

KATHOLIEKE UNIVERSITEIT
LEUVEN

Arenberg Doctoral School of Science, Engineering & Technology
Faculty of Engineering
Department of Electrical Engineering

ANALYSIS OF ELECTROPHYSIOLOGICAL MEASUREMENTS DURING STRESS MONITORING

Joachim TAELMAN

Dissertation presented in partial fulfillment of the requirements for the degree of Doctor in Engineering Sciences

January 2011

ANALYSIS OF ELECTROPHYSIOLOGICAL MEASUREMENTS DURING STRESS MONITORING

Joachim TAELMAN

Jury:
Prof. dr. ir. P. Moldenaers, president
Prof. dr. ir. S. Van Huffel, promotor
Prof. dr. ir. A. Spaepen, copromotor
Prof. dr. ir. R. Puers
Prof. dr. ir. D. Berckmans
Prof. dr. B. Van Houdenhove
Prof. dr. B. Van den Bergh (Universiteit van Tilburg)

Dissertation presented in partial fulfillment of the requirements for the degree of Doctor in Engineering Sciences

January 2011

© Katholieke Universiteit Leuven – Faculty of Electrical Engineering
Kasteelpark Arenberg 10, B-3001 Leuven (Belgium)

Alle rechten voorbehouden. Niets uit deze uitgave mag worden vermenigvuldigd en/of openbaar gemaakt worden door middel van druk, fotocopie, microfilm, elektronisch of op welke andere wijze ook zonder voorafgaande schriftelijke toestemming van de uitgever.

All rights reserved. No part of the publication may be reproduced in any form by print, photoprint, microfilm or any other means without written permission from the publisher.

D/2011/7515/7
ISBN 978-94-6018-304-1

Dankwoord

Deze thesis is het resultaat van 4 jaar onderzoek met veel inspanning, met soms lange dagen en korte nachten, maar ook met voldoende ruimte voor ontspanning (de ConText meetings, de congressen, de activiteiten met de collega's). Hoewel je een doctoraat grotendeels alleen schrijft, kan je dit toch niet tot een goed einde brengen zonder de steun van een aantal mensen.

Vooreerst wil ik mijn promotoren, prof. dr. ir. Sabine Van Huffel en prof. dr. ir. Arthur Spaepen, bedanken voor de begeleiding tijdens mijn onderzoek en om mij de kans te geven dit doctoraat te behalen. Bedankt Sabine om mij aan te moedigen tijdens de goeie momenten, maar ook om mij te blijven steunen tijdens de moeilijke momenten en om mij dan toch telkens weer te prikkelen en te motiveren om door te zetten. Dankzij jou heb ik dit tot een goed einde gebracht. Tuur, bedankt om mij de kans te geven om aan het project ConText mee te werken en voor het vertrouwen dat je in mij had tijdens dat onderzoek.

Verder wil ik ook de leden van de jury bedanken. Bedankt prof. dr. Boudewijn Van Houdenhove, prof. dr. ir. Daniel Berckmans, prof. dr. Bea Van den Bergh en prof. dr. ir. Bob Puers voor de positieve en opbouwende feedback die ik kreeg om deze tekst tot dit resultaat te krijgen. Bea, het was mij een waar genoegen om met jou samen te werken en hopelijk leidt de enorme inspanning van jouw studie tot goeie resultaten. Hierbij wil ik ook prof. dr. ir. Paula Moldenaers bedanken om de rol van voorzitster op haar te nemen.

Een groot deel van het onderzoek werd uitgevoerd in het kader van het Europese project ConText. Hierbij gaat mijn dank uit naar iedereen van het consortium voor de heel goede samenwerking met diepgaande discussies en de aangename 'social events'. In het bijzonder wil ik hier mijn directe collega's op FaBeR, Katrien, Tine, Elke en Anskje, bedanken voor de vlotte samenwerking. Verder wens ik de goeie samenwerking met prof. dr. Gunnar Buyse en prof. dr. Gunnar Naulaers van het UZ Gasthuisberg in de verf te zetten. De goesting om te gaan werken wordt mede bepaald door werksfeer en die wordt gecreëerd door je dagelijkse collega's. Die verdienen hier natuurlijk ook een speciale vermelding: Bedankt Steven, Alexander, Devy en Bogdan (voor de goeie samenwerking); Ivan en Vladimir (to allow a small

part of Belgium into the Serbian office); en verder ook Katrien, Wouter, Bori, Maarten, Diana, Maria Isabel, Marya, Rosie, Aileen, Kris, Ann-Sofie, Anca, Milica, Thijs, Vanya, Ben, Jan, Lieven en Kirsten (ESAT) en Ilse, Erik, Lennart, Gerlinde, Annelies, Karen en Marijke (FaBeR). Voor veel van jullie zou ik hier eigenlijk een aparte paragraaf moeten schrijven, maar dat zou mijn doctoraat dubbel zo dik maken.

Ik kan ook niet anders dan mijn huisgenootjes (Simon, Ann, Piet, Elise) hier vermelden voor de gezellige avondjes (al dan niet met fonduevleesjes). Verder wens ik alle familie, vrienden, broers, kennissen, collega's die ik hier niet heb vernoemd... te bedanken die van ver of van dichtbij ook maar enige interesse hebben getoond in mijn werk. Ook al was ik er niet altijd voor jullie, jullie waren toch een grote steun voor mij. Heel speciaal wil ik hier nog mijn ouders, Francky en Resi, vermelden voor hun steun en vertrouwen in mij!

Tot slot wil ik Leentje bedanken, gewoon om er altijd voor mij te zijn. Sorry dat ik de laatste maanden niet zoveel tijd over heb gehad om leuke dingen te doen, maar ik maak dat zeker en vast goed. Dat beloof ik! Jij blijft mijn kleintje!

Abstract

Work-related musculoskeletal disorders are a growing problem in todays society. These musculoskeletal disorders are caused by, amongst others, repetitive movements and mental stress. Stress is defined as the mismatch between a perceived demand and the perceived capacities to meet this demand. Although stress has a subjective origin, several physiological manifestations (e.g. cardiovascular and muscular) occur during periods of perceived stress. New insight and algorithms to extract information, related to stress are beneficial. Therefore, two series of stress experiments are executed in a laboratory environment, where subjects underwent different tasks inducing physical strain, mental stress and a combination of both.

In this manuscript, new and modified algorithms for electromyography signals are presented that improve the individual analysis of electromyography signals. A first algorithm removes the interference of the electrical activity of the heart on single-channel electromyography measurements. This interference signal is the major source of contamination in the electrical activity of the muscles in the shoulder and needs to be removed. The algorithm is based on a single-channel extension of independent component analysis to identify statistically independent sources in the signal. The extension consists of the decomposition of a single recording, using ensembled empirical mode decomposition or wavelets and on which traditional independent component analysis is applied.
A second data-driven algorithm estimates the rest-activation period from a muscle. Several applications need an accurate estimation of the period when a muscle is in rest. A new approach is presented, using the frequency content of the signals, which is able to distinguish between the rest and the active state of a muscle without a reference measurement or without the unreliable amplitude domain thresholding. The signals of the muscles in the shoulder area showed an interesting specific pattern during the stress experiments after removing the different artefacts. In approximately 65% of the subjects, a continuous firing of a single motor unit, was visible. This indicates a very low and subconscious muscle contraction without a postural benefit. An algorithm to detect these single motor unit firings is presented. The algorithm, based on an energy operator and correlation calculation, showed an excellent performance as it reaches a sensitivity of 100% and a specificity of

94,8%.

Another focus of the thesis is the physiological data interpretation during the stress experiments. The muscle activity analysis of the muscles in the shoulder girdle did not reveal any statistically significant increase in muscle activity. An activation of the muscles in the shoulder girdle during the stress test was identified, but this increase was not restricted to the periods where a mental task was executed. Even more, several subjects showed also reactions on other muscles (in the face, the lower back), revealing that the muscle activity analysis should not be limited to the trapezius muscle, but broadened to a group of muscles where reaction due to a mental stressor could be expected.
The analysis of the heart rate variability, a noninvasive estimation of the autonomic nervous system modulation on the heart rate, showed a statistically significant difference between the different tasks and revealed an extra reduced vagal modulation when the physical and the mental task are combined compared to both tasks seperately. Time-frequency analysis revealed that the effect of the mental task on the physiological signals reduces over time. In an additional study on pregnant women, we were not able to correlate the amount of reaction in the heart rate variability during different conditions with the subjective scores of anxiety and stress susceptibility of the pregnant women. This reveals that there is a clear effect of the tasks on the heart rate variability itself, but this is not one-to-one related with the stress level of the test subjects.
Both, the analysis of the muscle activity and the heart rate variability reveal the need for individual analysis during stress monitoring. The stress system consists of very complex interactions in the brain, which are at this moment not completely understood. Those interactions, however, are responsible for the variability in reaction of individual people on stressors: both in the intensity of the reaction as in the physiological reaction itself.

A last focus of this thesis was the analysis of the combination of the oxygenation and the electrical activity in the muscle, respectively measured and quantified by near-infrared spectroscopy and surface electromyography, during a muscle fatigue test. The combination of these two signals provides complementary information regarding muscle fatigue. A typical four-phase response was identified in the muscle oxygenation index, where different parameters could be linked with the physiology. A medical application, of which a pilot study is described, where both measurements are used, is the analysis of the progress of the disease in children with a muscle disease (Duchenne Muscle Dystrophy).

Samenvatting

Werkgerelateerde musculoskeletale aandoeningen zijn een groot probleem in de hedendaagse samenleving. Deze worden veroorzaakt door onder andere repetitieve beweging en stress. Stress wordt veroorzaakt door een onevenwicht tussen de subjectieve perceptie van een specifieke opdracht en de subjectieve perceptie van de individuele capaciteiten om die opdracht tot een goed einde te brengen. Alhoewel stress duidelijk een psychologische oorsprong heeft, worden fysiologische reacties veroorzaakt door de stress. Nieuwe inzichten en algoritmes om stressgerelateerd informatie uit de fysiologische signalen te halen, zijn nuttig. Daarom werden experimenten uitgevoerd in een labo waar de proefpersonen verschilllende taken ondergaan waar fysieke en mentale belastingen worden geïnduceerd.

In dit manuscript worden nieuwe en aangepaste algoritmes voorgesteld voor verbeterde individuele analyses van de spiersignalen. Een eerste algoritme verwijdert het interferentie signaal van het hart op een éénkanaalsmeting van het electromyogram. Dit algoritme is gebaseerd op een éénkanaalsuitbreiding van onafhankelijke componenten analyse, waarbij onafhankelijk signaalbronnen geïdentificeerd worden in het signaal. Deze uitbreiding maakt eerst een decompositie van het oorspronkelijke signaal via wavelets of via de empirische mode decompositie techniek en gebruikt deze decomposities om onafhankelijke componenten analyse toe te passen.
Een tweede algoritme gaat op zoek naar de periode van rust in de spiersignalen. Dit is nodig voor verschillende toepassingen. Een nieuwe benadering wordt beschreven waar gebruik wordt gemaakt van informatie in het frequentiedomein. Deze benadering maakt het mogelijk om te differentiëren tussen een spier in rust en een actieve spier, zonder gebruikt te moeten maken van een voorafgaande referentiemeting of de onbetrouwbare amplitudeparameters.
De signalen van de spieren in de schouderstreek tonen, na verwijdering van de interferentiesignalen, een specifieke activiteit tijdens de stressexperimenten bij ongeveer 65% van de proefpersonen: de continue activatie van slechts één motoreenheid. Dit betekent dat op dat moment slechts een aantal spiervezels actief zijn die zorgen voor een zeer kleine en onbewuste contractie. Een algoritme dat deze activiteit kan detecteren en lokaliseren is beschreven. Het algoritme maakt

gebruik van de energie in het signaal en correlatieberekeningen en toont zeer goede resultaten met een sensitiviteit van 100% en een specificiteit van 94,8%.

De focus van deze thesis richt zich op de interpretatie van de fysiologische metingen tijdens de stress experimenten. De analyse van de spieractiviteit in de schoudergordel toont geen statistisch significante toename van de spieractiviteit bij een mentale belasting. Activatie van de schouderspieren tijdens de stresstaak werd wel waargenomen, maar deze activatie was niet enkel beperkt tot de taken met een mentale belasting. Verschillende proefpersonen toonden ook spieractiviteit in de gezichtspieren en de spieren in de onderrug. Dit betekent dat de analyse van de spieren tijdens stressmomenten niet beperkt mag worden tot de spieren in de schoudergordel, maar dat ook de activiteit van de andere spieren in rekening gebracht moet worden.
Hartritmevariabiliteit, een niet-invasieve maat voor de activiteit van het autonoom zenuwstelsel, toont statistisch significante verschillen tussen de verschillende taken en toont zelfs een additief effect van de mentale taak op de fysieke belasting. Tijds-frequentie analyse toont dat het effect van de mentale belasting vermindert over tijd. In een bijkomstige studie bij zwangere vrouwen werd er geen verband gevonden tussen de sterkte van de fysiologische reactie en de subjectieve score van angst en angstgevoeligheid van de zwangere vrouwen. Deze bevindingen tonen aan dat met hartritmevariabiliteit kan aangetoond worden dat er een duidelijk reactie vanwege de taak is, maar dat er geen één-op-één verband is met het stressniveau van de proefpersoon.
Zowel de analyse van de spieractiviteit als van de hartritmevariabiliteit tonen aan dat er nood is aan individuele analyse tijdens stressanalyse. Het stresssysteem bestaat uit een heel aantal complexe interacties tussen verschillende gebieden in de hersenen, die op dit ogenblik nog niet volledig uitgeklaard zijn. Deze interacties zijn ervoor verantwoordelijk dat de stressrespons van verschillende personen heel individueel verschillend is: zowel wat de intensiteit van de reactie betreft, als de betrokkenheid van de verschillende fysiologische systemen.

Een laatste deel van de thesis is de analyse van zowel het zuurstofniveau als van de elektrische activiteit van een spier, respectievelijk opgemeten via nabij-infrarood spectroscopie and oppervlakte EMG, tijdens een spiervermoeiingstest. De combinatie van de informatie die gehaald kan worden uit beide fysiologische systemen zorgt voor complementaire informatie met betrekking op spiervermoeidheid. Het zuurstofniveau vertoont een typisch patroon tijdens een contractie, waaruit verschillende parameters gehaald kunnen worden die verband houden met de fysiologie. Een medische toepassing van het gebruik van beide meettechnieken is de analyse van spierwerking tijdens een contractie bij kinderen met spierdystrofie (ziekte van Duchenne) om de voortgang van de ziekte te kwantificeren.

Nomenclature

Symbols

$a, b, \ldots$	scalars
$\mathbf{a}, \mathbf{b}, \ldots$	vectors
$\mathbf{A}, \mathbf{B}, \ldots$	matrices
$[\mathbf{a}\,\mathbf{b}]$	matrix with columns $\mathbf{a}$ and $\mathbf{b}$
$\lvert a \rvert$	absolute value of a
$\mathbf{A}'$	transpose of the matrix $\mathbf{A}$
r	Pearson correlation coefficient
$\sum$	sum

Metrics

nm	nanometer
μm	micrometer
cm	centimeter
m	meter
g	gram
kg	kilogram
ms	milliseconds
s	seconds
h	hour
Hz	Hertz
ml	milliliter
mmHg	millimeter mercury
mV	millivolt
y	year

Abbreviations

$1/f$	1/f slope
ACT	Activity Level of the muscle
ACTH	AdrenoCorticoTropic Hormone
ANOVA	ANalysis Of VAriance
ANS	Autonomic Nervous System
ApEn	Approximate Entropy
AV	AtrioVentricular
BMI	Body Mass Index
bpm	beats per minute
BPV	Blood Pressure Variability
BSS	Blind Source Separation
CD	Correlation Dimension
CI	Confidence Interval
CNS	Central Nervous System
CO	Cardiac Output
ConText	European project: Contactless sensors incorporated in Textiles
CP	Phosphocreatine
CRH	Corticotropin Releasing Hormone
CWT	Continuous Wavelet Transform
Cytox	Cytochrome Oxydase
DAP	Diastolic Arterial Pressure
DFA	Detrended Fluctuation Analysis
DGC	dystrophin-glycoprotein-complex
difNN	difference between longest and shortest NN interval
DMD	Duchenne Muscle Dystrophy
DPF	Differential Path Length
DWT	Discrete Wavelet Transform
DYN	Semidynamic contraction
ECG	ElectroCardioGram
EEG	ElectroEncephaloGram
EEMD	Ensemble Empirical Mode Decomposition
EEMD-ICA	Ensemble Empirical Mode Decomposition in combination Independent Component Analysis
EMD	Empirical Mode Decomposition
EMG	ElectroMyoGrapm
FD	Fractal Dimension
FT	Fourier Transform
FFT	Fast Fourier Transform
GAS	General Adaptation Syndrome

Hb	haemoglobin
HbO_2	oxyhaemoglobin
HbR	deoxyhaemoglobin
HD-EMG	High Density Electromyography
HF	High Frequency (in absolute values)
HFnu	High Frequency (in normalized units)
HPA-axis	Hypothalamus-Pituitary-Adrenocortical axis
HR	Heart Rate
HRV	Heart Rate Variability
ICA	Independent Component Analysis
IMF	Intrinsic Mode Function
IMT	Intrinsic Mode Type Function
LE	Lyapunov Exponent
LF	Low Frequency (in absolute values)
LFnu	Low Frequency (in normalized units)
MAP	Mean Arterial Pressure
Mb	myoglobin
MPF	Mean Power Frequency
MPT	phase with combined Postural and Mental Task
MSD	MusculoSkeletal Disorders
MT	phase with Mental Task
MU	Motor Unit
MUAP	Motor Unit Action Potential
MVC	Maximal Voluntary Contraction
NIRS	Near Infrared Spectroscopy
NL	Noise Limit
NLdr	Noise Limit detection rate
NLEO	Non Linear Energy Operator
NN interval	Normal-to-Normal interval
np	noise parameter for EEMD
ns	non-significant
O_2	Oxygen
PCS	Post-Conceptional Age
PANAS	Positive Affect Negative Affect Schedule
pNN50	number of interval differences of successive NN intervals greater than 50 ms divided by the total number of NN intervals
PNS	Peripheral Nervous System
PSD	Power Spectral Density
PT	phase with Postural Task
R	Rest (phase)
REM	Rapid Eye Movement
RLE	Rest Level Estimation
RMS	Root Mean Square
RMSSD	Root Mean Square of Successive Differences

RRI	R peak to R peak Interval
RSI	Repetitive Strain Injury
RSA	Respiratory Sinus Arrhythmia
RVC	Relative Voluntary Contraction
S	Sigh
SR	Self-Rating
SAP	Systolic Arterial Pressure
SampEn	Sample Entropy
sEMG	surface ElectroMyoGram
SENIAM	Surface Electropmyography for the Non-Invasive Assessment of Muscles
SD	Standard Deviation
SDNN	Standard Deviation of NN intervals
SDSD	Standard Deviation of the Successive Differences
SMUF	Single Motor Unit Firings
SNR	Signal To Noise Ratio
STAT	Static contraction
STAI	State-Trait Anxiety Inventory
STFT	Short-Time Fourier Transform
SV	Stroke Volume
TFA	Time-Frequency Analysis
TFR	Time-Frequency Representation
TOI	Tissue Oxygenation Index
TP	Total Power
VDU	Visual Display Unit
VLF	Very Low Frequency (in absolute values)
wICA	Wavelets in combination with Independent Component analysis
WT	Wavelet Transform

Contents

Dankwoord i

Abstract iii

Samenvatting v

Nomenclature vii

Contents xi

1 Overview 1

1.1 Introduction 1

1.2 Aim of the thesis 3

1.3 Collaboration 4

1.3.1 Department of Kinesiology and Rehabilitation Sciences, K.U. Leuven 4

1.3.2 ConText 5

1.3.3 Other Collaborations 7

1.4 Chapter-by-chapter overview 8

1.5 Personal Contribution 13

2 Methodology 15

2.1 Mathematical background 15
2.1.1 Independent Component Analysis (ICA) 15
2.1.2 Time-Frequency Analysis (TFA) 18
2.1.3 Ensemble Empirical Mode Decomposition (EEMD) 23
2.2 Surface Electromyography 26
2.2.1 Muscle Physiology: Overview 26
2.2.2 Surface Electromyography 30
2.2.3 Parameters 33
2.3 Heart Rate Variability 35
2.3.1 Introduction 35
2.3.2 Processing 38
2.3.3 Heart Rate Variability Parameters 40
2.4 Near-Infrared Spectroscopy 46
2.5 Stress 51
2.6 Conclusion 55

3 sEMG processing and analysis 57

3.1 Introduction 58
3.2 Data acquisition: stress assessment 59
3.2.1 Stressexp 1 59
3.2.2 Stressexp 2 64
3.3 Preprocessing: ECG interference removal 68
3.3.1 Introduction 68
3.3.2 Algorithms 69
3.3.3 Data 72
3.3.4 Results 74
3.3.5 Discussion 82
3.4 Single motor unit firings: Detection algorithm 84

3.4.1 Single Motor Unit Firing 84
3.4.2 Detection algorithm 85
3.4.3 Results 87
3.4.4 Discussion 89
3.5 Rest Level Estimation 90
3.5.1 Introduction 90
3.5.2 Rest Level Estimation Algorithm 91
3.5.3 Results 93
3.5.4 Discussion 98
3.6 Stress: Data analysis 100
3.7 Conclusion 106

4 Heart Rate Variability **109**

4.1 Introduction 109
4.2 Instantaneous changes in heart rate variability during physical, mental and combined stress in laborartory environment 110
4.2.1 Objective 110
4.2.2 Methodolgy 111
4.2.3 Results 113
4.2.4 Discussion 124
4.3 Stress during pregnancy: Is the autonomic nervous system influenced by Anxiety? 127
4.3.1 Introduction 127
4.3.2 Methods 128
4.3.3 Results 130
4.3.4 Discussion 132
4.4 Respiration 134
4.4.1 Introduction 134
4.4.2 Sighing: a psychophysiological resetter 134

4.4.3 Respiration versus HRV 136
4.5 Conclusion 137

5 Near Infrared Spectroscopy: processing applied to muscle fatigue 139
5.1 Introduction 139
5.2 Methods 140
5.2.1 Experimental procedure 140
5.2.2 Muscle fatigue parameters 142
5.3 Results 142
5.4 Discussion 144
5.5 Muscle activity assessment for patients with Duchenne Muscle Distrophy (DMD) 146
5.6 Conclusion 148

6 Conclusions and future research 151
6.1 General conclusions 151
6.1.1 Mathematical techniques 151
6.1.2 Stress 152
6.1.3 Other Applications 154
6.2 Future work 155
6.2.1 EMG analysis 155
6.2.2 Heart Rate Variability and respiration 156
6.2.3 Near Infrared Spectroscopy in muscle analysis 156
6.2.4 Stress 157

Bibliography 177

Publication list 195

Curriculum vitae 199

Chapter 1

Overview

1.1 Introduction

Work-related musculoskeletal disorders (MSD) are a growing problem in todays society. MSD cover a wide variety of phenomena and experiences (discomfort, disorders, pain) [61]. Musculoskeletal disorders are injuries of the muscles, nerves, tendons, ligaments, joints, cartilage, or spinal discs and are not typically the result of any instantaneous or acute event (such as a slip, trip, or fall) but reflect a more gradual or chronic development. A wide range of acronyms and terms are used to give a unified name to syndromes that are work-related, and appear at different sites of the human musculoskeletal system. They give different names according to the body part affected or the presumed pathomechanics of the injury. Other expressions used to describe MSDs are: Repetitive Strain Injuries (RSIs), Cumulative Trauma Disorders, Overuse Injuries, Repetitive Motion Disorders. Medical terms used to describe MSDs to various parts of the body include low back pain, carpal tunnel syndrome, trigger finger, myalgia .... MSD have personal consequences, such as discomfort, pain, malfunctioning and disability. Moreover, MSD have socio-economical consequences such as reduced productivity, reduced performance and absenteeism. Forty to fifty percent of all work related absences are affected by work-related MSD. This problem leads to losses of 0.5 to 2% of GNP per year. The problem is noticed by the European Commission [52, 55]. These MSD occur when there is a mismatch between the physical requirements and the physical capacity of the human body. The injuries are mainly associated with effort, movements, postures and vibrations, but also with work organisation and psychosocial factors. In the last decades, its prevalence has increased in a varied range of occupations. This can be related to changes in work contents: there has been a shift from work being dynamic and varied to work being more

static, repetitive and monotonous. Workload has also become more stressful [52, 53, 54]. Mental stress occurs from an imbalance between perceived demands of the environment and perceived capacities of the person to meet those demands. This imbalance can be originated by a too low, a boring demand or a too difficult taks. In the last decades, the focus of research on the pathomechanisms of WMSD has broadened from singularly physical mechanisms towards psychophysiological pathomechanisms and its relation to stress.

Stress results in an activation of several physiological systems as described in 2.5. Stress, whether purely physical or psychophysiological, generates a fight or flight reaction to prepare the body to withstand the stressful situation. Stress activates the hormonal system through the secretion of adrenalin and noradrenalin into the blood stream. Noradrenalin is secreted to mobilize energy for stimulating the cardiovascular system and the muscular system (high muscle tension). This fight or flight reaction ceases when the balance between perceived demands and perceived capacity is restored, i.e. when the stressor is no longer present. However, a chronic exposure to stressors, such as experienced in working situations, can lead to a chronic activation of the physiological systems such as amongst others the muscular systems. Long term consequences can be musculoskeletal overload due to insufficient recovery and repair of the muscle fibers. During prolonged mental load and/or low physical activity, low threshold motor units are being 'overused'. Although these units are assumed to be fatigue-resistant, overactivity can cause metabolic disturbances and degenerative processes. Accumulation of inflammatory substances and elevated muscle stiffness leads to increased pain sensitivity which evolves into a vicious circle of increasing muscle tension and pain. The trapezius muscle has been found to be particularly sensitive to stress [67, 82, 73]. Prolonged muscle tension, joint overloading, reduced blood perfusion and acidification of the muscle which compromises the tissue quality, can cause musculoskeletal disorders.

Electromyography (EMG) can help to understand the mechanisms and the impact of stress on muscle activity. In laboratory studies, researchers have studied EMG-signals during the performance of a mental task (e.g. Stroop Color Word test, mental arithmetic test, memory tasks). They found that mental workload increases trapezius muscle activity [6, 17, 50, 89, 92, 96, 181]. Stressful circumstances, such as verbal provocation during performance and time pressure also increase muscle activity [180]. However, several researchers have reported considerable inter-individual differences in muscle activity response to a stressor [186, 98, 115, 173].

The relationship between EMG-activity and pain or musculoskeletal disorders has been studied in several case-control studies in varied types of occupation, such as VDU-workers (video-display-unit-workers), supermarket cashiers, chocolate packers, medical secretaries, etc. An important finding is that the number of EMG rest periods or 'EMG-gaps' (very short periods of muscle rest) is lower in pain-afflicted subjects [67, 115, 139, 167]. These findings emphasize the importance

of (micro-) pauses in the battle against MSD. Crenshaw et al [32] found that pauses did not influence muscle activity, but pauses do benefit the blood circulation and muscle oxygenation. Moreover, pain-afflicted subjects have less and slower deactivation or recuperation after work compared with pain-free subjects [73, 95]. This suggests that relaxation during work and in leisure time is essential to prevent MSD.

EMG activity does not always correlate with other physiological parameters, such as heart rate, blood pressure, level of cortisol and catecholamines [89, 82, 135]. This suggests that other physiological parameters are also necessary to measure stress. Also, perceived muscle tension, perceived general tension or mood states do not always correlate with EMG activity [135, 173]. Therefore, other physiological parameters can be analyzed. One of the most important parameters is the beat-to-beat alterations of the heart rate, known as heart rate variability (HRV). Several researchers [1, 165] have shown that information extracted from HRV can be linked with activity of the autonomic nervous system. The autonomic nervous system is not only affected by postural activity, but also by changes in the psychological state of a subject. HRV may therefore offer a powerful tool for clarifying the relationship between psychological and physiological processes.

The myoelectric signal is not the only physiological signal that can be measured from the muscle. Near-Infrared Spectroscopy (NIRS) is an important technique to retrieve information about the oxygenation in the muscle. Information about the muscle oxygenation can benefit in the battle against MSD and muscle pain as stated earlier. The analysis of the combination of EMG and NIRS can improve the insight into the functioning of a muscle and can result in a better estimation of possible malfunctioning of the muscle.

1.2 Aim of the thesis

A first goal of the thesis is the development and modification of new or existing algorithms to improve the individual analysis of electromyography signals. A first algorithm aims to remove the interference of the electrical activity of the heart on single-channel electromyography measurements, which is the major source of interference in the signals of the muscles in this region. Hereafter, a data-driven algorithm is presented that estimates the rest-activation period from a muscle using its electrophysiological signal.

A second goal of the thesis is the determination of the influence of mental stress on different physiological signals: the heartrate variation and the electrical activity of the muscles in the shoulder girdle. Next to the traditional electromyography parameters to quantify the EMG activity, the aim was to identify specific EMG patterns during periods with mental load and detect this patterns using signal

processing.
The beat-to-beat variability of the heart is investigated, to study the autonomic nervous system, influenced by the mental load. In addition to the traditional HRV parameters, time-frequency analysis can be applied to improve the time resolution of the detect changes.
In a study on pregnant women, the relationship between the amount of perceived stress, measured via questionnaires, and the amount of physiological reactions, via HRV analysis is investigated.

A last goal of this thesis is combining oxygenation information from the muscle with its electrophysiological activation during a muscle fatigue test. A combination of this multimodal data can provide additional information in different applications. This information is used in a medical application where the progress of a muscle disease (Duchenne Muscle Dystrophy) in children is investigated.

The most important hypotheses of this manuscript are:

1. The electrical interference of the heart on the electromyography signals can be removed from a single surface electromyography measurement using advanced signal processing techiques.
2. The trapezius muscle activity and the variability of the heart rate are influenced by all types of mental stress.
3. The complexity of the stress system and the interindividual physiological reaction profiles require algorithms that are applicable on individual basis.
4. Combining myoelectrical and muscle oxygenation information during sustained contraction improves the physiological insight in healthy and pathological muscles.

1.3 Collaboration

1.3.1 Department of Kinesiology and Rehabilitation Sciences, K.U. Leuven

A huge part of my work is executed in the labo of ergonomics and biomechanics under the supervision of prof. dr. ir. Arthur Spaepen at the department of Kinesiology and Rehabilitation Sciences (FaBeR). The main focus of the research in this group is the use of surface electromyography (sEMG) as a qualitative measure in ergonomics, consultancy in ergonomics and biomechanical modelling during gait analysis and the upper limb movement. Together with Katrien Van Damme and Tine Adriaensens, I worked as a researcher for the ConText project

(see section 1.3.2). The sEMG data acquisition, data analysis and interpretation were performed in this laboratory. Besides this, we supported the development of the capacitive sensors, the design of the shirt and the positioning of the electrodes in the ConText shirt via different measurements and analysis.

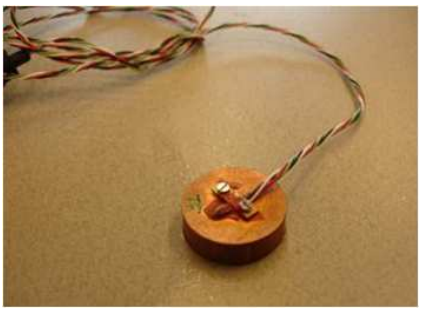
1.3.2 ConText

The main part of the work was performed within the framework of the European project ConText (Contactless sensors incorporated in Textiles for stress monitoring; IST-027291). The project ran 3 years from January 2006 till December 2008. The objectives of the project were the development of a home monitoring shirt to obtain unobtrusive sEMG signals enabling long term recordings with applications in stress monitoring and musculoskeletal disorders by acquiring the EMG signals using contactless capacitive sensors. These sensors are incorporated into textiles to increase comfort for the end user. This project was in collaboration with several partners across Europe.

- **Philips Research (The Netherlands),** was the project leader. Their main focus was the development of a capacitive sensor with the focus on sEMG signals.
- **TNO (The Netherlands),** developed the design of the shirt with the focus on comfort and usability. TNO also developed a printing technology to print conductive wires on the textile. They went to the end user in collaboration with Clothing + to look for other applications with the developed technology.
- **TITV (Germany),** compared the different existing conductive wires and incorporated the best suitable material in textiles via weaving.
- **T.U. Berlin (Germany),** created the embroidered capacitive sensor. They also worked on the encapsulation of the electronics onto the textile with respect to comfort and sustainability.
- **Clothing+ (Finland),** investigated the use of lamination and for the development of a capacitive sensor. They looked for potential new applications of the developed technology with TNO.
- **K.U. Leuven (Belgium),** worked on the application of the project. Several measurements of sEMG and ECG were performed in a laboratory environment and the signals were analysed. They supported the development of the capacitive sensors, the design of the shirt and the positioning of the electrodes in the shirt.



(a) Prototype II ConText vest.



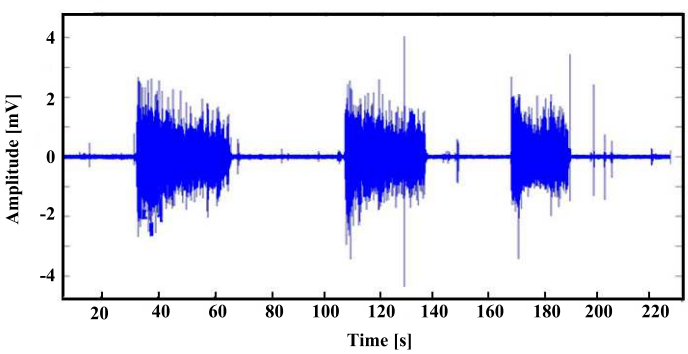
(b) Optimised capacitive sEMG sensor (Philips).



(c) Embroidered capacitive sensor (T.U. Berlin).



(d) Laminated capacitive sensor (Clothing + and T.U. Berlin)



(e) sEMG measurement with the laminated capacitive sensor on the Biceps Muscle (Philips and K.U. Leuven)

Figure 1.1: *Pictures of achievements in the European project ConText*

The most important achievements of the projects are presented in figure 1.1. Figure 1.1(a) shows the second prototype of the ConText vest, designed by TNO and Clothing+. The materials were selected and the design was optimised to have a narrow fit in the areas where perfect contact is needed (e.g. shoulder area). The EMG sensors were incorporated in the demoshirt to measure the trapezius muscle. The conductive area at the back of the shirt measures the reference signal for the EMG signals. Figure 1.1(b) shows the optimized capacitive sensor, developed by Philips. This sensor is more robust to movement artifacts. Figure 1.1(c) is an enlargement of the shoulder of the first prototype shirt and shows an embroidered capacitive sensor made by T.U. Berlin. The electronics of the sensors are included on a flexible substrate and a textile bus structure to transfer the data is visible. The test sensor is shown in figure 1.1(d). This is a laminated capacitive sensor incorporated into textiles to measure the sEMG. This electrode has been used to test on different muscles. An EMG measurement, using this capacitive laminated sensor, is shown in figure 1.1(e). The sensor is placed on the biceps muscle and several contractions are executed. These contractions are clearly visible in the EMG signal.

1.3.3 Other Collaborations

Several collaborations with other groups are set up for several studies described in this manuscript:

- **Research Group on Health Psychology, K.U. Leuven**. One of the two stress experiments were executed in close collaboration with dr. Elke Vlemincx from the group of Prof. dr. Omer Van den Bergh. During these measurements, the test subjects underwent different tasks, imposing a mental effort on them, while several physiological signals (EMG, ECG and respiration) were acquired. One of the topics of the research of this group is the effect of sighing as a psychophysiological resetter in stress situations.
- **Developmental Psychology, Universiteit van Tilburg, The Netherlands**. A large study is performed in the group of prof. dr. Bea Van den Bergh about the influence of the stress of a pregnant mother on the cognitive development of their babies. At this moment, the level of stress and anxiety of the mothers is derived using psychological questionnaires, but the question is whether the physiological parameters, related to stress, could be a better classifier. Several physiological signals of the mothers are acquired at several time instants during their pregnancy next to different physiological parameters of the babies after birth. This study is part of a large European research project EuroSTRESS [46].
- **U.Z. Gasthuisberg, Division of Neonatology, K.U. Leuven**. Together with dr. Joke Vanderhaegen from the group of prof. dr. Gunnar Naulaurs,

we explored the combination of surface electromyography and Near Infrared Spectroscopy (NIRS) during and after muscle fatigue exercises. In the group of neonatology, the NIRS is used to monitor the oxygenation of the brain of premature babies for more effective threatment.

- **U.Z. Gasthuisberg, Division of pediatric neurology, K.U. Leuven**. This group of prof. dr. Gunnar Buyse works with children with Duchenne Muscle Distrophy. The diagnosis of DMD is based on clinical signs and indirect measures. They are starting up research to measure the response of the oxygenation and the electrophysiology of the muscle after a physical effort.

1.4 Chapter-by-chapter overview

In this section, the content of the different chapters is provided. Figure 1.2 shows an overview of the different chapters in this manuscript and their relationship with each other. Table 1.1 gives an overview of the different experiments and shows in which section each dataset is used.

Chapter 1

In this chapter, a general introduction and an overview of the work is presented. Furthermore, the different goals of the thesis are addressed and an overview of the personal contributions is provided.

Chapter 2

Chapter 2 provides a scientific basis for the following chapters. In a first subsection, the different mathematical techniques, used throughout the thesis, are summarized. The described techniques are Independent Component Analysis (ICA), Wavelet Transform (WT), ensemble empirical mode decomposition (EEMD) and time-frequency analysis (TFA).

The anatomy of a muscle is introduced in section 2.2 next to the use of the surface electromyography (sEMG) to measure the electrical activity of the muscle and the traditional time and frequency parameters that are derived from the sEMG signals to analyze the signals.

Section 2.3 provides an overview of the different steps to retrieve heart rate variability (HRV) results from ECG signals, including the peak detection and the

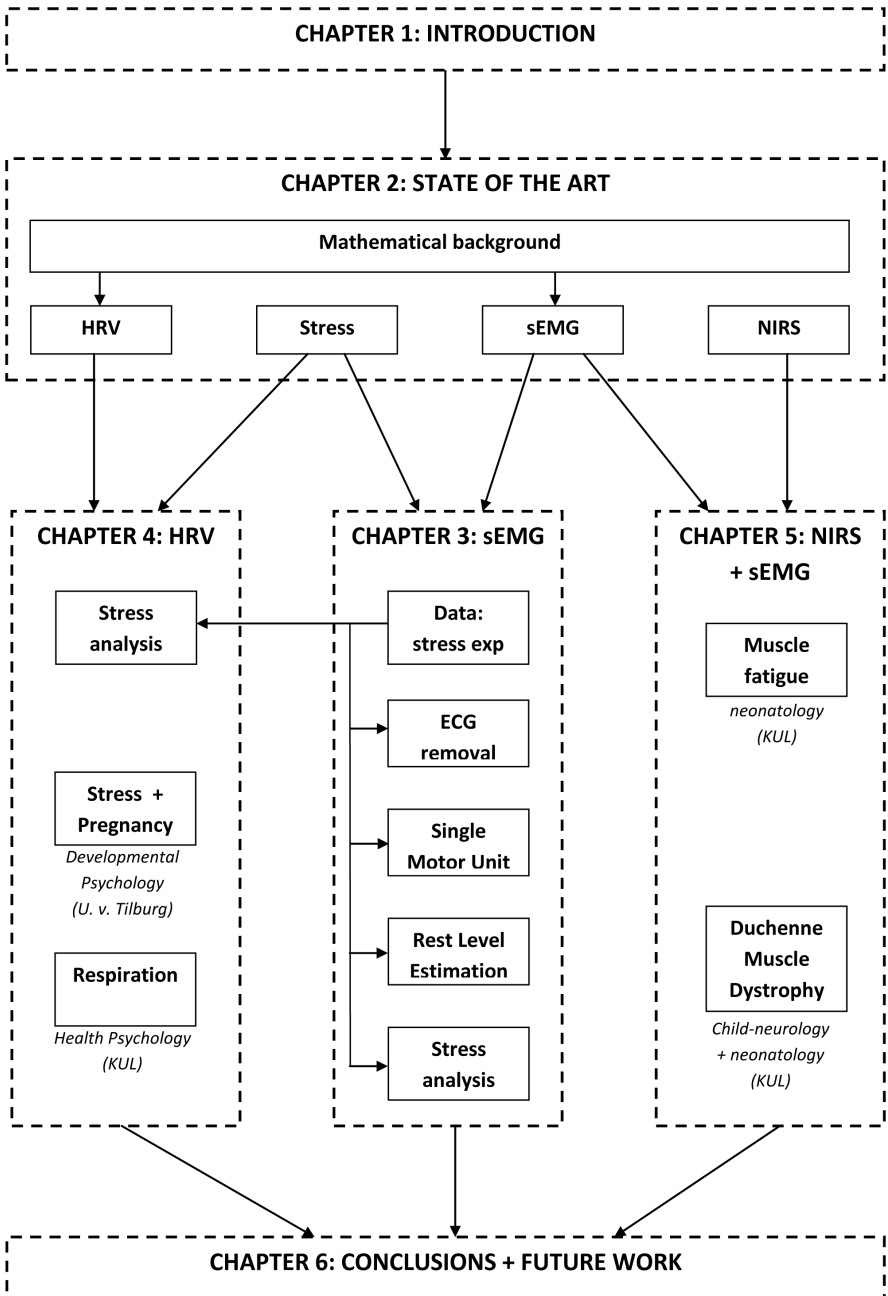


Figure 1.2: *Overview of the chapters in this thesis.*

Table 1.1: *Overview of the different experiments used in this thesis. This table shows in which section each data set is used.*

Experiment	Description (Section)	Subjects (#)	Duration	Analyses		Collaboration
Stressexp 1	3.2	28	max 39min	ECG Removal	(3.3)	ConText
				Single motor unit firing	(3.4)	
				Rest Level Estimation	(3.5)	
				EMG analysis	(3.6)	
				HRV analysis	(4.2)	
Stressexp 2	3.2	43	42min	ECG Removal	(3.3)	ConText
				EMG analysis	(3.6)	KUL Psychology
				HRV analysis	(4.2)	
Stress pregnancy	4.3.2	180	24h	HRV vs. Anxiety	(4.3)	University Tilburg
EMG + NIRS	5.2	34	± 40min	Muscle fatigue	(5.3)	KUL Neonatology
DMD	5.5	18	15min	Muscle contraction	(5.5)	KUL pediatric neurology KUL Neonatology

preprocessing. Afterwards, the linear, nonlinear and time frequency parameters, used in this manuscript, are summarized.

The near infrared spectroscopy (NIRS) measurement and the parameters to measure the oxygenation of the tissue is described in section 2.4.

In the last part of this chapter (section 2.5), an introduction of stress is described. Stress is introduced as both a psychological and physiological phenomenon. Therefore, we refer to stress as a psychophysiological phenomenon.

Chapter 3

Chapter 3 gives an overview of the signal processing and the analysis of the sEMG signals. In a first section 3.2, the data, used within the manuscript, are described. Two stress experiments are conducted where a mental stress was induced on the test subjects. This mental task was combined with and without an extra physical load. These data were collected and analysed for the European project ConText.

In section 3.3, the removal of ECG interference in sEMG signals of the shoulder girdle is described. This ECG interference signal is the most important noise influence in these sEMG signals. Together with my colleague Bogdan Mijovic, a single channel approach of independent component analysis was elaborated and I applied it to remove the ECG interference signal from a single EMG signal. These techniques were expanded to situations where a simultaneous ECG measurement is available. The results of these techniques were compared with a standard technique to remove the interference signal.

During the analysis of the sEMG signal of the trapezius muscle during the stress assessment tasks, a specific pattern of muscle activity could be identified which is not published earlier in this situation using this type of electrodes. This muscle activity is a continuous activation of single type I motor unit. A spike train detection algorithm is modified to detect this type of activity. This observation and detection algorithm is described in section 3.4.

In the next section (3.5), an algorithm to estimate whether a muscle is active or in rest is presented. This algorithm is based on the frequency properties of the sEMG signals in both situations. We used this algorithm to estimate the baseline of the different sEMG signals during the stress assessment task.

The last section (3.6) shows the most important results of the analysis of the different sEMG parameters during the stress experiments. The effect of the mental task on the standard parameters is discussed, next to the analysis of muscle fatigue during the different tasks. We also looked at the additional effect on the muscle activity from the mental load on a physical load.

Chapter 4

The results of the HRV analysis on the two stress experiments (described in section 3.2) are presented in section 4.2. More specifically, the additional effect on the different HRV parameters of a mental load on top of a physical load is studied using the traditional linear HRV parameters. To increase the time resolution of the variations of the parameters during the test, time frequency analysis are applied.

In the next section 4.3, the aim was to investigate whether anxiety during pregnancy, as indicated by the questionnaires, can be linked with differences in the autonomic heart rate modulation via HRV parameters during both a 24h recording of the ECG and a stress test where a mental load is induced. The hypothesis was that perceived stress, indicated via subjective questionnaires, will be reflected in differences in HRV measures so that we would be able to distinguish between a low and a high anxiety group using these HRV parameters. The nonlinear HRV measures are used next to the traditional linear HRV measures.

In the last section 4.4, a short overview of the most important influences of respiration are discussed. The effect of the respiration, and more specific sighing, during a stress task will be explored. The psychophysiological interpretation of sighing as a physiological resetter has become a large topic in research. During the second experiment, the respiration was included as one of the physiological signals, so this analysis could be included. In the literature, there is a huge ongoing discussion about the role of respiration in HRV analysis which is discussed in the second part of this section.

Chapter 5

In a first part, the myoelectric and oxygenation mechanisms of muscles during muscle fatigue is described. More specifically, the behavior of the indiviual sEMG and NIRS parameters and their relationship in the biceps brachii muscle until exhaustion after isometric static and semidynamic exercises are investigated.

In a second part, the sEMG and NIRS parameters are used to investigate the response of the oxygenation and the myoelectric signals of the muscle after a physical effort on patients with Duchenne Muscle Dystrophy in a pilote study.

Chapter 6

The last chapter summarizes the work presented in the different chapters and formulates the main conclusions of this manuscript. Moreover, several suggestions for future research are described.

1.5 Personal Contribution

As discussed previously, I collaborated in several projects both in EU context and in a bilateral agreement with various divisions in K.U.Leuven and U.Z. Leuven. In general, I contributed to the data acquisition, the signal analysis, the algorithm modifications and the interpretation of the results.

I was involved in the acquisition of all the data used throughout this manuscript. I was responsible, together with my colleagues at FaBeR, for the design of both protocols, the laboratory set up and the acquisition of the data of the stress tests (described in section 3.2). The second set of experiments were performed in collaboration with dr. Elke Vlemincx of the group of psychology at the K.U. Leuven. These data were used for the HRV and sEMG analysis. I included the stress assessment task in the protocol during the recording of the ECG of the pregnant women (section 4.3).

I did all the data analysis of the sEMG signals and the interpretation of these results was done together with my colleagues at FaBeR. I modified and tuned several algorithms that were used in the sEMG signal analysis. Together with my colleague Bogdan Mijovic, we worked on a single channel approach of independent component analysis and I applied it to remove the ECG interference from the sEMG signals. I compared its results with the results of the standard method that is used nowadays. During the visual inspection of the sEMG signals of the trapezius muscle, I observed the single motor unit firing and modified and tuned an existing algorithm to detect this specific sEMG signal pattern. This algorithm was able to localize all these types of sEMG activity. I developed an easy-to-use algorithm, based on the frequency properties of sEMG signals, that is able to distinguish between rest and contraction in a muscle. This algorithm is applied to estimate the baseline of the different sEMG signals during the stress assessment task as no baseline session was included in the measurements.

The HRV analyses of the two experiments were performed in close collaboration with my colleague at ESAT, Steven Vandeput. We collaborated in the analysis of the ECG signals, the statistics and in the interpretation of the results. The analysis and the interpretation of the data from the pregnant women is executed by myself in close collaboration with Steven Vandeput and Devy Widjaja. The analysis of the sighing was mainly performed by Elke Vlemincx, but I contributed to the interpretation of some results.

I set up a collaboration with the division of neonatology of prof. dr. Gunnar Naulaers and dr. Joke Vanderhaegen to use NIRS for muscle activity and with the division of pediatric neurology of prof. dr. Gunnar Buyse to measure the children with the Duchenne Muscle Dystrophy (DMD). I was responsible for the design of the protocols, the laboratory setup and the acquisition of the data of simultaneous sEMG and NIRS on both healthy subjects and children with DMD,

next to the data analysis, statistical analysis and the physiological interpretation of the results. These results are described in chapter 5. For the data analysis of the children with DMD, I worked together with my colleague Alexander Caicedo Dorado.

Chapter 2

Methodology: State of the art

Chapter 2 introduces the mathematics, the physiological background and signals, necessary for a good understanding of the thesis. First the mathematical techniques are presented in Section 2.1. This section gives an overview of Independent Componentent Analysis (ICA), Time Frequency Analysis (TFA) and the introduction to wavelets and finally Ensemble Empirical Mode Decomposition (EEMD). Section 2.2 describes the physiological background of a muscle and introduces surface electromyography and its most important parameters. The physiology of the heart, the heart rate variability, its preprocessing and linear and non linear parameters are discussed in section 2.3. The near infrared spectroscopy (NIRS) measurement and the parameters to measure the oxygenation of tissue is described in section 2.4. In the last section (section 2.5), an introduction of stress is described. A summary of the physiology and the psychology of stress is given in this section.

2.1 Mathematical background

2.1.1 Independent Component Analysis (ICA)

Blind Source Separation (BSS)

A good example to introduce the principle of blind source separation (BSS) is the so-called *cocktail party problem*. In one room, n people are speaking simultaneously producing each a signal $s_n(t)$. (k) microphones are located at different places in the same room and are recording simultaneously the conversations, denoted with

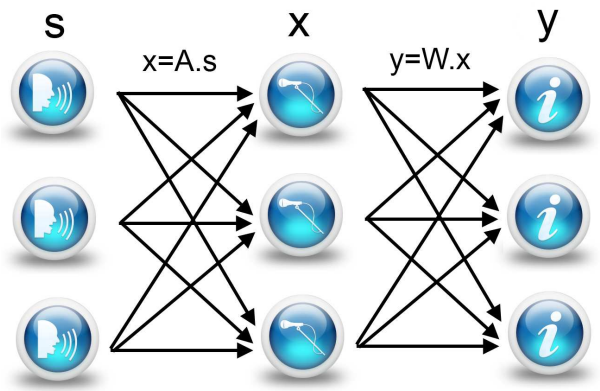


Figure 2.1: *Illustration of the cocktail party problem. A linear mixture of the three different conversations is recorded at the three microphones. (From [37])*

$x_k(t)$. The recordings $x_k(t)$ are a linear mixture of the different conversations $s_n(t)$ and is presented in equation 2.1.

$$\begin{cases} x_1(t) &= a_{11}s_1(t) + a_{12}s_2(t) + \ldots + a_{1n}s_n(t) \\ x_2(t) &= a_{21}s_1(t) + a_{22}s_2(t) + \ldots + a_{2n}s_n(t) \\ \ldots & \\ x_k(t) &= a_{k1}s_1(t) + a_{k2}s_2(t) + \ldots + a_{kn}s_n(t) \end{cases} \tag{2.1}$$

where a_{11}, a_{21} ... are the mixing parameters that depend on the distances of the microphones from the speakers (to simplify the model, the delay of the signal, other extra factors and noise in the room are omitted). In signal processing, the challenge is to retrieve the signals $y_k(t)$, which are estimates of $s_k(t)$, from the recordings $x_k(t)$. Figure 2.1 gives an overview of the problem (with $k = 3$ and $n = 3$). $\mathbf{A}$ and $\mathbf{W}$ are respectively called the mixing and the unmixing matrix. When the information of the mixing matrix $\mathbf{A}$ is available, the source signals can be estimated using classical linear algebra. However in most real situations, this information is not present making the problem considerably more challenging. Extra assumptions and prior information needs to be included to retrieve the original sources $s_n(t)$. The mathematical techniques that focus on solving this problem are called blind source separation techniques. These techniques can be applied on several applications where the research problem can be estimated by equation 2.1.

Independent Component Analysis (ICA)

One approach to estimate the mixing matrix and calculate the different sources from equation 2.1 is using information on the statistical properties of the sources $s(t)$ to estimate the mixing matrix $\mathbf{A}$. Independent Component Analysis (ICA) assumes that the sources $s(t)$ are mutually statistically independent [78]. In the case of a cocktail party problem, this is a valid assumption. In more general terms for signal processing, ICA is a computational method for separating a multivariate signal into additive subcomponents supposing the mutual statistical independence. Statistically independency is a stronger assumption than uncorrelation: two statistically independent variables implies that they are uncorrelated, but the opposite is not valid. As ICA is trying to estimate the mixing matrix derived from properties of the sources, two limitations of the technique are appearing. The variances of the independent sources cannot be determined (assume that each independent component has unit variance $E\{s_i^2\} = 1$) and no order of the independent sources can be found. Fortunately, in most applications these limitations are insignificant.

One fundamental restriction in ICA is that the independent components must be nongaussian to make ICA applicable [78]. The mixing matrix $\mathbf{A}$ can not be identified for gaussian independent components. More specifically, at least one independent component has to be non gaussian. According to the central limit theorem (CLT), a mixture of two source signals will be more gaussian than the two original source signals. Several methods exist to distinguish between the different independent sources. The most used method is maximizing the nongaussianity of each of the independent sources. Several measures can be used to maximise this nongaussianity: the classical measure is the kurtosis or the fourth order cumulant, but also the negentropy and known approximations of negentropy are used. Another approach to look for independency is minimizing the mutual information between the sources. Hyvärinen showed in his book [77] that minimizing the mutual information is equivalent as finding the direction in which the entropy is maximized. In [77, 91], several implementations of ICA are described.

In this work, the fastICA algorithm [76] will be used. This algorithm uses a computationally more efficient approximation for negentropy to estimate the different independent sources. This approach is roughly 10 times faster than the conventional methods [192] to calculate the negentropy. The sources are extracted one after each other. This technique has been applied multiple times in the field of biomedical signal processing [76, 87, 64].

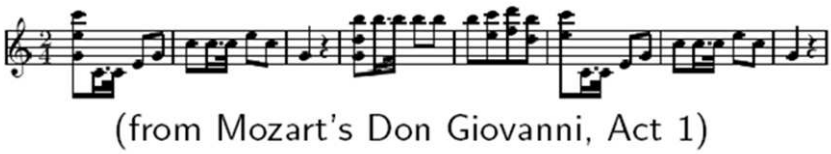


Figure 2.2: *The most known time-frequency representation: a music line (From [4]).*

2.1.2 Time-Frequency Analysis (TFA)

The traditional frequency domain analysis methods, applied on the whole signal, are not reliable when the signal is nonstationary, which means that different instantaneous signal properties, such as the signal amplitude or the spectrum properties, are not constant over time. The spectrum, extracted from the Fourier Transform, essentially tells us which frequencies are present in the signal, as well as their corresponding amplitudes and phases, but does not tell us at which times these frequencies occur. Luckily, techniques exist that combine both time and frequency information simultaneously, the so-called time-frequency representations (TFR). The best known example of a representation that gives both time and frequency information is a music line (see figure 2.2). The rhythm contains the time information while the note gives the tone (more specifically the frequency) at which the rhythm needs to be executed at that specific time instant.

In signal processing, different techniques are available to create a TFR from a time series. An overview of the most important techniques is given by Auger et al [7], but here the basic short-time Fourier transform (STFT) and the more advanced wavelet transform (WT) are discussed. A schematic illustration of the differences between time series representation, Fourier transform, STFT and CWT is shown in Figure 2.3 and will be explained more in detail in the following subsections.

Short-time Fourier Transform (STFT)

The traditional Fourier Transform (FT) decomposes the time signal in different sine waves with a specific frequency. A sine wave is an continuous oscillating signal, removing all the time information and thus implying stationarity from the signal. In order to introduce time-dependency in using a Fourier transform, a simple and intuitive solution consists in pre-windowing the signal $x(u)$ around a particular time t during which the signal is stationary, calculating its Fourier transform, and doing that for each time instant t. The resulting transform, called the short-time

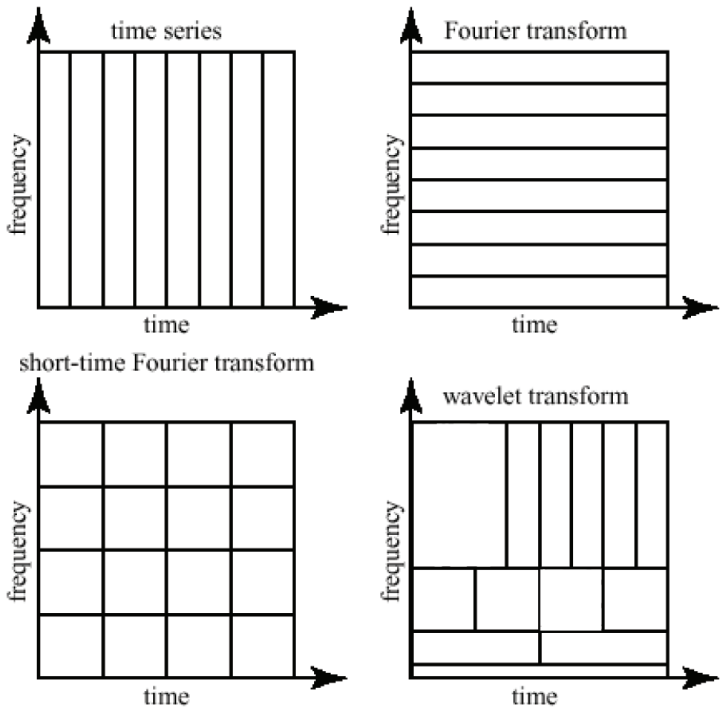


Figure 2.3: *A schematic illustration of the differences between time series analysis, Fourier transform, short-time Fourier transform and continuous wavelet transform regarding the time and frequency resolution. Time series analysis show a perfect time resolution and no frequency resolution, while the Fourier transform yields no time resolution. Short Time Fourier Transform has a fixed time and frequcy resolution while this is variable for wavelets.*

Fourier transform (STFT), is given in formula 2.2.

$$F_x(t, f; h) = \int_{-\infty}^{+\infty} x(u) \cdot h^*(u - t) \cdot e^{-j2\pi fu} \cdot du \tag{2.2}$$

where $h(t)$ is a short-time analysis window localized around $t = 0$ and $f = 0$. The STFT is also invertible, but this type of time-frequency representation has a trade-off between time and frequency resolutions. On one hand, a good time resolution requires a short window $h(t)$ while on the other hand, a good frequency resolution requires a narrow-band filter and thereore a long window $h(t)$. This limitation is a consequence of the Heisenberg-Gabor inequality.

If we consider the squared modulus of the STFT, we obtain a spectral energy density of the locally windowed signal $x(u)h^*(u-t)$:

$$S_x(t,f) = \left| \int_{-\infty}^{+\infty} x(u) \cdot h^*(u-t) \cdot e^{-j2\pi fu} \cdot du \right|^2 \tag{2.3}$$

This defines the *spectrogram*, which is a real-valued and non-negative distribution. Since the window h of the STFT is assumed of unit energy, the spectrogram satisfies the global energy distribution property :

$$E_x = \int_{-\infty}^{+\infty} \int_{-\infty}^{+\infty} S_x(t,f) \cdot dt \cdot df \tag{2.4}$$

Therefore, we can interpret the spectrogram as a measure of the energy of the signal contained in the time-frequency domain centered at the point (t, f).

Wavelet transform

The Fourier transform is a tool widely used for many scientific purposes. However it is only well suited to the study of stationary signals where all frequencies have an infinite coherence time. The Fourier analysis brings only global information which is not sufficient to detect compact patterns. Gabor introduced a local Fourier analysis, taking into account a sliding window, leading to a time frequency-analysis. This method is only applicable to situations where the coherence time is independent of the frequency. This is for instance the case for singing signals which have their coherence time determined by the geometry of the oral cavity. Morlet introduced the Wavelet Transform in order to have a coherence time proportional to the period. A wavelet is, as its name suggests, a 'small wave'. A small wave grows and decays essentially in a limited time period. The contrasting notion is obviously a 'big wave'. An example of a big wave is the sine function, which keeps on oscillating up and down. The sine function is, as described earlier, the basic function for Fourier Transform. A basic function $\Psi(t)$, called the mother wavelet, is a wavelet if the function satisfies 2 basic properties.

1. The integral of $\Psi(t)$ is zero:

$$\int_{-\infty}^{\infty} \Psi(t)\, dt = 0 \tag{2.5}$$

2. The square of $\Psi(t)$ integrates to unity:

$$\int_{-\infty}^{\infty} \Psi(t)^2\, dt = 0 \tag{2.6}$$

The first property indicates that every positive excitation of the wavelet is compensated by an equal negative excitation. The second property says that there is an excitation in a finite interval [-T,T]. The nonzero activity of the wavelet is limited to the finite interval. Several wavelets that satisfy both conditions are published (Haar, Morlet, Gaussian, Daubechies, Meyer, Mexican hat, ...)[34]. Some of them are illustrated in Figure 2.4.

The idea of wavelet transform is to project a signal $x(t)$ on a family of zero-mean functions (the wavelets) deduced from an elementary function (the mother wavelet) by translations and dilations:

$$T_x(t, a; \Psi) = \int_{-\infty}^{+\infty} x(s) \cdot \Psi^*_{t,a}(s) \cdot ds \tag{2.7}$$

where

$$\Psi_{t,a}(s) = |a|^{-1/2} \cdot \Psi\left(\frac{s-t}{a}\right). \tag{2.8}$$

The variable a corresponds now to a scale factor, in the sense that taking $|a| > 1$ dilates the wavelet Ψ and taking $|a| < 1$ reduces Ψ. By definition, the wavelet transform is more a time-scale than a time-frequency representation. However, for wavelets which are well localised around a central frequency f_0 at scale $a = 1$, a time-frequency interpretation is possible thanks to the formal identification $f = \frac{f_0}{a}$. The basic difference between the wavelet transform and the short-time Fourier transform is as follows: when the scale factor a is changed, the duration and the bandwidth of the wavelet are both changed but the waveform remains the same. In contrast to the STFT, which uses a single analysis window, the WT uses short windows at high frequencies and long windows at low frequencies resulting in a good frequency resolution at low frequencies and a good time resolution for higher frequency. This partially overcomes the resolution limitation of the STFT as the bandwidth B is proportional to f. When the scales are changed continuously and the wavelet is shifted continuously, this transform is called the *Continuous Wavelet Transform (CWT)*. In reality, these time and scale changes are discretised. The steps between two consecutive scales and time shifts are selected according to the application. In this situation, CWT is sometimes called the discretised CWT.

Using CWT, a similar distribution to the spectrogram can be defined. Since the continuous wavelet transform behaves like an orthonormal basis decomposition, it can be shown that it preserves energy:

$$E_x = \int_{-\infty}^{+\infty} \int_{-\infty}^{+\infty} |T_x(t, a; \Psi)|^2 \cdot dt \cdot \frac{da}{a^2} \tag{2.9}$$

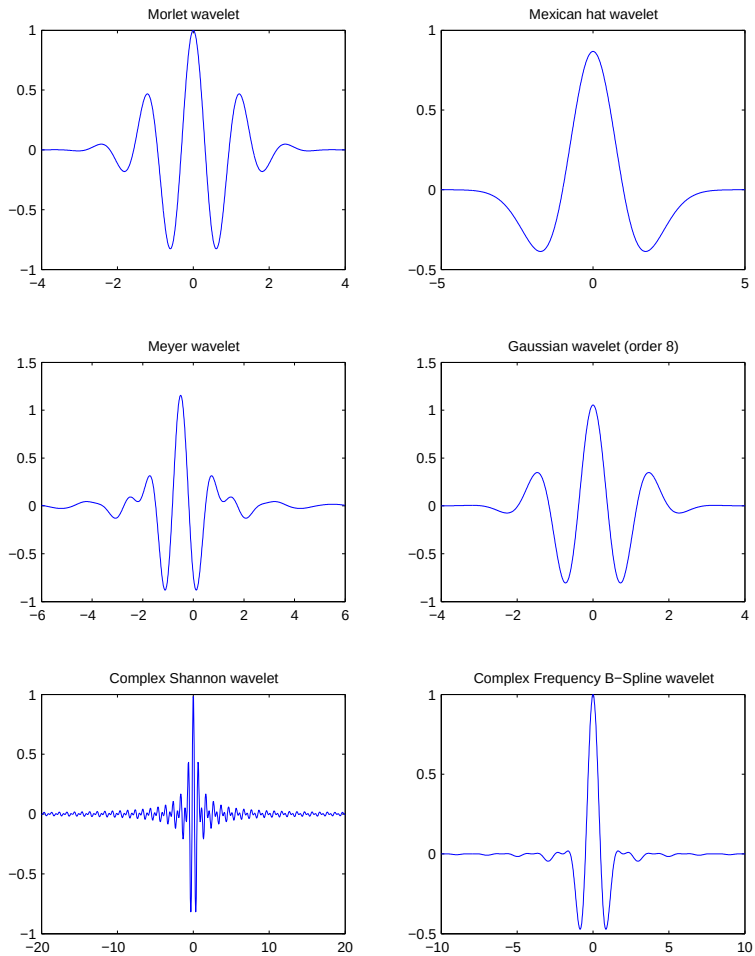


Figure 2.4: *Illustration of several types of mother wavelet functions: Morlet wavelet (top left), Mexican hat wavelet (top right), Meyer wavelet (middle left), Gaussian wavelet (middle right), complex Shannon wavelet (bottom left), complex frequency B-spline wavelet (bottom right).*

where E_x is the energy of x. This leads us to define the *scalogram* of x as the squared modulus of CWT. It is an energy distribution of the signal in the time-scale plane, associated with the measure $dt\frac{da}{a^2}$. As for the wavelet transform, time and frequency resolutions of the scalogram are related via the Heisenberg-Gabor principle: time and frequency resolutions depend on the considered frequency. As the STFT was inversible, the signal x can also be reconstructed from its continuous wavelet transform according to the formula:

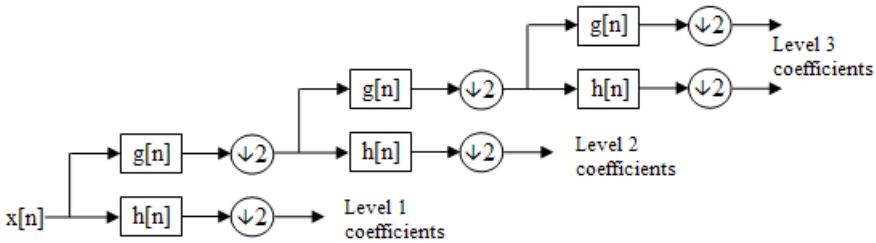
$$x(t) = \int_{-\infty}^{+\infty}\int_{-\infty}^{+\infty} T_x(s,a;\Phi)\cdot\Psi_{s,a}(t)\cdot ds\cdot\frac{da}{a^2} \tag{2.10}$$

A CWT contains a lot of redundant information. Using a good selection of scales, the redundancy can be removed. A specific example is when the distribution of the scales is dyadic (2^n). This is called the *Discrete Wavelet Transform (DWT)*. The DWT can also be seen as a filter bank analysis composed of band-pass filters with constant relative bandwidth. Figure 2.5(a) illustrates a 3 level DWT decomposition. The original signal is sent through a half band high pass filter $h[n]$ obtaining the details d_i and through a half band low pass filter $g[n]$ obtaining the approximations a_i. The details and the approximations are downsampled with a factor 2 and the approximations are again filtered using the same half band filters. The filter coefficient of $h[n]$ and $g[n]$ are dependent on the selected mother wavelet. The decomposition in figure 2.5(a) results in three levels of details and 1 approximation signal. The effect of the filtering in the frequency domain is presented in figure 2.5(b). This figure shows that each decomposition bisect the frequency content.

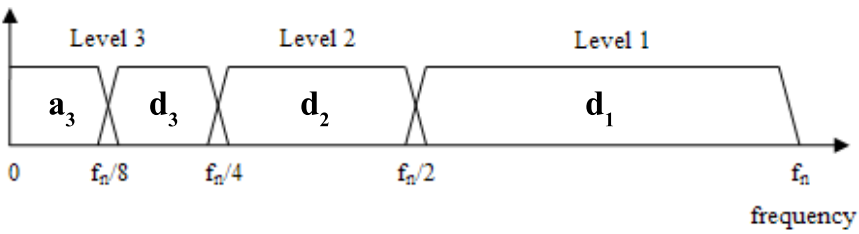
2.1.3 Ensemble Empirical Mode Decomposition (EEMD)

Empirical Mode Decomposition (EMD) [75] is a new tool to analyze the nonstationary signals. Like other methods (e.g. wavelets), EMD decomposes into different components [51]. Wavelets and other signal decomposition techniques tend to map the signal space onto a space spanned by a predefined basis, but once the selected basis does not match with the signal itself very well, the results are often unreliable. In contrast, EMD is a data driven algorithm which means that it decomposes the signal in a natural way where no a priori knowledge about the signal of interest embedded in the data series is needed. The idea is that a time series is a sum of spectrally independent oscillatory modes (see equation 2.11), called Intrinsic Mode Functions (IMFs) with specific properties [190].

$$x(n) = \sum_{i=1}^{N} d_i(n) + r(n) \tag{2.11}$$



(a) DWT Filterbank



(b) Frequency domain of a 3 level decomposition

Figure 2.5: *A 3 level decomposition using DWT. (a) shows the filterbank sequence, (b) shows the effect of the filter banks on the frequency domain (From* `http://www.wikipedia.org`*).*

where d_i denotes the i-th IMF, $i = 1, \ldots, N$ and $r(n)$ is the trend.

Each IMF is a mono-component signal [26], which means that each IMF consists of one frequency at any time instance (instantaneous frequency). Next to this, the number of zero crossings and extrema within one IMF differ at most by one. The local mean in the IMF is approximately zero at all times. The different IMFs are mutually orthogonal. The different IMFs are calculated one after each other using a sifting process.

The sifting processes to calculate the different IMFs:

1. Find the locations of all the extrema of the signal $x'(n)$. For initialisation: $x'(n) = x(n)$.
2. Interpolate (using spline interpolation) between all the minima (resp. maxima) to obtain the signal envelope passing through the minima, $e_{min}(n)$ (resp. the maxima $e_{max}(n)$).
3. Compute the local mean $m(n) = (e_{min}(n) + e_{max}(n))/2$.

4. Subtract the mean from the signal to obtain the oscillating signal $s(n) = x'(n) - m(n)$.

5. If the resulting signal $s(n)$ obeys the stopping criteria ($s(n)$ has zero mean or the maximum number of iterations is reached), $d(n) = s(n)$ becomes an IMF and go to step 6, otherwise set $x'(n) = s(n)$ and iterate from step 1.

6. Calculate the residual $r(n) = x(n) - m(n)$ and restart from step 1 with the residual as starting signal. The algorithm stops when the residual $r(n)$ is a monotonic signal.

As the algorithm is data driven and calculates local maxima and minima, the EMD algorithm is very sensitive to noise. Therefore, a more robust, noise-assisted version of the EMD algorithm, called Ensemble EMD (EEMD) [75] is defined. The algorithm defines the IMF set for an ensemble of trials. For each trial, a set of IMFs is obtained by applying EMD to the signal of interest with added independent, identically distributed white noise. The added noise for each trial differs, but has an equal standard deviation. The ratio of SD of the the added noise to the SD of the signal is also called noise parameter (np). The ensembled set of IMFs is obtained by calculating the mean of the corresponding IMFs from the decompositions of the different trials.

The np and the number of trials need to be optimised for each application and are dependent on the amount of noise of the original signal. If the added noise is high, the signal properties of the original signals are altered, while a too low np will not be able to cancel out the noise in the original signal. The number of trials needs to be high enough to cancel out the added noise at each time instant. Being different from the Fourier decomposition and the wavelet decomposition, EEMD has no specified basis. Its basis is adaptively produced depending on the signal itself, which makes not only the decomposition very effective, but also makes the localization on frequency and time much sharper and most important of all, it makes more physical sense [190]. On the other hand, unlike the techniques with a predefined basis which have a straight forward approach, EMD is an iterative process of selecting local maxima and minima for each IMF. The noise robust extension of EMD, the EEMD, ensembles the outcome of multiple trials of a single EMD. The computational time of this technique is much higher compared to other decomposition techniques. In matlab, a decomposition of a signal (10.000 datapoints, 150 decompositions) with wavelets is 1.1±0.09s while for EEMD (np = 0.2, number of trials =100), the calculation time is 446±49s.

EMD decomposes a signal into different IMFs using an adaptive basis. This could lead to problems in the interpretation of the IMFs extracted from different signals seperately. Standard EMD yields disjointed set of IMFs (corresponding to different frequency bands) for multiple channels and, hence, makes their comparison meaningless. The IMFs of the different signals should be matched in terms of

frequency to facilitate the analysis and the interpretation of the joint IMFs. Tanaka et al [164, 3] proposed methods to overcome this shortcoming by using complex Empirical Mode Decomposition. Two signals are fused by making one complex equivalent where one signals is the real part and the other signal the imaginary part. These technique create complex IMFs, taking into account the information in both signals. The complex EMD is a bivariate extension of the standard EMD. A more generalised approach to multivariate data, where no restriction is imposed on the number of different data channels, is the recently developed multivariate emperical mode decomposition [132] (MEMD). The MEMD is a generic multidimensional extension of the standard EMD. MEMD processess the input signal directly in higher dimensional spaces, where it generates multiple n-dimensional envelopes. This results in matched IMFs in terms of frequency of each of the multivariate input signals.

EMD has already shown its usefulness in a wide range of applications, but the mathematical basis of the technique and the derivation of the IMFs is still unclear and the attempts have been mostly exploratory [51]. Ingrid Daubechies introduced recently the synchrosqueezed wavelet transform [35], that captures the advantages of EMD, but with a mathematical background. This techniques forms Intrinsic Mode Type Functions (IMT), with similar properties of IMFs, but with a different approach in constructing the components. Synchrosqueezing reallocates the coeffcients resulting from a continuous wavelet transform to get a concentrated time-frequency picture, from which instantaneous frequency lines can be extracted. Daubechies showed in [35] on simulations and real life data that synchrosqueezing an appropriate wavelet transform give a single line on the time-frequency plane, at the value of the instantaneous frequency of a corresponding IMF. In future, synchrosqueezing wavelet transform could help in the understanding of EMD or could be used as a computational more efficient alternative of the EMD.

2.2 Surface Electromyography

2.2.1 Muscle Physiology: Overview

A muscle is the contractile tissue in humans. The most important function is to produce force and cause motion being locomotion of the organism itself or movement of the internal organs. Muscles can be divided in three types.

- **Skeletal muscle** or voluntary muscle. These muscles are also known as striated (banded) muscles. They are responsible for all the conscious movements that are controlled by the central nervous system. The muscles are inhibited subconsciously via a reflex or consciously via the brains through the nervous system. Their main functionality is the control of the skeleton

for postural control or movement. The skeletal muscle is attached to bone via tendons.

- **Smooth muscle** or unvoluntary muscle. They are found in organs and structures such as the stomach, intestines, bronchi, uterus, bladder, blood vessels ... They tend to enclose a certain volume and work in most situations by squeezing on that volume. Unlike a skeletal muscle, a smooth muscle is not under conscious control and is not striated.
- **Cardiac muscle** is the contracting tissue of the heart. It is striated and looks like a skeletal muscle, but acts like a smooth muscle: the central nervous system is not required for contraction, although the central nervous system has its influence on the operation of the heart muscle (see heart rate variability).

In this text, we refer to skeletal muscle when muscle is mentioned. When referred to another muscle type, the name of the type will be mentioned explicitely. A muscle is built up mainly of two types of tissue: connective tissue and contractile tissue. The connective tissue cannot actively contract and can be divided into two groups. A first group connects the muscle to bone and is called tendon. A muscle has typically two tendons: one is found at the origin, where the muscle is anchored to and is the point that remains in fixed position during a particular movement, while the other is connected to the opposite end, the insertion. The insertion is the point that is moved by the muscle. The second group of connective tissue is wrapped around the contractile tissue and is called the fascia. Their main functions are protecting the muscle and holding the contractile tissue together into a functional unit.

The contractile tissue consists of different layers and an overview is given in figure 2.6. A complete muscle is built up from several fasciculi (bundles of muscle fibers). A single muscle fiber is called a skeletal muscle cell and consists of nuclei (source of new proteins and is influenced by muscle fiber strength and anaerobic/aerobic capacity), mitochondria (responsible for the aerobic metabolism), sarcoplasm (glycolisis reactions and stores of glycogen). The contractile elements within a muscle cell are the myofibrils. A single cell consists of many of these myofibrils. A myofibril has a repeating structure, a sarcomere, which is a complete and functional unit for contraction. The successive sarcomeres can be distinguished via the vertical lines (Z-lines) on the myofibril. When looking into detail to one sarcomere, different regions can be distinguished. The lighter region next to a Z-lines is called the isotropic or I-band, while the darker region between two Z-lines is the anisotropic or the A-band. In the middle of the A-band, a smaller less dark region is visible. This is called the H-zone. These different bands are formed by the filaments that are responsible for contraction. The two filaments are actin (small filaments, attached to the Z-lines) and myosin (thick filaments). The latter is the active filament and is moving when activated along the actin filaments towards

the Z-lines reducing the H-band. A muscle fiber consists of hundreds of these sarcomeres one after each other and a shortening of all the subsequent sarcomeres causes a contraction. When deactived, the binding between the actin and the myosin disappear and the muscle fibers can be stretched again to the original length.

Around a muscle fiber, there is a membrane, called the sarcolemma. This membrane conducts the nerve pulses, in a form of action potentials, rapidly along the muscle fiber. Within the muscle fiber, t-tubuli connect one side of the sarcolemma to the other side and enable the action potentials to enter the cell. These t-tubuli are in close collaboration with the sarcoplasmic reticulum. This is an extensive internal membrane system that controls the release of Ca^{2+}–ions. When an action potential is conducted from the sarcolemma into the t-tubuli, the sarcoplasmic reticulum starts to release Ca^{2+}, causing the contraction to proceed. When the action potential is over, the sarcoplasmic reticulum captures the Ca^{2+} from the cell, ending the contraction.

Every muscle fiber is controlled by an α-motor neuron, that receives a stimulus from the brain by the synaps in the spinal cord. The motor neuron sends the motor unit action potential to the sarcolemma of the muscle fiber, where it is conducted

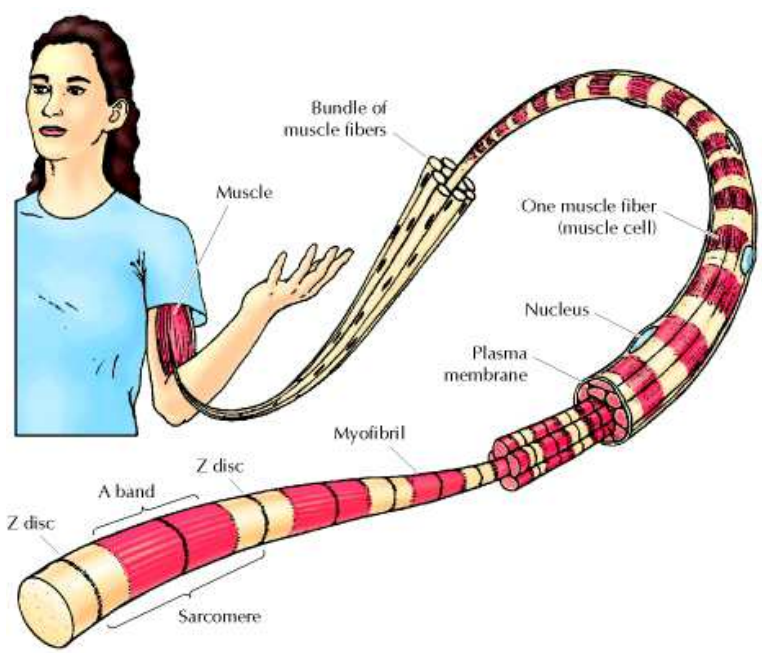


Figure 2.6: *Overview of the structure of a skeletal muscle [29].*

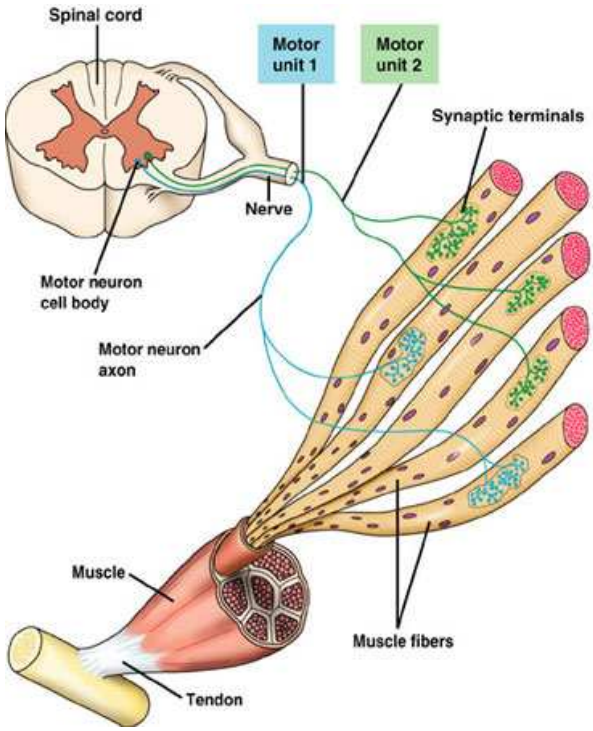


Figure 2.7: *Motor units are controlling the muscle fibers. One muscle has several motor units and one motor unit can control more muscle fibers [21].*

through the muscle fiber to initiate the contraction. Pulse trains towards the muscle fibers are needed to maintain the contraction. This is called a motor unit pulse train. Each muscle fiber is controlled by at most one motor unit, while one motor unit innervates several muscle fibers. This number of muscle fibers, controlled by one motor neuron, is called the innervation ratio which can vary considerably, related to the function of the muscle unit. In muscles where the innervation ratio is low (around 5), it is possible to produce very fine motion like the muscles of the eye. In contrast, the quadriceps where the main function is producing a huge amount of force, one motor neuron initiates several thousands of muscle fibers. A motor neuron with its fibers is called a motor unit. Figure 2.7 shows two motor units to control several muscle fibers.

There are three types of motor units in correspondence with the muscle fibers they control. Within one motor unit, all of the fibers are of the same type. The type of fibers depends on their physiology, metabolic characteristics and mechanical and electrical properties. Here, a short overview of the properties of the different fibers is given.

- **Type I or slow oxidative**. These muscle fibers are known as the red fibers and are used for sustained activity. These muscle fibers have a high oxidative capacity. The mitochondria may occupy as much as 40% of the fiber volume and together with the large amount of myoglobin and blood capillaries, they are responsible for the red color. Oxygen is used to produce the energy within the mitochondria revealing the need for myoglobin and blood capillaries. These muscle fibers are also fatigue resistant so they can contract for a longer time. The contraction velocity of the muscle fibers is low. The conduction velocity of the action potential in the motor neuron to the muscle is fast. A motor neuron of this type can easily be stimulated to produce an action potential that inhibits a muscle contraction. Type I motor units have a low innervation ratio and the produced force by one motor unit is low. These motor units are recruited at low force levels. The recuperation time of type I muscle fibers is longer than the recuperation time of type II muscle fibers.

- **Type IIa or fast oxidative glycolytic**. These muscle fibers have both oxidative and glycolytic energy production. The properties of these muscle fibers are a combination of the type I and type IIb properties. As the fibers have oxidative energy production, the fibers contain mitochondria, myoglobin and blood capillaries and have a red color. These fibers are more resistant to fatigue compared to the type IIb fibers, while the contraction velocity is higher than the type I fibers. The conduction velocity through the motor neuron of the action potential is very high. The innervation ratio is rather high and the force produced by a single motor unit is in between type I and type IIb motor units. These motor units are typically recruited at moderate force levels.

- **Type IIb or fast glycolytic**. These muscle fibers are the white fibers (pink in reality). The energy of these muscle fibers is retrieved from glycolytic processes that take place in the sarcoplasm, so mitochondria and myoglobin are almost not present. These muscle fibers contract very fast and have a large fiber diameter. These muscle fibers are fatigue prone. The conduction velocity of the action potential in the motor neuron to the muscle is very fast. A motor neuron of this type has a higher threshold to produce an action potential that inhibits a muscle contraction. The innervation ratio of type II muscle fibers is high resulting in a very high force production per motor unit. These motor units are recruited at high force levels.

2.2.2 Surface Electromyography

One method to quantify the muscle activity is to look at the electrical currents generated by the muscle fibers to produce muscle force as described in 2.2.1.

Electromyography (EMG) [104] is a technique for evaluating and recording this electrical activity. EMG is performed using an instrument called an electromyograph, to produce a record called an electromyogram. There are two types of EMG: surface EMG and intramuscular (needle and fine-wire) EMG. To perform intramuscular EMG, a needle electrode or a needle containing two fine-wire electrodes is inserted through the skin into the muscle tissue. A trained professional observes the electrical activity while inserting the electrode to achieve good localization for optimal information. The insertional activity provides valuable information about the state of the muscle and its innervating nerve. The shape, size, and firing frequency of the resulting motor unit potentials can be monitored. Intramuscular EMG has the advantage that information at motor unit level can be extracted.

Nevertheless, intramuscular EMG is an invasive technique and not needed in several applications. Instead, a conductive electrode at the skin may be used to monitor the general picture of muscle activation, as opposed to the activity of only a few fibres as observed using a intramuscular EMG. This is called surface electromyography (sEMG). sEMG is the more common method of measurements, since it is non-invasive and no specialist is needed to conduct the measurements. The signal is a differential measurement of two electrodes placed on the same muscle. Where intramuscular EMG measures the activity of a single motor unit, sEMG picks up the summation of the electrical activity of all the motor units that are in its detection range. The information reveals the general muscle state. The measurement of sEMG depends on a number of factors and the amplitude of the sEMG signal varies from μV to the low mV [13]. The properties of the signal are dependent on several factors:

- the timing and intensity of the muscle contraction
- the distance of the electrode from the active muscle
- the properties of the overlying tissue (e.g. thickness of overlying skin and adipose tissue)
- the electrode and amplifier properties
- the quality of contact between the electrode and the skin

In most applications, only information of the timing and intensity of the muscle contraction is desired. The other factors only exacerbates the variability in the sEMG recordings, making the interpretation of results more difficult. Nevertheless, there are methods to reduce the impact that non-muscular factors have on the properties of the EMG signal. SENIAM (Surface Electromyography for the Non-Invasive Assessment of Muscles, [57]), a European consortium of sEMG experts, developed recommendations for sEMG. The key items, when working with sEMG

were considered to be sensors, sensor placement procedures, signal processing and modelling. The SENIAM guidelines for monitoring sEMG of muscles with contact sensors concerns the skin preparation to reduce the skin resistance, type and specifications of the electrodes, technical specifications of the equipment etc. Besides these recommendations, they searched for the optimal electrode position to retrieve good and stable sEMG. Factors which influence the recording of a good and stable sEMG are: presence of motor points, muscle tendons and cross-talk (presence of other active muscles near the sEMG-sensor). For this reason, SENIAM has developed recommendations for sensor locations on 27 muscles that can be measured with sEMG. These recommendations include for each muscle a description of the muscle anatomy, the electrode location and orientation.

As described before, the voltage potential of the sEMG signal detected by the electrodes strongly depends on several factors other than muscle contractions, varying between individuals and also over time within an individual. This makes the use of the amplitude of the signal not useful in group comparisons or to follow events over a long period of time. The fact that the recorded sEMG amplitude is never absolute is mainly due to the fact that the impedance varies between the active muscle fibres and the electrodes and is unknown [62]. Therefore, when comparing amplitude variables between measurements, normalization is required. A commonly used technique is normalization of the signal with respect to a force. Typically, the sEMG is related to a maximal voluntary contraction (MVC) of a typical movement. SENIAM also described for each muscle a specific movement that should be used for reference measurement.

High density electromyography (HD-EMG) is a new approach of sEMG signal processing that came up the last decade. Instead of using two electrodes to have a differential measurement, an array or a grid of electrodes is used to retrieve multichannel data. A typical example of a grid is an 8 by 13 grid, resulting in 104 simultaneously recorded sources. These multichannel data can be decomposed using multichannel decomposition techniques into channels with underlying information. A straight-forward approach is to decompose the data during a contraction into its single motor unit pulse trains [72, 103]. This is information that could only be retrieved using intramuscular EMG. This approach combines the advantages of the two previous methods: the information of single motor units can be found with non-invasive measurements and there is the information of the total muscle activity which is not present while using the intramuscular EMG. The HD-EMG is at this moment still in the research phase and still copes with several drawbacks (high amount of data, computational cost of the decomposition algorithm), but it has a high potential for several medical applications.

The data, used in this manuscript, were recorded for the project described in 1.3.2. One objective of the project was the use of textile integrated capacitive electrodes to measure sEMG and analyse these signals. This technology is not appropriate

for use for HD-EMG at this moment. Therefore, despite the big potential of HD-EMG, the widely used differential sEMG is used. The capacitive electrodes were not reliable at the beginning of the different measurements, restricting us to the use the traditional contact electrodes.

2.2.3 Parameters

Time domain

There are several techniques for data processing using the raw sEMG-signals. All these techniques are performed on the amplitude of the signal. However, in 2.2.1, a remark was made about the use of the amplitude as a measure for the signals. SENIAM suggests to solve this problem by measuring the sEMG signals during a reference measurement, which is the maximal voluntary contraction (MVC) during a specified movement. The amplitude of the muscle activity during a measurement can be expressed as a percentage of this reference MVC. SENIAM [57] stipulated general recommendations for contact electrodes, not only for the positioning and shape of the electrodes, but they also made a description for basic signal processing of the sEMG-signals. The most common methods are:

- **Analog rectification (RECT)**: the absolute form of all the values

$$x_{RECT} = |x| \tag{2.12}$$

- **Average rectified value (ARV)**: The average value of the rectified signal in a moving window of 0.25 – 2s in the signal.

$$x_{ARV}(t) = \frac{1}{N} \sum_{i=0}^{N-1} x_{RECT}(t-i) \tag{2.13}$$

  where N is the number of sEMG samples in the selected window.

- **Root Mean Square (RMS)**: calculation of the root mean square in a moving window of 0.25 –2s in the signal. RMS is a statistical measure of the magnitude of a varying quantity. It is especially useful when variates are positive and negative. The next formula gives the calculation of the RMS-value

$$x_{RMS}(t) = \sqrt{\frac{1}{N} \sum_{i=0}^{N-1} x^2(t-i)} \tag{2.14}$$

  where N is the number of sEMG samples in the selected window.

- **Envelope detector (ENV)**: low-pass filtering of the rectified signal. This operation gives an idea of the amplitude of a sEMG-signal.

At present, RMS is the most used technique for interpretation of the amplitude of sEMG-signals and will be used in the manuscript.

Frequency domain

The common measure to quantify the frequency content of a sEMG signal is calculating the mean power frequency (MPF) of the power spectral density PSD (see equation 2.15). To introduce time-dependency, the STFT is used. Ranniger et al [131] showed that the wavelet analysis method consistently over-estimates the MPF and that the signal characteristics and shapes of the MPF curves of both techniques are similar. Therefore, the STFT (window length of 500ms and overlap of 50%) is used to characterize the MPF due to the reduced complexity of the calculations.

$$MPF = \frac{\sum_{n=1}^{f_s/2} f_n \cdot PSD(f_n)}{\sum_{n=1}^{f_s/2} PSD(f_n)} \tag{2.15}$$

Activity Level (ACT)

A last parameter which can be derived from sEMG is the activity level of the muscle. This parameter is an indication of the real muscular effort. An algorithm to derive this physiological muscle activity (ACT) was described by Spaepen et al [150, 70], using both amplitude and frequency information. Similarly to RMS or integrated sEMG-values, this ACT-parameter estimates a sEMG-parameter proportional with its isometric contraction. In contrast, a lower sensitivity to a slowly changing baseline and lower dependence on the time interval are advantages of the ACT-parameter. The recursive algorithm (2.16) to calculate muscular activity (A) from a series of raw sEMG signals (E) at equally spaced time series can be summarised as follows: the algorithm computes the activity at time t_{n+1} from a known activity at time t_n and the corresponding raw sEMG values E_{n+1} and E_n.

$$A(t_n) = p \cdot A(t_{n-1}) + q \cdot \sqrt{|E(t_n) - E(t_{n-1})|} \tag{2.16}$$

Where

$A(t_n)$: the muscle activity at time t_{n+1}
$A(t_{n-1})$: the muscle activity at time t_n
p: constant value, equal to 0.9938
q: constant scaling value, equal to 0.05
$E(t_n)$: EMG-signal at time t_{n+1}
$E(t_{n-1})$: EMG-signal at time t_n

The activity parameter can be explained as the sum of two terms. First, the force production in a muscle fibre, the twitch force, does not stop abruptly when stimulation is terminated, but continues for a limited time. The constant value p indicates the rate of force decay. P denotes the amount of force following the previous activity. Secondly, activity obtained from the amount of force resulting from the new sEMG activity has to be added to the previous term. The force delivered by a muscle is related to the change in electrical activity (E), which is measured by sEMG.

2.3 Heart Rate Variability

2.3.1 Introduction

The heart, visualised in Figure 2.8, is divided into two pumps lying side by side, pumping in phase but distributing blood in series. The right side receives blood from the body and then propels it at low pressure through the vascular system of the lungs (the pulmonary circulation) while the left side receives blood from the lungs and then propels it at high pressure to all other tissues of the body, the so called systemic circulation. In one cycle all the output of the right part has to circulate through the lungs but, since the circulations of the different tissues are arranged in parallel, not all the output of the left heart reaches every single organ. Normally, there is no direct blood transfer between the two pumps.

Each side of the heart has two chambers: atrium and ventricle. The atrium receives the blood from the veins and aids its flow into the ventricle. The contraction of the ventricle propels the blood into the arterius. This phase is called systole. The filling of the ventricle is called dyastole. The pumps generate pulsatile pressure, 0 to ∼25 mmHg in the right ventricle and 0 to ∼120 mmHg in the left ventricle. When the body is at rest, diastole occupies two-thirds of the total cycle. The product of the frequency of pumping (heart rate - HR) and the volume ejected at each contraction by any one side (stroke volume - SV) is the cardiac output (CO). Typical values for a resting adult person are 60 – 70 beats per minute, 70 – 80 ml per beat and 5 – 6 litre per minute, respectively.

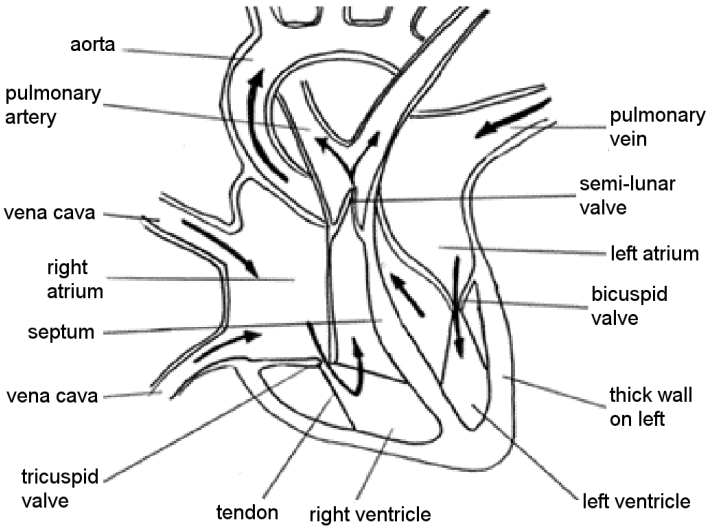


Figure 2.8: *Structure of the chambers and valves of the heart. The arrows indicate the direction of the blood flow.*
From `http://www.dr-sanderson.org/images/heart.gif`

Cardiac muscle has a myogenic rhythm, which means that it has the ability to contract rhythmically without nervous input. The action potential for each heart beat is generated by a pacemaker in the right atrium and transmitted through the heart along specialised conducting pathways. Pacemaker cells have a resting membrane potential which slowly and spontaneously depolarize to a threshold at which an action potential is initiated. Cardiac action potentials are typically of long duration (200 – 400 ms). There is a considerable overlap in time between the cardiac action potential and the contraction it initiates so that, in contrast to skeletal muscles, two contractions can not summate.

The synchronised depolarization spreading through the heart causes currents in the extracellular fluid that establishes field potentials over the whole body. These potential differences can be detected by electrodes placed on the body's surface. The signal (about Δ 1 mV) has to be amplified and the record produced is called the electrocardiogram (ECG).

The pattern of the ECG varies depending on the position of the electrodes but certain features are always present. A typical ECG of one heart beat is shown in Figure 2.9. The P wave is produced by the spread of electrical activity during atrial depolarization. The QRS complex is produced by ventrical depolarization and the T wave by ventrical repolarization. When no depolarization or repolarization is occuring, there is no potential difference in the ECG leading to the isoelectric

line. Atrial repolarization does not produce any detectable wave because it occurs during the much larger QRS complex. Since ventricular repolarization is less well synchronised than ventricular depolarization, the T wave is longer in duration but smaller in amplitude than the QRS complex. Depending on the electrode position, the QRS complex may have one, two or sometimes three components. If after the P wave the first deflection from the isoelectric line is negative (by convention downwards), it is called a Q wave; if positive, it is called an R wave and if the next deflection falls below the isoelectric line, it is called an S wave. The PQ or PR interval is the time required for excitation to spread through the atria, atrioventricular (AV) node and bundle of His while the QS interval is the required time of excitation to spread through the ventricles. The duration of the ventricular and atrial action potentials is therefore given by respectively the QT and PS interval.

The pacemaker firing rate, and consequently heart rate, is influenced by the nervous system. The nervous system is a network of cells specialised for the reception, integration and transmission of information. It comprises on one hand the central nervous system (CNS) and on the other hand sensory and motor nerve fibers that enter and leave the CNS or are completely outside the CNS (peripheral nervous system or PNS). The CNS comprises the brain lying within the skull and the spinal cord lying within the vertebral column. The PNS is that portion of the nervous system that lies outside the spinal cord and brain. It comprises both the somatic and the autonomic divisions. The somatic division contains all the peripheral pathways responsible for communication with the environment and the control of skeletal muscle. The autonomic nervous system (ANS) comprises all the pathways from controlling centres in the brain and spinal cord to effector organs other than skeletal muscle. As heart rate variability is linked with autonomic nervous modulation, we will focus on the ANS. The actions of the peripheral autonomic nervous system are normally involuntary and are directed to the control of individual organ function and to homeostasis. The ANS is often regarded as the 'solely motor' in function with fibres going to cardiac muscle, smooth muscles and glands. Sensory information comes from visceral and somatic afferent inputs. The peripheral autonomic nervous system is anatomically divided into the sympathetic and parasympathic system. The latter is often also called vagal system. Many tissues are innervated by both systems, having opposing effects. The heart rate is increased by sympathetic and decreased by parasympathetic nerve activity. The autonomic nervous system also influences the conduction velocity of the action potentials through the heart and the duration of the cardiac action potential.

The focus of this work is on the R peaks as the distance between two consecutive R peaks indicates the time between two successive heart beats. Based on the RR intervals, we can extract different parameters to analyze the variation between the heart beats and link these parameters to retrieve information of the autonomic nervous system.

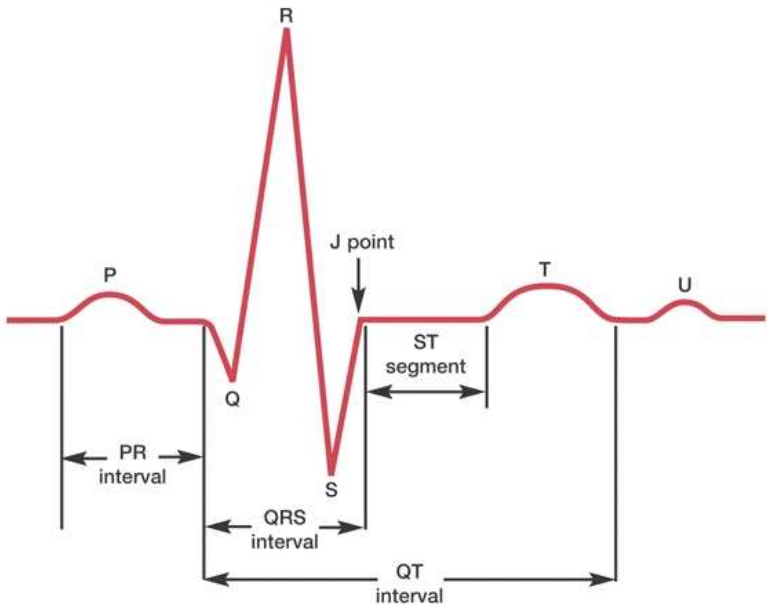


Figure 2.9: *The basic pattern of electrical activity across the heart. A typical ECG of one heart beat with P wave, QRS complex and T wave. From [5].*

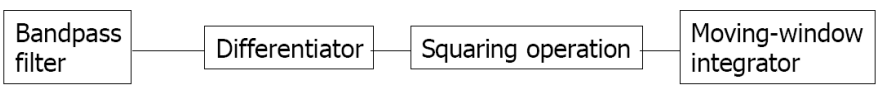


Figure 2.10: *Block diagram of the Pan-Tompkins algorithm for QRS peak detection.*

2.3.2 Processing

Peak detection: Pan-Tompkins

HRV analysis is based on the fluctuations in RR intervals. This implies the first step in processing the ECG is to determine the R-peaks of the QRS-complexes. Pan and Tompkins [120] proposed a real-time QRS detection algorithm based on analysis of the slope, amplitude and width of the QRS complexes. The algorithm includes a series of filters and methods that perform low-pass, high-pass, derivative, squaring, integration, adaptive thresholding and search procedures. Figure 2.10 illustrates the steps of the algorithm in schematic form.

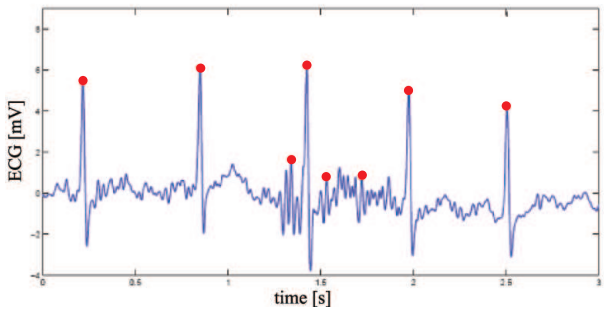


Figure 2.11: *Example of wrong peak detections by the Pan-Tompkins algorithm. The result after preprocessing is given on top and shows that the wrong intervals were concatenated correctly [187].*

Data preprocessing

The Pan-Tompkins algorithm has a good performance in general. Nevertheless, errors will be introduced via wrong peak detections and missed peaks. An example of a data fragment with wrong peak detections is shown in Figure 2.11. Therefore, an extra preprocessing of the data is unevitable. Missed beats can be replaced via interpolation while wrong peak detections can be discarded if needed, based on information of the previous beats. An example can be seen on top of Figure 2.11. Moreover, also premature supraventricular and ventricular beats need to be removed as HRV can only reliably extract information from normal sinus rhythms. To exclude these typical beats, filters are available with omission of one subsequent beat and linear interpolation of the corresponding periods. This way, type A errors (QRS detected prematurely when in fact a sinus conducted wave has not occurred) and type B errors (failing to detect an R wave that is present) could be largely avoided [83, 69]. A 20%-filter [86] was used, meaning that every RR-interval that differ more than 20% from the previous one, is replaced by an interpolated value, defined via spline interpolation over the 5 previous and 5 next intervals. The assumption that underlies this correction is that the RR interval does not oscillate abruptly from the mean value and that the use of the interpolated value will introduce less high frequency noise.

Secondly, a trend removal algorithm is applied that removes any linear trend in the signal. This has no influence on regular stationary baseline data, but it prevents artificial low frequency power. After the preprocessing steps, the corrected RR intervals are called normal-to-normal intervals (NN).

Finally, a file containing the consecutive NN intervals is exported for later processing. Such an NN interval time series, illustrated in Figure 2.12, is called a tachogram and is the signal on which the different HRV techniques will be applied.

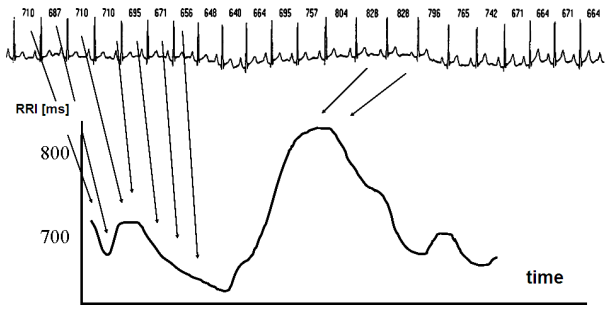


Figure 2.12: *Illustration how to derive the tachogram (RR interval time series) from the ECG signal. First, R peaks are detected (see Figure 2.9) and the time between two successive R peaks, which is called the RR interval (RRI), is calculated and expressed in milliseconds as indicated on top. Then, all these RR intervals become the samples of a new signal, called tachogram or RR interval time series shown at the bottom, where the RR intervals (ms) are plotted on the Y axis versus the time (s) at which the heart beat occurs on the X axis [170].*

2.3.3 Heart Rate Variability Parameters

The linear time and frequency domain techniques for HRV were standardised in a report of the Task Force of the European Society of Cardiology and the North American Society of Pacing ans Electrophysiology [165].

Time domain analysis

Time domain analyses are simple techniques, most of them are based on statistical properties of the tachogram:

- **Mean NN (ms)** is the average duration of the RR intervals over the defined period. This measure is inversely correlated to the widely used heart rate in beats per minute.

$$MeanHR(bpm) = 60 * 1000/MeanNN(ms) \tag{2.17}$$

- **diffNN** is the difference between the longest and shortest NN interval
- **SDNN (ms)** is the standard deviation of the NN intervals and equals the square root of variance. SDNN reflects all the cyclic components responsible for variability in the period of recording. It correlates well with total power in the frequency domain since variance equals total spectral

power. In many studies, SDNN is calculated over a 24h period and thus encompasses both short-term high frequency variations, as well as the lowest frequency components seen in a 24h period. As the period of monitoring decreases, SDNN estimates shorter and shorter cycle lengths. It should also be noted that the total variance of HRV increases with the length of analyzed recording [142]. Thus, on arbitrarily selected ECGs, SDNN is not a well defined statistical quantity because of its dependence on the length of recording period. Consequently, in practice, it is inappropriate to compare SDNN measures obtained from recordings of different durations. However, durations of the recordings used to determine SDNN values (and similarly other HRV measures) should be standardised. 5-minute recordings for short-term and nominal 24h for long-term recordings seem to be appropriate options.

- **pNN50 (%)** is the percentage of successive NN intervals differing more than 50 ms in length from the previous interval.
- **rMSSD (ms)** is the square root of the mean of the squares of differences in length between adjacent intervals. The RMSSD gives an estimate of the short-term component of HRV.
- **SDSD** the standard deviation of successive differences.

The last three measures are highly intercorrelated and relate to high frequency spectral power in the frequency domain. The rMSSD is preferable to the pNN50 because it has better statistical properties [165]. This activity is linked with the parasympathetic activity of the nervous system [165].

Frequency domain analysis

Various spectral methods for the analysis of the tachogram have been applied. Power spectral density (PSD) analysis provides the basic information of how power, and therefore the variance, distributes as a function of frequency. Independent of the method employed, only an estimate of the true PSD of the signals can be obtained by proper mathematical algorithms.

Methods for the calculation of PSD may be generally classified as nonparametric and parametric. In most instances, both methods provide comparable results. The advantages of the nonparametric methods are: (a) the simplicity of the algorithm employed (Fast Fourier Transform - FFT - in most of the cases) and (b) the high processing speed, whilst the advantages of parametric methods are: (a) smoother spectral components which can be distinguished independently of preselected frequency bands, (b) easy post-processing of the spectrum with an automatic calculation of low and high frequency power components and easy identification of

the central frequency of each component, and (c) an accurate estimation of PSD even on a small number of samples on which the signal is supposed to maintain stationarity. The basic disadvantage of parametric methods is the need to verify the suitability of the chosen model and its complexity (the order of the model).

One has to distinguish between short-term and long-term recordings. During short-term recordings, three main spectral bands are distinguished in a spectrum: an ultra-low frequency component (ULF) below 0.003 Hz, very low frequency (VLF) (from 0.003 to 0.04 Hz), low frequency (LF) from 0.04 to 0.15 Hz, and high frequency (HF) fluctuations from 0.15 to 0.4 Hz (Figure 2.13). The distribution of the power and the central frequency of LF and HF are not fixed but may vary in relation to changes in autonomic modulations of the heart period. In each frequency band, the power is calculated as the area under the PSD curve between the corresponding lower and upper bound. The total power (TP) is defined as the power in the frequency band going from 0 Hz to 1 Hz. Calculation of ULF, VLF, LF and HF powers are usually made in *absolute values of power* (ms^2), but LF and HF may also be measured in *normalised units (n.u.)*:

$$LF(n.u.) = \frac{LF}{TP - VLF} \quad , \quad HF(n.u.) = \frac{HF}{TP - VLF} \tag{2.18}$$

The representation of LF and HF in n.u. emphasizes the controlled and balanced behaviour of the two branches of the autonomic nervous system. Moreover, normalization tends to minimize the effect on the values of LF and HF components of the changes in total power. Another measure is LF/HF, calculated as the ratio of the power in LF and HF band.

Vagal activity is the major contributor to the HF component. Disagreement exists concerning the LF component. While some studies suggest that LF, when expressed in normalised units, is a quantitative marker for sympathetic modulations, most studies view LF as reflecting both sympathetic and vagal activity. Consequently, the LF/HF ratio is considered to mirror mainly sympathovagal balance. The physiological explanation of the VLF component is much less defined and the existence of a specific physiological process attributable to these heart period changes might even be questioned. The non-harmonic component which does not have coherent properties and which is affected by algorithms of baseline or trend removal is commonly accepted as a major constituent of VLF. Thus VLF assessed from $\leq$5 minute recordings is a dubious measure and should be avoided when interpreting the PSD of short-term ECGs. The ULF component is discussed when 24h recordings are analyzed. This parameter reveals information of the circadian variations of the heart rate.

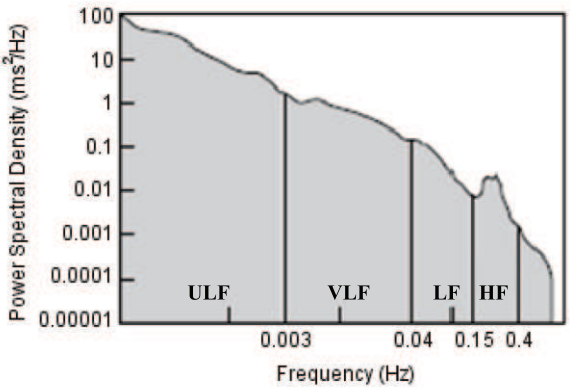


Figure 2.13: *Example of an estimate of power spectral density obtained from the entire 24h interval of a long-term Holter recording. The different frequency bands are clearly indicated: ultra-low frequency component (ULF), very low frequency component (VLF), low frequency component (LF) and high frequency component (HF). From [165].*

Time-frequency analysis

Because of the problem of stationarity, frequency domain HRV parameters are not reliable in case of quick changes in heart rate or its autonomic modulation. The spectrum essentially tells us which frequencies are contained in the signal, as well as their corresponding amplitudes and phases, but does not tell us at which times these frequencies occur. Therefore, time-frequency representation (TFR) can be made from the signal as described in section 2.1.2. The Morlet wavelet is selected as mother wavelet as literature showed that this is an appropriate function to study HRV [90]. From this TFR, a time course of spectral parameters can be extracted. The spectral bands are chosen similarly to the Task Force description [165], so as to keep the physiological interpretation of the results: LF band (0.04 - 0.15 Hz) and HF band (0.15 - 0.40 Hz). The instantaneous frequency of a signal, calculated as the derivative of the phase of its analytical signal, often produces results that, in some ways, may seem paradoxical [127], and which, in any case, make their physical interpretation difficult. This drawback can be avoided by defining the instantaneous frequency as the mean frequency of the spectrum at each instant [25]. The spectrum is obtained as a section of the time-frequency distribution at

this instant.

$$f_s(t) = \frac{\sum_{n=n_b}^{n_e} f_n \cdot TFR(t, f_n)}{\sum_{n=n_b}^{n_e} TFR(t, f_n)} \tag{2.19}$$

with n_b, n_e respectively the beginning and end frequency of a selected frequency band and f_n the frequency representation of the scales a. Each mother wavelet has a central frequency, which can be modified by rescaling the mother wavelet. The scale a is thus directly related to a frequency. The instantaneous frequency is calculated in the high frequency band (f_{HF}), while the analysis in the low frequency band is neglected because no agreement exists on physiological meaning of this frequency. Analogously, in the two frequency bands the power can be calculated by integrating the spectrogram, expressed in absolute values or normalised units (respectively e_{LF} and e_{HF} for the power in the low frequency and the high frequency band).

$$e_s(t) = \sum_{n=n_b}^{n_e} f_n \cdot TFR^2(t, f_n) \tag{2.20}$$

Non-Linear HRV parameters

Next to the time and frequency measures, several non linear techniques are used to describe the dynamics of the cardiovascular system. These methods for non-linear dynamics enable other insight in HRV. They allow the quantification of the complexity and the chaos of processes, induced by the biological system. Here, a short overview of the methods used in this manuscript is given, a more extensive explanation about the different techniques is given in [170].

- **1/f slope.** The 1/f slope [88] is the slope of the linear regression of the log(PSD)to log(frequency) relationshop in the frequencyband of 10^{-4} till 10^{-2} Hz. This measure is an indication of the long term scaling characteristics of the signal. A value of -1 indicates a young, healthy person.
- **Detrended Fluctuation Analysis (DFA).** DFA [122] quantifies the presence or absence of fractal-like properties in non-stationary time series. In HRV, short term DFA α_1 (by agreement from 4 to 11 heartbeats) and long term DFA α_2 scaling factors are calculated. The long term and short term self-similarity of the signal is characterised by these scaling factors.

- **Sample Entropy (SampEn).** The sample entropy [134] is an estimation of the entropy as measure for the complexity of the system. SampEn quantifies the conditional probability that subseries of length m that match pointwise within a tolerance r, match also at the next point. In this study, the values of $m = 2$ and $r = 0.2$ are used. The higher the values of SampEn the more complex a time series is [178].

- **Fractal Dimension (FD).** The FD [84] measures the irregularity of the fractals within the time series and is a measure for the complexity. To estimate the FD, the tachogram is divided in squares with length r and the number of squares, needed to cover the complete tachogram are calculated. Several methods exist to calculate the FD. Here, the box-counting method is used.

- **Lyapunov Exponent (LF).** LE [124] is used to discriminate between chaotic dynamics and periodic signals. It is a measure of the rate at which the trajectories separate one from the other. The trajectories of chaotic signals in phase space follow typical patterns. Closely spaced trajectories converge and diverge exponentially, relative to each other. The LE is an indication of the predictability of a time series. A positive value of LE indicates the presence of chaos in the time series.

- **Numerical Noise Titration.** Numerical Noise Titration [126] is a better alternative for the Lyapunov exponent (LE), which is a measure of the exponential divergence of nearby states. LE fails to specifically distinguish chaos from noise and cannot detect chaos reliably unless the data series are inordinately lengthy and virtually free of noise, but those requirements are difficult mostly even impossible to fulfill for most empirical data. To apply numerical noise titration, the noise limit NL is calculated. NL estimates a linear and a nonlinear model to model the data. If the linear model is a better estimation of the data, it can be concluded that the data are not chaotic and the NL equals 0. The non linear model indicates that the data are both chaotic and non chaotic. After adding noise, both models are calculated. As long as the nonlinear model is a better predictor, extra noise is added. The amount of noise added is the noise limit (NL). $\mathrm{NL} > 0$ indicates the presence of chaos, and the value of NL gives an estimate of relative chaotic intensity. Conversely, if $\mathrm{NL} = 0$, then the time series may be non-chaotic or the chaotic component is already neutralised by the background noise. Therefore, the condition $\mathrm{NL} > 0$ provides a simple sufficient test for chaos.

  Two measures to assess the changes in the chaos level can be extracted. The detection rate (NLdr) is defined as the percentage of all time segments in which nonlinearity is detected. This measure gauges the mean cardiac chaos level. NLmean is calculated as the average of all the NL's excluding the segment with $\mathrm{NL} = 0$. It estiamtes the chaos level directly and can be used as a highly time-resolved measure.

2.4 Near-Infrared Spectroscopy

Near Infrared Spectroscopy (NIRS) is a technique that uses light in the near infrared spectrum for noninvasively clinical monitoring of tissue oxygenation. The method is based on the property that biological tissue is relative transparent to light in the near-infrared part of the light spectrum i.e. 700 to 1000 nm. As light photons can penetrate several centimetres into the tissue, some of the optical properties of the tissue can be measured noninvasively ([80]). The signal detection is based on levels of light directed into the tissue through the skin and picked up by the detector after the light has traveled through tissue ([99]). The light will be attenuated due to a combination of absorption by chromophores and scattering through the inhomogeneous medium (skin, adipose tissue, muscle). In human tissue, three main chromophores that absorb light causing the light attenuation are oxyhaemoglobin (HbO_2) and deoxyhaemoglobin (HbR) in the red blood cells and the oxidized form of Cytochrome oxidase (Cytox) in the cell mitochondrial membrane. Attenuation of transmitted light in the tissue due to other causes can be assumed to be constant over the period of monitoring. Consequently, any change observed in attenuation is due to a change in the concentration of the chromophore. The purpose of NIRS is to quantify the concentrations of these chromophores in tissue ([41, 112]). Light attenuation increases as the light scatters away from the original linear path. The scattering rate is unknown due to the inhomogeneous tissue and the unknown deviation from the linear path. This deviation is expressed in differential pathlength factor (DPF) and describes the actual distance traveled by the light through tissue ([117]). However, as most commercially available NIRS systems can not measure the actual pathlength, DPF is usually set to a fixed value in clinical studies. For the studies described in this manuscript, the DPF is set to a constant value of 4.39 ([44, 108]). Figure 2.14 shows the principle of the NIRS. Although the absorption is relatively low in biological tissue, it is still difficult for NIR light to penetrate more than a few centimeter. Due to the high scattering, however, a detector, placed a few centimeters from the source on the same surface, can collect light that has passed through the tissue beneath the optodes. Assuming homogeneous tissue, the sample volume corresponds to a banana-shaped volume beneath the optodes [20]. The assumption here is that light attenuation arises only due to changing concentrations of chromophores in tissue, because DPF and other factors attenuating the light can be considered constant during measurement at the same position in tissue. The Modified Beer-Lambert equation (equation 2.21) [30] makes it possible to convert changes in absorption and attenuation to changes in concentration of the chromophores, recognizing that the distance between the optodes (light source to detector) is constant and known.

$$A = \log \frac{I_0}{I} = \alpha \cdot C \cdot d \cdot B + G \tag{2.21}$$

Where

$A =$ attenuation
$I_0 =$ incident light intensity
$I =$ emergent light intensity
$\alpha =$ optical characteristics of a compound at a given wavelength
$C =$ concentration of the absorbing compound
$d =$ distance between optodes
$B =$ differential pathlength factor (DPF)
$G =$ additive geometry-dependent term reflecting scattering loss

Here, the additive geometry-dependent term G reflecting scattering is an unknown but constant factor in time. To avoid this factor G another equation is used, calculating the difference between two moments in time.

We have the attenuation A at two time instants.

$$A_1 = \log \frac{I_0}{I} = \alpha \cdot C_1 \cdot d \cdot B + G \tag{2.22}$$

$$A_2 = \log \frac{I_0}{I} = \alpha \cdot C_2 \cdot d \cdot B + G \tag{2.23}$$

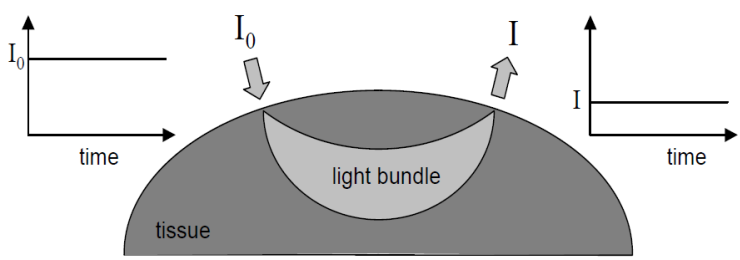


Figure 2.14: *Schematic representation of the sample volume (light bundle) when source and detector are placed on the same surface. The incoming light (source) has intensity I_0, the emerging light (detector) is attenuated and has intensity I (From [108]).*

When taking the difference in attenuation between these two measurements, the unknown factor G disappears.

$$(A_2 - A_1) = \log \frac{I_0}{I} = \alpha \cdot (C_2 - C_1) \cdot d \cdot B \tag{2.24}$$

A disadvantage is that NIRS only measures concentration changes of the chromophores ([112]). The spectrum of HbO_2 and HbR is given in figure 2.15. The analysis of the light in the tissue in selected wavelengths in the range of interest can give a qualitative assessment of changes in the tissue concentration HbO_2 and HbR. The largest differences in the spectrum between HbO_2 and HbR are in the range of 600 - 1000nm. The more wavelengths that are measured in the equipment, the better the assessment of the changes in concentration. These changes in tissue oxygenation take place at the level of small blood vessels, capillaries and intracellular sites of oxygen uptake ([97]). The NIRS measurements are able to display on real-time basis the changes in HbR (ΔHbR) and in HbO_2 (ΔHbO_2) and the difference in total haemoglobin concentration (ΔHbt) can be determined by summing ΔHbR and ΔHbO_2. Changes in Cytox concentration (ΔCytox) are a relative rate of cellular oxygenation. The total blood volume can be estimated by the total haemoglobin concentration (ΔHbt). The blood flow is calculated from the changes in O_2 saturation and HbO_2 recorded over a small epoch. A good correlation between blood flow and volume has been notified in previous work ([112, 117]).

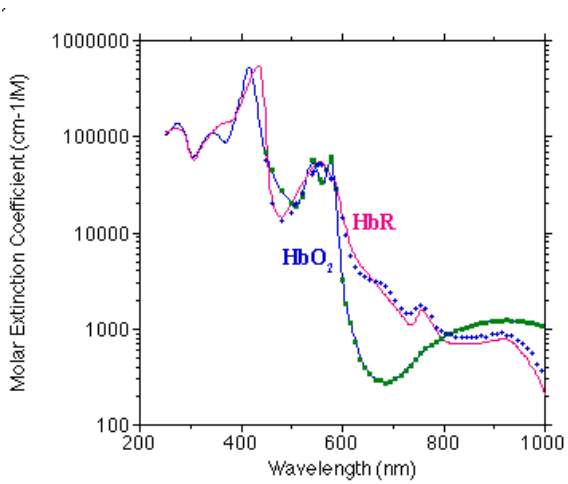


Figure 2.15: *The spectrum of HbR and HbO_2. (From* `http://omlc.ogi.edu/spectra/hemoglobin/moaveni.gif`*)*

Spatially resolved spectroscopy (SRS) uses the diffusion approximation in addition to the modified Beer-Lambert Law. This method describes the propagation of photons in a highly scattering medium such as living tissue [79]. This equation is given in 2.25.

$$\frac{1}{c}\frac{\delta\phi(r,t)}{t} = \nabla[D(r)\nabla\phi(r,t)] - \mu_a(r)\phi(r,t) + S(r,t) \tag{2.25}$$

Where

$\phi(r,t) =$	diffuse photon fluence rate at position r and time t
c =	speed of light in the tissue
S(t) =	photon source
D(r) =	diffusion coefficient: $D(r) = (3(\mu_a + \mu_s))^{-1}$
$\mu_a =$	absorption coefficient
$\mu_s =$	scattering coefficient

For a semi-infinite, homogeneous half-space geometry, it can be shown that the solution of equation 2.25 for an impulse is given by [108, 112]:

$$R(\rho,t) = \frac{1}{4\pi DC}\frac{1}{\mu_s}t^{-5/2}exp(-\mu_a ct)exp(\frac{-(\rho^2+\mu_s^2)}{4Dct}) \tag{2.26}$$

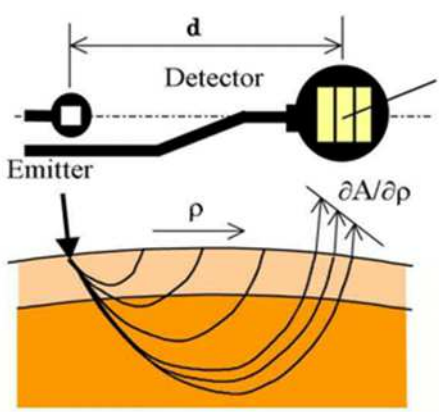


Figure 2.16: *Detector of spatially resoveld spectroscopy [112].*

With $R(\rho, t)$ = the intensity of the reflected light at a distance ρ and time t.

Patterson et al [121] proposed that the effective attenuation coefficient of tissue can be measured using non-time resolved measurements by measuring the spatial variation of the intensity of retroreflected light as a function of the distance between between the light source and detector ρ. They showed that the scatter loss becomes homogenous if ρ is large enough (ρ >3). From this distance, the attenuation coefficient can be estimated as $(3\mu_a\mu_s)^{1/2}$. The detector consist of three sensors at varying distances from a light source (see figure 2.16). At the point of the detector, the differences in intensity measured at the three different sensors can be interpreted as differences in absorption loss and the relationship can be noted as $\delta A/\delta\rho$, where A is the surface of one detector. Any difference in intensity measured by the three detectors gives an indication of the variation in absorption. This enables the measurement of the dynamic balance between O_2 supply and O_2 consumption in tissue capillaries, arterioles and venules which is impossible in larger blood vessels because the light would be absorbed fully by the high haemoglobin concentration. The tissue oxygenation index (TOI) is measured as a local change in absorption in function of distance between source and detector. The TOI can be calculated according to equation 2.27.

$$TOI(\%) = \frac{k \cdot HbO_2}{k \cdot HbO_2 + k \cdot HbR} \tag{2.27}$$

Where

HbO_2 =	concentration in oxydised haemoglobin
HbR =	concentration in reduced haemoglobin
k =	constant scattering distribution

The main advantage of the tissue oxygenation index, TOI, compared to the HbO_2, HbT and HbR separately is that an absolute value is calculated. This enables the use of this parameter for group analyses without the need of a reference measurement.

For the measurements in this manuscript, the NIRO 300 (Hamamatsu Photonics K.K., Tokyo, Japan) is used (figure 2.17). NIRO 300 uses spatially resolved spectroscopy (SRS) with four different laser diodes emitting near-infrared light at four wavelengths, i.e. 775, 810, 850, and 910 into tissue. The laser diodes sequentially irradiate the skin through the same emitter which is made from a fiber bundle. The pulse width of each laser diode is about 100ns and the repetition rate is 2 kHz. The total average power of the irradiation to the skin is about 1 mW and classified as laser Class 1. Three closely spaced photodiodes measure the

attenuation as a function of source- detector distance. The different parameters that are extracted from a measurement with the NIRO 300 are the ΔHbO_2, ΔHbR, ΔHbT and TOI.

2.5 Stress

Everybody in todays society knows the phenomenon stress and lot of people have their own opinion on stress. But the real description of stress is vague as several definitions of stress exist, pointing to the situation, the feeling, the initiation and so on. In this text, we use a more fundamental and general definition described in the book of Van Houdenhove [74]: *Stress is a set of physiological and psychological mechanisms that initiates because of real or imaginative threats to our physical or psychological balance.* These threats are called stressors and can have a large variety in origin both physical as mental: lack of sleep, working under time pressure, coping with an annoying boss, performing a difficult task, shooting the decisive penalty in the final of the world championship, facing a bear in prehistoric ages ... All these stressors lead to changes in the body that make people feel stressed. Therefore, stress is called a psychophysiological phenomenon. Hans Selye [144], a physiologist, is generally accepted to be the pioneer of stress. He discovered the general adaptation syndrome (GAS) during an endocrinological experiment in which he injected mice with extracts of various organs. At first, he believed he discovered a new hormone, but was proved wrong when every irritating substance he injected produced the same symptoms. This, paired with his observation that people with different diseases exhibit similar symptoms, led to his description of

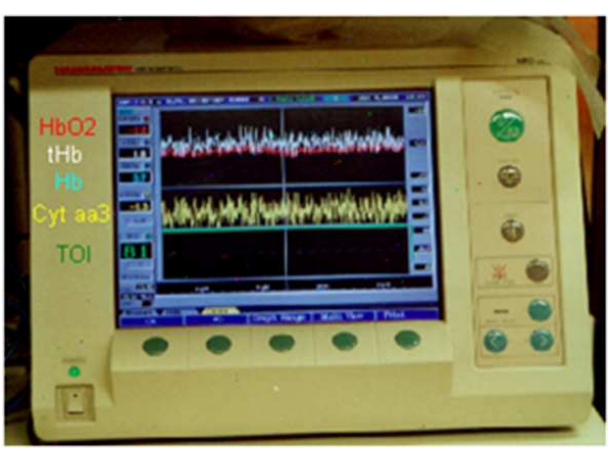


Figure 2.17: *NIRO 300.*

the effects of noxious agents. He later coined the term *stress* to stress, which has been accepted as the general term in various other languages. The work of Selye was greatly influenced by Walter B. Cannon, who had focused on the role of the sympathetic nervous system in adaptation called it the *fight-or-flight response*. When an animal is threatened by a predator, several changes in the physiology of the animal occur to bring the animal in a state of arousel where its body is prepared to attack or fly from the predator. A nice example is clapping in your hands when seeing a cat. The cat freezes immediately, moves down, open the eyes and after a while the cat runs away or attacks. Later, this fight-or-flight reaction was called the acute stress response in the work of Selye.

The body reacts to the different stressors with the complex stress reaction, but this reaction still works nowadays in a similar way as in the prehistory [74]. The appearance of a threat inhibits changes in the physiology and behaviour of the body with the only focus on survival. Some of these changes are an increase in heart rate, blood pressure and respiration; an increase in muscle tension that is responsible for fighting or flying. Other mechanisms that are not necessary for direct survival are reduced like sleep, pain, reproduction, sex ... The mood is anxious and nervous so the body remains focused on survival. All these processes are controlled by the brain [74]. When the threatfull situation is identified (by the amygdala, the cortex and the hippocampus), the locus coeruleus or the sympathetic system and the hypothalamus-pituitary-adrenocortical axis (HPA-axis) are activitated, while the prefrontal cortex is disabled. The sympathetic system becomes more activated via the locus coeruleus (situated in the brain stem), resulting in the secretion of the neurotransmitter noradrenaline. The activation of the sympathetic system innervates the production of adrenalin in the adrenal medulla. In addition, the parasympathetic system is shut down. The production of adrenalin is responsible for the increase in heart rate, respiration rate and vasoconstriction. From the initial threat on, the hypothalamus is releasing the corticotropin releasing hormone (CRH) to maintain the acute stress reaction (coping). It also activates the pituitary that activates the adrenal cortex via the adrenocorticotropic hormone (ACTH) to produce cortisol. The prefrontal cortex is shut down. This brain region is responsible for planning complex cognitive behaviors, personality expression, decision making and moderating correct social behavior. The basic activity of this brain region is considered to be orchestration of thoughts and actions in accordance with internal goals.

As described earlier, the stress response is a natural protection mechanism of the body to external danger and is *in se* not bad. Even more, in certain circumstances, stress enhances the functionality of an individual (both physical and mental). Selye introduced the term *eustress* for this phenomenon [145]. The opposite is called *distress*. A stress situation has a clear impact on the body and results in an extra load of the metabolism (See figure 2.18). Long term exposure to stress could load to exhaustion of several systems in the body. McEwen

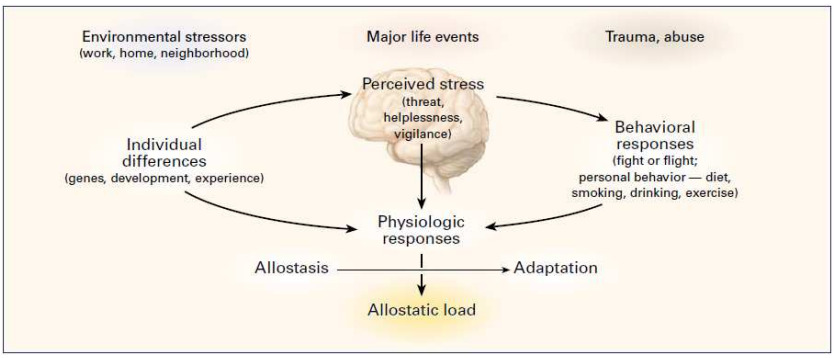


Figure 2.18: *The Stress Response and Development of Allostatic Load. The perception of stress is influenced by ones experiences, genetics, and behavior. When the brain perceives an experience as stressful, physiologic and behavioral responses are initiated, leading to allostasis and adaptation. Over time, allostatic load can accumulate, and the overexposure to mediators of neural, endocrine, and immune stress can have adverse effects on various organ systems, leading to disease. (From [100], with permission of the New England Journal of Medicine. ©[1998] Massachusetts Medical Society. All rights reserved.)*

[101] introduced the word *allostatic load* for this as a failure of the allostasis. Allostasis [153] is the ability from the body to adapt to external situations and cope with the environment(awake, asleep ...). The top plot of figure 2.19 shows normal allostasis, where a response is initiated by a stressor, sustained for an appropriate interval and is turned off when the stressor disappears. However, if the deactivation is inefficient, there is overexposure to stress hormones. Long term over exposure (months to years) to these hormones can result in allostatic load and its pathophysiologic consequences. The first type is the frequent stress. The body can cope with occasional stressors, but is not adapted to face long term periods with stressors (for example long periods of elevate blood pressure increases the risk of myocardial infarction). The second type refers to the lack of adaptation of the body to cope with repeated stressors of the same type. The learning process to similar external stimuli (habituation) is absent. A third mechanism that leads to allostatic load is the failure of the body to shut down the allostatic responses after the stress is terminated. In normal circumstances, the increase of stress hormones in the body is answered with negative feedback to the mediators to control the stress mechanism and to recover the body once the stressor disappears. This feedback mechanism fails to work for some people when the stress mechanism is exhausted due to long term exposure. These above described types of allostatic load are all three related to the stress system in overdrive. The opposite, when the stress system is in underdrive, is the fourth type of allostatic load. The reaction of some allostatic processes to a new stressor is inadequate, resulting in a compensatory increase of other allostatic processes. This is also responsible for the exhaustion

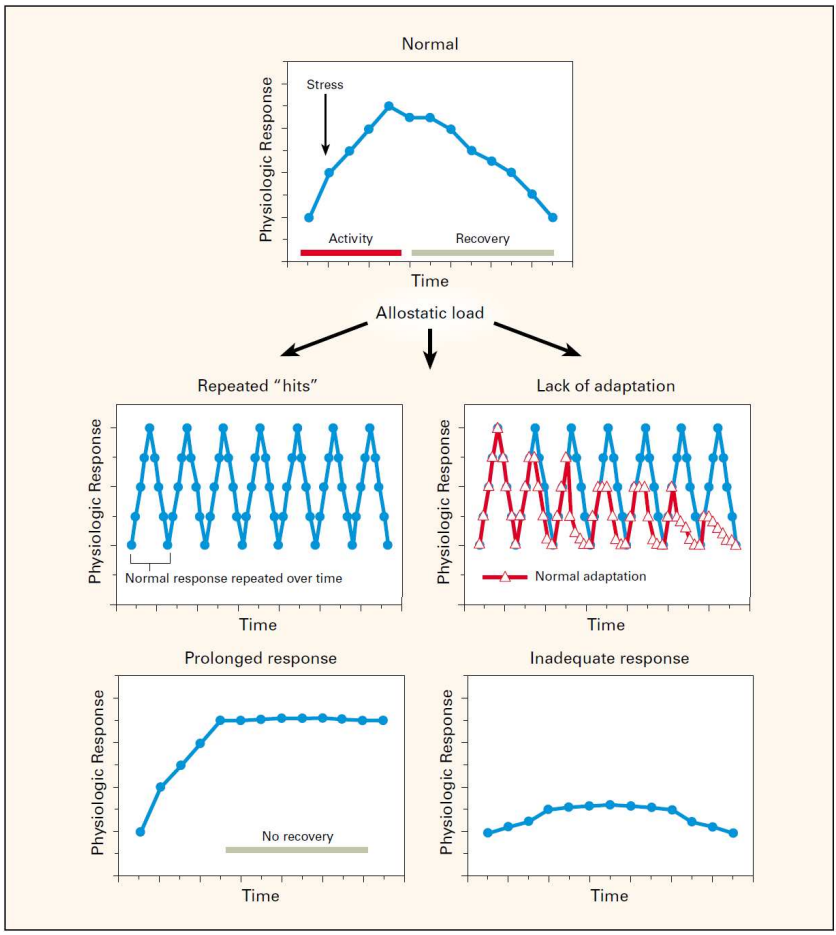


Figure 2.19: *Different types of allostatic load. The top panel illustrates the normal allostatic response, in which a response is initiated by a stressor, sustained for an appropriate interval, and then turned off. The remaining panels illustrate four conditions that lead to allostatic load: repeated hits from multiple stressors; lack of adaptation; prolonged response due to delayed shutdown; and inadequate response that leads to compensatory hyperactivity of other mediators (From [100], with permission of the New England Journal of Medicine. ©[1998] Massachusetts Medical Society. All rights reserved.)*

of several physiological processes. Underactivitation of the HPA axis leads to a shortage of cortisol in the blood [74]. This shortage has a direct influence in the malfunction of the immune function of the body with its direct consequences to health.

Allostatic load has a huge impact on the equilibrium of the human body. This results in numerous diseases that are related with long exposure to stressors. The most common stress diseases are coronary diseases (elevated blood pressure, myocardiac failure), type 2 diabetes, obesitas, depression, fybromyalgia, chronic fatigue syndrome, burn-out.

2.6 Conclusion

In this chapter, the most important methodology is introduced to understand this manuscript. In a first section, the mathematics that are used in this manuscript are described. The next sections introduce the physiological and technical background of the physiological signals (muscle activity, variability of the heart and the oxygenation of tissue) that are used within this manuscript. Finally, Stress, which is the basis of the collected data and the analysis used in this manuscript is introduced. A summary of the physiological impact of mental stress is described.

Chapter 3

Surface Electromyography: processing and analysis applied to stress monitoring

This chapter gives an overview of the signal processing and the analysis of the sEMG signals. In a first section 3.2, two series of stress experiments are described that are used within this manuscript. Each stress experiment consisted of different tasks where a mental stress was induced on the subjects. This mental task was combined with and without an extra physical load. In a next section 3.3, the removal of ECG interference in sEMG signals of the shoulder girdle is described. This ECG interference signal is the most important noise influence in these sEMG signals and need to be removed for reliable analysis. A single channel approach of independent component analysis was elaborated and applied on the data to remove the ECG interference signal. These techniques were expanded to situations where a simultaneous ECG measurement is available. The results of these techniques were compared with template subtraction, which is the standard technique to remove the interference signal. During the analysis of the sEMG signal of the trapezius muscle during the stress assessment tasks, a specific pattern of muscle activity could be identified which is not published earlier in this situation using this type of electrodes. This muscle activity is a continuous activation of single type I motor unit. A spike train detection algorithm is modified to detect this type of activity. This observation and detection algorithm is described in section 3.4. In the next section (3.5), an easy-to-use algorithm, based on the frequency properties of the sEMG signals, to estimate whether a muscle is active or in rest is presented. This algorithm was used to estimate the baseline of the different sEMG signals during the stress experiments. The final section of this section (3.6) describes the most

important results of the analysis of the different sEMG parameters during the two stressexperiments tests. The effect of the mental task on the sEMG parameters is discussed, next to the analysis of muscle fatigue during the different tasks. The additional effect on the muscle activity from the mental load on a physical load..

3.1 Introduction

The use of surface Electromyography is of importance in the battle against musculoskeletal disorders. More specific, the influence of mental stress on spontaneous activation of the muscle in the shoulder girdle (and the trapezius muscle more specific), is a main topic in research [67, 82, 73]. The prolonged activation of the muscle fibers in the shoulder area could lead to overload of the fibers and in a further stadium to MSD.

In laboratory studies, researchers found that mental workload increases trapezius muscle activity [6, 17, 50, 89, 92, 96, 181]. Stressful circumstances, such as verbal provocation during performance and time pressure also increase muscle activity [180]. However, several researchers have reported considerable inter-individual differences in muscle activity response to a stressor [186, 98, 115, 173]. EMG activity does not always correlate with other physiological and psychological parameters [89, 82, 135]. This proves the necessity of the monitoring and the analysis of the sEMG in the battle against MSD.

Two series of stress experiments were conducted where several muscles in the shoulder area (trapezius, deltoideus and infraspinatus muscle) were monitored. The test subjects carried out different tasks, imposing physical, mental and a combination of physical and mental stimuli. The reaction of the muscles on these different tasks was investigated. So far, researchers have mainly investigated the amplitude of the EMG signals via the Root Mean Square. These results are described shortly in a paragraph. But in this study, we focus also on possible patterns in the sEMG signals to possibly discriminate between activity caused by the physical stimuli and the mental stimuli.

To increase the performance of the analysis, the most important artefacts need to be removed. When looking at the sEMG signals in the shoulder area, the interfernce of the electrophysiological signal of the heart is identified as a major source of interference and needs to be removed. A single channel approach of independent component analysis (ICA) was described to remove the ECG interference signal from sEMG signal. The results were compared with a standard technique to remove the interference signal.

After removing the ECG interference signal from the EMG data, a specific pattern of muscle activity was identified: the burst of spikelike activity. This muscle

activity is a continuous activation of a single type I motor unit and does not benefit in for the postural load. This continuous activity could be one of the cause of the muscle overload, leading to MSD. A detection algorithm is presented and validated.

3.2 Data acquisition: stress assessment

As described earlier, a large part of the study was performed under contract of a European project. This study aimed to evaluate the effect of mental stress on the muscles of the shoulder girdle. Our group was responsible for the data collection and the design of the protocol and the interpretation of the signals. Two experiments were executed to collect the data and the design, the protocol, the materials are described seperately in this chapter. In this manuscript, we will refer to both experiments as *stressexp 1* and *stressexp 2* respectively.

3.2.1 Stressexp 1

Overview

The first experiment was designed to investigate the effect of a mental load on the electrophysiological signals of the body. Therefore, the test subjects executed different tasks (body in rest and during a physical load) with and without an superimposed mental load. The physiological signals in this experiment include sEMG signals in the shoulder girdle to monitor the muscle activity and heart rate to investigate its variability. The muscles of interest were the m. Trapezius pars descendens, m. Deltoideus medius, and the m. Infraspinatus of both left and right side (see figure 3.1). The m. Trapezius pars descendens was included because literature showed that its muscle activity is very sensitive to changes related to mental stress [98, 95]. The Deltoideus is the prime mover of the shoulder abduction which is used as physical load during this experiment and the m. Infraspinatus is the muscle that is responsible for the posture of the body.

The study population was limited to healthy students and young people working at the Katholieke Universiteit Leuven from 19 to 26 years old, 14 men and 14 women, aged 22 ($\pm 1,96$) years and an average body mass index (BMI) of 22 $\pm$ 2,33 kg/m^2. Before the experiment, information about neck or shoulder complaints, cardiovascular problems and whether subjects were right- or left handed was noted. Upon arrival, the participants were informed on the course of the experiment and signed an informed consent. The experiments were approved by the Ethics committees of the Department of Psycholgy and the Faculty of Medical Sciences. The study is in accordance with the Declaration of Helsinki.

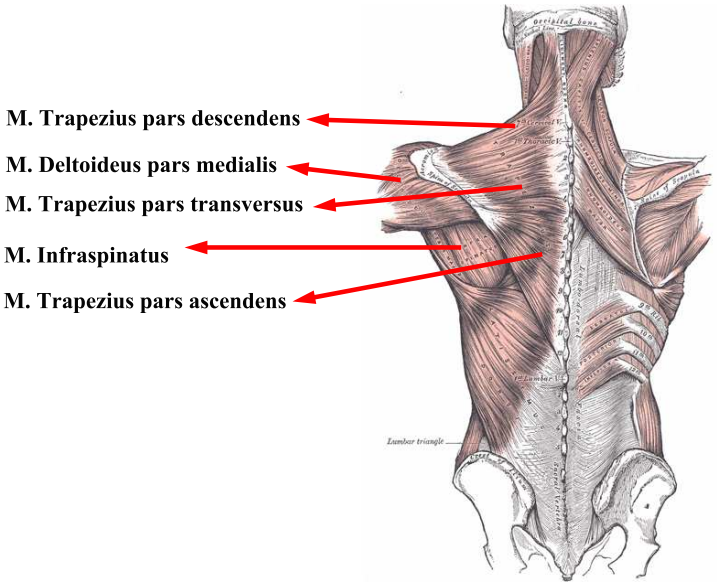
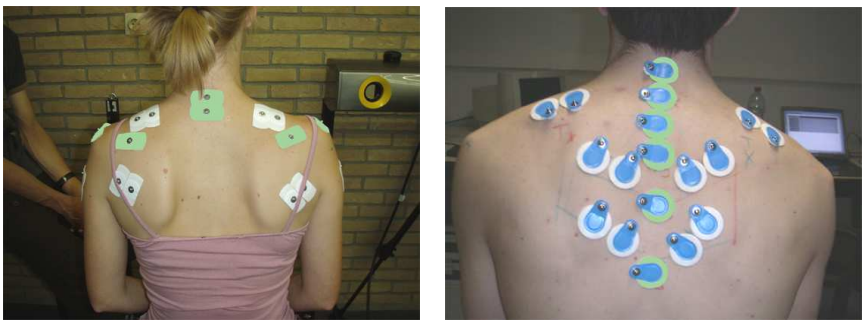


Figure 3.1: *Position of the muscles used during both stress experiments. In stressexp 1: m. Trapezius pars descendens, m. Deltoideus medius, and the m. Infraspinatus. For stressexp 2: m. Trapezius pars descendens, m. Trapezius pars transversus, m. Trapezius pars ascendens.*

Materials

On arrival, the participants were prepared for the recordings. The hair on the body was removed if appropriate and the skin was cleaned. Contact electrodes (Ag-AgCl, 10 mm diameter, Nikomed, Denmark) were used and positioned on the muscles according to SENIAM recommendations [57] and palpation of the muscle. During this experiment, left and right of the m. Trapezius pars descendens, m. Deltoideus medius, and the m. Infraspinatus were measured (see picture 3.2(a)). Two electrodes plus one reference electrode were placed for each muscle. Heart rate was measured with two electrodes plus a reference electrode on the lower part of the sternum. The exact position of the two electrodes is not crucial as long as the heart is in between the two electrodes. We standardized the positioning of the two electrodes (as shown in figure 3.3. The electrodes were placed on the ribs and the upper part of the sternum to reduce the EMG interference of the m. pectoralis major on the ECG data. Six channels of sEMG and one channel of ECG were recorded via EMG preamplifiers (Mega Electronics Ltd, Finland). These analogue signals were low pass filtered (450Hz) to avoid aliasing during digitization. The Daqbook 2005 (IoTech, Ohio, USA) was used to digitize the signals at a sampling rate of 1000Hz. An extra channel was added with a pulse generator (3V, 0.5s).

This pulse was used to distinguish the different tasks during the test. Posture of the participants was recorded during the test with a Sony (DCR-HC37E) camera. The data were analyzed using MATLAB and LABVIEW 8.2.



(a) stressexp 1 (b) stressexp 2

Figure 3.2: *Pictures of the positioning of the electrodes during the two stress experiments. The reference electrodes are indicated in green.*

Setting

The environment and the positioning of the subjects were controlled. Subjects were seated in an ergonomic office chair, adjusted to the subjects body geometry and comfort. Seat height was adjusted so that the subjects feet were flat on the floor with a knee angle of $\pm 90°$. Seat depth was adapted to the length of the upper legs so that the distance between the front of the seat and the back of the knees was approximately 5cm. Backrest height was positioned ergonomically for

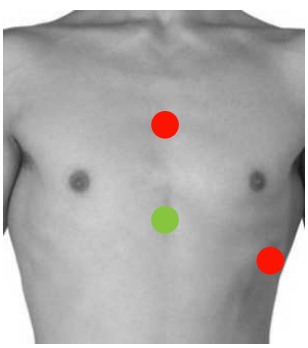


Figure 3.3: *Position of the electrodes to measure the ECG in red, the reference electrode is given in green.*

optimal support to the lower back. The office chair had no arm support. The table was adjusted to elbow height. The top of the computer screen was positioned at the eye level of the subject. Horizontal distance between the eyes and the screen was approximately 60 cm. This ergonomic adaptation of the test environment ensured good posture of the neck, shoulders and back, with minimal postural load. The participants were explicitly instructed not to speak, mumble or move the lips, except for giving the answer during the mental task, to sit comfortably, not to change posture or to move the body (except for the physical task). The experimenter was seated next to the participant.

Overall Stress Level

To estimate the subjects overall stress levels, questionnaires were completed before the experiment. In the first experiment the Positive Affect Negative Affect Schedule (PANAS) is used [182]. PANAS is a psychometric scale developed to measure the largely independent constructs of positive and negative affect, both as states and traits. Positive and negative affect have been proven to be in relationship with typical personality states and traits, such as anxiety.

Maximal Voluntary Contraction

Before the start of the experiment, the maximal voluntary contraction (MVC) of the different muscles were recorded to allow the interpretation and comparison of intersubject sEMG-signals during the experiments as described in the section 2.2. The MVC of the trapezius pars descendens, the deltoideus and the infraspinatus were measured respectively during a static maximal shoulder elevation with stretched arms against a resistance, a maximal static shoulder abduction with stretched arms at an angle of 45° and a static exorotation of the shoulder joint where the elbow was fixed against the body. The maximal contraction was built up over 5 seconds. The subjects performed 3 maximal contractions per muscle with a rest interval of 1 minute. The highest sEMG-value of the 3 contractions was used as the MVC. The amplitude of the muscle activity during different conditions of the experiments could then be expressed as a percentage of the MVC.

Protocol

The participants were instructed to perform different tasks to change the mental and the physical load and a combination of both mental and physical load. These different tasks were:

1. **Rest(R)**: the subjects were sitting at ease with their hands in their laps. During this rest period, a series of relaxing photos were shown on the computer screen to reduce boredom. A complete test starts with rest and after each active phase, there was another rest condition.

2. **Physical task (PT)**: the subject performed a shoulder abduction of 45° with stretched arms during 6 minutes. This prolonged static posture was intended to induce muscle fatigue.

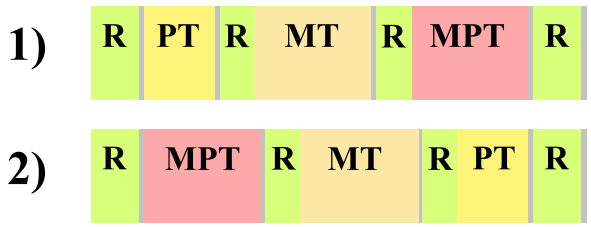
3. **Mental task (MT)**: the subjects were sitting with their hands in their laps and performed a complex and challenging mental task, part 1 of the home version of the MENSA test [102]. Time to complete the test was limited to 10 minutes without visual feedback of the remaining time. The answers were formulated orally and noted by the experimenter.

4. **Mental and physical task (MPT)**: the subjects performed a shoulder abduction of 45 with stretched arms and solved part 2 of the MENSA test. Time to complete the MENSA test was limited to 10 minutes without visual feedback of the remaining time. The answers were formulated orally and noted by the experimenter.

5. **Self rating (SR)**: following each active task (MT, PT, MPT) the subjects were asked to rate their subjective perception of stress at that moment on the short version of the Spielberger State-Trait Anxiety Inventory (STAI) [39]. This provided subject perceptions of their stress or anxiety levels at the instant of rating. The scale comprises 6 terms rated on a scale of 1 to 4: 3 of negative affect (tense, nervous, worried) and 3 of positive affect (calm, content, relaxed). The self rating lasts for 30 seconds.

In the protocol sequence, shown in figure 3.4(a), prior muscle fatigue from PT may contribute to muscle load in MPT, confusing interpretations of mental task muscle activity. We therefore used two task sequences and one with PT and MPT switched, and assigned subjects randomly to one of both protocols. The different phases are indicated in color and the most important conditions are indicated with their acronym.

During the analysis of stressexp 1, several limitations appeared regarding the design. A first remark is that with this randomization of the tasks, influence of a preceeding task on the signals during MT could not completely be excluded. A larger problem, especially for HRV analysis, was the inequality in length of the different conditions: there was a maximum of 10 minutes to solve the MENSA test during MT and MPT, but most participants finished the test earlier. Therefore, a new experiment was set up to tackle these shortcomings.



(a) stressexp 1



(b) stressexp 2

Figure 3.4: *The different protocols for both series of experiments. Rest (R, green), Mental load (MT, orange), Physical load (PT, yellow), Mental in combination with physical load (MPT, red). For stressexp 1, grey means Self Rating (grey), while for stressexp 2, grey shows the instance of the instructed sigh.*

3.2.2 Stressexp 2

Overview

The second experiment was designed to investigate the additional effect on different physiological signals of a mental load on a physical task. The results of stressexp 1 showed the presence of muscle activity during the mental task without a postural load, but no effect could be seen on the muscle activity when an additional mental task was applied to a physical load. Therefore, this second stress experiment was designed to answer this question. During the design, the shortcomings of stressexp 1 were taken into account and the physical load was modified to a more realistic office task: the clicking of a mouse. This second stress experiment

was performed in collaboration with psychologists (Research Group on Health Psychology, Katholieke Universiteit Leuven) where research is devoted on the effect of sighing as a relief factor in stress situations.Muscle activity and heart rate were recorded during this experiment next to the respiration. The deltoideus and the infraspinatus muscle did not reveal any change due to a mental stimuli and were discarded during this experiment. The scope was narrowed to the three parts of the m. Trapezius (pars ascendens, transversus and descendens). Figure 3.1 gives the position of these three muscles.

The study population for this experiment was limited to healthy students and young people working at the Katholieke Universiteit Leuven from 18 to 26 years old, 21 men and 22 women, aged 22 ($\pm 1,97$) years and an average body mass index (BMI) of 22 $\pm$ 1,89 kg/m^2. No other exclusion criteria were used. Before the experiment, information about neck or shoulder complaints, cardiovascular problems and whether subjects were right- or left handed was noted. Upon arrival, the participants were informed on the course of the experiment and signed an informed consent. The experiments were approved by the Ethics committees of the Department of Psycholgy and the Faculty of Medical Sciences. The study is in accordance with the Declaration of Helsinki.

Materials

The preparation of the test subjects is similar to the preparation during stressexp 1. The hair on the body was removed if appropriate and the skin was cleaned. Contact electrodes (Ag-AgCl, 10 mm diameter, Nikomed, Denmark) were used and positioned on the muscles according to SENIAM recommendations [57] and palpation of the muscle. For each muscle, 2 recording electrodes plus one reference electrode were used. In this case, the three parts of the trapezius muscle were recorded on the left and the right side of the back. The positions of the electrodes is visualized in figure 3.2(b)). Heart rate was measured with two electrodes (one on the ribs and one on the upper part of the sternum to reduce the EMG interference of the m. pectoralis major on the ECG data) plus a reference electrode on the lower part of the sternum (see figure 3.3). Six channels of sEMG and one channel of ECG were recorded via EMG preamplifiers (Mega Electronics Ltd, Finland). These analogue signals were low pass filtered (450Hz) to avoid aliasing during digitization. The cDAQ 9174 with modules NI 9239 (4 channels, channel-to-channel isolated, 24 bit) from national instruments (Austin, Texas) was used to digitize the signals at a sampling rate of 1000Hz. An extra channel was added with a pulse generator (3V, 0.5s). This pulse was used to distinguish the different tasks during the test. The breathing data were continuously collected by means of respiratory inductive plethysmography (RIP), using the LifeShirt System© (Vivometrics Inc., Ventura, CA). Two RIP transducers at the level of the rib cage and the abdomen, sewn into a LifeShirt garment including three accelerometers, were connected to the LifeShirt

recorder, a digital processing unit including a data storage card. Posture of the participants was recorded during the test with a Sony (DCR-HC37E) camera. The data were analyzed using MATLAB and LABVIEW 8.2.

Setting

The environment and the positioning of the subjects were controlled similarly to the stressexp 1 to ensure good posture of the neck, shoulders and back, with minimal postural load. Subjects were seated in an ergonomic office chair, adjusted to the subjects body geometry and comfort, with an adjusted seat height to ensure that the subjects feet were flat on the floor with a knee angle of $\pm 90°$. Seat depth was adapted to the length of the upper legs so that the distance between the front of the seat and the back of the knees was approximately 4 fingers. Backrest height was positioned ergonomically for optimal support to the lower back. The table was adjusted to elbow height and the top of the computer screen was positioned at the eye level of the subject. Horizontal distance between the eyes and the screen was approximately 60 cm. The participants were explicitly instructed not to speak mumble or move the lips, to sit comfortably, not to change posture or to move the body. The experimenter was seated next to the participant.

Overall Stress Level

To estimate the subjects overall stress levels, several questionnaires were completed before the start of the experiment: the Positive Affect Negative Affect Schedule (PANAS) [182], the Relaxation Inventory [33], the Perceived Stress Scale [27] and a Daily Life Complaints List. This latter checklist is based on Wientjes and Grossman [189] and contains the original 35 items and 4 additional dummy items [68].

Maximal Voluntary Contraction

The maximal voluntary contraction (MVC) was measured to allow intersubject sEMG-signals during the experiments as described in the section 2.2. The MVC of the m. Trapezius pars descendens was measured from a static maximal shoulder elevation with stretched arms against a resistance. The measurement of the MVC of m. Trapezius pars transversus and m. Trapezius pars ascendens is difficult to control and therefore less reliable. In stead, reference voluntary contraction (RVC) was measured during maximal voluntary shoulder elevation. The left and right muscles were measured simultaneously. The maximal contraction was built up over 5 seconds. The subjects performed 3 maximal contractions per muscle with a rest interval of 1 minute. The highest sEMG-value of the 3 contractions was used

as the MVC. The amplitude of the muscle activity during different conditions of the experiments could then be expressed as a percentage of the MVC or RVC.

Protocol

During stressexp 2, the focus of the tasks was on the additional effect of the mental task to the physical task. Therefore, a mental taks without a postural load was not included. The sigh was included for the collaboration with the group of psychology. The effect of the instructed sigh is mainly visible in the rest conditions and does not influence our analysis on the activity during the different tasks.

1. **Rest (R)**: participants are watching a relaxing movie ('The march of the Penguins') exposing them to neutral stimuli reducing boredom during this phase. Participants were ensured that no questions about the documentary would be asked later so they can relax and enjoy the movie. A complete test starts with rest and after each active phase, there was another rest condition.

2. **Physical task (PT)**: PT consists of a pure physical office task of indicating the largest number of three alternatives using the mouse cursor. Participants used the mouse cursor to indicate the correct answer choosing between three alternatives, but was not stressful: in contrast to the MPT, task difficulty was extremely low, no time constraints were applied and no task evaluation or reward for performance was given.

3. **Mental and physical task (MPT)**: The task consists of continuous mental calculations of five operations with a two- or three digit number (e.g. 287 +24 /2 -43 /3 +28) which had to be performed without verbal stimulation. This task required the same motor movement as the PT (indicating the correct answer with the cursor), but was executed after a mental task. After the decision, feedback of the answer was given. Participants were informed that at the end of the study, the five best performing participants would be rewarded with a movie ticket. The experimenter was seated next to the participant. MPT was considered to be stressful as task difficulty was high. Feedback was given, evaluation and rewards were given related to performance within time constraints and an observer was present [58, 85]. This task was repeated twice, where one task was followed by an instructed sigh.

4. **Sigh (S)**: The instructed sigh implied to sigh within the following 30-sec time window. Participants were asked to practice an instructed sigh before the test, so that the experimenter could check whether participants understood and succeeded in executing the instructions.

The different active phases are fully randomized to prevent any bias on the electrophysiological signals of preceding tasks. The first rest period is denoted to be the baseline session and after each active task, the participants have 6 minutes of recuperation. Figure 3.4(b) gives an overview of the different protocols. The grey line indicates the sigh after MPT. The participants are assigned randomly to one of the 6 protocols.

3.3 Preprocessing: ECG interference removal

3.3.1 Introduction

When looking at the raw sEMG signals of both experiments, a major source of noise can be distinguished: the interference of the electrical activity of the heart on the surface electromyography signals in the shoulder girdle. This interference signal is influencing the signal analysis [24]. Therefore, the data needs to be preprocessed to remove this ECG interference. The difficulty of the ECG interference removal is mainly due to the large overlap between the ECG interference spectrum and that of the considered sEMG signal (0-45Hz for ECG, 5-500Hz for sEMG). Regular high pass filtering is not applicable as it removes a substantial part of the sEMG information. Several approaches have been proposed to remove the ECG interference signal. The template subtraction algorithm [12] uses the quasi-periodic property, assuming a similar waveform of successive heartbeats in the sEMG signals. This data driven method estimates the template of the interference signal from the signal and subtracts this template on the occurrence of a heart beat to eliminate the interference signal. The template subtraction algorithm was applied successfully, but is sensitive to changes in the waveform of the ECG interference signal. Other methods, like adaptive filtering [137] or convolutive ICA were also proposed [43]. All these techniques require an ECG reference signal.

A new trend in biomedical signal processing is employing blind source separation (BSS) to unmix a set of recorded signals (based on an extra constraint) into its original sources. Independent Component Analysis (ICA) is one of these BSS techniques assuming independency between the sources. Unfortunately, these techniques are only applicable to multichannel data. Recently, several approaches to extend this idea to single channel data are published in the literature. A first approach, single channel ICA (SCICA), was presented by Davies and James [36]. The original data is chopped into several blocks of equal length and ordered in a matrix before applying the ICA algorithm. This algorithm separates successfully the sources of interest provided they have perfect disjoint spectra. The algorithm also requires stationary data. Both limitations are not fulfilled in this specific application. Another approach to enable the use of ICA in single channel analysis is to decompose the signal into a multichannel representation before applying ICA.

Several decomposition methods exist. Mijovic et al [106] combined ICA with either of two decompositions, Ensemble Empirical Mode Decomposition (EEMD) [75] and wavelets, and compared their performance with the SCICA method. They referred to the EEMD and wavelet approach respectively as EEMD-ICA and wICA. For electrophysiological signals, they showed that the latter two methods outperformed the SCICA algorithm. The wICA method has already been shown successful in removing the ECG artifact [8].

In this chapter, several methods are compared to remove the ECG interference from the sEMG signals. A distinction is made whether a corresponding ECG measurement is available or not. The performance of the wavelet-based decomposition, the EEMD based decompostion and the template subtraction, to our opinion still the golden standard in removing the ECG artifact, is compared. These methods are modified to be applicable in both situations. In addition, we look whether the extra ECG signal has an added value in the removal performance. In a first simulation study, the effect of the parameter settings for EEMD to remove the ECG artifact is investigated. Optimal parameters for EEMD-ICA are retrieved from this study and used further in the analysis. In a second part, the performance of EEMD-ICA to remove the ECG interference is compared with wICA and template subtraction for both simulated and real data.

The ICA based algorithms are published in a joint paper with my colleague Bogdan Mijovic, published in the IEEE Transactions on Biomedical Engineering [106]. I contributed to the idea, the simulations and the applications in this paper. These results have been presented earlier at the 29th Annual International Conference of the IEEE, Engineering in Medicine and Biology Society (IEEE/EMBC) in Lyon in 2007 and more results will be presented on the international Conference on Bio-inspired Systems and Signal Processing, subconference of the 4th International Joint Conference on Biomedical Engineering Systems and Technologies (BIOSTEC 2011), Rome in January 2011. Both presentations resulted in a paper that is published in the corresponding proceedings [159, 157].

3.3.2 Algorithms

Ensemble Empirical Mode Decomposition-Independent Component Analysis (EEMD-ICA)

The idea behind the algorithm is to decompose a measurement into different components before applying a blind source separation technique. Here, a single sEMG channel is decomposed using Ensemble Empirical Mode Decomposition (EEMD) before applying ICA [106]. EEMD [75] is a novel signal analysis tool which is able to decompose any complicated time series into a set of spectrally independent oscillatory modes, called Intrinsic Mode Functions (IMFs). While

wavelets and other signal decomposition techniques tend to map the signal space onto a space spanned by a predefined basis, EMD is a data driven algorithm which means that it decomposes the signal in a natural way where no a priori knowledge about the signal of interest embedded in the data series is needed. The advantage of EMD is that this technique is able to deal with nonstationary and nonlinear data. The more noise robust, noise-assisted version of the EMD algorithm, called Ensemble EMD (EEMD) is used in this study. The algorithm defines a set of IMFs for an ensemble of trials, each one obtained by applying EMD to the signal of interest with added independent, identically distributed white noise of the same standard deviation (SD). The ratio of the added noise standard deviation to the standard deviation of the signal will be further referred to as a noise parameter (np).

After EEMD is executed and a set of averaged IMFs is derived, independent component analysis (ICA) is applied to the decompositions to retrieve independent sources S. ICA is applied to the whole set of IMFs. It is worth noting that no IMF subset has been preselected as input to the ICA algorithm in order to keep this part of the algorithm as automatic as possible. Afterwards, the independent sources that represent the ECG artifact signal are set to zero before reconstruction of the cleaned sEMG signal without the ECG contamination.

The above described algorithm is the single channel approach. When in addition to the sEMG signal,a simultaneously recorded ECG channel is present (two-channel approach), both the ECG channel and the sEMG channel are decomposed separately into a set of IMFs and are used together as input for ICA without further preprocessing.

Algorithm 1 EEMD-ICA [106]

1: Add independent, identically distributed white noise with zero-mean and SD equal to *np* times the SD of the original sEMG signal.
2: Apply EMD to derive a set of IMFs.
3: Repeat steps 1 and 2 a number of times, resulting into an ensemble of IMF sets.
4: Average over the ensemble to obtain a set of averaged IMFs.
5: If the simultaneously recorded ECG channel is present, apply step 1 to 3 to the corresponding ECG signal.
6: Perform the FastICA algorithm to the IMFs and derive the corresponding mixing and unmixing matrices $\mathbf{M}$ and $\mathbf{W}$.
7: Select the independent components (sources) of without the ECG interference and multiply it with mixing matrix $\mathbf{M}$ to back-reconstruct its appearance in the IMF set.
8: Sum over all the newly derived IMFs to reconstruct the original sEMG signal cleaned from the ECG interference.

Wavelet-Independent Component Analysis (wICA)

This algorithm is similar to the EEMD-ICA algorithm, but a single channel signal is decomposed into components of disjoint spectra using the discrete wavelet decomposition (DWT) instead of EEMD. For this study we chose the Daubechies6 mother wavelet in accordance with the study of Azzerboni [8], but similar conclusion holds for other mother wavelets. The DWT has the property of a filter bank as shown in section 2.1.2. To maintain a good frequency resolution in the band of interest, the order of decompositions was set to 8 [159]. The algorithm was originally proposed by Azzerboni et al [8]. There, different, simultaneously recorded sEMG channels were decomposed using the discrete wavelet transform (DWT) before applying ICA.

In this study, both the sEMG signal and the ECG measurement (if present) are decomposed. In the case of the single channel approach, only the sEMG decomposition is used as input for the ICA algorithm, while for the approach with the two channels, both the sEMG and the ECG decomposition are used without any other preprocessing. After applying ICA on the decomposition, the sources containing the ECG contamination are set to zero and the sEMG signal is reconstructed.

Algorithm 2 wICA [106]

1: Select the mother wavelet of interest and the number of decompositions.
2: Apply the discrete wavelet transform on the sEMG signal to generate the decomposition.
3: If the simultaneously recorded ECG channel is present, apply step 2 on the corresponding ECG signal.
4: Perform the FastICA algorithm to the wavelet decompositions and derive the corresponding mixing and unmixing matrices $\mathbf{M}$ and $\mathbf{W}$.
5: Select the independent components (sources) of without the ECG interference and multiply it with mixing matrix $\mathbf{M}$ to back-reconstruct its appearance in the IMF set.
6: Sum over all the newly reconstructed wavelet decompositions to reconstruct the original sEMG signal cleaned from the ECG interference.

Template Subtraction

Template subtraction is a method that subtracts a data driven template of the artifact at its occurrence [12] in the signal. This method is at this moment still the golden standard in removing the ECG interference signal. ECG template subtraction uses the periodic characteristics of a heart beat in its electrophysiolical appearance. An ECG waveform template is subtracted from the sEMG signal at

each occurrence of the heartbeat. The moment of a heart beat can be localized very accurately from the QRS-complex in a simultaneously recorded ECG signal. This method has proven its ability to remove the ECG contamination artifact in previous studies and is, to our opinion, still the golden standard in removing the ECG artifact. The template subtraction is defined in the literature as a two-channel method where the corresponding ECG signal is present.

The two channel approach of the ECG template subtraction algorithm as described in [12] involves two steps. In the first step, a template of the ECG interference waveform is trained from the sEMG data. This is necessary because the waveform of the ECG contamination depends on the position of the electrodes and differs for each sEMG signal. From a training epoch selected in the sEMG signal, several 500ms sEMG signal segments each containing one heart interference signal are selected. One segment is selected by detecting the moment of QRS complex in the corresponding ECG signal and selecting the sEMG signal 250ms before and 250ms after this moment. The ECG template is calculated by averaging these different segments, assuming that sEMG has a zero mean Gaussian distribution. This results in a waveform template of ECG contamination of 500ms. In the second step, the template is used to clean ECG contamination in the complete muscle signal. At the occurrence of a heart beat, the ECG template is subtracted from the sEMG signal. Because the ECG template is data driven, the delay between the heart ECG signal and the ECG contamination in the sEMG is taken into account.

To have a fair comparison with the single channel wICA and EEMD-ICA, the template subtraction algorithm needs to be adapted to a single channel technique without the presence of the corresponding ECG signal. This adjustment is retrieving the occurrence of the heart beat from the sEMG signal itself. In the power spectrum of the contaminated sEMG signal, the ECG information is mainly present below 40Hz. Therefore, a bandpass filter of $5 - 40$Hz is used and this filtered sEMG signal is used to localize the ECG beats by applying the Pan Tompkins [120] algorithm. The further implementation of the algorithm is similar to the traditional two-channel approach: in a first step, the subtraction template is trained from the data itself and afterwards, this template is subtracted at the occurrence of a heart beat.

3.3.3 Data

Simulated Data

The simulation signals are derived from real-life contamination-free recordings. The sEMG signals are 60 second segments, selected from three different sEMG recordings (in the text referred as $ref(t)$) at different contraction levels. The signals are extracted from measurements of the right Biceps brachii muscle

and are not influenced by an ECG interference signal. This is confirmed by visual inspection in time and frequency domain of the sEMG signal. The ECG artifact templates were extracted from representative real-life contaminated sEMG measurements of the left and right trapezius muscle pars ascendens, transversus and descendens. Using these templates, seven artificially contaminated ECG signals (referred to as $ecg(t)$) are generated. The reference sEMG signals and artificial ECG signals are normalized. By mixing up the reference sEMG signals and the artificial ECG signals, a simulation data set is defined.

$$sig_i(t) = ref_e(t) + \lambda ecg_c(t) \tag{3.1}$$

with e the selected sEMG reference signal, c the simulated ECG contaminated signal and λ the proportion factor. For this study, λ was selected as one of the values (0.01, 0.1, 0.2, 0.5, 1, 2, 3, 5, 7, 10), resulting in 21 simulations per value of λ. An example is given in figure 3.5.

Real-life Data

The real-life signals were selected from both stress experiments as described in section 3.2. During visual inspection of the sEMG-signals, specific types of sEMG signals could be identified: muscle in rest, firing of a single motor unit, low force contractions, high force contraction, non-stationarity. 8 different sEMG segments are selected from the various recordings, each lasting for 30s. The selection was made to have a representative set of sEMG epochs compared to the complete data recordings of all the test subjects.

Validation

For the simulation data, the outcome of the ECG removal algorithms can be compared with the original reference signals for validation. Therefore, the relative root mean square error (RRMSE) is calculated to compare the performance of the different algorithms.

$$RRMSE(\%) = \frac{\sqrt{\frac{1}{N}\sum_{t=1}^{N}(ref(t) - \hat{a}(t))^2}}{\sqrt{\frac{1}{N}\sum_{t=1}^{N}\hat{a}^2(t)}} \times 100 \tag{3.2}$$

where $\hat{a}$ is the estimate of the signal of interest, $ref(t)$ the reference sEMG signal and N the number of samples.

For all the simulations, the number of independent components in ICA to be extracted was set to 5 according to the study by Mijovic et al (Mijovic, 2010) as he showed that 5 decompositions were sufficient. The EEMD-ICA and wICA algorithms were fully automated during the simulations. After applying ICA on the decompositions by both algorithms, the identification of the ECG sources is needed. Since the artificial ECG signal was available during the analysis, the independent ECG sources could be estimated automatically by analysing the correlation between the independent sources and the artificial ECG signal.

For the real-life data, the reference sEMG signal is not present, implying that the RRMSE cannot be calculated. Therefore, the outcome of the three different algorithms is visually scored by an expert regarding their performance in removing the ECG artifact. A good performance indicates a good removal of the ECG artifact while preserving the sEMG signal without distortion. The outcome of the three algorithms applied to the seven signals is scored regarding their removal performance of the ECG artifact (1 to 5; no removal to perfect removal) and their distortion of the sEMG signal (1 to 5; sEMG signal is completely removed to no distortion of the sEMG signal).

3.3.4 Results

The results of the algorithm during the simulations and real life data are presented. In the first part, the results of the single channel approach are presented where only the sEMG signal is available. In the second part, the results are shown when a corresponding ECG channel is used.

single sEMG channel

Figure 3.5 shows a fragment of a contaminated sEMG data. Several interference peaks of the heart are clearly visible in the data. The magnitude of the ECG interference is larger than the sEMG signal. On this signal, the EEMD-ICA algorithm is applied, resulting in 5 independent components derived from the ICA step. These independent components are shown in figure 3.6. ICA splits up the ECG interference and the sEMG signals in separate independent sources. Looking at the nature of the ECG contamination, we can identify the ECG sources as the sources number 2 and 4. These two sources are set to zero and the cleaned sEMG signal is reconstructed with sources 1, 3 and 5. Figure 3.7 shows the sEMG signal after reconstruction without the ECG interference sources. The ECG interference signal is visibly removed and the distortion of the reconstructed sEMG signal is limited. These figures reveal that the EEMD-ICA algorithm is able to remove the ECG artifact from a single sEMG measurement.

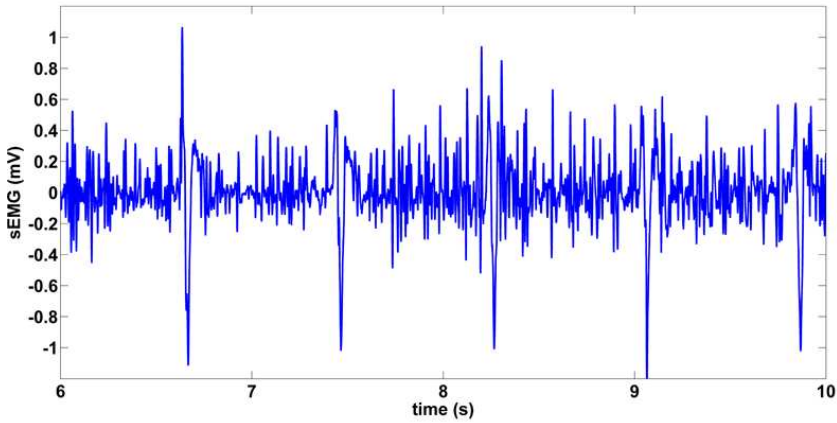


Figure 3.5: *Fragment of a typical sEMG with the ECG interference signal.*

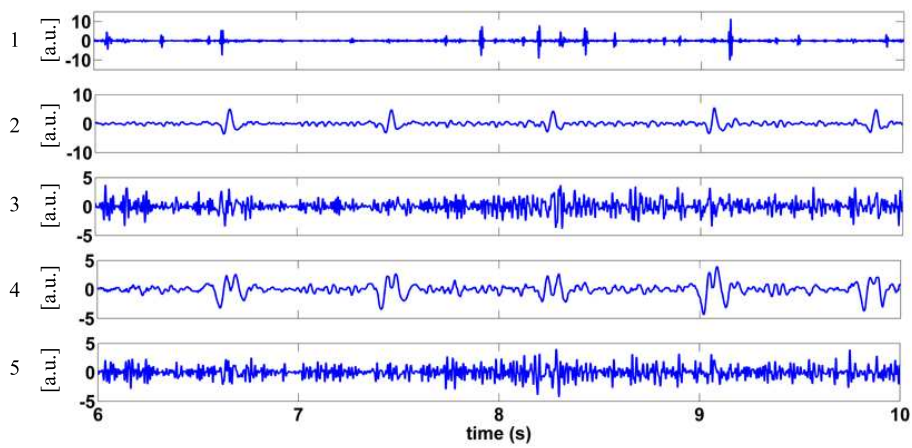


Figure 3.6: *5 independent sources after executing ICA on the IMFs after EEMD decomposition of the contaminated sEMG signal. Source 2 and 4 are related to the ECG interference signal*

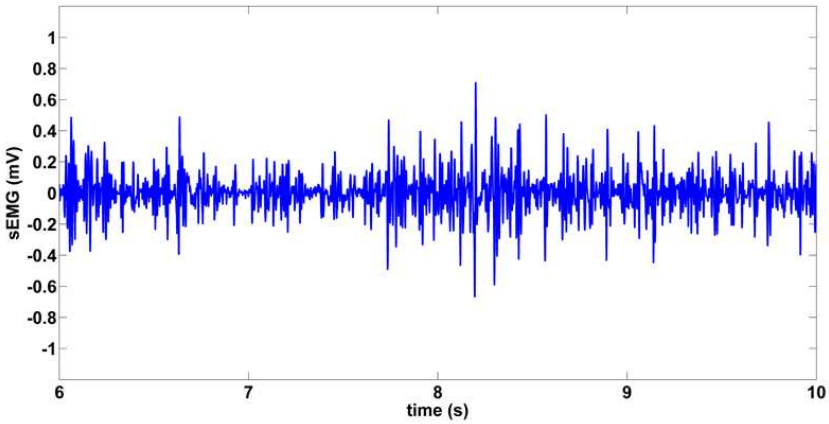


Figure 3.7: *Cleaned sEMG after ECG interference removal*

The noise parameter, the ratio of the noise standard deviation to the standard deviation of the signal power, and the number of trials have an impact on the outcome of the EEMD algorithm and are specific for the application. We need to look for the optimal number of trials and the optimal noise parameter. EEMD-ICA was executed on the simulation data set with varying EEMD parameters. The np varied between 0.2, 0.5 and 1 and the number of trials used for ensembling, varied between 100 and 200. Figure 3.8 shows the RRMSE for 6 different parameters. Each point is the mean of 21 simulations. To maintain the visibility of the figure, the standard error is not shown.

The simulations reveal that the selection of parameter settings has limited effect on the RRMSE in the range of -10 to 10dB. Only for higher and lower SNR, differences in parameter settings can be seen. For higher SNR, a lower np results in a lower RRMSE (green and black dot on the plot), while for lower SNR, a lower number of trials offers a better RRMSE (yellow and green dot on the plot). For higher SNR, the number of trials did not influence the results. Therefore, the decision is made to use a noise parameter np of 0.2 and an ensemble of 100 trials. These parameters will also be used for the decomposition of the simultaneous ECG signal in the two-channel approach.

Figure 3.9 shows the performance of template subtraction, the wICA and the EEMD-ICA method on the simulation data set when no simultaneous ECG signal was used. For a changing SNR the results are presented with their mean and standard error. The parameters used for the EEMD-ICA were set to 0.2 for the np and 100 for the number of trials as described earlier.

The discussion of the results of the algorithms using only the sEMG channel can be

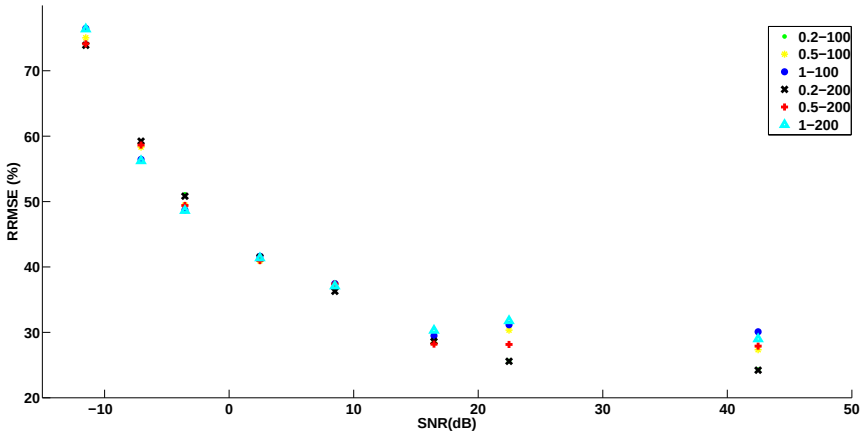


Figure 3.8: *RRMSE after removing the ECG contamination for various settings of the EEMD-ICA-parameters*

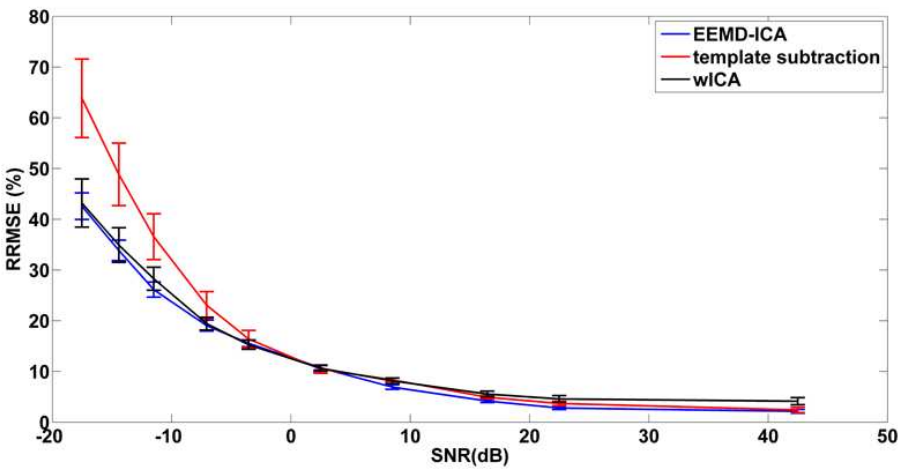


Figure 3.9: *Algorithm performances with only the sEMG channel available (RRMSE in %) for the described simulation. The results are presented as mean and standard error for the different SNR.*

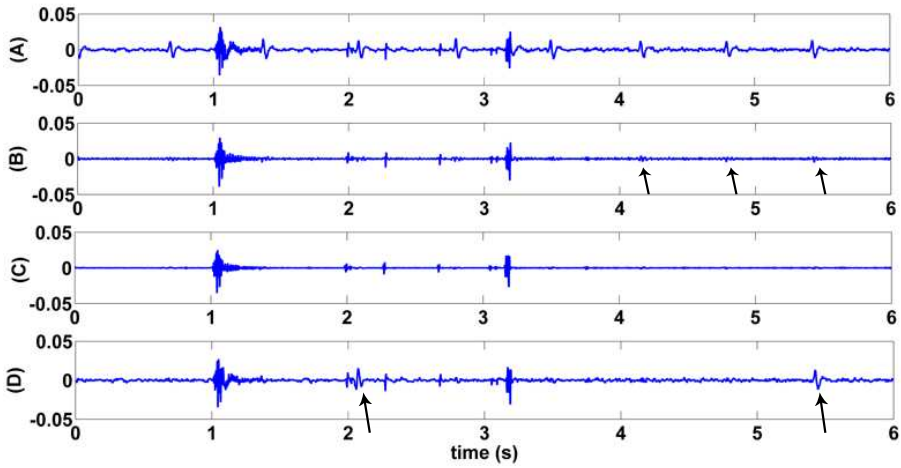


Figure 3.10: *ECG removal of a 5 second fragment of signal 2 using only the sEMG channel. (A) shows the original signal; (B) shows the result after wICA; (C) shows the result after EEMD-ICA; (D) shows the result after template subtraction.*

split up in two parts. Around the SNR of 2dB, the simulations reveal no difference between the three algorithms with a relative RMS error close to 10%. For higher SNR, where the power in the sEMG signal is higher than the power in the ECG interference signal, the RRMSE is lower than 10% for all three algorithms. The error made by the template subtraction and EEMD-ICA is similar to each other and is lower than the error using wICA. For the lower SNR, both ICA based algorithms perform much better compared to the template subtraction.

Figure 3.10 (a) shows a 5 second fragment of a representative real-life sEMG signal (signal 2 in table 3.1) where the ECG interference needs to be removed. The outcome of the wICA, the EEMD-ICA and the template subtraction algorithm is plotted respectively in figure 3.10 b, c and d. Both ICA based algorithms are able to reduce the ECG artifact completely, while template subtraction (D) induces a subtraction artifact at one ECG peak in this fragment. When examining the outcome of the wICA (B) algorithm, small residues of the artifact are still present. Only EEMD-ICA (C) is for this specific example able to remove the artifact perfectly. Both wICA and EEMD-ICA remove the baseline drift, and no distortion of the sEMG signal has been noticed. An overview of the removal of the ECG interference interference of all the real-life signals is shown in appendix A.

Table 3.1 gives the scores for the performance of the three algorithms on the real-life data set using the single channel approach. A general trend can be noticed. Both

Table 3.1: *scores on the performance of the three algorithms when applied to 8 real-life signals (numbered in the 1st column from 1 to 8) using only the sEMG channel. The scores range from 1 (very bad) to 5 (perfect).*

	ECG removal			EMG distortion		
	Templ Subtr	wICA	EEMDICA	Templ Subtr	wICA	EEMDICA
1	4	5	5	5	5	5
2	2	4	5	5	5	5
3	4	3	5	5	4	4
4	5	5	5	5	5	5
5	4	5	5	5	5	5
6	4	5	5	5	5	5
7	5	5	5	5	5	5
8	5	5	5	5	4	5

ICA algorithms perform better compared to the template subtraction in terms of removing the ECG artefact. On the other hand, template subtraction does not distort the sEMG signal, while wICA and EEMD-ICA did for several sEMG signals. This problem is more present for wICA compared to EEMD-ICA. Signal 6 shows a distortion of the sEMG signal after applying template subtraction, in contrast to wICA and EEMD-ICA. This reduced performance for template subtraction is caused by the presence of the 50Hz component in this signal. Both ICA based algorithms extracted this component as a separate independent source, which was removed in the ICA step.

sEMG and ECG channel

For the two-channel approach, the same parameters as for the single channel approach are used for EEMD (2 and 100 respectively for the noise parameter and number of trials). Figure 3.11 shows the performance of template subtraction, the wICA and the EEMD-ICA method on the simulation data set using both the ECG and the sEMG channel. The largest improvement is the performance of the template subtraction algorithm for lower SNR. Here, this algorithms achieves the best performance of the three described algorithms. For higher SNR, EEMD-ICA still performs the best of the three algorithms.

Figure 3.12 shows the outcome after removing the ECG interference signal of the same sEMG fragment of figure 3.10, but here the corresponding ECG channel is included to remove the interference signal. The results reveal that the ECG channel has no influence on the outcome of the EEMD-ICA and the wICA algorithm. An improvement is noticed for the performance of the template

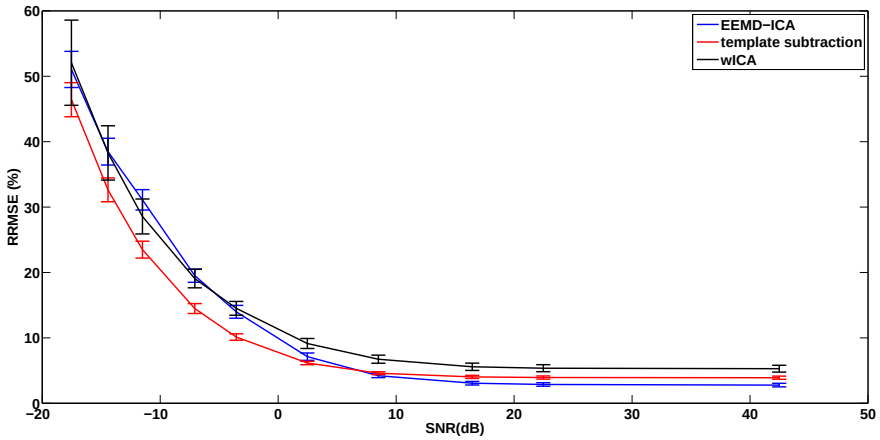


Figure 3.11: *Algorithm performances in the two-channel approach with sEMG and ECG simultaneously available (RRMSE in %) for the described simulation. The results are presented as mean and standard error for the different SNR.*

subtraction (D). Because the extra ECG channel allows a perfect localization of the occurrence of the interference signal, the subtraction of the interference waveform is more accurate and less subtraction artefacts are induced. A similar tendency can be concluded, looking at table 3.2. The differences with the single sEMG approach, shown in table 3.1, are indicated in bold. Template subtraction is able to remove all the ECG interference signals, whereas this was not the case when using only the sEMG signal. The ICA based algorithms show no improvement. An overview of the removal of the ECG interference interference of all the real-life signals is shown in appendix A.

Computational time

Table 3.3 gives an overview of the mean time needed to remove the ECG interference signal using the three techniques. The EEMD-ICA is slowest of the three techniques. The two-channel approach needs to decompose both the sEMG and the ECG channel using EEMD. The EEMD is an iterative algorithm that needs to be executed 100 times for noise robustness.

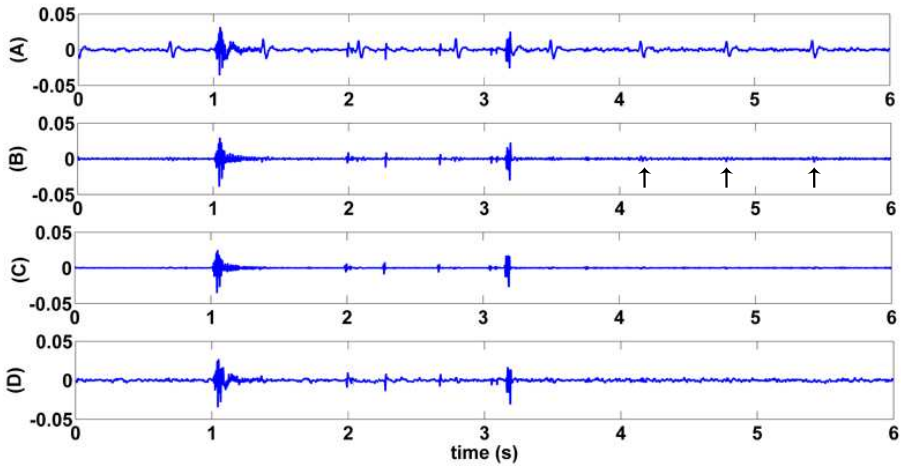


Figure 3.12: *ECG removal of a 5 second fragment of signal 2 using the simultaneous sEMG and ECG channel. (A) shows the original signal; (B) shows the result after wICA; (C) shows the result after EEMD-ICA; (D) shows the result after template subtraction.*

Table 3.2: *scores of the performance of the three algorithms using both sEMG and ECG channel when applied to 8 real-life signals (numbered in the 1st column from 1 to 8). The scores range from 1 (very bad) to 5 (perfect).*

	ECG removal			EMG distortion		
	Templ Subtr	wICA	EEMDICA	Templ Subtr	wICA	EEMDICA
1	**5**	5	5	5	5	5
2	**5**	4	5	5	5	5
3	**5**	**4**	5	5	4	4
4	5	5	5	5	5	5
5	**5**	5	5	5	5	5
6	**5**	5	5	5	5	5
7	5	5	5	5	5	5
8	5	5	5	5	4	5

Table 3.3: *Computational time to remove the ECG interference signal. Time is give in mean ± SD.*

	sEMG	sEMG + ECG
template subtraction	0.92 ± 0.08s	0.91 ± 0.09s
wICA	1.1 ± 0.09s	1.6 ± 0.10s*
EEMD-ICA	446 ± 49s	865 ± 53s*

* Significant difference with the one channel approach($p < 0.05$)

3.3.5 Discussion

The use of independent component analysis for removal of ECG artifacts has been described before [8]. However, all these algorithms are using a simultaneously acquired ECG channel as input. These algorithms show good performance in removing the ECG. In real-life measurements, a simultaneously recorded ECG channel is not always available, making the removal of the ECG artifact more complicated. In this study, we used recently developed single channel ICA techniques, described in the literature, to remove the interference signal and compared it with a widely used technique. The single channel is first decomposed into a multichannel signal using wavelets or ensemble empirical mode decomposition. The multichannel decomposition is then used as input to a subsequent independent component analysis in order to remove the ECG interference.

Both ICA based methods are able to remove the ECG artifact from the sEMG channel and perform better compared to template subtraction as soon as the ECG artifacts become more dominant (lower SNR). This can be explained by the limitations of the template subtraction technique. The algorithm uses the quasi-periodic property of the ECG artifact but assumes a constant waveform of successive heart beats. Furthermore, perfect localization of the occurrence of the heart beat is needed. If one of these assumptions is not fulfilled, the algorithm will introduce subtraction artifacts. In reality, the successive waveforms are slightly varying and perfect localization in the sEMG signal itself is more difficult, which is revealed in figure 3.10 for the real-life data. These subtraction artefacts are not present when the corresponding ECG channel is used (see figure 3.12). Thus, the larger the ECG interference signal is compared to the background sEMG signal, the larger these subtraction artifacts are. This explains the higher RRMSE for lower SNR. These limitations do not hold for both ICA based algorithms as these algorithms exploit statistical properties of both underlying signals to separate them.

The difference in performance between the results of wICA and EEMD-ICA can

be explained via differences in decomposing the original signal. The EEMD is a data-driven method and has a more natural decomposition, without a predefined base like the wavelet decomposition, that is able to cope with nonstationarities in the signal. Contrary to the wavelet decomposition, the extracted intrinsic mode functions can be spectrally overlapping. This leads to a more natural selection of the independent sources of the ICA afterwards, explaining the small differences in favor for the EEMD-ICA.

When the corresponding ECG channel is present, the performance of the template subtraction improves. The localization of the interference signal is more accurate and the subtraction of the interference waveform is better and less subtraction artefacts are induced. On the other hand, the ECG channel does not improve the performance of the wICA and the EEMD-ICA algorithm. The explanation is that the ECG channel in its pure form does not provide extra information. The waveform of the ECG interference signal and the corresponding ECG measurement are not equal and there is a delay between the ECG interference and the ECG channel. The results reveal that adding an extra channel do not offer extra information in the ICA decomposition.

A major drawback of the EEMD-ICA algorithm is its computational cost. The empirical mode decomposition is a data driven, iterative process of selecting local maxima and minima for each empirical mode. This is a computationally intensive decomposition. The noise robust extension of EMD, called ensemble EMD (EEMD), needs more time as the algorithm ensembles the outcome of at least 100 trials of a single EMD. In contrary, the wavelet decomposition is a straightforward method based on a predefined wavelet waveform. The computational load of wICA is similar to that of template subtraction, while EEMD-ICA is in the order of 300 times slower. This high computational load makes a real-time implementation impossible.

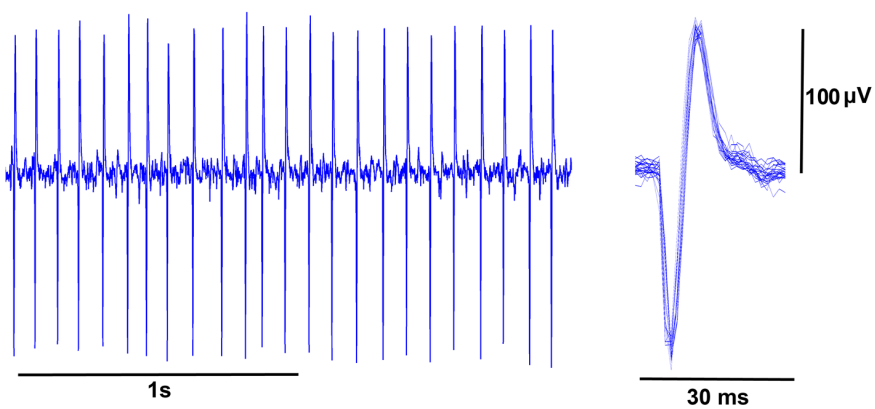
In general, when the corresponding ECG signal is not available, EEMD-ICA is better compared to wICA and yields similar performance as the template subtraction for higher SNR, while for lower SNR, EEMD-ICA is significantly better than template subtraction and slightly better than wICA. We can conclude that for offline use, EEMD-ICA has the best performance. When the ECG channel is present, the template subtraction is preferable.

For the removal of the ECG interference signal in the data, described in 3.2, template subtraction is used. The corresponding ECG channel was present for these measurements, which explains this decision. The results in this section showed that the performance of template subtraction is better compared to both ICA-based approaches and the computational time of the template subtraction is shorter compared to both ICA-based techniques.

3.4 Single motor unit firings: Detection algorithm

3.4.1 Single Motor Unit Firing

When analyzing the sEMG signals of the trapezius muscle parse descendens of the first experiment, a specific pattern was observed during the conditions without postural load: long lasting bursts of peak activity. Figure 3.13(a) shows a fragment of 2 seconds of a sEMG signal with this phenomenon. The peaks appeared at a rate of approximately 12 peaks per second. It is physiologically impossible that these peaks are the interference signal of the heart, although the shape is very similar to an ECG interference peak. The consecutive peak shapes are very similar. This can be seen in figure 3.13(b) where the peaks are plotted one on each other. We could conclude that this burst of peaks is a single motor unit action pulse train of a low-threshold motor unit. In this manuscript, we will refer to this as a single motor unit firing (SMUF). This sEMG signal differs from a common sEMG signal, induced by a normal and conscious contraction where several motor units are recruited for contraction and is an extra and undesired load of the active muscle fibers, possibly leading to musculoskeletal disorders due to exhaustion of this type of muscle fibers. Moreover, this contraction was present during conditions where the subject was informed not to change posture or move his hands. Possible conscious contractions during this period were of very short duration (less then 1 second). This is additional evidence that this type of muscle contraction is unconscious.



(a) (b)

Figure 3.13: *the left figure (a) shows an example of a spike train from a single motor unit of 2s. The right figure (b) plots the different spikes on top of each other [156].*

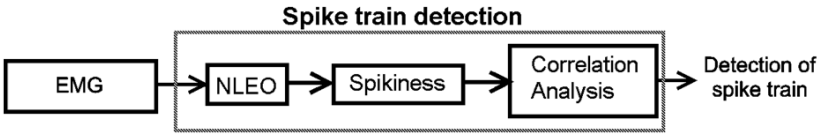


Figure 3.14: *Schematic overview of the spike train detection algorithm consisting of three consecutive steps: segmenting the high energetic part using the non linear energy operator, extracting different spikes and calculating the correlation between the spikes [156].*

Research has been devoted in understanding the behavior of this type of low-threshold motor units during low force contractions from the trapezius muscle with respect to the motor unit recruitment and derecruitment [184], conduction velocity [47] .... These low-threshold motor units were also a topic of research during stress monitoring where their behavior was studied during tasks of mental stress [152, 185]. In contrast to our study where single channel differential sEMG measurements on the surface of the skin were used, these motor unit firings were visible with measurements using invasive wire electrodes.

The sEMG signals, 6 per test subject and 28 subjects, were visually inspected by two independent experts and this type of activity was identified as low threshold motor unit firings. All segments with this single motor unit firing were labeled. The inclusion criteria were spiky activity as shown in figure 3.13(a), with isolated spikes and lasting for at least 10 spikes.

The observation, the detection algorithm and the results of the detection are published in the journal paper in Methods of Information in Medicine [156].

3.4.2 Detection algorithm

To detect the spikes in sEMG signals, we used the spike train detection algorithm as described by Deburchgraeve et al. [38]. The latter algorithm is developed for the detection of seizures in the EEG of neonates and is fully automated. This detection algorithm was adapted to our needs and consists of three consecutive steps as shown schematically in figure 3.14.

In a first step, high energetic parts of the EMG are segmented using a Non Linear Energy Operator (NLEO) proposed by Kaiser [81].

$$\psi_{kaiser}[x_n] = x_n^2 - x_{n-1} \cdot x_{n+1} \tag{3.3}$$

With basic properties:

$$\psi_{kaiser}[x_n] = A^2 \sin^2(\omega_0 n) \tag{3.4}$$

This operator is proportional to the square of both the immediate frequency and amplitude. Because of these properties, the NLEO amplifies the high-frequency spikes of the spike train relative to the background EMG, facilitating the segmentation. We can conclude that the NLEO accentuates the spikes. Here, the version described by Plotkin et al [125] is used which is more robust to noise.

$$\psi_{kaiser}[x_n] = x_{n-l} \cdot x_{n-p} - x_{n-q} \cdot x_{n-s} \tag{3.5}$$

$$l + p = q + s \tag{3.6}$$

The parameter settings were $l = 1$, $p = 2$, $q = 0$ and $s = 3$ for local energy calculation [37]. The NLEO calculates the energy of the signal based on only a few samples and is very local in time. The spikes have a magnitude of around 30ms as shown in figure 3.13(b). Therefore an extra smoothing (4 samples) of the NLEO output is performed by using a moving average filter. With simple thresholding of the smoothed signal, segments with high energy are located.

The second step analyzes the spikiness of the detected high energetic segments. This spikiness implies that the spikes need to be 'isolated' in the EMG by comparing the energy of the detected segment with its immediate background activity. The spikiness is calculated using formula 3.7. The segment in the formula is defined as the period of the smoothed NLEO that crosses the threshold. The background is period of activity of 50ms before and after this segment.

$$spikiness = \frac{max(segment)}{mean(background)} \tag{3.7}$$

The final step is the correlation analysis. To detect the occurrence of a repetitive pattern of segments, a correlation scheme was developed that grows a set of highly correlated segments with a correlation of 0.9 between two consecutive segments [38]. If more than 10 correlated segments are detected (approximately 1 second of single motor unit firing), the segments are classified as spikes of a spike train. Finally, the output of the algorithm is a set of highly correlated, high energetic spike-like segments corresponding to the spikes of the spike train.

Table 3.4: *Results of the detection of the single motor unit firings in the trapezius muscle using the described algorithm.*

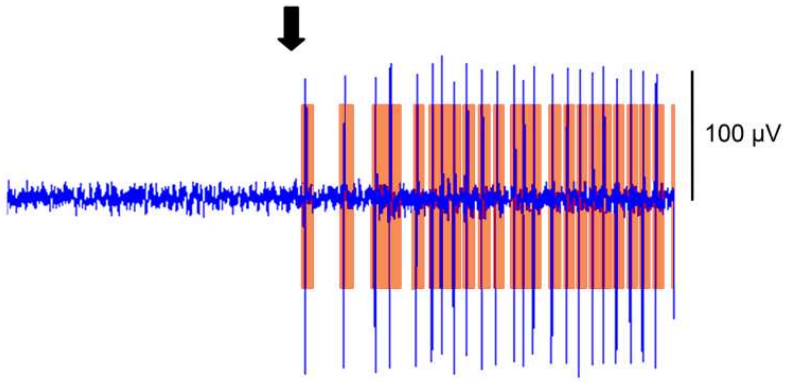
Description	Results
Presence of single motor unit firings	18 out of 28 subjects
Segments determined as single motor unit firings	74
Detected segments	78
Correct detections (true positives)	74
Sensitivity	100%
Specificity	94.8%

3.4.3 Results

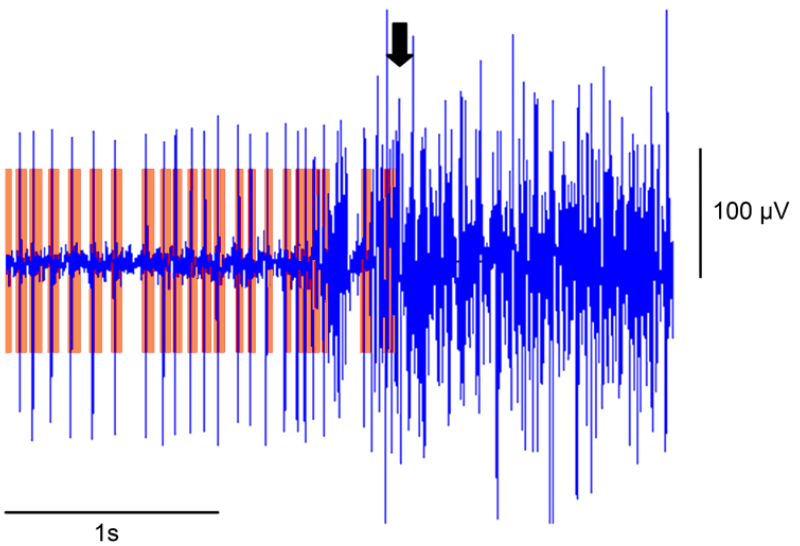
The analysis of this algorithm was performed on the data of stressexp 1 (section 3.2.1). The single motor unit firing was present in 18 out of the 28 test subjects on at least one of both trapezius muscles during a rest condition or during the condition with only the mental load. 74 different segments were observed with this single motor unit firing with an appearance rate from 1 up to 12 different segments per test subject, lasting from 10 to 189 seconds. In 6 of the 10 subjects without single motor unit firings, there was no muscle activity at all during the rest conditions or the mental condition. The other 4 subjects showed continuous muscle activity on both trapezius muscles and no single motor unit firing could be distinguished. These single motor unit firings were found only in the trapezius muscle and not on the sEMG signals of the other two muscles (deltoideus and infraspinatus muscle). The algorithm was performed on the complete data. However, only results during rest and the mental load condition are shown. This single motor unit firing could not be found during the postural condition (with and without mental load). This explanation is straight-forward as the trapezius muscle is a prime mover for shoulder abduction. For a conscious contraction, several motor units are firing, making the detection of a single motor unit impossible with the differential measuring method we used.

Figure 3.15(a) shows the beginning of a spike train. This is the same spike train as shown in figure 3.13. Initially, the muscle is at rest and on the moment of the black arrow, a single motor unit starts firing. This is detected by the algorithm. There was no change in posture noticed at this moment when analyzing visually the recorded movie. Figure 3.15(b) shows the end of the same spike train. The black arrow indicates the initiation of the shoulder abduction. This whole spike train with firings from a single motor unit (see figure 3.13) lasted in this particular case 46 seconds. These figures show that the algorithm is able to detect the spike trains originated by the firing of a single motor unit.

Table 3.4 gives an overview of the performance of the detection algorihtm. The



(a) Single motor unit firing on the trapezius muscle during the rest condition.



(b) Single motor unit firing before the shoulder abduction in combination with the mental task.

Figure 3.15: *Two examples of the performance of the detection algorithm [156].*

algorithm reached a sensitivity of 100% as all 74 segments with single motor unit firings were detected. The algorithm detected 4 more segments as single motor unit firings, leading to a specificity of 94.8%. By inspecting these false positives, it appeared that they were not really single motor unit firings, but at these time instants, there were just a few (2 or 3) motor units firing. These segments were not selected as single motor unit firings, but they are also not recognised as regular

sEMG contractions.

The sEMG signals of stressexp 1 were used for the analysis and validation of the algorithm. During the analysis of stressexp 2, this single motor unit firings on the trapezius pars descendens muscle was visible in 31 of the 43 subjects. In the 12 subjects without this pattern, 8 showed no activity in this muscle. In the other 4 cases, the muscle was fully active during the whole test, and no single motor unit firings could be distinguished.

3.4.4 Discussion

In this section, a special type of muscle contraction is described, discovered during a laboratory test. During the stress test, the participants were performing a mental task in combination with and without a postural task. In 65% of the test subjects, a pattern of the firing of a single low-threshold motor unit on the trapezius muscle was present. This is remarkable as the measurement of the electrical activity was a differential single channel measurement on the surface of the skin and not an invasive measurement with wire electrodes.

These specific patterns provide clear evidence of spontaneous muscle activity in the trapezius muscle. This type of activity is not seen in the other measured muscles: m. Infraspinatus and m. Deltoideus. The physiological meanig of a single motor unit firing is a very low contraction of the muscle performed by a limited number of muscle fibers, frequently performed subconsciously. Rekling et al [133] showed in their review study that the changes in the noradrenaline hormone, induced by mental stress, cause an increased excitability of the type I motor neurons due to a lower current threshold to induce repetitive firings. They assume that the trapezius muscles have more noradrenalin receptors and are part of the basic stress response of the body. This is in accordance with the fight-or flight reaction where the body is prepared to fight or to flight. The arms of the subjects are the front paws of the animals. Putting pretension on the muscles in the shoulder girlde enables a faster reaction for fighting or running away. Westgaard [185], however, considers that this low-threshold motor unit activation may come possibly from respiratory activity as they found respiratory modulation of the firing rate of single motor units. In this study, no respiration signal was measured, so this could not be verified. In chapter 4, we will show via heart rate variability (HRV) analysis that stress was induced during the mental task. Despite this, we have found this single motor unit firing in both the condition with rest and with the mental task. To link this activity with mental stress, we would have expected to see this activity more frequently during the condition with the mental load. Perhaps, the test subjects were not at ease during the rest periods, or were nervous for their results, but this would have been reflected in the HRV analysis, which was not the case.

We can not exclude completely that there is more than one motor unit firing and that this motor unit is outside the detection area of the detection volume. However, we reduced this possibility by placing the electrodes on the muscles according to SENIAM guidelines [57], to achieve more uniformity in the sEMG measurements. Therefore, guidelines are developed for muscles close to the skin surface with the optimal placement of the electrodes to achieve the best possible quality of sEMG signals and to have as many motor units in the detection volume as possible. A sustained contraction of a muscle fiber leads to exhaustion of that fiber, resulting in MSD. They may be significant for prevention of shoulder muscle strain injuries. These spontaneous firings of muscle fibers without contribution to physical activity should be avoided and therefore a detection algorithm is beneficial to make the subject aware of the muscle activity [146]. The presented algorithm showed excellent performance in localizing this specific type of muscle activity. Due to the simplicity of the presented algorithm, it shows potential to be used in a real time biofeedback system.

Further research is necessary to draw conclusions on the origin of these firings which might better motivate the benefits of detection of this phenomenon. In future research, we suggest to use high density sEMG, to have both spatial and temporal information of the muscle activity.

3.5 Rest Level Estimation

3.5.1 Introduction

During stress assessment algorithms, the estimation of the reference rest level of the sEMG signals is needed. During most tests, a baseline session is included in the protocol to determine the rest level. An initial baseline measurement before the measurement is often used, but however it can have ambiguous results, with no guarantee that subjects can definitely relax. A common method to estimate the rest level of a sEMG measurement without reference baseline is to determine, by agreement, a threshold at a certain percentage of the sEMG value during the maximal voluntary contraction (MVC). In the literature, common measures are ranging from 1 tot 5% of MVC [32, 139, 143, 167]. When the RMS value is above this threshold, the muscle is considered as active; while values below this threshold indicate a muscle in rest. When validating the rest level of the data described in section 3.2 visually, the rest level of the sEMG data ranged from 0.3 to 3.5% MVC. This range implies that a threshold on the MVC value is not reliable for indication of the rest level of the sEMG signal. When taking the threshold too high, for example, a value of 2%MVC, for several muscles this already is indicative for a muscle in contraction, while for other muscles this is not even the level of a muscle in rest.

To overcome these problems, there is a need to estimate the rest level of an sEMG signal for every single sEMG measurement. Therefore, we proposed a new, data driven method, to estimate the rest level of the muscle to automate this process: Rest Level Estimation (RLE). This method uses properties of the frequency domain of a sEMG signal.

This algorithm has been presented at the Annual Symposium of the IEEE/EMBS Benelux Chapter, Heeze (The Netherlands) in December 2007 [158].

3.5.2 Rest Level Estimation Algorithm

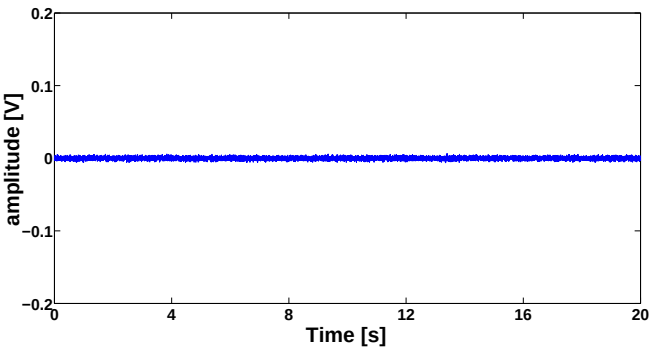
Figures 3.16 and 3.17 show representative sEMG signals from respectively a muscle in rest and a muscle in contraction. The top plot shows the time domain of the sEMG signal and the bottom plot presents its corresponding PSD plot. The frequency content from a muscle in rest is mainly noise. There is no contraction and no electrical activity is recorded. The active muscle shows that most energy in the frequency domain is below 200 Hz. Bearing this in mind, 2 regions in the frequency can be defined [13, 104]:

- 10-200Hz: dominant frequencies in active state of the muscle.
- 300-500Hz: low energy in both rest and active state.

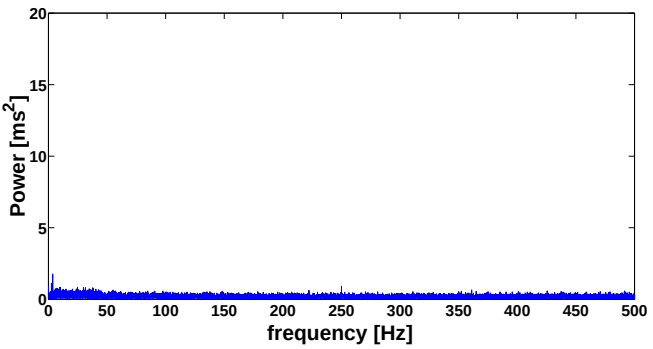
When calculating the ratio of the mean energy in both frequency bands, the ratio of a muscle in rest is approximately one, while the ratio for the muscle in contraction is much higher.

This parameter is used to distinguish between the active and the rest state of a muscle and not meant to deliver precise information on the state of activity. We can therefore filter out heuristic frequencies without losing information related to the state. In section 3.3, the interference of the ECG signal has been identified as a major source of noise of the sEMG signals, especially for the muscles in the shoulder girdle. The main energy of the ECG signal is below 40Hz [155]. Bearing this in mind, the active region is selected from 50-150Hz, to discard the ECG contamination and the power line interference. The rest level estimation value (RLE) is the ratio of the mean energy in the activity band (50-150Hz) in the frequency domain and the lower activity band (350-500Hz) as presented in the equation below.

$$RLE = \frac{\frac{1}{150-50}\int_{50}^{150} PSD_{EMG}(f)df}{\frac{1}{500-350}\int_{350}^{500} PSD_{EMG}(f)df} \tag{3.8}$$



(a) Time domain



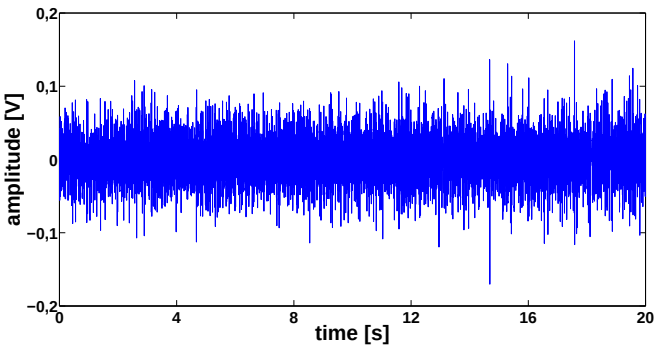
(b) Frequency domain

Figure 3.16: *sEMG signal from a muscle in rest. 3.16(a) shows the signal in time domain, 3.16(b) shows the signal in frequency domain.*

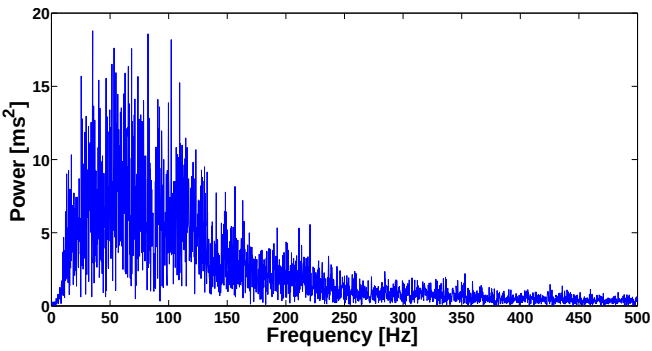
Where PSD_{EMG} is the PSD of the sEMG signal of interest.

This ratio is approximately one for a muscle in rest while for a muscle in contraction this ratio is much higher (typically >20). The exact value of this ratio depends on different factors like the amount of produced force, the amount of muscle fatigue, the overall fitness of the muscles and so on, but for each contraction, this ratio is much higher than one. As we are interested in the distinction between a muscle in rest and an active muscle, these flutctuation of the ratio do not influence the decision whether a muscle is in rest. We can set intuitively a decision threshold, where a higher ratio depicts an active muscle and a lower value of RLE is equivalent for a muscle in rest.

To apply this algorithm on a larger data set, the PSD is calculated based on a time window of m samples and the ratio of the mean power in both frequency bands is



(a) Time domain



(b) Frequency domain

Figure 3.17: *sEMG signal from an active muscle. 3.17(a) shows the signal in time domain, 3.17(b) shows the signal in frequency domain.*

derived. The window is shifted afterwards over n samples. In this study, we use a time window of m = 125ms and a shifting of n = 25ms. The distinction between the active and rest state is made on this series of RLE-values.

3.5.3 Results

Simulations

To find the optimal threshold value to discriminate between a muscle in rest and a muscle in contraction, a simulation study is executed. Different 10 second recordings from the biceps bracchii muscle, the deltoideus muscle and the trapezius muscle in rest is used. On top of one of these sEMG signals, the sEMG signal

from a contraction of 5s is superimposed. We selected 10 different sEMG signals of 5s muscle contractions, denoted as $\mathrm{EMG}_k(\mathrm{t})$, from different muscles: biceps bracchii muscle, deltoideus muscle, trapezius muscle, infraspinatus muscle. We selected also 10 different ECG signals. These ECG signals are derived from an ECG interference template, extracted from different muscles in the shoulder girdle. The ECG signals differ from each other with respect to the timing of the heart beats and waveform of the ECG interference. The amplitude of the different test signals is normalised. 1000 simulation signals are derived using equation 3.9. λ_m is proportional to the muscle contraction and ranged from 2 (a very small contraction) to 10 (a large contraction). This factor λ_m starts from 2 to ensure the presence of a muscle contraction within the simulation signal. λ_c is a factor proportional to the amount of ECG interference on sEMG signal. The value of λ_c ranged from 0 (no interference) to 10 (a large interference of ECG on the sEMG signal). The indices k and l select one of the 10 EMG respectively ECG channels. For each simulation, the moment of contraction, λ_k, λ_c, k and l are randomly chosen.

$$sig_i(t) = ref(t) + \lambda_m \cdot EMG_k(t) + \lambda_c \cdot ECG_l(t) \tag{3.9}$$

To validate, the total contraction time detected by the algorithm is plotted. This time was, by design, fixed to 5s. Figure 3.18 shows the mean contraction time ($\pm$ standard error) detected by the algorithm for the 1000 simulations in function of a changing threshold value. In the threshold range between 3 and 10, the algorithm estimates the correct contraction time while this is not correct for a higher or lower threshold value. Therefore, the threshold is fixed to value of 5.

Figure 3.19 shows the outcome of one the simulations with $\lambda_c = 7$ and $\lambda_m = 4$. The top figure shows that the ECG signal is overwhelming the sEMG signal. The RLE signal however is able to enlarge the period of muscle contraction to facilitate a distinction between rest and contraction. In this specific case, the threshold is set to 5.

Real Life Examples

Figure 3.20 shows an example where the active muscle is distinguished from the muscle in rest using this RLE algorithm. In the top chart, a raw EMG signal is shown with two large contractions and several smaller contractions in between. The ECG interference signal was not removed from the sEMG signal. The middle chart shows the RLE equivalent derived from the raw signal. This signal differs substantially between the rest and active states. The threshold is set to 5 as derived from the simulations, but the RLE-values range from 1 to over 200. A clear distinction could be made between a muscle in contraction and a muscle in rest. The lower chart shows the original sEMG signal with the active/rest state,

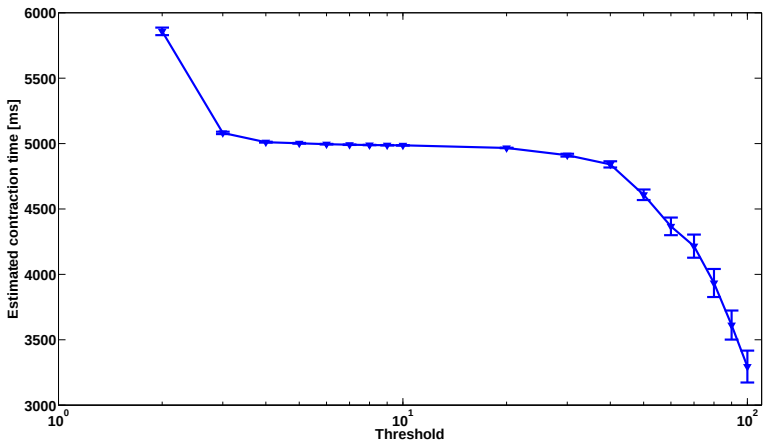


Figure 3.18: *The estimation of the contraction time for a changing threshold (log scale). The mean contraction time ± standard error is plotted.*

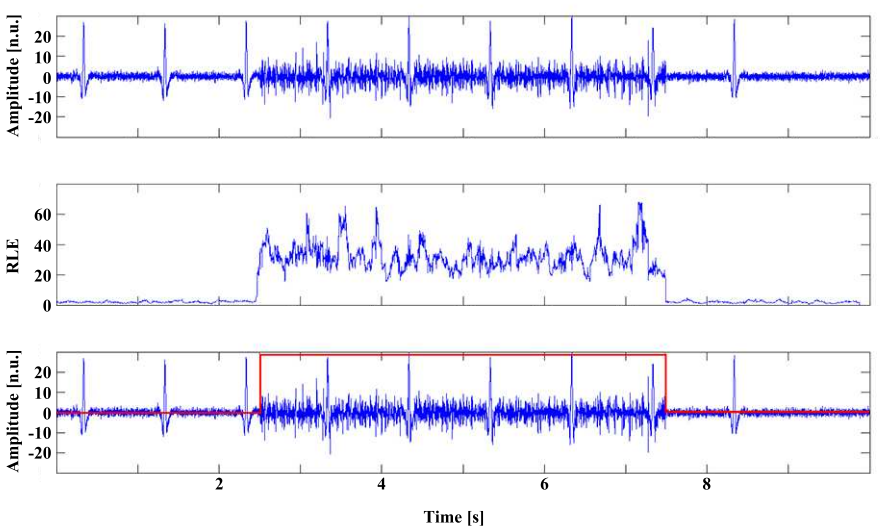


Figure 3.19: *sEMG simulation signal (top), the RLE equivalent (middle) and the active/rest state on top of the sEMG signal (bottom).*

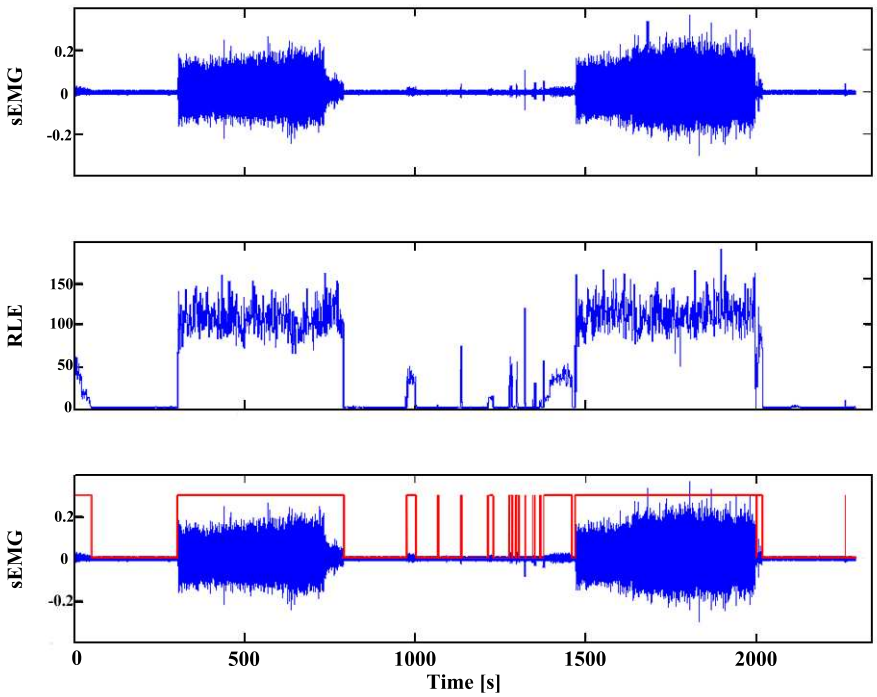


Figure 3.20: *Real life raw EMG signal (top), the RLE calculated from the raw EMG signal (middle) and the active/rest state of the muscle (below).*

estimated from the RLE value, superimposed. The match shows that the algorithm is able to make a clear distinction between rest and active states. Figure 3.21 enlarges on a period with several small active periods. Even with the presence of the ECG contamination in the raw signal, the algorithm is still able to distinguish very small periods of muscle activity from periods of rest, which are very difficult to detect with the commonly used thresholding in the time domain. In offline analysis, the ECG contamination signal can be removed before further analysis (as described in section 3.3), but for real-time usage, robustness to the ECG interference signal makes this a strong algorithm.

An application of this algorithm is to estimate the baseline values for the sEMG parameters, used in this manuscript. The baseline value is defined as the mean value of the sEMG parameters when the muscle is in rest. For the deltoideus and the infraspinatus muscle (section 3.2), the estimation of the rest period is straight forward: when no physical activity is imposed, these muscles are at rest. The behaviour of the trapezius muscle however is more complex. In section 3.4, the spontaneous activity of several muscle fibers of the trapezius muscle were

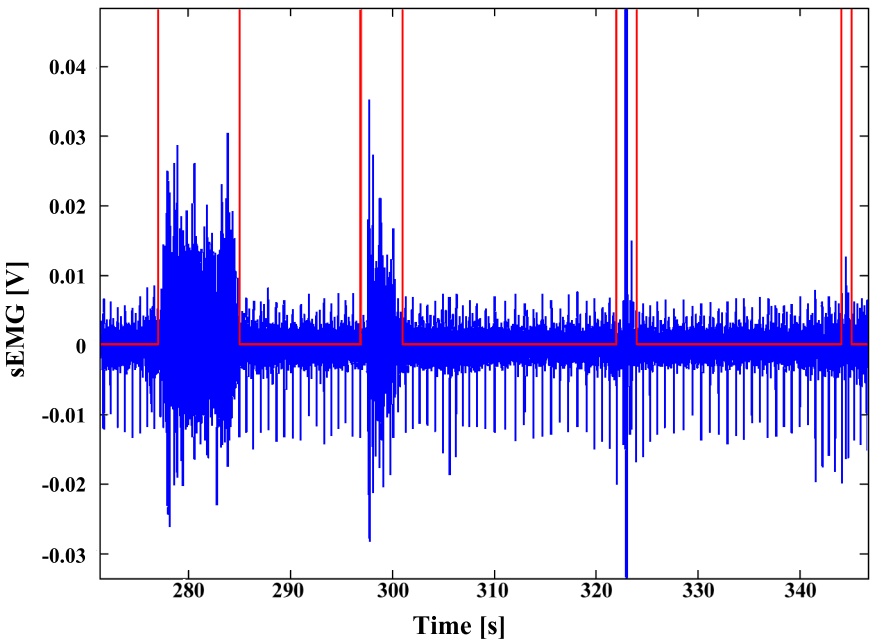


Figure 3.21: *Shows an enlarged part of figure 3.20. 4 separate periods of muscle activity can be distinguished from rest, even with the presence of ECG interference.*

described and in the literature, several studies report on muscle activity of the trapezius muscle in stress situations [6, 17, 50]. Therefore, we need to estimate the periods of rest using the sEMG information. The analysis is performed on the data of stressexp 1 (section 3.2.1) and an overview is presented in table 3.5. For each of the 6 muscles of the 28 subjects, the periods of true muscle rest are calculated from the sEMG signals using this algorithm. This mean RMS value of the rest sEMG signals is compared with the mean RMS value during the first rest period in the protocol, which is often used as the baseline session and where rest in the muscles is supposed, and with a manual estimation of the rest level. Periods without muscle activity are identified visually in the sEMG signals and the mean RMS value of the sEMG signals during this period is calculated. The values in the table are presented as percentage of the maximal voluntary contraction of each individual muscle. The table shows that there is no statistically significant difference between the value estimated using the RLE algorithm and the value which is estimated manually. These values differ from the RMS value estimated via the baseline session. Figure 3.22 shows the mean RMS value of each rest period (R1 is used as the baseline value in table 3.5) as percentage of the MVC, together with the RLE estimated value for the 6 muscles of interest (deltoideus,

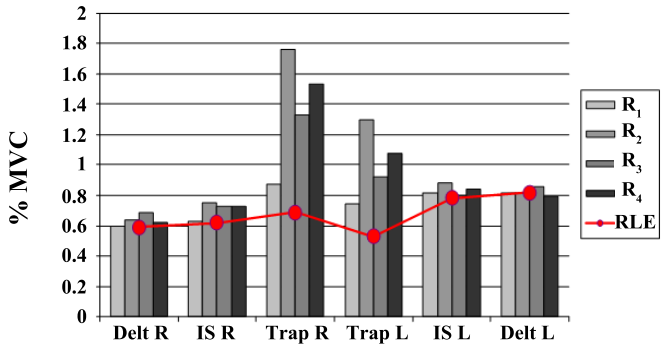


Figure 3.22: *RLE value versus mean RMS value for 28 subjects of stressexp 1 during 4 rest periods (Delt=m. deltoideus; IS=m. infraspinatus; Trap=m. trapezius; L=left; R=right).*

infraspinatus and trapezius left and right).

The figure confirms that the deltoideus and infraspinatus are in rest during the periods where rest is assumed. There is no difference between the rest level, estimated via RLE and the muscle activity during the rest periods. The results of sEMG analysis of the trapezius muscle confirm the behavior of the trapezius muscle: although no postural change is desired during the rest periods, there is muscle tension present. The rest periods 2 and 4 are the two rest periods following a physical load. These two periods show more muscle activity compared to the other two rest periods. These results reveal the need for a signal based estimation of the rest level of each muscle.

3.5.4 Discussion

In this section, an algorithm is presented that is able to distinguish between an active muscle and a muscle in rest based on the frequency content. There is clear distinction between the frequency content of a sEMG signal from a muscle in rest and a muscle in contraction and a feature could be extracted. We showed that with setting a threshold on this feature, we can easily differentiate between the two states. A feature of this type is beneficial for studies where the muscle of interest is very difficult to relax. We showed that there was muscle activity of the trapezius muscle during rest periods where no postural need of the muscle activity was present.

In several studies, the rest level is nowadays estimated when the sEMG amplitude is below a certain percentage of a maximal voluntary contraction (MVC). In literature, these values range from 1% to 5% of MVC [32, 139, 143, 167]. This

Table 3.5: *Estimation of mean RMS value of the rest sEMG signals using the baseline (base), the Rest Level Estimation algorithm (RLE) and manual estimation (real) of the 6 different muscles in stressexp 1 for the 28 subjects. (Values expressed in %MVC).*

	Deltoideus R			Infraspinatus R			Trapezius R			Trapezius L			Infraspinatus L			Deltoideus L		
subj	base	RLE	real	base	RLE	real	base	RLE	real	base	RLE	real	base	RLE	real	base	RLE	real
1	0,79	0,79	0,79	1,05	1,02	1,02	2,46	1,29	1,23	2,39	1,89	1,89	1,48	1,48	1,48	1,68	1,67	1,67
2	0,50	0,48	0,48	0,44	0,36	0,36	1,43	0,52	0,52	1,13	0,14	0,14	0,49	0,46	0,46	0,44	0,43	0,43
3	0,74	0,71	0,71	0,93	0,90	0,40	1,48	0,89	0,89	0,75	0,32	0,31	0,70	0,68	0,68	1,19	1,19	1,19
4	0,32	0,31	0,31	0,45	0,44	0,43	1,44	0,33	0,32	0,86	0,13	0,13	0,48	0,46	0,46	1,20	1,21	1,20
5	0,37	0,58	0,57	0,75	0,73	0,73	0,70	0,68	0,69	0,37	0,39	0,39	0,84	0,84	0,84	0,38	0,37	0,37
6	0,77	0,68	0,68	0,69	0,64	0,65	0,41	0,22	0,22	0,78	0,81	0,81	0,54	0,56	0,54	0,67	0,68	0,67
7	0,37	0,38	0,37	0,55	0,46	0,46	0,19	0,21	0,22	0,26	0,26	0,26	0,31	0,31	0,31	0,37	0,37	0,37
8	0,71	0,61	0,61	1,22	1,06	1,06	3,19	3,00	3,01	0,71	0,68	0,68	2,02	1,99	1,99	0,89	0,85	0,85
9	0,51	0,50	0,51	1,33	1,26	1,27	1,09	1,10	1,09	0,42	0,42	0,41	0,44	0,43	0,44	0,32	0,31	0,31
10	1,00	1,00	1,00	0,64	0,64	0,65	0,88	0,88	0,88	0,76	0,76	0,75	0,76	0,76	0,77	0,94	0,95	0,94
11	0,62	0,62	0,62	0,40	0,40	0,40	0,97	0,99	0,98	0,31	0,31	0,31	0,60	0,60	0,60	0,82	0,81	0,81
12	1,84	1,83	1,83	2,42	2,31	2,30	9,35	3,08	3,08	4,81	1,85	1,86	2,49	2,10	2,10	2,18	2,16	2,16
13	0,69	0,71	0,69	0,48	0,50	0,47	1,07	1,07	1,07	0,91	0,91	0,92	0,81	0,85	0,85	0,54	0,54	0,54
14	0,58	0,59	0,57	0,42	0,44	0,42	0,41	0,42	0,42	0,53	0,55	0,53	0,58	0,58	0,58	1,24	1,27	1,24
15	0,68	0,68	0,68	0,72	0,74	0,72	1,13	0,33	0,32	1,19	0,67	0,67	0,72	0,76	0,76	0,64	0,64	0,64
16	0,58	0,58	0,57	0,62	0,61	0,61	0,45	0,46	0,46	0,78	0,73	0,75	1,05	1,06	1,04	1,05	1,01	1,01
17	0,48	0,47	0,47	0,16	0,18	0,18	1,52	1,57	1,52	2,77	2,85	2,77	0,21	0,24	0,21	0,42	0,43	0,44
18	0,49	0,51	0,50	0,82	0,77	0,77	0,47	0,43	0,43	0,38	0,34	0,34	0,73	0,71	0,71	0,65	0,64	0,63
19	1,06	1,01	1,01	1,71	1,64	1,65	1,57	1,47	1,47	0,96	0,93	0,93	2,72	2,79	2,72	1,45	1,49	1,45
20	1,17	1,15	1,16	0,77	0,71	0,72	0,34	0,33	0,33	0,47	0,44	0,44	2,11	1,98	1,99	0,98	0,98	0,98
21	0,79	0,72	0,72	0,25	0,23	0,23	0,54	0,90	0,49	1,16	1,09	0,93	0,29	0,28	0,28	0,56	0,51	0,51
22	0,13	0,15	0,13	0,66	0,42	0,42	1,98	0,28	0,28	0,18	0,18	0,18	1,62	1,66	1,66	1,26	1,26	1,26
23	0,32	0,30	0,30	0,69	0,58	0,58	0,49	0,19	0,19	2,33	0,31	0,31	0,43	0,43	0,42	0,36	0,38	0,36
24	0,49	0,49	0,49	0,40	0,41	0,41	0,58	0,42	0,42	0,40	0,32	0,32	0,56	0,59	0,56	0,54	0,51	0,51
25	0,92	0,95	0,92	0,37	0,34	0,34	0,76	0,75	0,75	0,27	0,28	0,27	0,39	0,39	0,39	2,24	2,05	2,05
26	0,18	0,17	0,16	0,29	0,29	0,28	0,22	0,23	0,23	0,54	0,52	0,52	0,27	0,26	0,26	0,52	0,50	0,50
27	0,48	0,49	0,47	0,36	0,37	0,36	0,20	0,19	0,19	0,13	0,13	0,13	0,40	0,39	0,39	0,67	0,58	0,59
28	0,39	0,31	0,31	1,06	0,71	0,71	1,89	0,51	0,51	2,78	1,17	1,17	1,17	1,21	1,21	0,65	0,46	0,46

approach has two drawbacks: the first one is that there is a need for a reference measurement. A second drawback is that there is a fixed threshold, which is fixed before the study. When analyzing the signals during our experiments, we found values ranging from 0.3 to 3.5% MVC making the use of a fixed threshold unreliable. A data driven approach as described here is beneficial.

In the literature, several techniques that differentiate between rest and a muscle contraction exist [18, 59, 93, 140, 151]. These techniques use the amplitude information or statistical information of the sEMG signal to find the initiation of a muscle contraction. However, the application of these techniques is different: the main objective of these techniques is to estimate an accurate initiation of the muscle contraction which occurs in response to a stimulus. These methods are optimised to find this initiation after a period of rest. These methods have a very good time resolution and are more accurate for this specific application than the RLE method that looses the time resolution by using a windowed Fourier transform. As these methods need a reference rest period, they are not applicable in the presented applications.

The presented algorithm is computationally not complex and has therefore potential to be used in real time. A real time application where the algorithm can be applied is the battle against musculoskeletal disorders. Several studies showed that muscle recuperation and rest is essential in the prevention of musculoskeletal disorders [32, 67, 115]. This method can track in time the amount of rest compared to the muscle activation or count the number of EMG gaps [167].

3.6 Stress: Data analysis

In the last section of this chapter, the most important results of the interpretation of the sEMG signals during the stress assessment tasks (see section 3.2) are presented. The additive effect of a mental load on the muscle activity in the shoulder girdle is presented in the situation with and without an extra physical load. Afterwards, an indication of muscle fatigue is presented. We studied the individual sEMG profiles during the different subtasks.

Rest versus mental load

Comparing EMG amplitude (RMS) for MT_1 and RLE values for the first experiment showed a significant difference ($p<0.05$) for both trapezius muscles (see figure 3.23). The RLE value is selected to see the effect of the mental task on the total muscle activity as no muscle activity is expected for postural changes. These results are confirming the results in previous studies [98, 95] that the trapezius muscle is sensitive to a mental load and leads to an activation of this muscle.

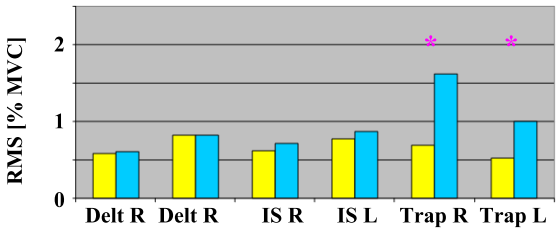


Figure 3.23: *Significant differences (*) between EMG amplitude (RMS) for MT_1 and RLE value for the data of stressexp 1(28 subjects; Delt=m. deltoideus; IS=m. infraspinatus; Trap=m. trapezius; L=left; R=right).*

Postural load versus combined mental and postural load

Conform to the findings that there is an increase in muscle activity in periods of mental load when the muscle should be in rest, we expected muscle activity during the combined mental and physical load (MPT) to be higher than activity during physical load (PT). Table 3.6) shows the results of the analysis of one muscle and one parameter during both experiments, but similar conclusions hold for the other parameters (ACT, MPF) and the other muscles. The results of the analysis of the stressexp 1 where the mental task was combined with a a shoulder abduction of 45° with stretched arms showed no significant change in muscle tension. The possible additive effect of the mental load was assumed to be low and was probably overshadowed by the muscle activity for the postural load. Therefore, stressexp 2 was deducted and the protocol was modified to answer this question. The postural task was to click a computer mouse, emulating a lower postural load more similar to office tasks. The new protocol also addressed earlier design issues: condition times were consistent, and the rest period was sufficiently long for subjects to relax muscles. The results for the second experiment were similar to the results of the first one. At a group level, muscle activity did not differ significantly for a postural task with or without a mental task for both the left and the right shoulder muscles. So no evidence could be found about the additional effect of the mental stress as induced with our mental task on the muscle activity.

Muscle fatigue

In the second experiment, the postural load for the three parts of the Trapezius muscle was very low during the entire test. During the clicking task, the right Trapezius muscle had a stabilizing function. The left arm was resting on the table during rest and active periods. Muscle fatigue was not expected to occur due to the low postural load. However, analysis of EMG signals showed that 13 out

Table 3.6: *Results of the comparison between the RMS parameter during postural load and combined mental and postural load for both stress experiments.*

Stressexp	Muscle	Parameter	Conditions	p-value
1	Trap D L	RMS	PT_1 - MPT_1	0.2141
1	Trap D R	RMS	PT_1 - MPT_1	0.1854
2	Trap D L	RMS	PT_2 - $MPT1_2$	0.9818
2	Trap D L	RMS	PT_2 - $MPT2_2$	0.4255
2	Trap D L	RMS	$MPT1_2$ - $MPT2_2$	0.4662
2	Trap D R	RMS	PT_2 - $MPT1_2$	0.3624
2	Trap D R	RMS	PT_2 - $MPT2_2$	0.0842
2	Trap D R	RMS	$MPT1_2$ - $MPT2_2$	0.0976

Trap D L: m. Trapezius pars descendens Left
Trap D R: m. Trapezius pars descendens Right

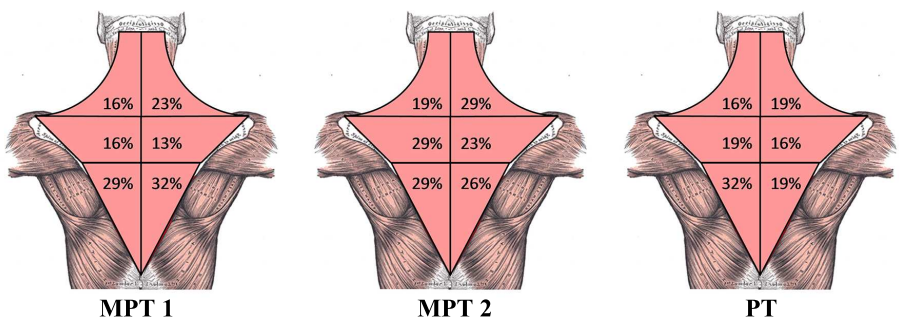


Figure 3.24: *Percentage subjects with muscle fatigue in specific muscles after specific tasks during experiment 2. MPT1 = first mental and postural task: MPT2 = second mental and postural task: PT = postural task.*

of 31 subjects (42%) experienced muscle fatigue in one or more muscles after 42 minutes. This phenomenon not only occurred in the right more active muscles, but especially in the left Trapezius muscle. Figure 3.24 shows the percentage of test subjects that showed signs of muscle fatigue after each individual task for the different muscles.

Muscle fatigue is defined [143, 150] as a variation of different sEMG parameters: a linear increase of the amplitude parameter (RMS), a linear decrease of the mean power frequency (MPF) and a constant activity parameter (ACT) and this was identified visually.

These observations are indications that not only the postural task, but also the extra mental effort plays a role. Muscle fatigue is a good indicator of potential

Table 3.7: *Most important p-values of the Spearman correlation analysis between the mean sEMG parameters (RMS: Root Mean Square, ACT: activity and MPF: Mean Power Frequency) and the questionnaires (PANAS, PSS: Perceived Stress Scale and DLC: Daily Life Complaints list) during stressexp 2.*

Muscle	Side	Questionnaire	Parameter	Condition	p-value
Trap T	Right	PANAS	RMS	Rest	0.0711
Trap T	Left	PANAS	MPF	PT	0.0621
Trap D	Left	PANAS	MPF	MPT1	0.0934
Trap D	Left	PSS	RMS	PT	0.0966
Trap D	Left	PSS	ACT	PT	0.0897
Trap D	Left	PSS	RMS	MPT1	0.0651
Trap D	Left	PSS	ACT	MPT1	0.0651
Trap T	Right	DLC	RMS	Rest	0.0834
Trap A	Right	DLC	RMS	Rest	**0.0025**
Trap A	Right	DLC	RMS	PT	**0.0130**
Trap A	Left	DLC	ACT	PT	0.1109
Trap T	Left	DLC	RMS	MPT2	0.0818

Trap D: m. Trapezius pars descendens
Trap T: m. Trapezius pars transversus
Trap A: m. Trapezius pars ascendens

overload of the muscle fibers.

Correlation of EMG and questionnaires

Table 3.7 shows the most important p-values of the Spearman correlation analysis between the mean sEMG parameters per condition and the questionnaires of stressexp 2. There was no evidence that sEMG signals were related to results from the questionnaires (PANAS, Relaxation inventory, Perceived Stress Scale, Daily life complaints list). The questionnaires refer to perceived stress levels and complaints over a longer period of time. The test protocol was designed to induce acute stress. It is clear that these questionnaires measure other aspects of stress than sEMG.

Individual sEMG profiles

On group level, no statistically significant difference could be identified for the muscle activity on the trapezius muscle during the different mental stress and physical load conditions. To look for individual differences, the video recordings of the stress test (stressexp 2) were analysed visually by two professional ergonomical

scientists. The video images were labeled with the presence of postural changes, muscle reactions and signs of stress, that were not related with the physical activity. Afterwards, the occurrence of these reactions were compared with the sEMG data of the left and the right trapezius muscle, pars descendens. Figure 3.25 shows different sEMG profiles. The RMS-values during the 6 minutes per condition are plotted on top of each other as percentage of the Maximal Voluntary Contraction. For some subjects, sEMG signal patterns matched with what was actually happening at a particular moment of the test, as viewed in the video images. For other subjects, however, there was a clear discrepancy between the sEMG signals (e.g. indicating much activity) and what was actually happening as viewed in the video images (e.g. no change of posture and no movement). This means that the muscle builds up muscle tension without the benefit for the posture of the test subject. An example of the latter activity is the single motor unit firing, as described in section 3.4. In this speicific case, only one motor unit was firing, indicating that only a few muscle fibers are contracting. These few muscle fibers are insufficient to influence the posture significantly.

When comparing the sEMG signals of the left and the right trapezius muscle, several subjects showed an increase in sEMG activity in the left muscles during the postural task, although the clicking movements during both PT and MPT were the same. These subjects may have become bored by the clicking task itself and therefore showed stress signals in the EMG. The subjects did not make random movements or change their posture during the test.

On the other hand, the video analysis revealed that most subjects have repeating typical stress reactions of their body which differ amongst the different test subjects. these reactions were not limited to the trapezius muscle. Even more, some subjects showed reactions on other muscles, but not on the trapezius muscle. Different reactions were seen in the face where some subjects were chewing (masseter and temporalis muscle) and others were frowning there forehead (frontalis muscle), while others were wobbling with their upper body or with their legs. Because of the absence of quantitative and qualitative measures of the muscle activity of these different muscles, no further analyses could be performed to study this large interindividual differences. But the observation of this differences in muscle reaction could be a interesting basis for a next study.

Discussion

The two stress experiments differed in the level of postural load imposed. For stressexp 1, test subjects performed a heavy 6-minute shoulder abduction with and without a mental task. Muscle tension did not increase significantly with the addition of a mental task. The possible additive effect of the mental load was assumed to be low and was probably overshadowed by the muscle activity for the

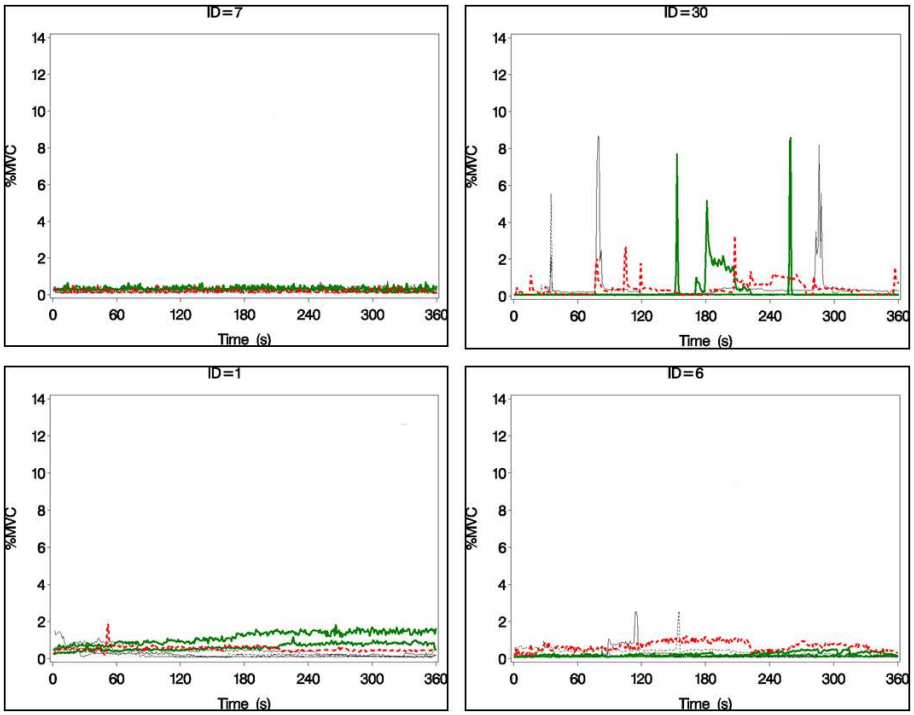


Figure 3.25: *4 profiles of the muscle activity of the different tasks for stressexp 2. The RMS-values during the 6 minutes per condition are plotted on top of each other as percentage of the maximal voluntary contraction. The green traces are MPT1 and MPT2, the red trace is PT and the gray traces are R.*

postural load. In stressexp 2, the postural task was to click a computer mouse, emulating a lower postural load more similarly to office tasks. The new protocol also addressed earlier design issues: condition times were consistent, and the rest period was sufficiently long for subjects to relax muscles. The results for stressexp 2 were similar to the results of the first one. At a group level, muscle activity did not differ significantly for a postural task with or without a mental task for the left shoulder muscles.

The sEMG parameters of the trapezius muscle revealed no direct relation with an extra imposed mental task. However, this muscle showed spontaneous activity without any beneficial effect on the posture. Signs of muscle fatigue after these tests were present even after the very small postural load that could lead to exhaustion and possible to MSD afterwards. Therefore, the monitoring of the trapezius muscle in the battle against MSD is of importance.

On an individual basis, there were differences in muscle reaction between the

test subjects on the different conditions with and without a mental load. On the trapezius muscle, different muscle contraction patterns could be identified between the different subjects. Some subjects showed an increase in muscle activity during the condition with a postural load compared to the condition where a combined physical and mental load was applied. This could reveal that these subjects were bored during the postural load, imposing another type of stress to the subjects. Another explanation could be that the mental task, as imposed here, did not initiate the same amount of mental stress on the subjects. There were subjects that have a very strong stress reaction by solving these tasks, while others were not stimulated to solve these tasks as good as possible. Several subjects showed an increase in muscle activity during the first rest period, which means that they were not at ease at the beginning of the experiment. In general, the reactions of the muscle activity of the trapezius were so individual and so different between the different subjects that, on group level analysis, no statistically significant differences could be identified. We can conclude that the analysis of solely the trapezius muscle activity as physiological measure is insufficient to see the effect of mental stress on the muscle activity.

In the literature, the trapezius muscle is the most important muscle that has been linked with mental stress reactions and the aim of the European project ConText was to develop a biofeedback system using physiological information distributed by this muscle, but research articles about stress are not limited to this muscle. The video analyses during the stress experiments revealed that muscle reactions also involve other muscle groups. To have a broader view on the muscle reactions due to stress, other muscles of the body should also be included in future studies: in particular, different face muscles (masseter, frontalis and temporalis muscle), the paravertebral muscles and the multifidus muscle.

In summary, the results in this section reveal the need for individual analyses or at least for smaller clusters in the population, to identify which muscles are activated and quantify their muscle activity to differentiate between stress and conscious muscle contractions.

3.7 Conclusion

The major source of interference (i.e. cardiac activity) on the sEMG signals need to be removed. Therefore, two recently developed single channel approaches of independent component analysis (ICA) are used to remove the ECG signal and the performance is compared with the standard technique to remove the ECG interference signal. The two techniques are based on the idea to decompose a single measurement using wavelets or ensemble empirical mode decomposition before applying ICA on these decompositions. When the corresponding ECG signal is not available, EEMD-ICA has the best performance compared to wICA and yields

similar performance as the template subtraction for higher SNR, while for lower SNR, EEMD-ICA is significantly better than template subtraction and slightly better than wICA. We can conclude that for offline use, when the calculation time is not important, EEMD-ICA has the best performance. When the ECG channel is present, the template subtraction is preferable.

sEMG signals of the trapezius muscle showed an interesting specific pattern during the stress assessment experiments. In approximately 65% of the subjects, for both experiments, spike trains appeared in the signals. We have evidence that these spike trains are the continuous firing of a single motor unit. This indicates a very low and subconscious muscle contraction that induces no postural change. We could not relate this pattern directly to stress, as it appeared randomly in the right and left muscles, during rest and the mental task. This could suggest that the presence of a mental load restrains the muscle from relaxing and recuperating. Frequent prevalence of single motor unit firing can lead to overload and exhaustion of these muscle fibers, resulting in pain and tissue damage. An algorithm to detect spike trains is capable of detecting single motor unit firings. The algorithm, based on an energy operator and correlation calculation, showed an excellent performance as it reaches a sensitivity of 100% and a specificity of 94,8%.

An algorithm to detect the absolute rest level of a muscle, the Rest Level Estimation (RLE), is developed. This algorithm uses a feature based on the frequency properties of the sEMG signal during contraction and in rest. Via easy thresholding, this algorithm is able to differentiate between the signals of the muscle in rest and in contraction. The RLE also has other useful applications. As it measures the rest level of a muscle in an objective way, without a reference measurement, we are able to distinguish in a daily task between the active and rest state of the muscle. The RLE can therefore be used in a biofeedback system to alert users if there are too few rest periods, and in the long term, help prevent musculoskeletal disorders of the neck and shoulder.

The two experiments, used for these analysies differed in the level of postural load imposed. For stressexp 1, the test subjects performed a heavy 6-minute shoulder abduction with and without a mental task. Muscle tension did not increase significantly with the addition of a mental task. The possible additive effect of the mental load was assumed to be low and was probably overshadowed by the muscle activity for the postural load. For stressexp 2, the postural task was to click a computer mouse, emulating a lower postural load more similarly to office tasks. The results for the second experiment were similar to the results of the first one. At a group level, muscle activity did not differ significantly for a postural task with or without a mental task for the left an right shoulder muscles. On an individual basis, there were differences in muscle reaction between the test subjects on the different conditions with and without a mental load. There are subjects that have a very strong stress reaction by solving the mental tasks imposed in the experiments, while others are not stimulated to solve these tasks as good as

possible. Several subjects showed an increase in muscle activity during the first rest period, which means that they were not at ease at the beginning of the experiment. In general, the reactions of the muscle activity of the trapezius are individual and different along the subjects that no statistically significant differences could be identified. The analysis of the trapezius muscle activity as physiological measure is insufficient to see the effect of mental stress on the muscle activity. This is confirmed via video analysis, which reveals that other muscle groups also show muscle activity during periods with stress. To have a broader view on the muscle reactions due to stress, other muscles of the body should also be included in future studies: different face muscles (masseter, frontalis and temporalis muscle), the paravertebral muscles and the multifidus muscle.

The results reveal the need for individual analyses or at least for smaller clusters in the population, to identify which muscles are activated and quantify their muscle activity to differentiate between stress and conscious muscle contractions. The complexity of the stress system and the interindividual physiological reaction profiles require algorithms that are applicable on an individual basis.

Chapter 4

Heart Rate Variability: analysis applied to stress monitoring

In this chapter, the results of the HRV analysis are discussed. In section 4.2, the HRV analysis applied on the two stressexperiments (described in section 3.2) are presented. The effect of the mental and the physical load to the different HRV parameters is studied next to the additional effect of a mental load on a physical task. Besides the traditional linear HRV measures, time-frequency analysis (TFA) is used. TFA has the advantage over the traditional HRV measures that it enables continuous tracking of different HRV parameters to gain extra insight in the effect of the mental load within one task. In a next section 4.3, an additional study is described where the effect of anxiety, which is quantified using psychological questionnaires, is reflected in changes of the HRV parameters during day-night comparisons and a stress assessment test. In a final section 4.4, the close link between HRV and respiration will be elaborated.

4.1 Introduction

Stress is a psychophysiological phenomenon that changes the physiological balance of, amongst others, the autonomic nervous system (ANS) [148, 174]. The ANS is divided into a sympathetic and parasympathetic or vagal branch. Both components operate simultaneously and balance each other dynamically in normal conditions. When a person is exposed to a stressor, the sympathetic system becomes more activated via the locus coeruleus, resulting in the secretion of the neurotransmitter norepinephrine [129]. The activation of the sympathetic system innervates the production of epinephrine in the adrenal medulla. In addition,

the parasympathetic system is shut down. This brings the body in an arousal state, called the fight or flight reaction since Walter Cannon's work on the fight-or-flight response in the 1930s [166]. This result in changes in several physiological systems such as an increase in heart rate (HR) via the stimulation of the sinus node of the heart. When the stressor disappears, the vagal system takes over and the sympathetic activation disappears. A message is sent to the medulla, which responds by releasing a hormone, called acetylcholine. This hormone slows down the heart rate, delaying the muscle contractions of the heart. The stress reaction is hormonal, neurological, cardiovascular, metabolic and muscular [89]. Chronic stress can lead to an overload or exhaustion of these physiological systems. Frequently used biomarkers for detection are blood pressure, heart rate variability, catecholamine and cortisol secretion.

Heart rate variability (HRV) refers to alterations in heart beat time-intervals and provides quantitative markers of autonomic regulation [1, 165]. Moreover, it is a simple and powerful noninvasive methodology having enormous practical advantages with a minimum of technical constraints, which makes it useful in many applications. Therefore, HRV has been used to examine the responses to mental and physical demands on the ANS. Expressed physical tasks strongly influence HRV indices related to ANS as shown for static handgrip at 25% of maximal voluntary contraction (MVC) [118], bicycle exercise [123] or static leg extension at 30% MVC [65]. Mental stress in laboratory experiments (cognitive demands, mental arithmetic) has been associated with decreased HRV, indicating a disturbed ANS [111, 149, 105, 180].

4.2 Instantaneous changes in heart rate variability during physical, mental and combined stress in laborartory environment

4.2.1 Objective

The results of the HRV analysis on the two stress experiments, called stressexp 1 and stressexp 2 in section 3.2, are presented in this section. The design of the experiments allow us to answer two research questions: 'What is the effect of a mental load on the different HRV parameters, revealing information of the ANS?' and 'Is there an additional effect on the different HRV parameters of a mental load on top of a physical load?'.

The goal of this study was to evaluate the changes in HRV parameters due to a specific physical, mental or combined load. More specifically, the difference in effect between mental load and physical activity, in literature known to be

methodologically difficult [138], is studied. Many studies only focus on either physical or mental load, but only a few consider both [60, 71]. In addition, the effect of the combined physical and mental demand on the HRV parameters was examined and compared with the changes during the single task. However the relative contribution of mental and physical stress on HRV parameters is still not completely clear. We hypothesize a bigger change of the HRV parameters, and therefore autonomic modulation of heart rate, in the combined task compared to a single task. The effect of applying a similar mental task at different time instances is investigated by looking at the differences in HRV parameters during the two periods of combined physical and mental load.

While almost all previous studies were either interested in the relation between HRV and a questionnaire based stress level or the influence of imposed demands on HRV, here, the time evolution is included using time-frequency analysis. Time-frequency analysis, as applied here, was rarely used in literature, although it enables the study of trends within the same condition or transitions between different conditions. Moreover, it enables the comparison of these trends within one condition as well as between the various conditions.

The results of stressexp 2 have been accepted for publication as journal paper in European Journal of Applied Physiology [161]. The results of both experiments have also been presented at the 4^{th} European Congress of the International Federation for Medical and Biomedical Engineering (ECIFMBE) in Antwerp in 2008 and at the 6^{th} International Workshop on Biosignal Interpretation (BSI) in New Haven in 2009 and resulted in a paper that is published in the corresponding proceedings [160, 171]. The results of stressexp 1 have been submitted in revised form to the Journal of NeuroEngineering and Rehabilitation [172] in close collaboration with my colleague Steven Vandeput.

4.2.2 Methodolgy

Data

During stressexp 1, the test subjects underwent three active periods while performing a task with respectively a physical (PT_1), a mental (MT_1) and a combined physical and mental load ((MPT_1)). The three tasks were randomised and followed by a rest period. After each active period, the test subjects reported their perceived tension. The physical task was a shoulder abduction and the mental task consisted of solving the home version of the mensa test.

The stressexp 2 had one physical task (PT_2) and two times a mental one in combination with a physical task (in order of appearance $MPT1_2$ and $MPT2_2$). The order of the tasks was fully randomised. Each active task was followed by a rest condition. Each condition had an equal duration of 6 minutes. The physical

task during this experiment was closer to an office task and consisted of clicking with the mouse. The mental task was solving complex calculations.

When referring to the tasks of one of the two experiment explicitely, the tasks will be denoted with the number of experiment (PT_1, MT_1, MPT_1 and R_1 for stressexp 1; PT_2, $MPT1_2$, $MPT2_2$ and R_2 for stressexp 2). The more general statements that refer to both experiments will be denoted without a reference to the experiment.

HRV analysis

After deriving the tachogram from the ECG signal, the data was checked manually for missing and ectopic beats and extra ventricular beats were replaced by a 20%-filter. Linear HRV parameters were obtained in agreement with the standards of measurement, proposed by the Task Force of the European Society of Cardiology and the North American Society of Pacing and Electrophysiology [165]. Mean, SDNN, RMSSD and pNN50 were calculated in the time domain. After resampling the tachogram at 2 Hz, the power spectral density (PSD) was computed by using fast Fourier transformation. In the frequency domain, LF, HF, LFnu, HFnu and LF/HF were calculated. The length of the different conditions in the first experiment is variable. As some HRV parameters, such as SDNN, depend on the recording length, a comparison between conditions can only be done by calculating each HRV parameter on segments of equal duration. Segments of 2 minutes during the first stress experiment were selected, which is the duration of the shortest condition in the dataset. The HRV parameters of all rest periods are averaged. This problem was not present for the analysis of the data of the second experiment as the length of the different conditions was equal for all conditions (duration of 6 minutes).

Additionally, to overcome the possible non-stationarity and to describe the changes in HRV spectra during transients, time-frequency analysis (TFA) is used by applying continuous wavelet transformation (CWT). The Morlet wavelet is used as the literature showed that this is an appropriate function to study HRV [90]. TFA enables to track LF and HF parameters reliably over time: the power as well as the instantaneous frequency [25] in each frequency band. For the first experiment, the duration of the different conditions is not consistent, which complicates the TFA. Therefore, the analyses are limited either to the 4 first minutes or to the length of the condition per test person. This means that the first minute recordings are available from all the test subjects, but this is not the case for the following minutes. For the rest condition, the mean is taken over each minute from the four rest conditions. To have a better representation, the standard error will be used which is a better estimation of the error when the number of test subjects per group is different.

Statistical analysis

Statistical analysis on the linear HRV parameters was executed using the nonparametric Friedman test adjusted for possible between-subject effects to test whether the different conditions (experiment 1: R_1, PT_1, MPT_1 and MT_1 and experiment 2: R_2, PT_2, $MPT1_2$ and $MPT2_2$) affected the HRV parameters. Post hoc Tukey contrasts were used in order to explore further differences between two conditions, taking into account multiple testing. $P < 0.05$ was considered statistically significant.

Several analyses are performed for the time frequency analysis of the first experiment. In a first analysis the effect of the executed task within one condition is studied. Therefore, the first and the fourth minute per condition are compared pairwise with the Wilcoxon Signed rank test. In addition, we look for the effect of the executed task within one condition by analyzing the differences between the conditions in the first and also in the fourth minute. The analysis of the first and the fourth minute is performed analogously as the two minute segments of the traditional HRV measures described in this section.

To statistically characterize the differences between the active conditions in the time-frequency analysis in the second experiment, a minute-to-minute analysis is performed, analogously to Orini et al [116]. At each time instant, the nonparametric Wilcoxon signed rank is used to find pairwise differences between two conditions, resulting into a continuous estimation of the p-value. The resulting time series allows assessing the time at which conditions start to differ and for how long this difference is significant. As such, insight in the additional effect of the mental load is revealed. $P < 0.05$ was considered statistically significant.

4.2.3 Results

Stressexp 1

A typical tachogram with indication of the different conditions is given in Figure 4.1. During a first visual inspection of the signal, a clear transition between the different conditions can be noticed. The condition had a significant ($p<0.0001$) effect on mean RR of which the boxplot is shown in figure 4.2. Contrast analysis revealed a significantly higher mean RR in R than in the active conditions MT_1, PT_1 or MPT_1 (all $p<0.001$) as could be expected from figure 4.1. The heart rate was highest during MPT_1 ($p<0.01$ vs. PT_1 and $p<0.05$ vs. MT_1) followed by MT_1 ($p=0.24$ vs. PT) and PT_1. Results on HRV showed that condition had no significant effect on SDNN for the first two minutes ($p=0.34$). SDNN, shown in figure 4.3, provides information about the total variability of heart rate control.

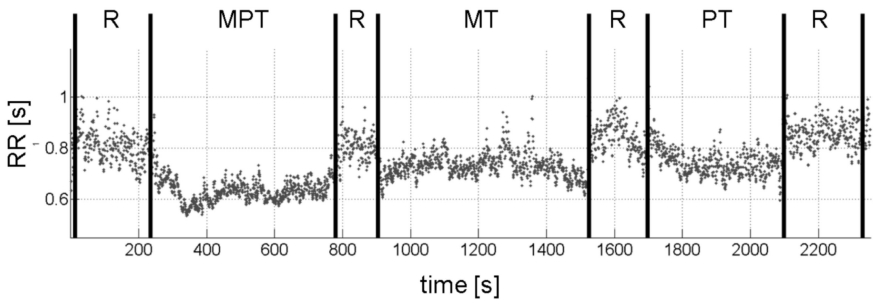


Figure 4.1: *Typical tachogram of a subject with indication of the different experimental conditions for the first experiment.*

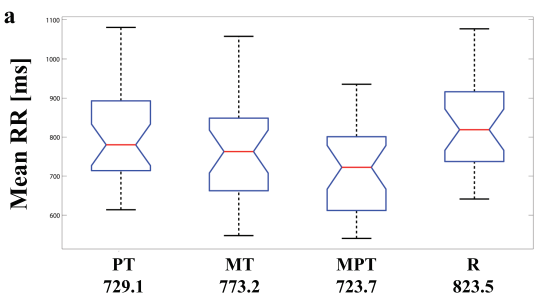


Figure 4.2: *Boxplots of mean RR intervals for the different conditions of the first 2 minutes of the first experiment.*

Statistically significant differences between conditions were found for rMSSD ($p<0.0001$), pNN50 ($p<0.001$), LF ($p<0.001$), HF $p<0.0001$). Figure 4.4 presents the results for rMSSD, which reflects vagal modulation of ANS as pNN50 and HF do according to the literature. These three parameters showed similar evolutions as expected. The differences are quasi identical to meanRR, namely significantly higher in R_1 compared to PT_1, MT_1 and MPT_1. In addition, those parameters were significantly lower in MPT_1 compared to PT_1. LF/HF, characterizing the sympathovagal balance is depicted in figure 4.5. Statistics reveal a significantly increased MPT_1 compared to the other three periods.

Figure 4.6 shows a typical time series of one subject for HF power and LF/HF. This figure visualizes changes in these parameters within and between the conditions. The time series giving the instantaneous frequency in the high frequency band of the same subject is also presented in the lower plot of figure 4.6 reflecting fluctuations between 0.22 and 0.26 Hz. Especially during MT, an increased HF frequency is observed.

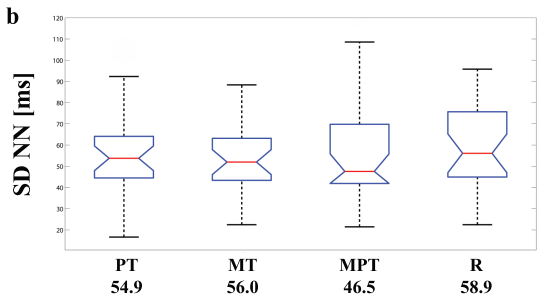


Figure 4.3: *Boxplots of SDNN (total heart rate variability) for the different conditions of the first 2 minutes of the first experiment.*

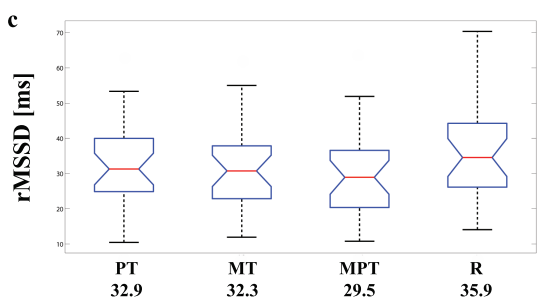


Figure 4.4: *Boxplots of RMSSD (vagal autonomic modulation) for the different conditions of the first 2 minutes of the first experiment.*

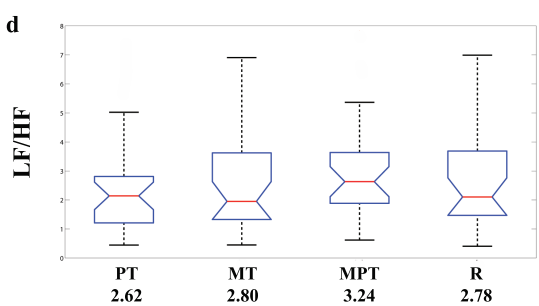


Figure 4.5: *Boxplots of LF/HF (sympathovagal balance) for the different conditions of the first 2 minutes of the first experiment.*

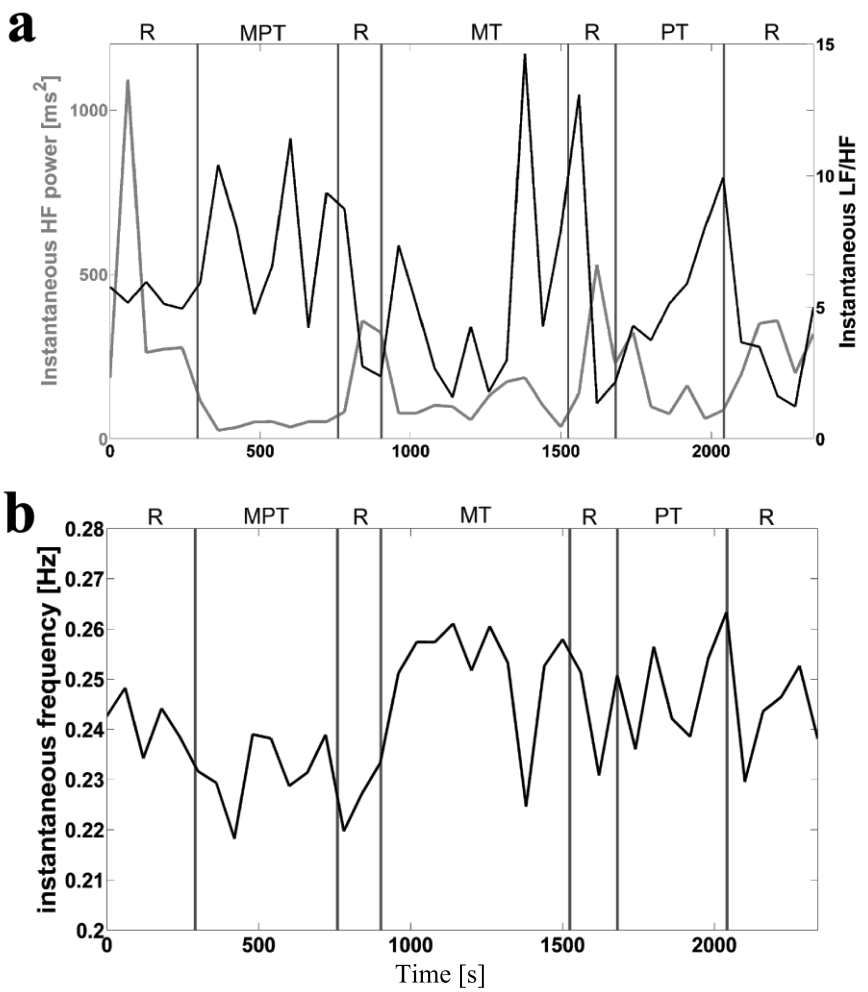


Figure 4.6: *Typical evolution of (a) instantaneous HF power (grey line) and LF/HF ratio (black line) over time and (b) instantaneous frequency in the HF band with indication of the different conditions (R = rest, PT = physical task, MT = mental task, MPT = mental and physical task combined).*

Figure 4.7 shows the time series of all the subjects for HF, LF, LF/HF and fHF. The time series of the mean (± standard error) are given for the 4 minutes per condition to see the evolution. In addition, Table 4.1 shows the mean value of the different time-frequency parameters for the 4 conditions at the first and the fourth minute. The results of the statistics are also included in this table. An underlined value indicates a statistically significant difference with the first minute of the condition. In addition to this analysis, the first and the fourth minute per condition are mutually compared and indicated with letters.

The HF time series shows that HF power is statistically significantly higher during the rest period compared to the three active conditions for the complete 4 minutes. In the beginning, there are no differences between the three active conditions, but from minute 3 on the two conditions with physical load have a lower HF power. However at minute 4, this difference is only statistically significant between PT_1 and MT_1. Only PT_1 has a significant change within the condition. The LF power during rest shows in the first minute a significantly higher value compared to the three active conditions. We also see that the LF power during PT_1 is statistically significantly higher compared to the two conditions with the mental load. Within the condition, these differences disappear. The decrease of LF power during R was statistically significant. Concerning the sympathovagal balance, LF/HF shows no difference in the beginning of each condition. After two minutes, the conditions with the physical load (PT_1 and MPT_1) show a strong increase. In minute 3, the LF/HF balance during these two conditions are statistically significantly higher compared to the beginning of the condition and compared to the two other conditions without physical load. In the fourth minute, the LF/HF of PT_1 remains high while the LF/HF of MPT_1 decreases back to the level of R_1 and MT_1. The instantaneous frequency in the high frequency band shows a constant frequency during the rest period. During MT_1, the instantaneous frequency shows a linear decrease, while it shows a linear increase during PT_1. Both changes are statistically significant from the first till the last minute of the condition. During MPT_1 both effects are combined: a decrease because of the mental load and an increase because of the physical load, resulting in a constant frequency. In the first minute, the instantaneous frequencies of both mental conditions are statistically significantly higher compared to those of the two conditions without the mental load. Within the conditions, the instantaneous frequency shifts towards a higher frequency during the physical conditions compared to that of MT_1 and R_1 in the fourth minute.

Table 4.2 shows the scores on subjective experiences (tensed, nervous, worried, calm, happy and relaxed). For three subjective experiences (tensed, happy and relaxed), the test subject gave significantly different scores during rest compared to the active conditions. They reported to be more happy, less tensed and more relaxed during the rest period compared to the MT_1, PT_1 and MPT_1 (not significant for happy) condition. The subjects also revealed to feel significantly

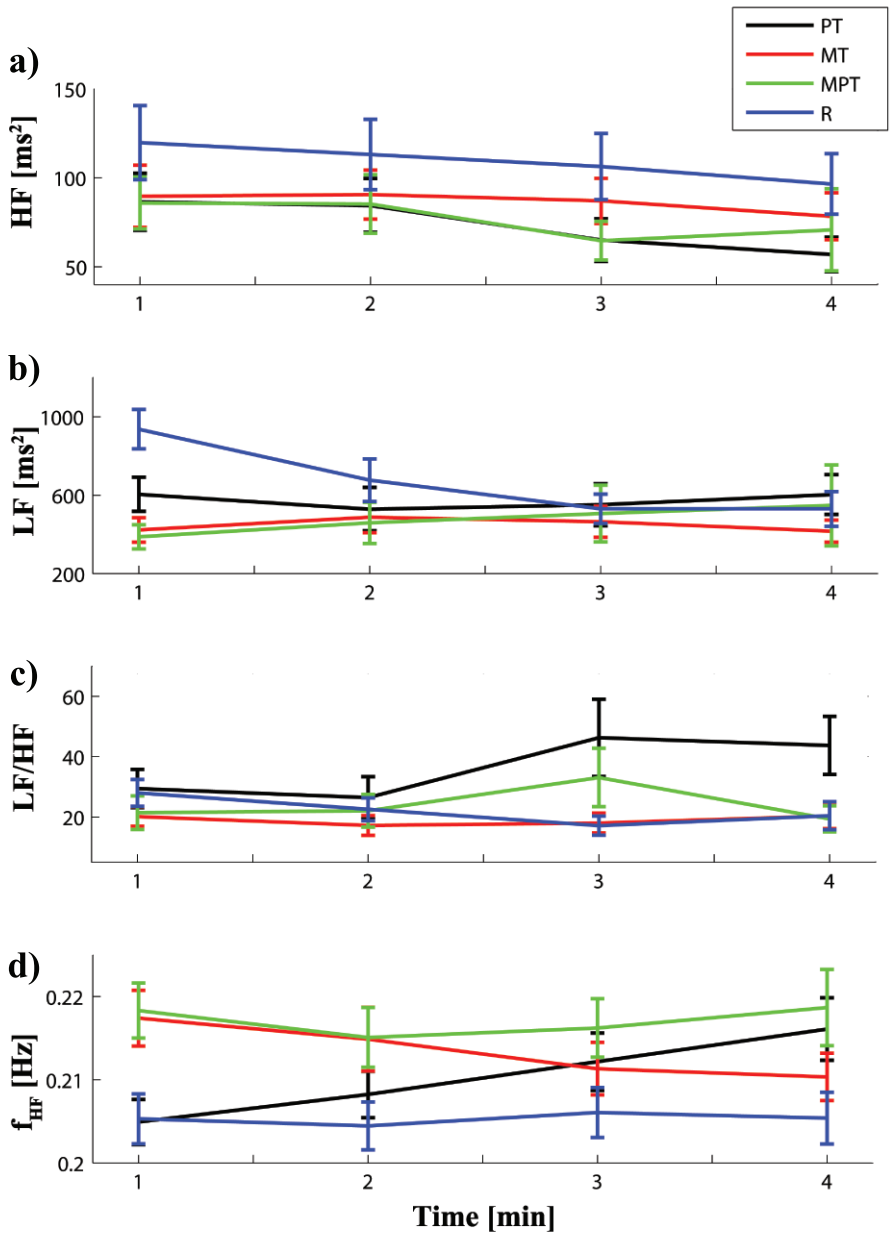


Figure 4.7: *Mean + standard error of the first four minutes of (a) instantaneous power in HF, (b) instantaneous power in LF, (c) instantaneous LF/HF ratio and (d) instantaneous frequency in the HF band. The four conditions are colored: PT = physical task (black); MT = mental task (red), MPT = mental and physical task combined (green) and R = rest (blue).*

Table 4.1: *Mean value for different time frequency measures of minute 1 and 4 during different conditions (R, PT, MT, MPT) of the first experiment. ($n = 28$)*

	R		MT		PT		MPT	
min	1	4	1	4	1	4	1	4
HF	86.51	56.87	89.64	78.33*	85.88	70.73	119.80 $^{\star,\diamond,\dagger}$	96.57 $^{\star,\diamond,\dagger}$
LF	604.32	603.25	422.85*	416.41	387.34*	547.54	935.92$^{\star,\diamond,\dagger}$	529.88
LF/HF	29.44	43.71	20.15	20.34	21.42	19.377	28.01$^{\diamond,\dagger}$	20.41*
f_{HF}	0.205	0.216	0.217*	0.210*	0.218*	0.219$^{\diamond}$	0.206$^{\diamond}$	0.205$^{\star,\diamond,\dagger}$

* Significant difference with PT ($p < 0.05$)
$^{\diamond}$ Significant difference with MT ($p < 0.05$)
† Significant difference with MPT ($p < 0.05$)
underlined: Significant difference within the condition ($p < 0.05$)

Table 4.2: *Mean (SD) for scores on subjective experiences during the different conditions (R, PT, MT, MPT) of the first experiment. Scales ranged from 1 to 4 (1 = not and 4 = extremely). (n=28).*

Variable	R	MT	PT	MPT
Tensed	1.66 (0.56)	2.14 (0.65)*	2.79 (0.74)$^{\star,\diamond}$	2.54 (0.79)*
Nervous	1.52 (0.44)	1.64 (0.73)	1.68 (0.82)	1.79 (0.69)
Worried	1.23 (0.55)	1.46 (0.74)	1.39 (0.69)	1.36 (0.73)
Calm	3.16 (0.61)	2.50 (0.75)	2.21 (0.79)	2.25 (0.75)
Happy	2.88 (0.50)	2.46 (0.79)*	2.25 (0.89)*	2.57 (0.74)
Relaxed	2.95 (0.61)	2.36 (0.62)*	1.79 (0.92)*	1.68 (0.77)*

$\star$ Significant difference with R ($P < 0.05$)
$\diamond$ Significant difference with MT ($P < 0.05$)

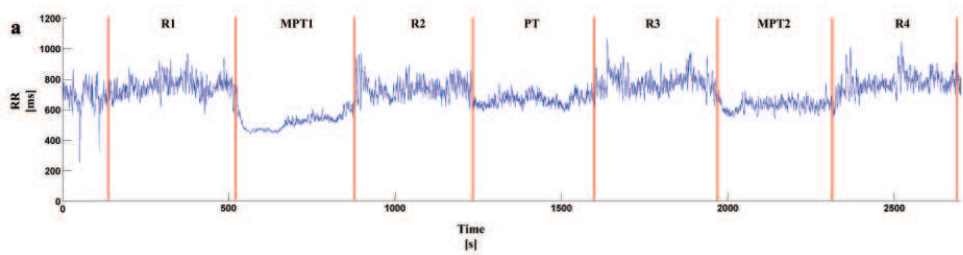


Figure 4.8: *Typical tachogram of a subject with indication of the different experimental conditions for the second experiment [161].*

more tensed during PT_1 compared to MT_1.

Stressexp 2

Figure 4.8 shows a typical tachogram of an individual during execution of the protocol. The different conditions, four rest conditions (indicated with R_2) and three active conditions are indicated in the figure: one physical clicking task (PT_2) and two clicking tasks in combination with the mental arithmetic task ($MPT1_2$ and $MPT2_2$). Visual inspection of the tachogram shows a clear transition between the active and the following rest condition. The time series also reveals a reduced variability of the heart rate in the three active conditions compared to the preceding and following rest condition.

The Friedman statistics reveal that the condition has a statistically significant effect on mean NN, SDNN, rMSSD, pNN50, LF and HF (all $p<0.0001$). Table 4.3 shows the post hoc contrasts. The mean values and standard deviation for the different HRV parameters are presented and the pairwise statistically significant

Table 4.3: *Mean values (SD) of different HRV parameters for the four conditions (R, PT, MPT, MPT) of the first experiment.*

Mean(SD)	R	PT	MPT1	MPT2
MeanNN [ms]	863.46(147.98)	821.17(141.18)*	755.44(134.47)$^{\star,\diamond}$	803.46(147.98)$^{\star,\diamond,\dagger}$
SDNN [ms]	46.73(19.48)	35.84(15.26)*	35.40(16.35*)	40.41(18.74)$^{\star,\diamond,\dagger}$
rMSSD [ms]	28.74(16.58)	22.83(14.09)*	19.39(13.77)*	22.94(15.66)*,†
pNN50 [%]	31.83(18.73)	27.68(17.00*)	26.82(16.10)$^{\star,\diamond}$	28.68(18.73)*,†
LF [ms2]	868.42(641.04)	522.10(463.72)*	466.87(460.20)*	645.06(600.61)$^{\diamond,\dagger}$
HF [ms2]	1005.48(782.59)	591.50(550.31)*	552.46(427.99)*	615.08(569.34)*

* Significant difference with R ($p < 0.05$)
$^{\diamond}$ Significant difference with PT ($p < 0.05$)
† Significant difference with MPT1 ($p < 0.05$)

differences between the conditions are indicated. The post hoc contrasts reveal that the changes between the rest condition and the three active conditions are statistically significant for all the HRV measures. SDNN, providing information about the total variability of heart rate control, was higher during rest compared to the active tasks. RMSSD, pNN50 and HF, all reflecting vagal modulation of ANS showed similar behavior and react conform to the literature, i.e. these values were significantly higher in rest condition (R_2) compared to the activity conditions PT_2, $MPT1_2$ and $MPT2_2$. More interesting are the differences between the three active conditions. $MPT1_2$ has the lowest meanNN, followed by PT_2 and $MPT2_2$. All these differences are statistically significant. The total variability (SDNN) is lower during PT_2 and $MPT1_2$ compared to $MPT2_2$, while mutually there are no differences. The combined mental and physical task has lower vagal modulation than the physical task as expected, being significant for pNN50 but not for RMSSD. More remarkable is that repetition has an effect on vagal modulation as both HRV parameters are lower during $MPT1_2$ than during $MPT2_2$. Even more, there is no difference between $MPT2_2$ and PT_2, indicating that the additional effect of the mental load has decreased.

Figure 4.9 shows the time evolution on group level of the power in the low frequency (a) and high frequency (b) band (respectively LF and HF) and the instantaneous frequency (c) in the high frequency band (HF). For visualization, the data are presented via the mean standard error in blocks of 1 minute. The time series of p-values are presented in figure 4.10.

The P_{LF} power (figure 4.9a and 4.10a,b,c), revealing information of both sympathetic and parasympathetic activity, is higher during the rest periods compared to the three active conditions. The evolution of LF power within the condition is similar for PT_2 and $MPT2_2$. The time series of the p-values shows that although the evolution of $MPT2_2$ and PT_2 is similar, the LF power is significantly higher in $MPT2_2$ compared to PT_2 (figure 4.10b) for almost the complete duration

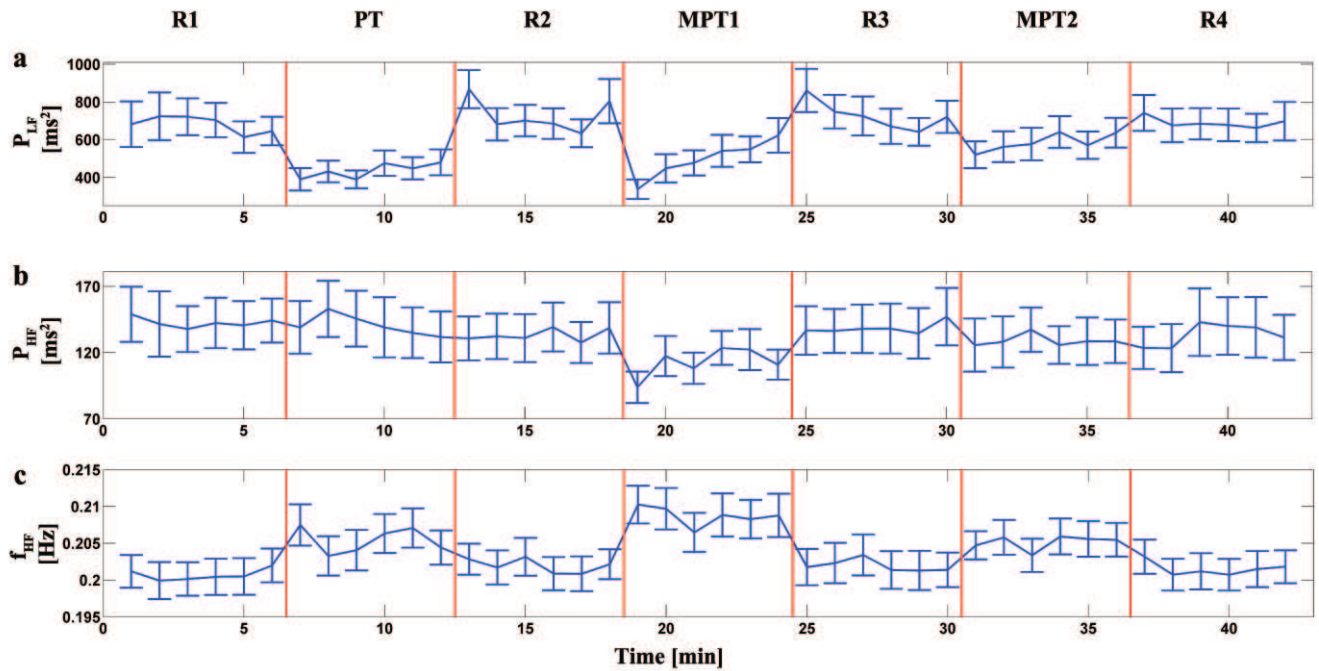


Figure 4.9: *Time evolution of different parameters during the second experiment, indicated as mean ± standard error, of the power in the low frequency (a) and high frequency (b) band (respectively P_{LF} and P_{HF}) and the instantaneous frequency (c) in the high frequency band (f_{HF}) [161].*

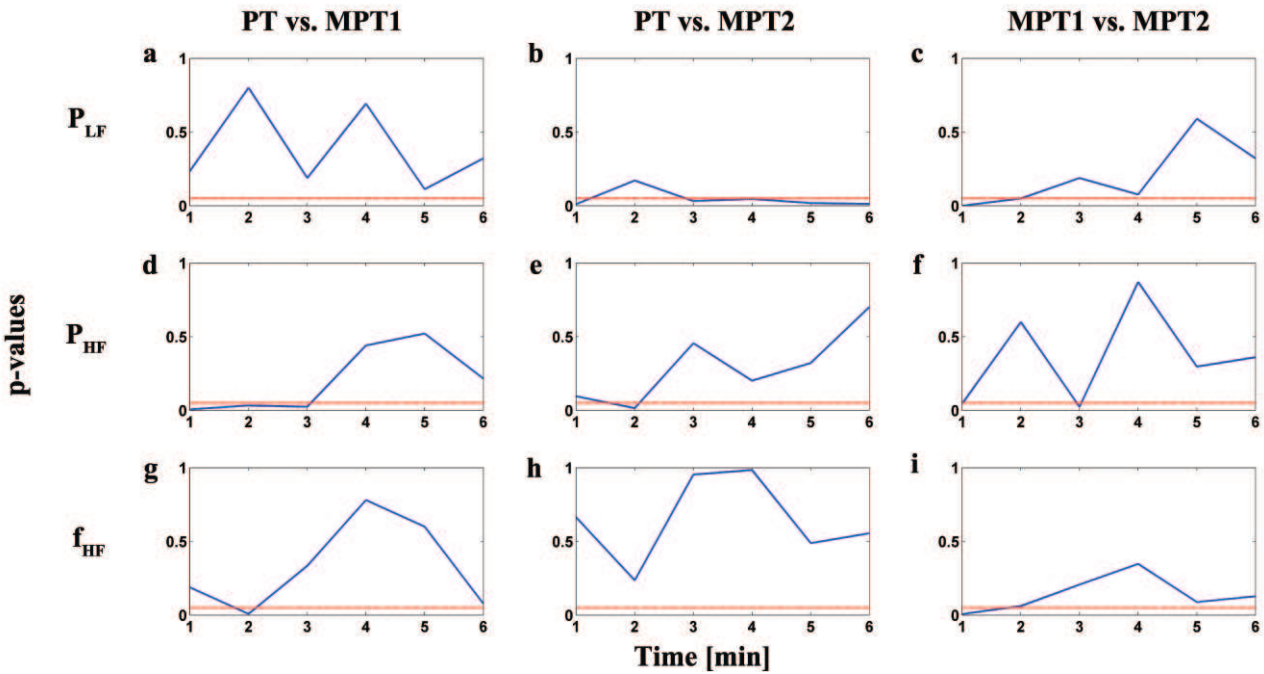


Figure 4.10: *The time series of p-values. The rows depict from top to bottom the power in the LF(P_{LF}) band, the power in the HF band (P_{HF}) and the instantaneous HF frequency(f_{HF}) [161].*

of the test. The values during MPT2 are tending more towards the values during the rest period compared to those of $MPT1_2$. Although $MPT1_2$ shows a linear increasing P_{LF} over time, statistics reveal that the differences between $MPT1_2$ and $MPT2_2$ (figure 4.10c) are only present during the first two minutes of the test. Although PT_2 has a more or less constant evolution and $MPT1_2$ is linearly increasing, there are almost no statistical differences between the two periods (figure 4.10), except at the end of the condition (minute 5). Information of the parasympathetic modulation on the heart rate is shown in the HF power band (figure 4.9b and 4.10d,e,f). The time evolution is similar as for the LF power, but statistics reveal other differences. The statistical differences between the active conditions are all present in the first three minutes of the condition. The effect of the mental task differs in time. During $MPT1_2$, P_{HF} differs from the period without mental load during the first three minutes (figure 4.10d), while the second condition with mental load is only significantly different during the second minute (figure 4.10e). This is also confirmed as the difference between $MPT1_2$ and $MPT2_2$ is statistically not different during the second minute (figure 4.10f). The instantaneous frequency in the high frequency band shows an equal frequency during the four rest periods. The mean frequency increases during the active conditions. Especially during $MPT1_2$, the mean frequency in the HF-band is the highest, but only significant during the first two minutes (compared to $MPT2_2$, figure 4.10i) and during the second minute (compared to PT_2, figure 4.10g).

4.2.4 Discussion

HRV parameters were calculated in several conditions: rest (R_1), physical task (PT_1), mental task (MT_1) and a combination of both tasks (MPT_1) for stressexp 1 and rest (R_2), physical task (P_2T) and a combination of both tasks ($MPT1_2$ and $MPT2_2$) for stressexp 2. During both experiments, almost all described measures (Mean RR, rMSSD, pNN50, HF) could distinguish the active conditions (PT, MPT, MT) from the rest condition (R), meaning that the variations in heart rate is a sensitive marker to any change in mental or physical state, regardless the task itself. For stressexp 1, the physical task consisted of a heavy shoulder abduction leading to fatigue. During this test, changes in the heart rate variability were expected while for stressexp 2, the physical load was low with a simple clicking task. This confirms the findings in previous work [60, 71, 105, 118, 123, 193] where evidence was found that physical and mental tasks influence HRV related to disturbances in the ANS.

A focus of this study was the additional effect on HRV parameters of a mental load. The combination of the physical and mental task (resp. MPT_1 and $MPT1_2$) was expected to result in a higher load compared to the physical task (resp. PT_1 and PT_2) or the mental task (MT_1) separately. The hypothesis was confirmed by a significantly higher heart rate and a significantly lower vagal modulation (rMSSD,

pNN50, HF) during the combined physical and mental load in both experiments. The effect of the single mental load (increased HR, decreased vagal modulation) is superposed to the cardiovascular effect of the physical load. This suggests an additional effect when multiple tasks are combined. Nevertheless, earlier studies found no effect of mental stress on physiological parameters [180]. One study reported that the addition of mental demands to a physical computer task does not elicit any further effect on HRV parameters related to autonomic modulation [60]. Therefore, they suggested that the physical demands have a major influence on the observed ANS changes whereas the influence of the mental load is insignificant, while these results reject their hypothesis. An additional effect of a mental task is identified with both a heavy and a low physical load. A mental load as such influences autonomic cardiac modulation, even in combination with a simultaneous physical task.

The power in the low frequency band is described in the literature as the measure that reveals information of both sympathetic and vagal modulation [165]. The hypothesis for the study was an increased LF power during the active conditions compared to the rest conditions, as mental and physical load activate the sympathetic branch of the ANS [40]. Contrarily, our results reveal a lower LF power confirming the findings in Hjortskov et al [71] where a withdrawal of vagal modulation during short-term stress was suggested [63, 147]. They also reported lower power in the LF band during tasks where mental stress was induced.

The time frequency analysis shows that the described differences are not present during the complete condition. For example, the PHF in Figure 4.10 was only significantly different for the first three minutes between the task with the mental load ($MPT1_2$) and the task without the mental load (PT_2). There were clear differences for the HRV parameters during this short period, although the physical load was similar for both periods. The protocol was fully randomised for the active conditions, so we can conclude that these changes are originated by the mental load and not by time. The differences caused by the additional mental load disappear when repetition took place. This reveals that our ANS is able to cope with mental load. In the literature, this has been discussed by McEwen [101] from the prospective of homeostasis and homeostatic load. He explained the adaptability mechanism of the human body to unknown stress situations. Translated to this situation, the mental arithmetic is the stress situation and the HRV parameters change significantly at the beginning of the exposure to the task. After being exposed to this stress situation for several minutes, the body habituates and at the end of this condition, the HRV parameters tend to those of PT_2. More evidence for homeostasis can be found by comparing the HRV parameters of $MPT1_2$ and $MPT2_2$. For almost all described parameters, there were significant differences between the first mental load and the second one, showing lower heart rate, more vagal modulation activity, lower instantaneous frequency in the HF band, related to the breathing rate. Moreover, except for the mean heart rate and the power in

the low frequency band, no significant differences were observed between $MPT2_2$ and PT_2, revealing that the additional effect of the mental arithmetic is minimal during this second time. The participants know what to expect and are used to the mental task. The steep increase in heart rate during the $MPT1_2$, as shown in Figure 4.8 for one participant and in Figure 4.9 with the time-frequency analysis, is less present explicitely. There is still a small effect as the time-frequency analysis of the power in the HF band revealed no statistically significant difference between $MPT1_2$ and $MPT2_2$ during the second minute, while the difference between PT_2 and $MPT2_2$ is significant for this minute.

The changes in instantaneous HF frequency can be related to changes in respiration frequency as the main peak in the HF band is normally caused by respiration [154, 127]. Assuming this, the tasks with mental load have a significantly higher respiration rate compared to PT and rest in both experiments. A possible assumption for the increase in respiration rate during the first experiment could be the effect of speaking as the subjects answered orally on the MENSA test. Allthough the subjects underwent the tasks with the mental load and answered orally, this instantaneous HF frequency had a linear decrease within MT_1. This decrease is not to be expected when the increase in respiration rate is only related to the influence of speaking where a constant frequency during the complete task would be expected. The increase in the beginning can be related to the effect of the mental task and the decrease within one condition to habituation. An increased respiration frequency during a 1h low-grade mental stress task in healthy subjects was already found in Nilsen et al [113]. Vlemincx et al [177] also reported an increased breathing rate during mental stress, although Bernardi et al [16] observed oppositely a lower respiration frequency. The linear increase in instantaneous frequency during PT_1 can be related to incoming fatigue, which is an ongoing physiological process that initiates from the beginning of the physical load. During MPT_1, the effect is the combination of both the physical and the mental effect on the frequency: a linear increase due to fatigue during the physical load and a decrease due to habituation of the mental load, resulting in a constant frequency. The respiration frequency during MPT_1 is at each time instant the highest of the four conditions of the first experiment. This indication of the fatiguing process of the body during the physical performance can also be seen in other parameters. In particular, the LF/HF ratio is increasing monotonously during PT_1 and MPT_1 (Figure 4.7), indicating the fast increase in sympathetic dominance caused by the heavy physical task. Evolutions in time were also observed within other conditions. The decrease in LF during rest condition can indicate recuperation after a physical load [85]. With respect to the sympathovagal balance, there is a decrease during rest (not significant), but an increase during both conditions with mental load showing that the vagal pathways of ANS became relatively a bit more active in rest while the sympathetic modulation gained importance in case of mental stress.

During stressexp 1, the subjects reported their perceived tension using a

questionnaire (table 4.2). The subjects reported there to be less happy, more tensed and less relaxed during the active conditions compared to rest, the different active tasks brought the participants into another emotional state. The fact that the subjects revealed to feel more tensed during PT_1 compared to MT_1 is probably due to the interpretation of tension as physical tension. MT_1 and MPT_1 being not significantly different with respect to the tension level confirmed this idea. Because of the mental distraction, the perception of tension due to the physical task is reduced during MPT_1. Despite the marked difference in several HRV parameters between the active conditions, this was not visible in the self rating scores. Therefore, even if subjects do not indicate a difference in stress level, often there are changes in their physiology which can be observed via amongst others heart rate variability.

Studies conducted in a laboratory have the advantage that the experimental conditions are carefully controlled. However, it is also a limitation that the results and conclusions cannot necessarily be extrapolated to office settings, although we believe that the stressors and the physiological stress reactions in the present study may reflect the reactions during office work. Even more, the stress task as used in both experiments, does not initiate a similar amount of mental stress to all the subjects. On the other hand, different people react physiologically different to the same stressor due to the complex processes in the brain to control the stress system. Although the results of these analyses reveal an effect of the mental load on different HRV parameters, group analyses do not reveal the amount of physiological reaction. Therefore, in this type of analyses, there is a need for individual models to have a better insight in the effect of stress on the physiology..

Calculating HRV parameters is at low computational cost making the findings of this study useful in daily life. This study supports the conclusion of Nolan et al [114] that HRV can be promising to be used in a biofeedback system.

4.3 Stress during pregnancy: Is the autonomic nervous system influenced by Anxiety?

4.3.1 Introduction

Stress and anxiety during pregnancy can influence the development of the fetus. A low birth weight [119] and prematurity [110] of the child are possible consequences resulting in long term problems [141]. Several studies reveal that cognitive, emotional and behavioral disorders occur more often when fetuses are more exposed to prenatal stress and anxiety [169]. The perceived stress level of the pregnant mothers are derived from traditional questionnaires such as STAI [39] and EDS [31].

Recently, there seems to be more and more interest in studying all kinds of emotions by means of physiological signals. It is known that stress influences the cardiac system, which is regulated by the autonomic nervous system (ANS). The sympathetic and parasympathetic modulation on the cardiac system can be quantified using heart rate variability (HRV) [165]. Mental stress in laboratory experiments (cognitive demands, mental arithmetic) has been associated with decreased HRV, indicating a disturbed ANS [105].

This study is conducted in collaboration with the group of prof. Bea Van den Bergh (Developmental Psychology, Universiteit van Tilburg, The Netherlands). A large study is performed about the influence of the psychological characteristics and physiological responses of the mother during pregnancy on the development of their babies. The mothers are monitored at several time instants during their pregnancy. After birth, several physiological parameters of the babies are measured at different moments to monitor their development. This is, at this moment, an ongoing project.

In this section, one initial study deducted from the data is described. The aim was to investigate whether anxiety during pregnancy, as indicated by the questionnaires, can be linked with differences in the autonomic heart rate modulation via HRV parameters during both a 24h recording of the ECG and a test where a mental load is induced. The hypothesis was that perceived stress, indicated via subjective questionnaires, will be reflected in the differences in HRV measures so that we would be able to distinguish between a low and a high anxiety group using these HRV parameters.

The results of this study has been presented at the 37th Annual Computing in Cardiology conference (CinC 2010), in Belfast (Northern Ireland) and the conference paper has been published in the proceedings [162].

4.3.2 Methods

Data

180 women, aged from 18 to 40, were recruited from 10 to 12 weeks gestation onwards and monitored during each semester of the pregnancy. Inclusion criteria were: no current substance abuse problems, no severe psychiatric problems and no pregnancy-associated medical problems such as diabetes or hypertension. Each semester, the participants underwent a 24h ECG recording at 1000 Hz using the Vrije Universiteit - Ambulatory Monitory System (VU-AMS [179]) during daily activity. At the end of the 24h recording in the first and the third semesters, the participants underwent an additional stress test of 25 minutes. The stress test consists of 5 periods of 5 minutes, in which alternating periods of rest and mental stress occurred (phases are numbered 1 to 5 in order of appearance; 1,3,5

= rest and 2,4 = mental task). The mental stress was induced by solving complex continuous mental calculations of five operations with a two or three digit number. This period was considered to be stressful as task difficulty was high. During rest, relaxing pictures were shown and music was played, exposing the participants to neutral stimuli reducing boredom during this phase. This study considered the data of the pregnant women during the first semester.

At the beginning of the 24h recordings, the women were requested to fill in several questionnaires. The most important one for this study was the State Trait Anxiety Inventory (STAI) to determine the amount of anxiety present. The STAI consists of a state and a trait subscale; state anxiety is conceptualised as a transient emotional condition, while trait anxiety reflects a dispositional anxiety proneness and is known as continuous anxiety. This study only considered the state anxiety. Based on the STAI score, subjects were divided into three groups regarding their anxiety level: a low (STAI ≤ 28), medium ($28 <$ STAI < 40) or high (STAI ≥ 40) anxiety group.

Heart Rate Variability analysis

A tachogram is derived from the raw ECG signals using the Pan-Tompkins algorithm. The Pan-Tompkins algorithm has a good performance in general. Nevertheless, errors will be introduced via wrong peak detections and missed peaks. Therefore, the tachogram is preprocessed as described by Widjaja et al [188].

Linear HRV parameters were obtained in agreement with the standards of measurement, proposed by the Task Force committee [165]. Mean and standard deviation (SD) of the tachogram, the square root of the mean squared differences between consecutive RR intervals (rMSSD), the percentage of intervals that vary more than 50 ms from the previous interval (pNN50) and the mean of the standard deviations within 5 minute segments ($SDNN_i$) were calculated in the time domain. After resampling the tachogram at 2 Hz, the power spectral density (PSD) was computed by using the Welch method. In the frequency domain, low frequency power (LF: 0.04–0.15 Hz), high frequency power (HF: 0.15–0.40 Hz) and total power (0.01–0.40 Hz), as well as the ratio of low over high frequency power (LF/HF), were calculated. In addition, the power can be expressed in absolute values (ms^2) or in normalised units (n.u.). These linear HRV parameters are used for both the day-night comparisons and the stress test.

Nonlinear parameters do not describe the amount of modulation as such, but are able to describe the scaling, complexity and chaotic properties of the signal. Often used parameters which study the scaling of the system are 1/f slope [88], fractal dimension (FD) [84] and detrended fluctuation analysis (DFA α_1 & α_2) [122] while the complexity is addressed via sample entropy (SampEn) [134]. Also a chaotic signature is calculated by means of the recently developed numerical noise titration

Table 4.4: *Comparison of HRV parameters of day and night between the different groups, based on their STAI score.*

	time	High	Middle	Low	p_{H-L}	p_{K-W}
$SDNN_i$	d	57,71 ± 16,95	51,13 ± 15,24	59,22 ± 16,15	0,557	**0,036**
TINN	d	399,53 ± 152,69	341,33 ± 165,88	425,52 ± 158,62	0,403	**0,049**
DFA α_2	n	1,10 ± 0,11	1,01 ± 0,12	1,05 ± 0,10	0,094	**0,013**
NLmean	d	11,82 ± 6,07	14,91 ± 8,75	16,59 ± 9,11	**0,024**	**0,049**

d: day, n: night, p_{H-L}: p-value or comparison between high and low anxious, p_{K-W}: p-value for Kruskal-Wallis

Table 4.5: *Most significant results for the different HRV parameters during the stress test between the three anxiety groups based on the STAI scores.*

	Phase	High	Middle	Low	p_{H-L}	p_{K-W}
meanNN	5	773,04 ± 109,30	739,45 ± 67,90	791,90 ± 74,49	0,547	**0,049**
RMSSD	2 - 4	-1,76 ± 8,59	1,67 ± 6,64	-3,03 ± 5,71	0,326	**0,027**
SDSD	2 - 4	-1,55 ± 8,35	1,44 ± 5,87	-2,62 ± 5,49	0,241	**0,018**
HF	2 - 4	-66,50 ± 161,38	150,86 ± 580,34	-83,07 ± 236,64	0,727	**0,026**
LF/HF	2 - 4	0,91 ± 1,73	-0,34 ± 2,23	-0,13 ± 0,96	**0,049**	**0,049**

p_{H-L}: p-value or comparison between high and low anxious, p_{K-W}: p-value for Kruskal-Wallis

technique (NLmean and NLdr) [126]. These parameters can only be calculated on sufficient long segments. Therefore, the non-linear parameters were only calculated when analysing the 24h recordings.

Statistical analysis

In order to quantify the relationship between the questionnaires and the HRV parameters, the Kruskal-Wallis test was used to differentiate between the three groups (between the high and the low group more specifically). Extra analyses were performed using the Spearman correlation coefficient ρ to look for possible correlation between HRV measures and the STAI score.

4.3.3 Results

The activity during day and night is different. Therefore, 6 successive hours during day and night were selected manually and the HRV parameters were analyzed. Table 4.4 gives the most important results of the comparisons between the three anxiety groups. The Kruskal-Wallis test revealed several statistically significant differences, but the post hoc-test shows that these differences were mainly between the middle and low anxiety group and not between the high and the low anxiety

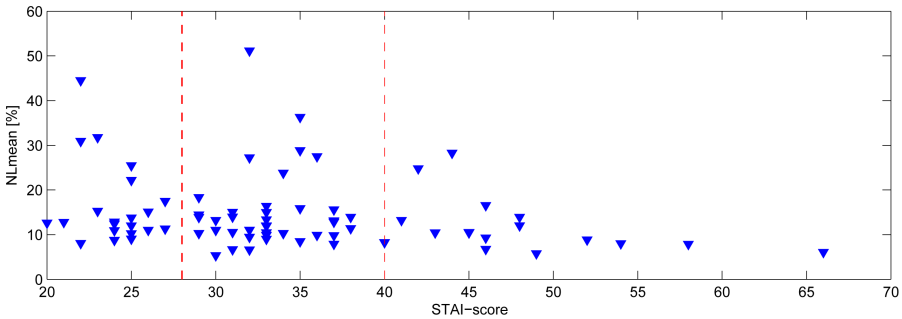


Figure 4.11: *NLmean for the 6h-day measurements in function of the STAI score.*

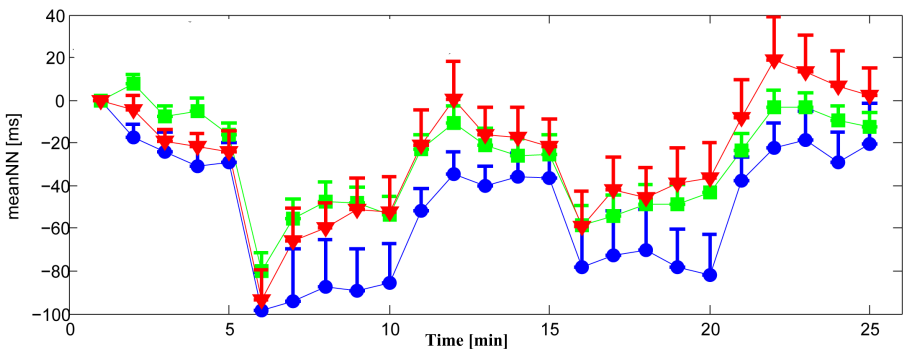


Figure 4.12: *the standardised meanRR intervals during the test for the three anxiety groups. (◯ = high; □ = middle; ▽ = low).*

group. A more general approach to look for a relationship between the STAI score and the HRV-parameters is calculating the correlation between the two variables. For the day-night comparisons, only a significant correlation coefficient is found for the NLmean parameter as shown in Figure 4.11 (ρ = -0.26, p = 0.021), but the figure does not reveal a convincing result. This negative correlation was more expressed during day than night time. Positive correlations were only found for parameters related to sympathetic activity (LF [n.u.] and LF/HF) and for the detrended fluctuation analysis (DFA) parameters. In contrast, the positive correlations were stronger at night compared to day time.

Figure 4.12 shows the normalised meanRR intervals during the stress test for the three anxiety groups. The different conditions can be distinguished for each group. The more interesting was the difference in reaction between the three different groups. Therefore, we deducted between-group analyses of the different HRV parameters for the different phases and for differences in phases. Table 4.5 gives

Table 4.6: *Significant correlation coefficients during the stress test between HRV parameters and the STAI scores.*

	Phase	ρ	p
SDNN	4	-0,233	0,040
pNN50	4	-0,225	0,048
	2 - 4	0,240	0,034
LF	3	-0,239	0,035
	4	-0,253	0,026
HF	2	-0,260	0,022
	3	-0,237	0,037
	3 - 4	-0,255	0,024
LF/HF	2 - 4	0,238	0,036

an overview of the most important results. Some statistically significant differences were present, but not to differentiate between the high and low anxiety group as hypothesised. This difference was statistically significantly present for LF/HF.

Table 4.6 shows the statistically significant correlation coefficients between the HRV parameters and the STAI scores. Several correlations are present, but ρ shows that these correlations are not persuasive. A general trend when analyzing the correlation coefficients is that the HRV parameters of the individual phases are negatively correlated with the STAI scores and are more present during phases with the mental load during the stress test.

4.3.4 Discussion

The goal of this study was to investigate whether anxiety during pregnancy, as indicated with a self-rating score (the STAI score), can be linked with the functioning of the autonomic nervous system via different HRV parameters. Therefore, the cardiac system of several pregnant women was investigated for its sleep-wake rhythms and during a stress test. The ANS, characterised via different HRV parameters, showed little influence of anxiety, indicated by the STAI score. This revealed that a strong correlation between a psychological self-rating score and the physiological response of the subjects is absent [109].

A statistically significant indication of anxiety could be found in the chaos of the RR intervals: more anxiety leads to less chaos. This difference was only statistically significant during the day, where the daily activity was not standardised and is therefore not a very strong evidence. Most other HRV parameters showed slightly negative correlations with the STAI score, indicating a reduced HRV for women with high anxiety that is in agreement with a reduced

HRV for several pathologies. Two measures (LF [n.u.] and LF/HF), both related to the sympathovagal balance, showed positive correlations during the day. These positive correlations were more present during the night. In general terms, we can state that anxiety results in a higher sympathovagal balance while sleeping and in a global reduction of HRV during the day, although these correlations were not statistically different.

Anxiety, reflected from the STAI scores, revealed hardly any influence on the cardiac reaction during the stress test. All time domain measures indicated a negative correlation with the STAI score during the different phases of the stress test. This confirms the hypothesis that anxiety reduces the variability of the heart rate. HF, a marker of the parasympathetic modulation on the heart rate, revealed a statistically significant negative correlation coefficient during the different phases indicating a reduced parasympathetic influence in women with high anxiety. This was more apparent during the periods with mental load.

The statistically significant differences, described here, were only marginal compared to the numerous analyses that were performed during this study. The conclusions that could be made were only from trends in the data. A limitation of the study was that the state anxiety of the STAI was used. The state anxiety is depending on the situation and can vary during day time. A better approach could be to use the trait anxiety of the STAI, that reflects the dispositional anxiety proneness. Another limitation during the stress test could be the task we used to induce stress. These women are pregnant and their main concern is to have a healthy baby. This concern is mainly responsible for the anxiety level. The mental arithmetic test could induce a different type of stress that is not linked with the concerns of the pregnant women. Even more, it is likely that the mental task, as imposed here, did not initiate the same amount of mental stress on the subjects. There are subjects that have a very strong stress reaction by solving these calculations, while others are not stimulated to solve these tasks as good as possible. Therefore, a combination of different types of stressors could improve the accuracy of the study, as the current study is only focussing on a very specific mental stress, which is not the type of stress why the women score high on anxiety.

Solving the above mentioned limitations could possibly lead to better correlations between the psychological score and the physiological responses of the cardiac system. However, the stress phenomenon is a very complex reaction. Stress is, in its nature, a subjective and psychological phenomenon that initiates different reactions in the brain of the subjects leading to physiological reactions. The results show that several people report to be very sensitive to mental stressors via questionnaires, which is by definition a subjective measure, does not result automatically in a very strong stress reaction in the physiological parameters. The absence of this correlation reveals that there are different processes in the brain that regulate the stress system and these processes interact with each other in a complex way. The nature of these complex interactions is still not clear and the

question will be whether this complex system will be unravelled completely in the future. This explains why there is not a 1 to 1 relation between the cause of the mental stress and the physiological stress response of the body.

This study is a part of a larger project at the university of Tilburg [46]. In this project, a follow up study of the influence of the stress and the anxiety of women during their pregnancy to the development of their babies is performed. For future analysis, the physiological scores via, for example, HRV can be used as predictor for the development of the fetus and its problems and compared with the results when the psychological questionnaires for anxiety are used. In this type of studies, the influence of genetic factors can not be neglected and should also be taken into account. For example, the susceptibility to stress and the genetic factors that are responsible for this susceptibility could be a more important factor than the stress itself.

4.4 Respiration

4.4.1 Introduction

In this section, a short overview of the most important influences of respiration on heart rate variability are discussed. In a first subsection, the effect of the respiration, and more specific sighing, during a stress task will be explored. The psychophysiological interpretation of sighing has become a large topic in research. During the stressexp 2, the respiration was included as one of the physiological signals, so this analysis could be included. In the literature, there is a huge ongoing discussion about the role of respiration in HRV analysis. This problem will be discussed in the last subsection.

4.4.2 Sighing: a psychophysiological resetter

During stressexp 2, the respiration was quantified using information retrieved from a capnograph (determines the CO_2 of the exhaled air), measured with a nose tube and the LifeShirt vest that measures thoracic and abdominal respiration via two resistive belts. These analyses are realised in close collaboration with the Research Group on Health Psychology (Katholieke Universiteit Leuven). The human respiration system is activated with physical and/or mental effort. This system responds in different ways to different efforts. For example, gradually increasing physical effort (such as walking or running) first results in an increase in breathing volume followed by an increase in respiration rate. Mental effort due to mental arithmetic tasks results mainly in an increase in respiration rate and

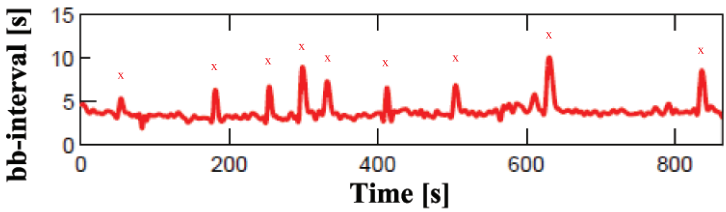


Figure 4.13: *Shows the tidal volume of one test subject. The respirations are presented in breath-to-breath intervals. The sighs are indicated with X.*

not in breathing volume. The respiratory system does not necessarily respond in the same way for different mental tasks.

Sighs, defined as single deep breaths, are often considered disturbances of spontaneous breathing. Nonetheless, sighing may play an important role in regulatory processes. Vlemincx et al [175] argued that sighs operate as general psychophysiological resetters. First, reductions in lung compliance and gas exchange efficiency are restored by sighing [22, 11]. Second, sighing resets parasympathetic control when sympathetic activity chronically dominates autonomic regulation [56]. Third, sighing resets various fractions of respiratory variability to a healthy balance representing a sensitive, yet stable respiratory system. Therefore, the effect of sighing during a mental load is of importance. Here the results of sighing during the second experiment are presented. The sighs could be identified using the above mentioned measurements as shown in figure 4.13.

The second experiment consisted of three active tasks (one sustained attention task with clicking, PT, and two tasks where a mental effort was asked in combination with clicking, MPT). The results are presented in figure 4.14. The expectation was that subjects would sigh when tension had built up and relief was necessary. The number of spontaneous sighs during MPT would therefore be a good indicator of tension. This expectation was confirmed. Statistical analysis revealed that the number of sighs was higher during MPT than during PT and rest periods. The prevalence of multiple sighs may indicate built up tension and mental overload, while no statistically significant difference was seen between the number of sighs during the physical task and the rest periods.

The collaboration with Elke Vlemincx resulted in two journal papers in Psychophysiology [177] and Physiology & Behavior [176]. I collaborated in the data acquisition, in the discussion of the results and in the preparation of the manuscripts.

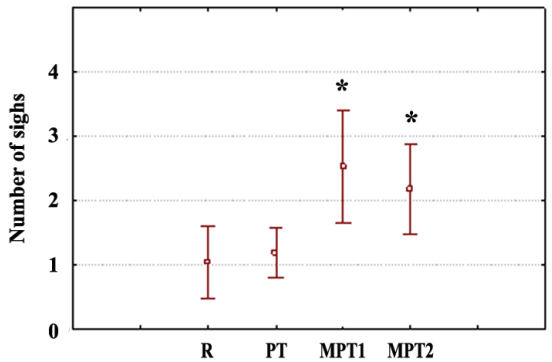


Figure 4.14: *Number of sighs during different conditions of the second experiment. R = mean rest; MPT1 = first mental and postural taks; MPT2 = second mental and postural task; PT = postural task. * Indicates statistically significantly different from R ($p<0.05$).*

4.4.3 Respiration versus HRV

In the literature, there is an ongoing discussion about the influence of respiration on the HRV parameters. Several studies reported on the effect of respiratory parameters, such as respiration rate, tidal volume, expiration/inspiration rate on the different HRV parameters [15, 128, 168], but no consensus exist.

The Respiratory Sinus Arrhytmia (RSA), the variation in heart rate due to respiration where the heart rate increases during inspiration and decreases during expiration, is seen as an index for parasympathetic control and therefore in the HF band. The peak frequency in this band is an indication of the mean respiration rate and the power in the HF band is measure for parasympathetic modulation of the heart. The respiration rate is nonstationary and the RSA can shift outside the boundaries of the HF band due to very slow or fast respiration. Bailon et al [9] therefore proposed to work with a variable HF frequency band, localised around the respiration rate and calculate the HF power. Recent studies however show that variations in the respiration rate and volume alter the amount of RSA, independent from the parasympathetic control. Therefore, the information in the HF band due to RSA is the topic of recent papers, but no consensus is reached for the real physiological interpretation [42, 66].

In fact, Bernardi et al [15] claimed that in the absence of simultaneous analysis of respiration, the changes in the LF/HF ratio should be taken as a clear evidence of changes in sympathovagal balance. In orde to incorporate respiration into the interpretation of the frequency domain of the HRV, one must look closely into the mechanisms of interaction between respiration and the heart rate control system.

Despite many past studies, the precise physiological mechanisms of LF and HF components of HRV and their relation to respiration are still beign debated [168].

Even more, Wessel et al [183] gave an example of cardiorespiratory modeling which demonstrates that the complex behaviour of the heart rate is mainly caused by the respiration which influences the coupling of heart rate and blood pressure. They suggested therefore that the complex heart rate fluctuations resulted from a modulation by breathing and that this complex respiratory behaviour can be explained by the regulation of ventilation.

The main question is to what extent we need to correct for respiration in HRV analysis. On one side, there is the theory that the main goal of HRV analysis is to retrieve information about the ANS. It is less important whether this information is originated by respiration and therefore no correction is needed. Others hypothesise that correction for respiration during HRV analysis is necessary because the HRV reveals information of the heart and not of the respiratory system. Nevertheless, this correction uses the respiration parameters as covariates during the statistical analysis [136, 42]. Presumably, this approach overestimates and overcompensates the respiratory influences on the HRV and removes information that is not related to the respiration.

In the future, there is need for new signal processing methods to correct the tachogram for influence of respiration to improve HRV analyses. This could probably add new information to the above mentioned discussion. Moreover, there is a clear interaction between the cardiovascular and the respiratory system and research has been devoted to the synchronisation between both systems. In biomedical signal processing, there is a tendency to combine different signals using multimodal signal processing techniques to extract additional information compared to the different signals analyzed separately. This will become more important as it is possible to extract respiration information from the ECG signal using ECG derived respiration signals [10]. From the raw ECG signal, a respiration signal can be extracted. This respiratory signal arises from the movement of electrodes with respect to the heart during respiration. This causes changes in the electrical impedance, which modifies the waveform of the ECG signal.

4.5 Conclusion

The analysis of the heart rate signal during both experiments showed that heart rate variability (HRV) is a powerful tool to see the effect of mental stress. The HRV characteristics could differentiate between rest, physical and mental load. The addition of a mental load to a physical task elicited further effect on HRV parameters related to autonomic cardiac modulation. Time-frequency analysis revealed that the mental stress level changes in time within one phase. The effect

of the stressor used in this study was reduced after three minutes. This type of analysis is able to detect changes within the 6 minute phase that were not visualised by the standard HRV parameters when evaluated across the 6 minute phases. This clarifies the importance of using time-frequency for this type of applications. In addition, calculating HRV parameters is at low computational cost making the findings of this study useful in a biofeedback system.

The study of the effect of anxiety in pregnant women showed that anxiety, reflected from subjective questionnaires, revealed hardly any influence on the amount of cardiac reaction during the stress test and the day-night comparison. All time domain measures indicated a negative correlation with the STAI score during the different phases of the stress test. This confirms the hypothesis that anxiety reduces the variability of the heart rate. On the other hand, no correlations were statistically significantly different. The frequency content in the HF band, a marker of the parasympathetic modulation on the heart rate, revealed a statistically significant negative correlation coefficient during the different phases indicating a reduced parasympathetic influence in women with high anxiety. This was more apparent during the periods with mental load, although not in a statistically significant way. The mental task to initiate stress in this study could be questioned, as this task aims to initiate a very specific type of mental stress. For several pregnant women this task did not initiate stress as they were not interested in solving the arithmetic calculations.

The stress phenomenon is a very complex reaction. Stress is a subjective, psychological phenomenon that initiates different reactions in the brain of the subjects leading to physiological reactions. The results show that several people report to be very sensitive to mental stressors via questionnaires, which is by definition a subjective measure, does not result automatically in a very strong stress reaction in the physiological parameters. The absence of this correlation reveals that there are different processes in the brain that regulate the stress system and these processes interact with each other in a complex way. The nature of these complex interactions is still not clear and the question will be whether this complex system will be unravelled completely in the future. This explains why there is not a one-to-one relation between the initiator of the mental stress and the physiological stress response of the body.

Chapter 5

Near Infrared Spectroscopy: processing applied to muscle fatigue

The first part of this chapter describes the myoelectric and oxygenation mechanisms of muscles during muscle fatigue. More specifically, the behavior of the indiviual sEMG and NIRS parameters and their relationship in the biceps brachii muscle until exhaustion after isometric static and semidynamic exercises are investigated. In section 5.5, the sEMG and NIRS parameters are used to investigate the response of the oxygenation and the myoelectric signals of the muscle after a physical effort on patients with Duchenne Muscle Dystrophy in a pilote study.

5.1 Introduction

Knowledge of myoelectric and oxygenation mechanisms in muscles is important to understand muscle fatigue [94]. A frequently used definition of muscle fatigue is the one established by Edwards [45]: *Fatigue is defined as a failure to maintain the required or expected force.* As a consequence, a fatigued muscle can not maintain the expected force and exhaustion occurs at a specific point in time. Note that the cause of muscle fatigue is not limited to metabolic limitations in the muscle. Neurological, physiological and circulatory changes influence the development of muscle fatigue. These changes already occur at the beginning of the contraction. These initial changes can only be measured using techniques as surface electromyography (sEMG) for myoelectric changes and near-infrared

spectroscopy (NIRS) for oxygenation changes. NIRS appeared to be a reliable method for non-invasive muscle consumption [28, 130].

sEMG records the electrical activity of a muscle and is a good indicator of muscle force and fatigue [94]. Standard parameters of sEMG signals are extracted to analyze the electrical activity of the muscle. NIRS allows the direct and non-invasive measurement of local blood circulation, blood volume, and changes in oxygenated haemoglobin (Hb) and myoglobin (Mb) in working muscles [107]. Muscle oxygenation is the number of Hb saturated with oxygen (O_2) in the blood of the muscle. Oxygenation and blood volume decrease significantly and similarly during restriction of blood flow due to intramuscular pressure for example when caused by exercise [191].

Although considerable research had been devoted to myoelectric or oxygenation changes during fatigueing exercises, rather less attention has been paid to the combination of myoelectric and oxygenation changes during development of muscle fatigue. The aim of this study is to investigate the relationship between sEMG and NIRS parameters in the biceps brachii muscle until exhaustion after isometric static (STAT) and semidynamic (DYN) exercises. Understanding their behaviour can lead to additional information in order to make a better assessment of muscle fatigue [49].

This study was a collaboration of the group of prof. dr. Gunnar Naulaers (division of neonatology at the university hospital UZ Gasthuisberg of Leuven), where NIRS is used to measure the oxygenation in the brain of premature babies and the group of prof. dr. ir. Arthur Spaepen (lab of biomechanics and ergonomics, faculty of sports and rehabilitation sciences at the Katholieke Universiteit Leuven) where sEMG is used to study the muscle fatigue. This study is accepted for publication as a journal paper in Advances in Experimental Medicine and Biology in December 2010 [163].

5.2 Methods

5.2.1 Experimental procedure

In total, 34 test subjects (17 male, 17 female, 21 $\pm$ 2.0 years) were requested to sit on a chair with the right upper arm relaxed against the body and elbow angle equal to 90°, forearm positioned in supination with hand palm up. A wooden handle attached with a solid rope to a load cell was held in the hand. The subject was instructed to bend his elbow using only arm muscles. This static isometric contraction caused activation of biceps brachii muscle (BB). sEMG electrodes and NIRS probe were placed in the direction of muscle fibres on BB symmetrically [48]

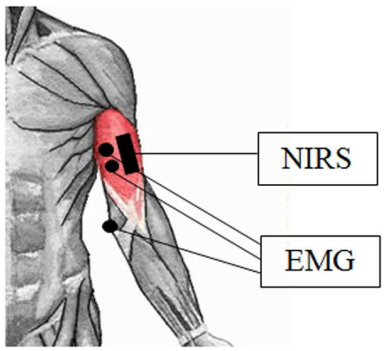


Figure 5.1: *Positioning of the sEMG electrodes and NIRS probe on the biceps brachii muscle [163].*

of the line between medial acromion and fossa cubit at 1/3 from fossa cubit [57] as shown in figure 5.1.

The exerted force on the load cell was amplified using a volt amplifier (HBM, Germany) and visual feedback of the force was given to the subject by a digital oscilloscope (Hewlett Packard, 54501A). sEMG signals (bipolar pre-gelled Ag/AgCl electrodes) were amplified. The NIRS probe (NIRO 300 , Hamamatsu Photonics K.K., Tokyo, Japan) was connected to the NIRO 300 measurement and display unit for visualization. All signals from sEMG, NIRO 300 and force transducer were digitised at a sampling rate of 1kHz with an analog-to-digital converter (National Instruments, cDAQ, 24 bit) before storage on a personal computer.

Figure 5.2 gives an overview of the protocol. Initially a maximal voluntary contraction (MVC) was measured as reference value for the sEMG signals and the total force of the test subject. After 5 minutes of recuperation, the subject performed a static contraction (STAT) at 50% MVC until exhaustion. On the oscilloscope, a line was fixed, representing the target level of force output. At the moment the force of the subject decreased to 90% of the required force, the muscle was defined as exhausted. After 20 min recuperation a isometric contraction with different load was exerted in the static position. In this manuscript, we will refer to this contraction as the semi-dynamic contraction (DYN) On the oscilloscope, two horizontal lines representing 20% and 60% MVC and time interval were displayed. Subject performed alternating 4s contractions at 20% MVC and 6s contractions at 60% MVC until exhaustion. The contractions at 50% and 60% of MVC are anaerobic, while a contraction at 20% MVC is aerobic.

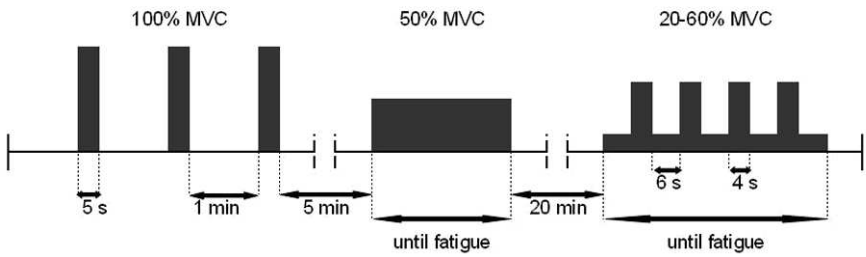


Figure 5.2: *Overview of the protocol to measure NIRS and sEMG during muscle fatigue.*

5.2.2 Muscle fatigue parameters

Surface electromyography (sEMG) is frequently used in kinesiology as an indicator of muscle activation, force production or fatigue index. This objective, non-invasive, and indirect method detects motor unit action potentials (MUAPs) in the muscle fibre during muscle activity. The summation of the MUAPs of the underlying muscle detected by the electrodes provides the sEMG signal that results in the ability to estimate non visible phenomena in the muscle such as muscle fatigue [94]. The tradiotional myoelectric parameters RMS and MPF are used next to the activity measure (ACT) which has been reported to be less sensitive to muscle fatigue. A last parameter, the ratio RMS/ACT, gives an indication of muscle fatigue that less dependent to changes of the muscle force [70].

Near-infrared spectroscopy (NIRS) is a non-invasive technique that can be used for the measurement of tissue oxygenation. This method is based upon the relative transparency of biological tissue to light in the near-infrared (NIR) part of the light spectrum. Signal detection is based on levels of light directed through the muscle and picked up by the detector after the light has travelled through tissue. Tissue oxygenation index (TOI) is a NIRS parameter and indicates the dynamic balance between O_2 supply and O_2 consumption in tissue capillaries, arterioles and venules [23, 112].

5.3 Results

All subjects successfully completed the protocol. The results are given in Table 5.1. MVC force produced by men was significantly larger than that produced by women ($p<0.001$) and women could significantly longer maintain the DYN test compared with men ($p<0.01$). The DYN test was significantly longer than the STAT test for all subjects ($p<0.001$) indicating that local muscle exhaustion was reached faster during the STAT test.

Table 5.1: *Duration of tests and MVC force, given as mean (SD)*

	STAT time (s) [s]	DYN time (s) [s]	MVC force (N) [N]
Total	78(20)	147(46)	175(7)
Men	73(20)	123(24)	235(5)
Women	83(19)	172(51)	116(3)

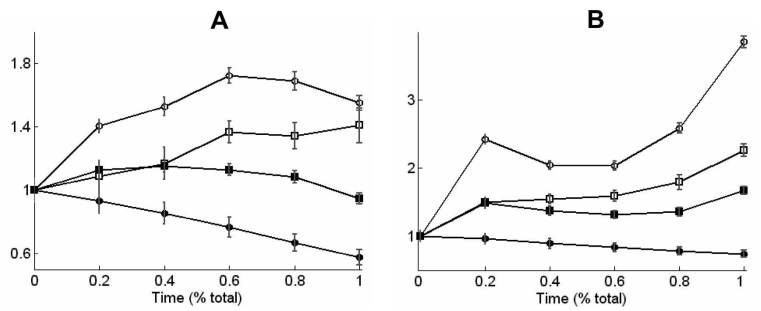


Figure 5.3: *the mean value of the sEMG parameters over all subjects during both tests (A: STAT, B: DYN) [163].*

Figure 5.3 shows the mean value of the sEMG parameters over all subjects during both tests (A: STAT, B: DYN). The time scale was normalised to the total contraction time until exhaustion. The figures reveal on group level an increasing RMS and RMS/ACT slopes ($p<0.001$), a decreasing MPF slope ($p<0.001$) and a flat ACT slope ($p>0.05$).

Figure 5.3 shows the TOI response of a representative subject during the STAT (A) and the DYN test (B). The TOI showed a typical four-phase response during both tests that could be identified for all the test subjects. The first 2-3 seconds after the initiation of the contraction, a small increase of TOI is noticed, indicating an increase in muscle oxygenation (phase 1). Secondly, a fast linear decrease of the TOI could be identified. The change in TOI during phase I and II was similar for both contraction modalities. There was no statistically significant difference of the duration of phase 2 within the subjects between the two tests. In the third phase, the TOI is on group level almost constant and dependent on the type of contraction. There is a flat line for the STAT test, while the trace of the TOI during the DYN test is following the contraction intensity. The ΔTOI, which is the difference between the initial value during phase I and the constant value of phase III (the mean value is taken during the DYN test), correlates negatively

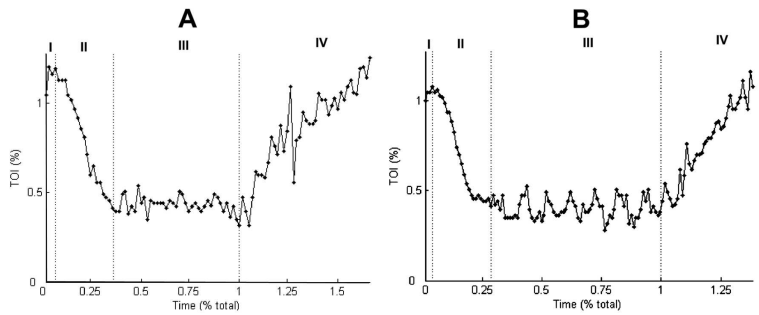


Figure 5.4: *the TOI response of a representative subject during the STAT (A) and the DYN test (B) [163].*

with the total exertion time (STAT: r = -0.56, p<0.001; DYN: r = -0.66, p<0.001). Higher differences in the TOI value resulted in a shorter duration of exercise and consequently exhaustion occurs faster. Subjects with a small negative TOI slope in phase II could maintain both tests longer (STAT: r=-0.64, p<0.001; DYN: r=-0.74, p<0.001). Finally phase 4 shows the TOI after the contraction. This phase shows the TOI during recuperation and was only recorded after the STAT test. There was an initial overshoot of the TOI after contraction, but the TOI recovered to the initial value within the 20 minutes of recuperation between the STAT and the DYN test. The TOI value at the beginning of the DYN test was not statistically significantly different with the initial TOI value.

The MPF and the TOI slope during phase 2 are significantly correlated during both the STAT and DYN test (p<0.001). During the DYN test, a statistically significantly negative correlation between the TOI slope during phase II and the RMS/ACT ratio is also identified (p<0.01), however, this correlation was not significant during the STAT test. In earlier studies, a strong positive correlation was reported between muscle oxygenation and MPF [48, 23].

5.4 Discussion

During both tests for all the subjects, an increasing RMS and RMS/ACT slopes, a decreasing MPF slope and an almost stable ACT slope was found for all the subjects. The sEMG parameters confirm that muscle fatigue is an ongoing linear process that initiates from the very beginning of the contraction [70]. Both pictures show that RMS/ACT corrects for movement compensation during the fatigue test. The RMS/ACT curve is more an increasing straight line compared to the RMS curve, which is generally used in literature. This confirms the finding of [70] that

RMS/ACT is a better parameter to estimate muscle fatigue. The RMS/ACT ratio and MPF are clear indicators for the myoelectric activity of local muscle fatigue.

The TOI showed a four-phase response during both tests, which was also demonstrated in earlier studies [48]. A short increase was identified, followed by a decrease in TOI. The duration of this decline seems parallel with the energy pathways for muscle exercise. The muscle firstly consumes any ATP stored in the muscle (about 2-3 seconds). Afterwards, it uses phosphocreatine (CP) as energy source to resynthesize ATP until the CP is depleted, which lasted according to the literature for 15-30s [2]. After the ATP and CP are used, the body will move on to either aerobic or anaerobic metabolism (glycolysis) to continue to create ATP to fuel exercise. The energy during the third phase is probably mainly taken from glycogen in anaerobic glycolysis due to a deficit in oxygen. The mechanical obstruction of the blood flow in the muscle during a contraction limits the supply of sufficient oxygen. This leads to the accumulation of lactic acid followed by an oxygen debt resulting in muscle exhaustion [2]. During the DYN test, the trace of the TOI is following the contraction intensity. This indicates an increased supply of oxygen during the 20% MVC contraction, which is an aerobic contraction, leading to a small recuperation period during the DYN test. These short periods of recuperation during the aerobic contraction were absent during the STAT test, where the contraction was the complete duration anaerobic, and explains why the STAT test was statistically significant shorter for all the test subjects. The duration of phases I and II were similar during both tests for all the test subjects, while the length of the third phase was dependent on the length of the contraction. After the exercise, during the fourth phase, there is an overshoot of the TOI revealing an increase in oxygen supply for recuperation.

The negative correlation between Δ TOI and total exertion time reveals that higher deoxygenation during the contraction results in earlier exhaustion of the muscle. A higher deoxygenation during phase II causes a larger oxygen debt resulting in a faster fatiguing process. Despite the evidence in sEMG that fatigue is an ongoing linear process, NIRS does not reveal this. On the other hand, a NIRS parameter gives an indication of the velocity of the fatigue process.

This study shows that although sEMG and NIRS measure two different physiological phenomena of muscle fatigue, there is a link between both measurements. The MPF of the myoelectric signal is strongly correlated with the muscle oxygenation. On the other hand, only sEMG shows that muscle fatigue is an ongoing linear process that starts from the beginning of the contraction, while the duration of the contraction was correlated with a parameter from the TOI. We can conclude that both sEMG and NIRS give complementary information concerning muscle fatigue.

5.5 Muscle activity assessment for patients with Duchenne Muscle Distrophy (DMD)

Duchenne muscular dystrophy (DMD) is an X-linked recessive neuromuscular disorder clinically characterised by progressive muscle weakness starting in childhood and leading to death around the age of 20 years. With an estimated birth prevalence of 1 in 4200 live born males, it is one of the most frequent neuromuscular disorders. DMD is a progressive muscle disease that starts with an abnormal gait with toe walking, but continues with a decrease in muscle strength. This decrease in muscle strength initiates from the distal muscles in the limbs and makes the children wheelchair bound at the age of around 12 with a complete loss of mobility. There is a progressive functional loss of the respiration muscles and the heart muscle and leads to a mortality at around 20-25 years [14].

DMD is caused by mutations of the dystrophin gene which is located on the short arm of the X-chromosome (Xp21). The protein product, called dystrophin, is situated at the sarcolemma in muscle fibres and is part of the dystrophin-glycoprotein-complex (DGC). The DGC provides a structural link between the actin cytoskeleton and the extracellular matrix, thereby stabilizing the sarcolemma during cycles of muscle contraction and relaxation [19]. Although the primary gene deficiency is known since 1996, the precise mechanism by which dystrophin deficiency causes the destruction of muscle fibres is still unknown and until now, there is no effective treatment and complete healing for this disease. Treatment goals are to maintain function, prevent contractures and keeping these children standing and walking as long as possible.

The diagnosis of DMD is based on clinical signs and indirect measures and is confirmed after a muscle biopsy. The progress of the disease is monitored via indirect measures: walking test, maximal force, breathing volume ... But at this moment, no objective measure exists at this moment. Therefore, we performed an explorative study to investigate the response of the oxygenation and the electrophysiology of the muscle after a physical effort on patients with DMD. For this measurement, NIRS and sEMG are acquired continuously and simultaneously. The probe of the NIRS and the sEMG electrodes are placed on the biceps brachii muscle of the test subject (as shown in figure 5.1). The ultimate goal is to look for differences in the muscular metabolism of these DMD patients during and after a contraction to establish an objective parameter of the progress of the disease. The protocol consisted of a rest period of 2 minutes, a submaximal (60% of MVC), aerobic, isometric elbow flexion during 1 minute, followed by a recuperation phase of 10 minutes where the muscle is at rest.

This project was a continuation of the research on muscle fatigue where sEMG and NIRS were used and was executed at the UZ Gasthuisberg with the group of prof. dr. Gunnar Buyse (Division of pediatric neurology). 18 test subjects

were measured in this pilote study where 16 DMD patients and 2 healthy children. The age of the DMD patients ranged from 7 years at which there is only initial manifestation of the disease to 20 years (severe manifestations of the disease: patients have limited mobility and are wheelchair bounded).

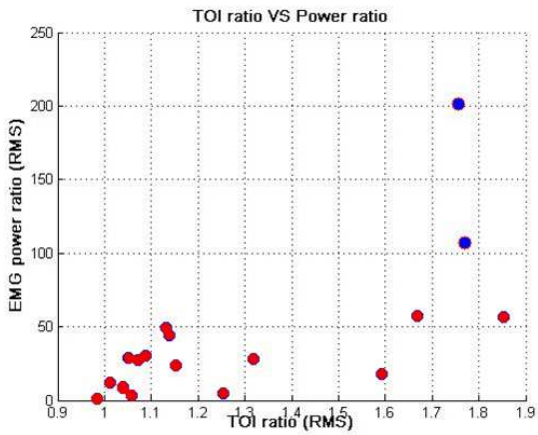


Figure 5.5: *The change in muscle oxygenation in function of the change in muscle amplitude. DMD patients are in red, healthy patients in blue.*

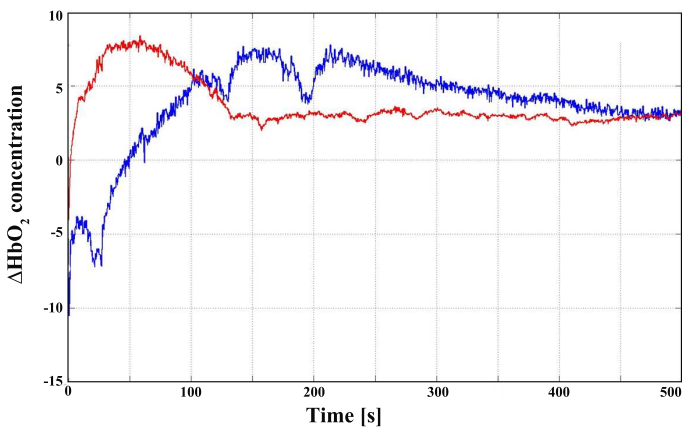


Figure 5.6: *Initial recuperation of the oxidised haemoglobin after the contraction. Red trace is the DMD patient, the blue trace is the healthy patient.*

The healthy patients can be differentiated from the DMD patients based on the results showed in figure 5.5. The change from rest to contraction in tissue oxygenation is plotted in function of the change in sEMG amplitude. The healthy

patients showed a larger difference in sEMG activity. The control children showed a decrease in TOI during the contraction, while for the patients with severe manifestations of the disease, this decrease in tissue oxygenation index was low or absent. The DMD patients (blue dots) at the right of the figure are the youngest patients that show limited manifestations of the disease. The older patients are clustered around each other as they show limited reaction in both physiological signals during the submaximal contraction.

Figure 5.6 shows the initial recuperation of the oxidised haemoglobin after the contraction. A different profile can be seen between the healthy patient and the DMD patient. The DMD shows a faster overshoot of the HbO_2, but a faster return to baseline.

A different profile in the dynamic of the oxidised and reduced heamoglobin can be observed between normal subjects and patients with Duchenne Muscle Dystrophy by means of Near-Infrared spectroscopy and sEMG signals. Preliminary studies have found that this profile presumably changes accordingly to the state of the muscle degeneration. In this patient a faster return to baseline, compared to normal patients, of the oxidised haemoglobine after contraction preceded by an overshoot was found, together with a undershoot in the reduced haemoglobine and a fast return to baseline values. A possible explanation of this behaviour can be related to the increase of the oxydative strees inside the cell, produced by a higher concentration of calcium, which can lead to a state where the muscle acts as it is still contracted even when the contraction has finished, together with a possible acceleration of the cell oxygen consumption; however, no evidence of persisted contraction has been found yet in patients with the distrophy. Further studies are needed in order to confirm this hypothesis and to find relation with the dystrophy pathophysiology.

In the first focus will be with the patients in the range of 6-12 years old. This is the group that receives medical interventions to increase their quality of life and is therefore the most interesting group at this moment.

5.6 Conclusion

The study presented in the first part of this chapter shows that although sEMG and NIRS measure two independent physiological phenomena during muscle fatigue, there is a link between both measurements. The MPF of the myoelectric signal is strongly correlated with the muscle oxygenation. On the other hand, only sEMG shows that muscle fatigue is an ongoing linear process that starts from the beginning of the contraction, while the duration of the contraction was correlated with a parameter from the TOI. We can conclude that both sEMG and NIRS give complementary information concerning muscle fatigue. The TOI showed a typical

four-phase response during contraction that could be related to the metabolic processes in the muscle

There are indications that the sEMG and NIRS combination reveal information about the muscle state and the progress of the disease. Different parameters could be defined that could distinguish between the healthy patients and the patients with the DMD disease.

Chapter 6

Conclusions and future research

6.1 General conclusions

6.1.1 Mathematical techniques

- To remove the major source of interference (ECG contamination) in a sEMG signal in the shoulder girdle, two recently developed single channel approaches of independent component analysis (ICA) were used and their performance was compared with the standard technique (template subtraction) to remove the ECG interference signal. These two techniques are based on the idea to decompose a single measurement using wavelets or ensemble empirical mode decomposition (EEMD) before applying ICA on their decompositions. When the corresponding ECG signal is not available which could be the case during different measurements, EEMD-ICA has the best performance compared to wICA and yields similar performance as the template subtraction for higher SNR, while for lower SNR, EEMD-ICA is significantly better than template subtraction and slightly better than wICA. We can conclude that for offline use, when the calculation time is not important, EEMD-ICA has the best performance. When the ECG channel is present, the template subtraction is preferable due to a better performance and lower computational time.

- An interesting pattern is discovered during the visual inspection of the sEMG signals of the trapezius muscle: spontaneous activation of a single motor unit. An algorithm to detect spike trains is capable of detecting single motor

unit firings. The algorithm, based on an energy operator and correlation calculation, showed an excellent performance as it reaches a sensitivity of 100% and a specificity of 94,8%.

- An algorithm to detect the absolute rest level of a muscle, the Rest Level Estimation (RLE), is developed and this algorithm is used to determine the true rest level of the muscle based on the frequency properties of the sEMG signal during contraction and in rest. Via easy thresholding, this algorithm is able to differentiate between the signals of the muscle in rest and in contraction. The RLE also has other useful applications. As it measures the rest level of a muscle in an objective way, without a reference measurement, we are able to distinguish in a daily task between the active and rest state of the muscle. The RLE can therefore be used in a biofeedback system to alert users if there are too few rest periods, and in the long term, help prevent musculoskeletal disorders of the neck and shoulder.

6.1.2 Stress

- sEMG signals of the trapezius muscle showed an interesting specific pattern: in approximately 65% of the subjects measured during a stress assessment task, spike trains appeared in the signals. We have evidence that these spike trains are the continuous firing of a single motor unit. This indicates a very low and subconscious muscle contraction without the benefit for postural change. This pattern could not be related directly to stress, as it appeared randomly in the right and left muscles, during periods with rest and with a mental load. This could suggest that the presence of a mental load restrains the muscle from relaxing and recuperating. Frequent prevalence of single motor unit firing can lead to overload and exhaustion of these muscle fibers, resulting in pain and tissue damage.

- The sEMG parameters of the trapezius muscle showed no relation with the imposed mental task. However, this muscle shows spontaneous activity without any beneficial effect on the posture. The SMUF is one example of this spontaneous activity, next to the recuperation that this muscle needs after a conscious contraction. There is more tension on this muscle than expected and overuse of these muscle fibers could lead to exhaustion and possible to MSD afterwards. Therefore, the monitoring of this muscle in the battle against MSD is preferable.

- Two experiments were conducted to reveal the effect of mental stress on the muscle activity of the trapezius muscle. This mental load was imposed in situations with and without a physical load. The two experiments differed in the level of postural load imposed. For the first experiment, test subjects performed a heavy 6-minute shoulder abduction with and without a mental

task. Muscle tension did not increase significantly with the addition of a mental task. The possible additive effect of the mental load was assumed to be low and was probably overshadowed by the muscle activity for the postural load. For the second experiment, the postural task was to click a computer mouse, emulating a lower postural load more similarly to office tasks. The results for the second experiment were similar to the results of the first one. At a group level, muscle activity did not differ significantly for a postural task with or without a mental task for the left an right shoulder muscles. The reactions of the muscle activity of the trapezius are individual and different among the subjects so that no statistically significant differences could be identified. The analysis of the trapezius muscle activity as physiological measure is insufficient to see the effect of mental stress on the muscle activity. This is confirmed via video analysis, which reveals that other muscle groups also show muscle reaction. To have a broader view on the muscle reactions due to stress, other muscles of the body should also be included in future studies such as different face muscles (masseter, frontalis and temporalis muscle), the paravertebral muscles and the multifidus muscle.

- The heart rate variability analysis during both experiments showed that this is a very promising tool to see the effect of mental stress. We were able to differentiate the HRV characteristics between rest, physical and mental load. The addition of a mental load to a physical task elicited further effect on HRV parameters related to autonomic cardiac modulation. Time-frequency analysis revealed that the mental stress level changes in time within one phase. The effect of the stressor used in this study was reduced after three minutes. This type of analysis is able to detect changes within the 6 minute phase that were not visualized by the standard HRV parameters when evaluatedacross the 6 minute phases. This clarifies the importance of using time-frequency for this type of applications. In addition, calculating HRV parameters is at low computational cost making the findings of this study useful in daily life. HRV can be promising to be used in a biofeedback system. In addition, calculating HRV parameters is at low computational cost making the findings of this study useful in a biofeedback system.

- The analysis of the effect of anxiety in pregnant women shows that there is no correlation between the subjective questionnaires and the amount of cardiac reaction during the stress test. Stress is, in its nature, a subjective and psychological phenomenon that initiates different reactions in the brain of the subjects leading to physiological reactions. The results show that although several people report via questionnaires to be very sensitive to mental stressors, they do not have automatically a very strong stress response in these physiological parameters. The absence of this correlation reveals that there are different processes in the brain that regulate the stress system and these processes interact with each other in a complex way. The nature of these complex interactions is still not clear and the question will be

whether this complex system will be unravelled completely in the future. This explains why there is not a one-to-one relation between the initiator of the mental stress and the physiological stress response of the body.

- Both, the analysis of the muscle activity and the heart rate variability reveal the need for individual analysis during stress monitoring. The stress system consists of very complex reactions in the brain, which are at this moment not completely understood. Those reactions, however, are responsible for the different reactions of individual people on stressors: both in the amount of the reaction as in the physiological reaction itself.

- The mental tasks to initiate stress in this manuscript could be questioned. These tasks initiate a very specific type of mental stress. There are subjects that have a very strong stress reaction by solving these specific tasks imposed in the experiments, while others are not stimulated to solve arithmetic calculations as good as possible. Several subjects showed a change in physiological reaction during the first rest period of the experiments, which means that they were not at ease at that time moment. In the study with the pregnant women, their main concern is to have a healthy baby. This concern is mainly responsible for the anxiety level. The mental arithmetic test could induce a different type of mental stress that is not linked with the concerns of the pregnant women.

6.1.3 Other Applications

- The study that analyses the myoelectric and oxygenation mechanisms of muscles during muscle fatigue shows that although sEMG and NIRS measure two independent physiological phenomena of muscle fatigue, there is a link between both measurements. The mean power frequency (MPF) of the myoelectric signal is strongly correlated with the muscle oxygenation. On the other hand, only sEMG shows that muscle fatigue is an ongoing linear process that starts from the beginning of the contraction, while the duration of the contraction was correlated with a parameter from the TOI. We can conclude that both sEMG and NIRS give complementary information concerning muscle fatigue. The TOI showed a typical four-phase response during contraction that could be related to the metabolic processes in the muscle.

- There are indications that the sEMG and NIRS combination reveal information about the muscle state and the progress of the Duchenne Muscle Dystrophy. Different parameters could be defined that could distinguish between the healthy patients and the patients with the DMD disease.

6.2 Future work

6.2.1 EMG analysis

High Density sEMG

In this work, traditional differential surface electromyography signals are used. The main functionality that can be monitored using these signals is related to the overal muscle activation and muscle force. A lot of valuable information is lost using these signals. Therefore, sEMG signal processing should continue in the direction of the HD-EMG. This enables to analyze the behavior of individual motor units and increases the information that can be retrieved from the sEMG signals. Moreover, recently developed multichannel techniques that proved to be successful in for example brain analysis using an electroencephalogram or image processing techniques could be modified to process these signals and improve the analysis.

We suggest that this HD-EMG should be introduced in the stress research as the analysis of the single channel sEMG do not provide that much information. The analysis reveal that there is muscle activity in the trapezius muscle during several periods, but more information about the origin of the activity, the number of motor units that are involved could help to identify the real cause of the muscle activity. To this extent, more specific information about the single motor unit firings that we discovered in the sEMG analysis during both experiments could be derived: where is the motor unit located, is it always the same single motor unit that starts firing or does this alters ... All these questions can be answered using HD-EMG.

Trapezius muscle

The behavior of the trapezius muscle needs special attention in the stress research. This muscle acts differently compared to other skeletal muscles and the complete functionality of this muscle is still not completely clear. There is a spontaneous activation of this muscle, but the origin of this activation is still unclear. Moreover, this muscle needs recuperation time after a conscious contraction, while other muscles are immediately in rest after a contraction. All these extra activations of the muscle are making it vulnerable to musculoskeletal disorders. A lot of people that suffer from long term exposure to stress know about tension and pain in this muscle. More research should be devoted to reveal the physiological processes that are taking place in this muscle and which measures could be taken to relax this muscle. The use of NIRS to investigate the oxygenation of this muscle

during different types of physical and mental load could increase the insight in the behaviour of this muscle.

6.2.2 Heart Rate Variability and respiration

There is an ongoing discussion in the literature about the role of respiration in heart rate variability. There is a clear relationship between the ECG signal (and the tachogram) on one side and the respiration on the other side. A respiration signal can be extracted from the ECG and several HRV parameters are related to respiratory influences. But the complete interaction between respiration and HRV is still not clear. The RSA component is the component that quantifies the increase in heart rate due to inspiration and the decrease with expiration. However, the information from this measure is also used as a measure for the vagal modulation of the autonomic nervous system on the heart rate. This implies that there is more information than only the respiration present in this component and signal processing techniques should be used to extract this extra information. Moreover, the interaction between the heart rate and respiration could provide extra information, so techniques need to be developed to quantify this interaction.

This result presented in this manuscript about the effect of anxiety on the difference in reaction of the HRV parameters is a small part of a bigger project with a follow up of the pregnant women and their babies. For future analysis, the physiological scores via HRV can be used as predictor for the development of the fetus and its problems and compared with the results when the psychologic questionnaires for anxiety are used.

6.2.3 Near Infrared Spectroscopy in muscle analysis

Muscle oxygenation

In the study presented in this manuscript, the tissue oxygenation index showed a typical four-phase evolution during a submaximal contraction until exhaustion. By analyzing these signals and looking at the timing, we could link several phases to metabolic processes in the muscles. But at this moment, there is no evidence that this metabolic information could be extracted from the tissue oxygenation index and more research in collaboration with physiologists needs to be devoted to this topic. At this moment, only the TOI is used, but also the oxidised, the reduced and the total amount of haemoglobin can be monitored over time.

Duchenne Muscle Dystrophy

The use of NIRS and sEMG is relatively new in the research of the patients with Duchenne Muscle Dystrophy. The results of the explorative pilote study reveal that there could be valuable information in these physiological signals, but a more thorough research should be executed where patients with the Duchenne Muscle Dystrophy and healthy children of the same age are monitored. The ultimate goal would be a standardised test using one or both physiological measurement to monitor the evolution of the disease and to see whether different interventions improve the disease and the quality of life of these patients. A next study will limit the study population between 6 and 12 years old as this is the range of patients where medical interventions could improve their quality of life.

6.2.4 Stress

Multidisciplinary research

The phenomenon of stress is a very complex system consisting of very various interactions in the brain. The nature of these complex interactions is still not clear and the question will be whether this complex system will be unravelled completely in the future. This explains why there is not a 1 to 1 relation between the cause of the mental stress and the physiological stress response of the body. Because of the complexity, stress is at this moment a hot topic in research and its impact will even increase more in the future. Many research groups with different backgrounds are working in the field of stress: Psychologists are elaborating the psychological aspect of the stress and well-being and the impact on the personality of persons; In psychiatry, there is a focus on the consequences of stress leading to chronic fatigue syndrome, depression, obesitas... Biomedical engineers start looking at changes that occur in different physiological signals such as the heart rate, muscle activity, respiration... And physiotherapists are studying meditation therapies and techniques to reduce the stress. A next step in the research should be a close collaboration between the different research divisions working in this area. Biomedical engineering and signal processing, for example, could benefit substantially from knowledge of the physiological processes in the brain and the body due to stress in order to increase the accuracy of analysis, while psychology can make a big step forward when taking the psychophysiological background of stress into account. Therefore, the research of stress should be tackled in a highly inter- and multidisciplinary way where the combination of the knowledge of the different scientific areas and the strong interaction between these multidisciplinary research groups should generate the required synergy to advance the insight and knowledge in stress and stress monitoring. At this moment, it is too early to say whether stress detection will be possible. Stress remains the mysterious interaction

between the body and the mind, which is not resolved at this moment. The question is whether this subjectivity and objectivity will be coincide at one time. Big leaps still needs to be taken in this direction. Multidisciplinary research could be a first step towards the good direction.

Appendix A

The results of the ECG removal (described in section 3.3) of the 8 real life signals are presented in this appendix. In this figures, the first 15 seconds are plotted for clarity, but these 15 seconds are a representative for the rest of the signal. The first eight figures (1-8) show the results of the single channel approach, where the ECG interference is removed using only the sEMG signal. The next eight figures (9-16) show the results of the same signals using the two channel approach where both the sEMG signal and the corresponding ECG signal are used. Each figure shows from top to bottom the original contaminated signal, the cleaned sEMG signal from respectively the template subtraction, the wavelet-ICA and the EEMD-ICA. The bottom plot shows the corresponding ECG signal to see the occurrence of each heart beat.

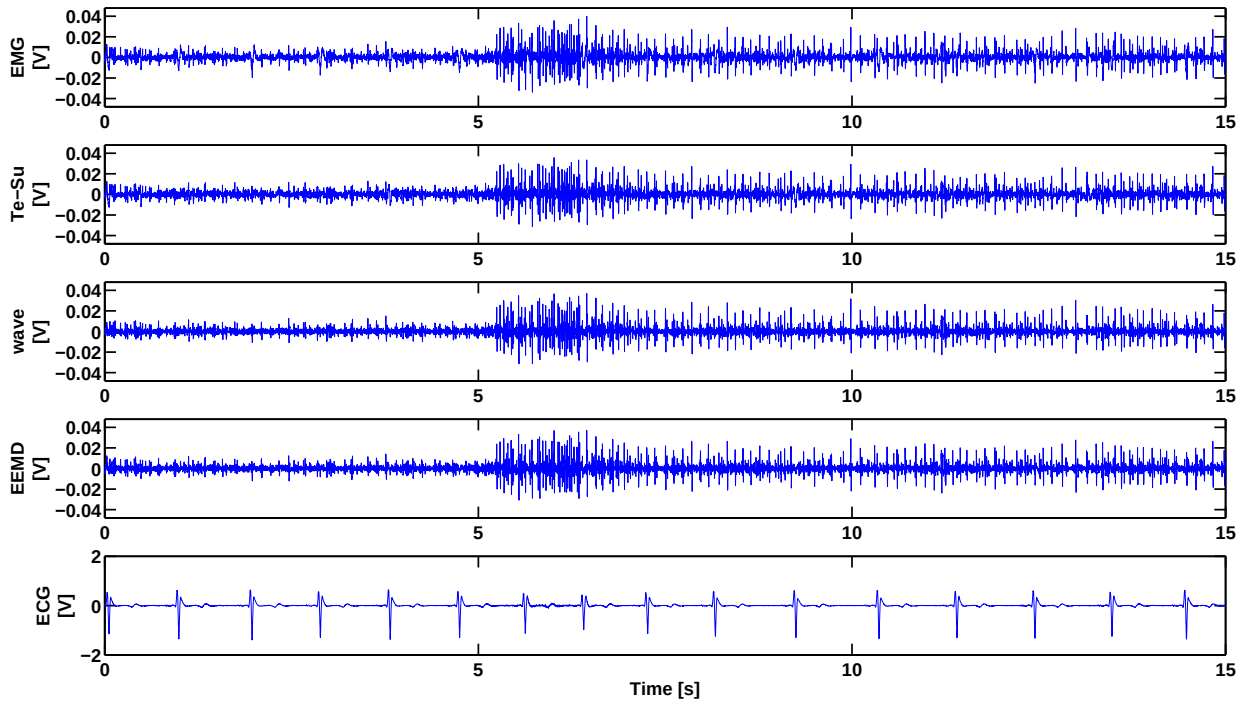


Figure 1: *ECG removal on real life signal 1 using the* ***single channel*** *approach. The top figure shows the contaminated sEMG signal. The middle three figures show the results after cleaning with the template subtraction (Te-Su) algorithm, after wavelet-ICA (wave) and Ensemble Empirical Mode Decomposition-ICA (EEMD). The lower trace show the corresponding ECG channel for validation.*

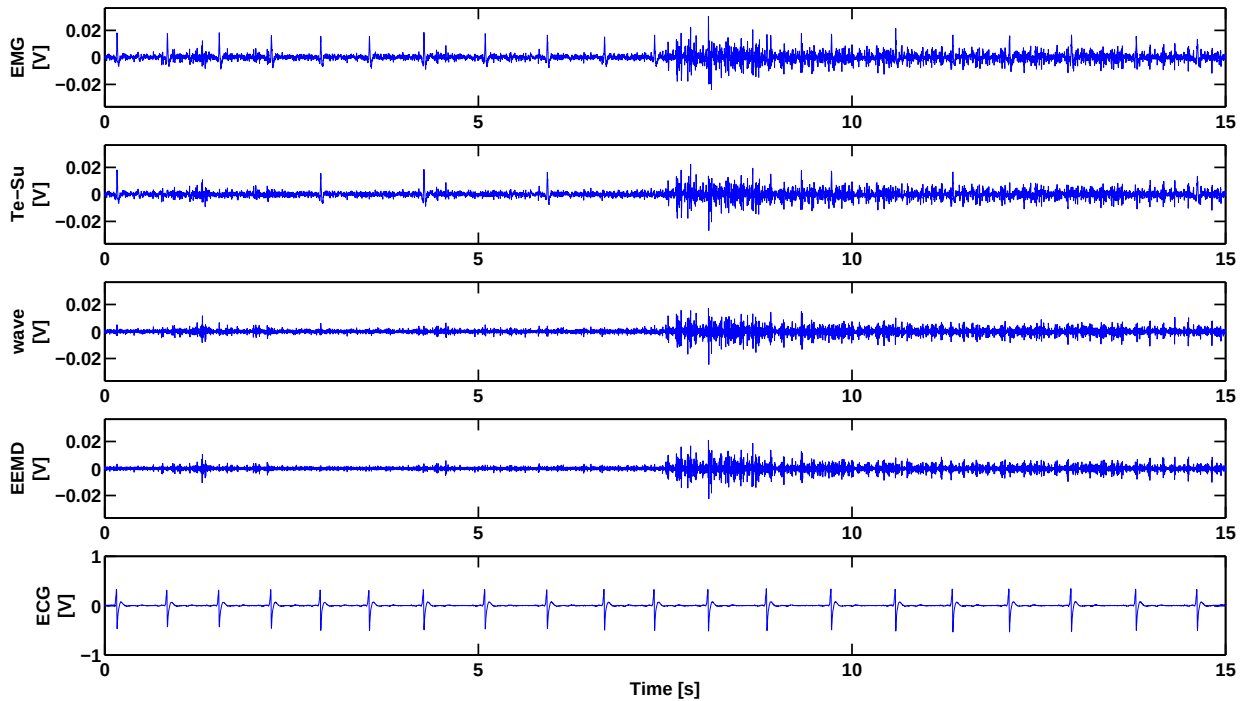


Figure 2: *ECG removal on real life signal 2 using the* ***single channel*** *approach. The top figure shows the contaminated sEMG signal. The middle three figures show the results after cleaning with the template subtraction (Te-Su) algorithm, after wavelet-ICA (wave) and Ensemble Empirical Mode Decomposition-ICA (EEMD). The lower trace show the corresponding ECG channel for validation.*

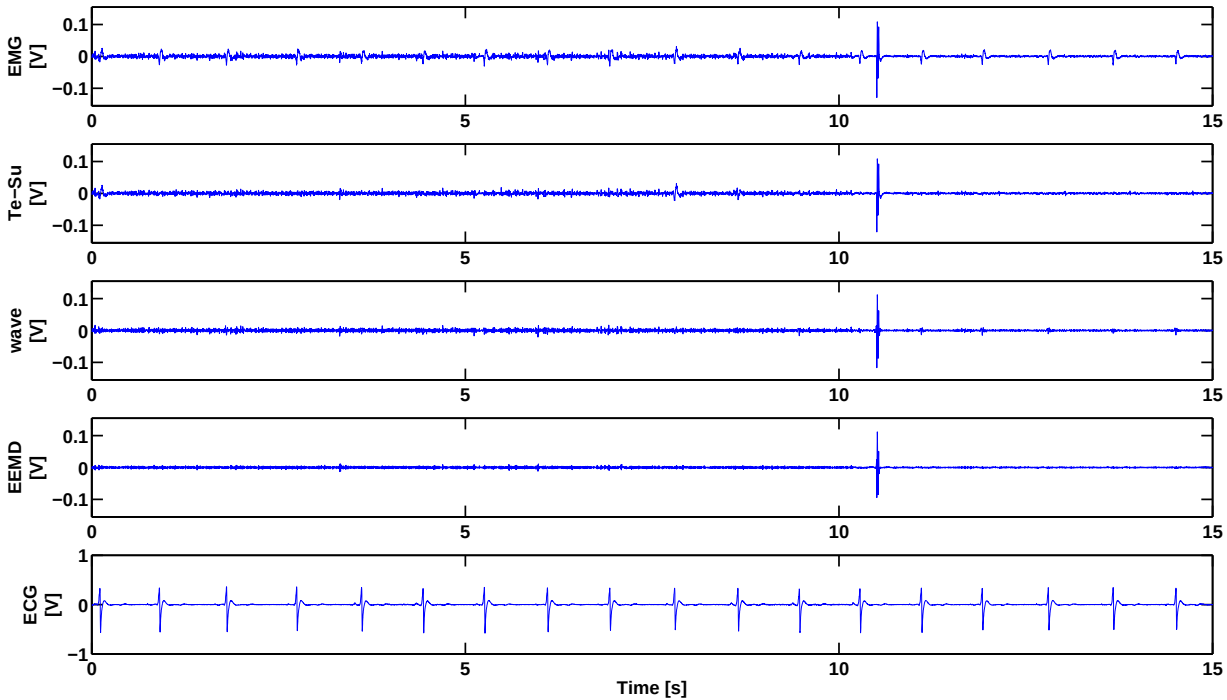


Figure 3: *ECG removal on real life signal 3 using the* ***single channel*** *approach. The top figure shows the contaminated sEMG signal. The middle three figures show the results after cleaning with the template subtraction (Te-Su) algorithm, after wavelet-ICA (wave) and Ensemble Empirical Mode Decomposition-ICA (EEMD). The lower trace show the corresponding ECG channel for validation.*

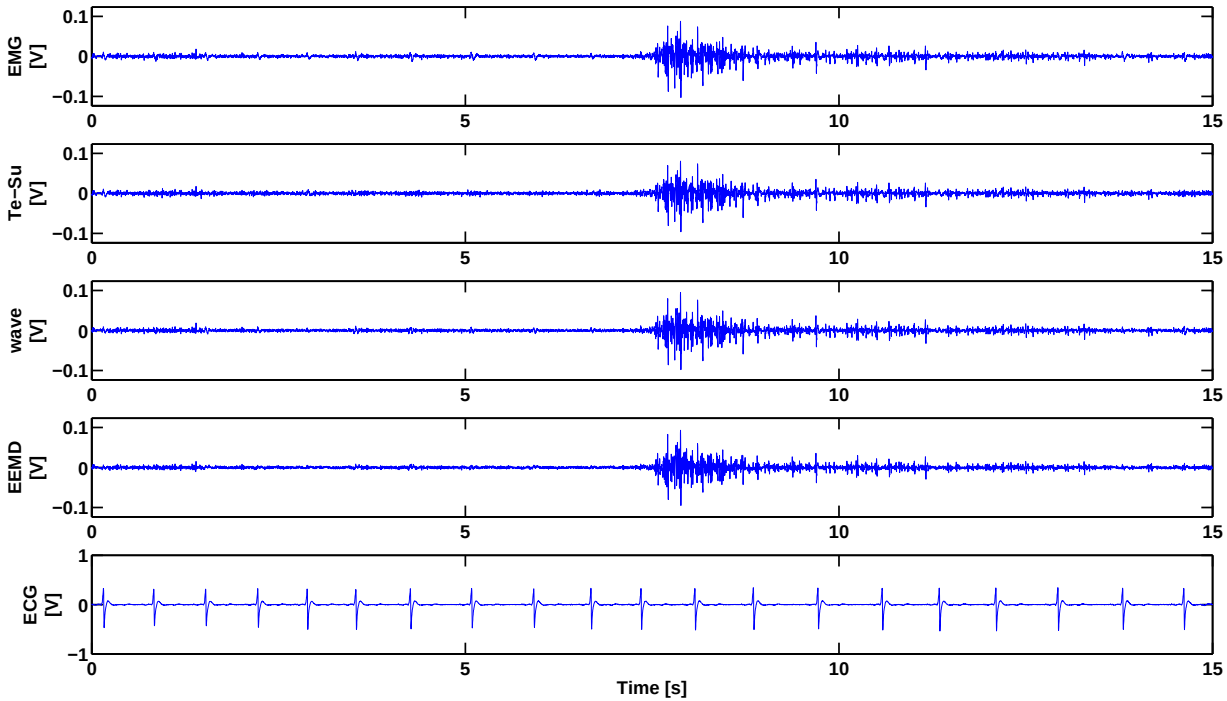


Figure 4: *ECG removal on real life signal 4 using the* ***single channel*** *approach. The top figure shows the contaminated sEMG signal. The middle three figures show the results after cleaning with the template subtraction (Te-Su) algorithm, after wavelet-ICA (wave) and Ensemble Empirical Mode Decomposition-ICA (EEMD). The lower trace show the corresponding ECG channel for validation.*

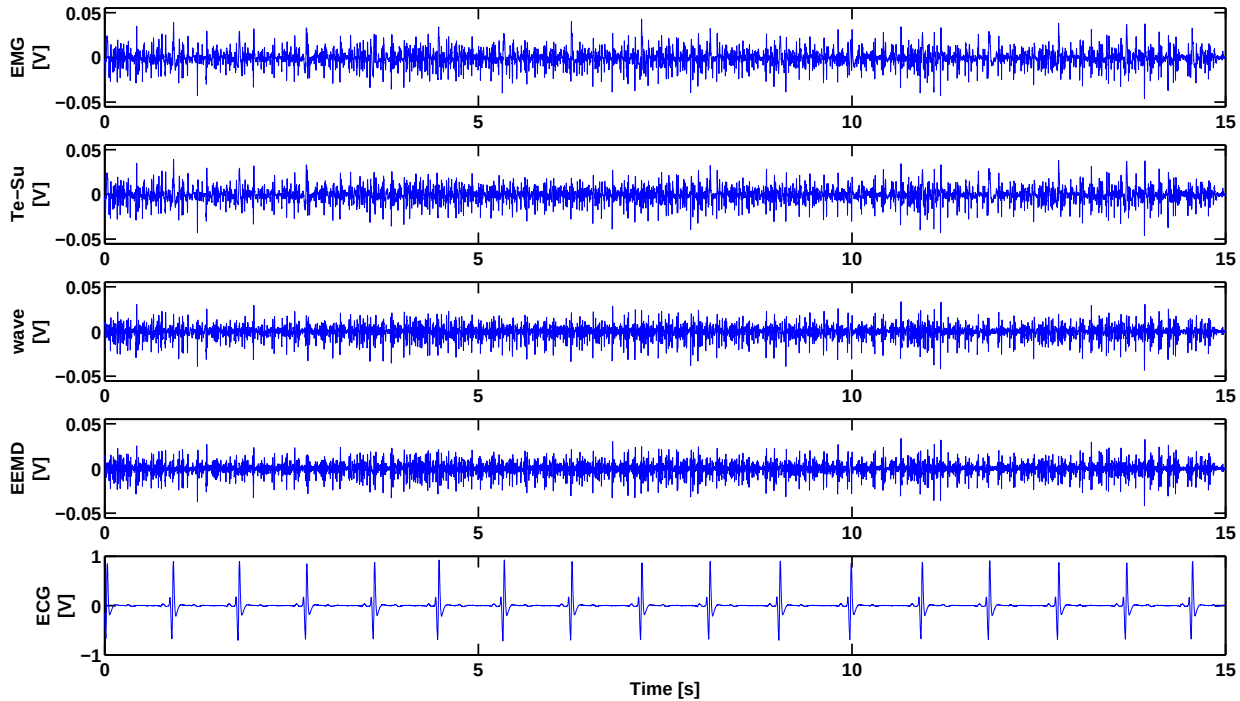


Figure 5: *ECG removal on real life signal 5 using the* ***single channel*** *approach. The top figure shows the contaminated sEMG signal. The middle three figures show the results after cleaning with the template subtraction (Te-Su) algorithm, after wavelet-ICA (wave) and Ensemble Empirical Mode Decomposition-ICA (EEMD). The lower trace show the corresponding ECG channel for validation.*

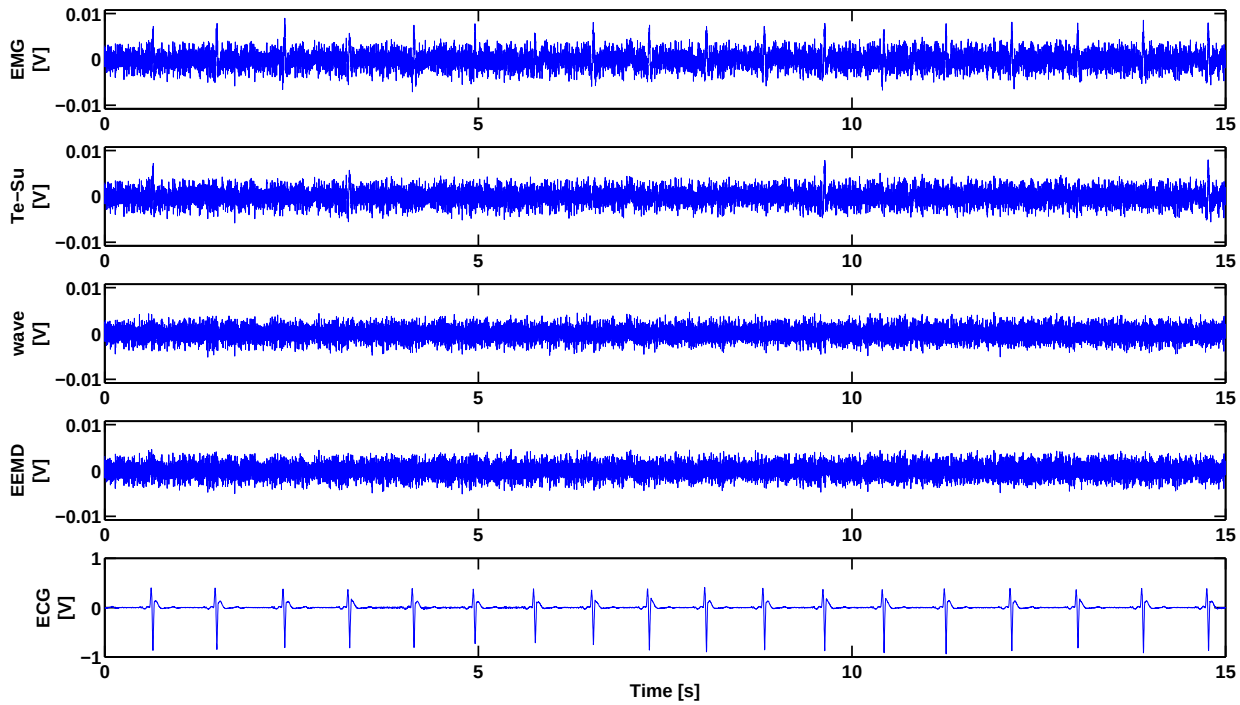


Figure 6: *ECG removal on real life signal 6 using the* ***single channel*** *approach. The top figure shows the contaminated sEMG signal. The middle three figures show the results after cleaning with the template subtraction (Te-Su) algorithm, after wavelet-ICA (wave) and Ensemble Empirical Mode Decomposition-ICA (EEMD). The lower trace show the corresponding ECG channel for validation.*

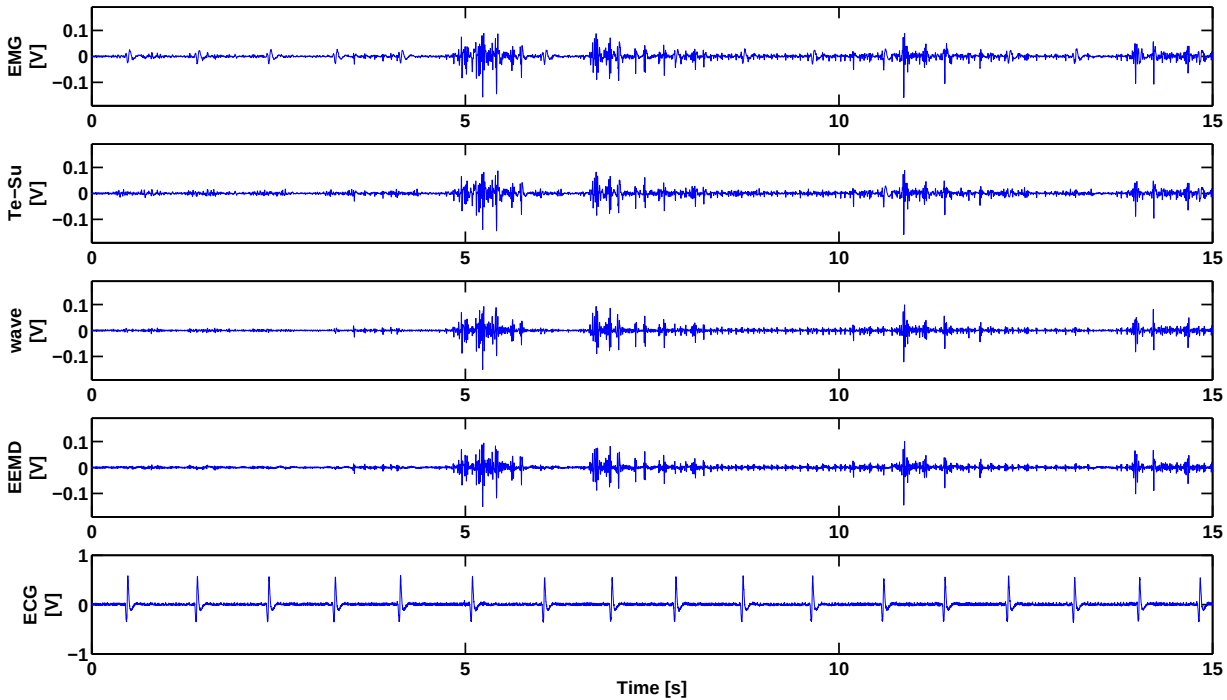


Figure 7: *ECG removal on real life signal 7 using the* ***single channel*** *approach. The top figure shows the contaminated sEMG signal. The middle three figures show the results after cleaning with the template subtraction (Te-Su) algorithm, after wavelet-ICA (wave) and Ensemble Empirical Mode Decomposition-ICA (EEMD). The lower trace show the corresponding ECG channel for validation.*

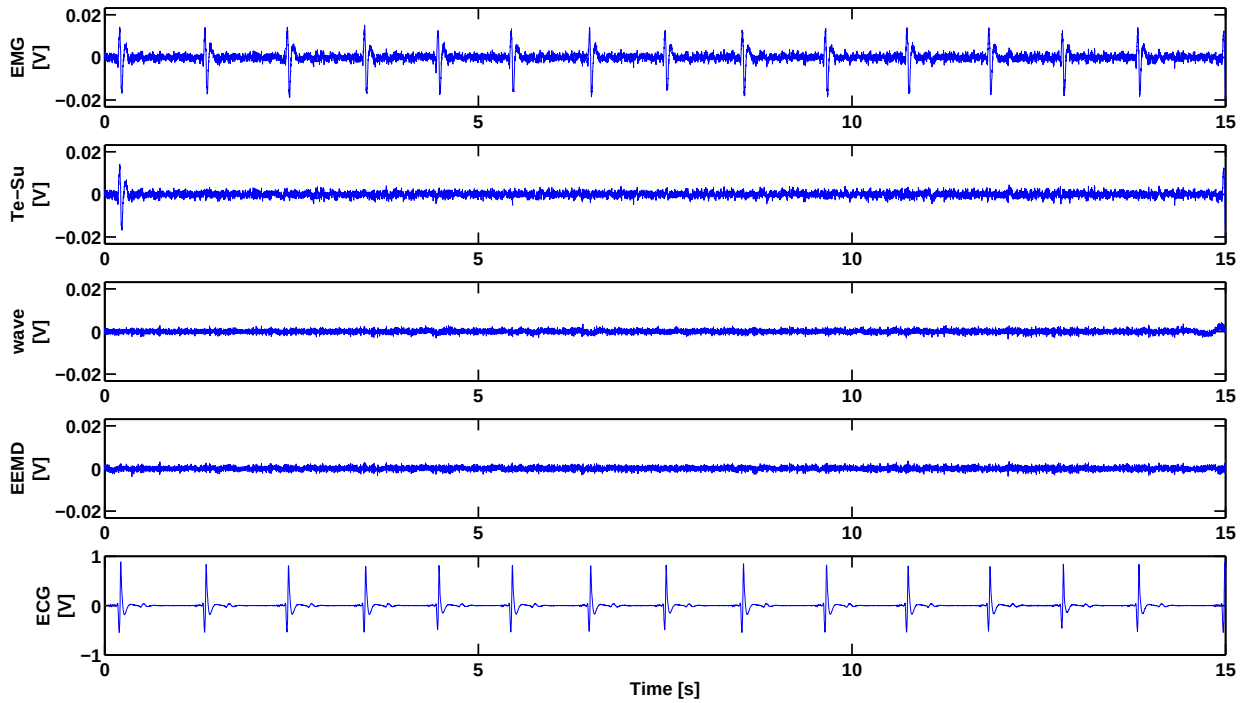


Figure 8: *ECG removal on real life signal 8 using the* ***single channel*** *approach. The top figure shows the contaminated sEMG signal. The middle three figures show the results after cleaning with the template subtraction (Te-Su) algorithm, after wavelet-ICA (wave) and Ensemble Empirical Mode Decomposition-ICA (EEMD). The lower trace show the corresponding ECG channel for validation.*

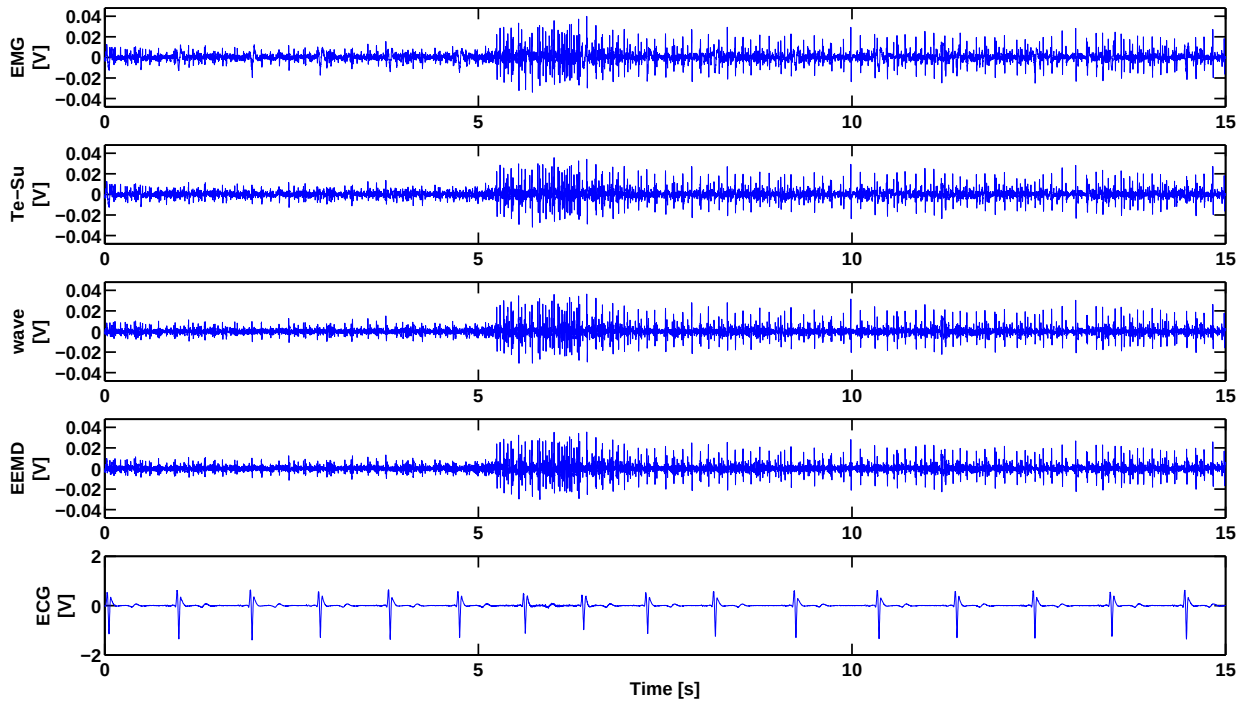


Figure 9: *ECG removal on real life signal 1 using the* ***two channel*** *(sEMG and corresponding ECG channel) approach. The top figure shows the contaminated sEMG signal. The middle three figures show the results after cleaning with the template subtraction (Te-Su) algorithm, after wavelet-ICA (wave) and Ensemble Empirical Mode Decomposition-ICA (EEMD). The lower trace show the corresponding ECG channel for validation.*

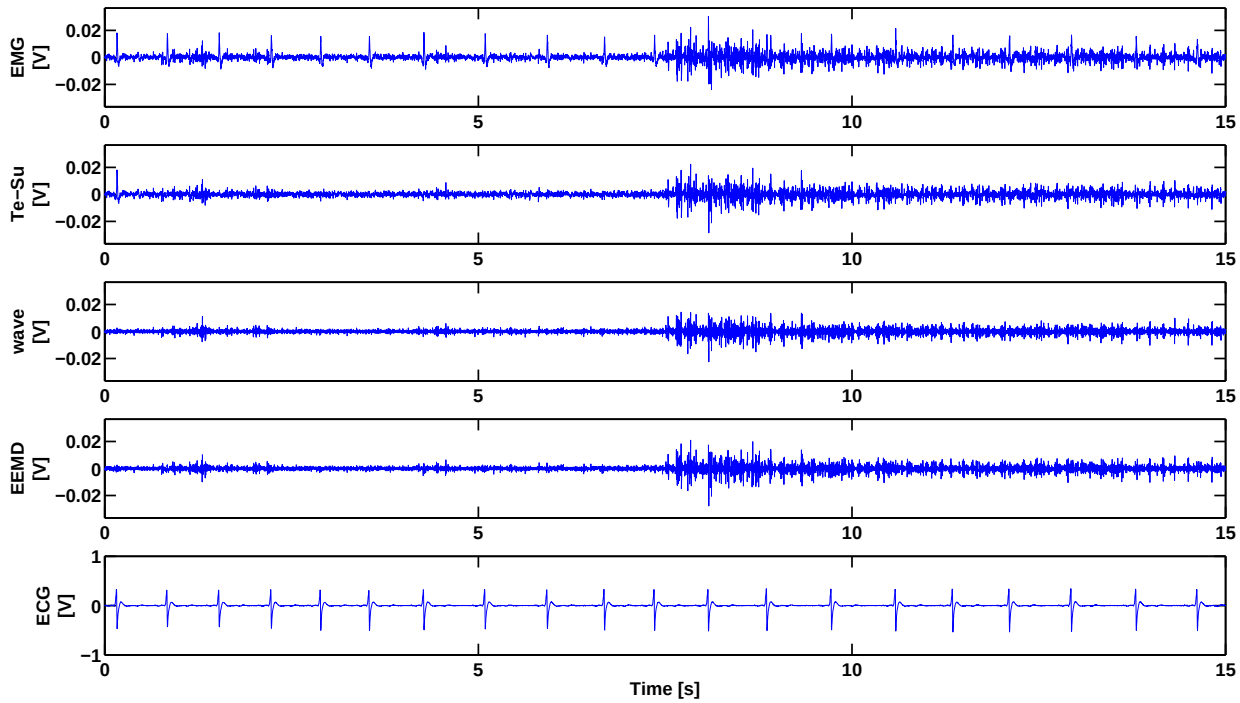


Figure 10: *ECG removal on real life signal 2 using the* ***two channel*** *(sEMG and corresponding ECG channel) approach. The top figure shows the contaminated sEMG signal. The middle three figures show the results after cleaning with the template subtraction (Te-Su) algorithm, after wavelet-ICA (wave) and Ensemble Empirical Mode Decomposition-ICA (EEMD). The lower trace show the corresponding ECG channel for validation.*

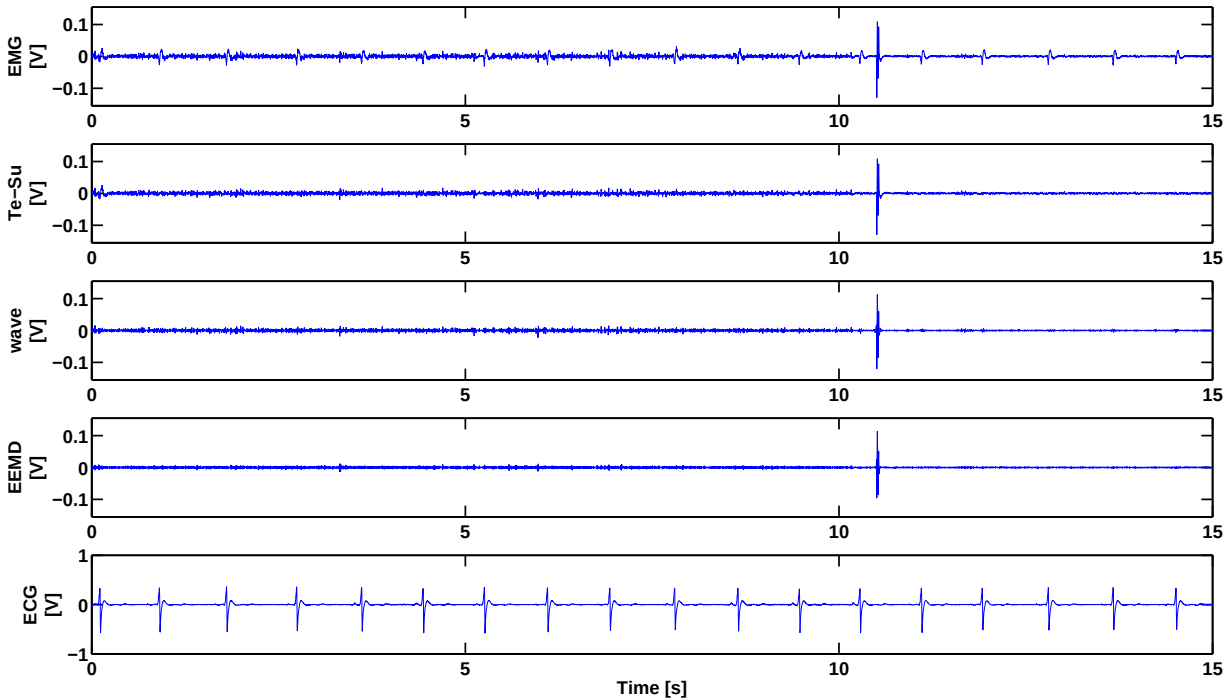


Figure 11: *ECG removal on real life signal 3 using the* ***two channel*** *(sEMG and corresponding ECG channel) approach. The top figure shows the contaminated sEMG signal. The middle three figures show the results after cleaning with the template subtraction (Te-Su) algorithm, after wavelet-ICA (wave) and Ensemble Empirical Mode Decomposition-ICA (EEMD). The lower trace show the corresponding ECG channel for validation.*

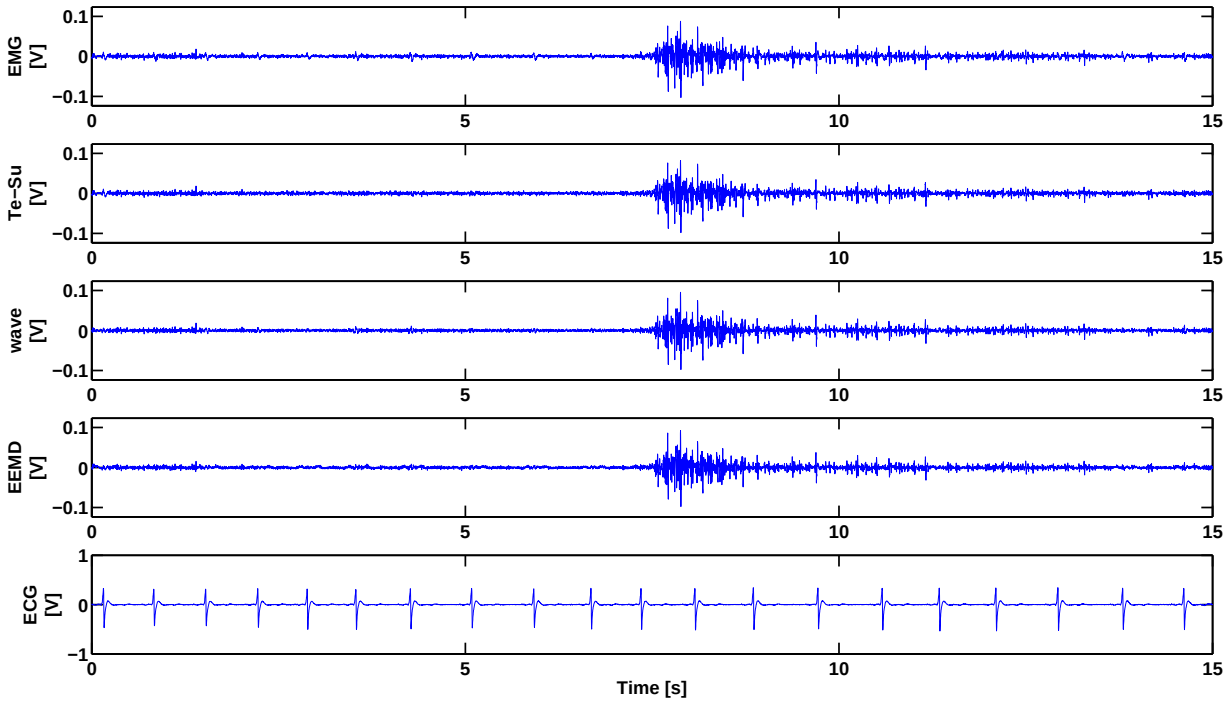


Figure 12: *ECG removal on real life signal 4 using the* ***two channel*** *(sEMG and corresponding ECG channel) approach. The top figure shows the contaminated sEMG signal. The middle three figures show the results after cleaning with the template subtraction (Te-Su) algorithm, after wavelet-ICA (wave) and Ensemble Empirical Mode Decomposition-ICA (EEMD). The lower trace show the corresponding ECG channel for validation.*

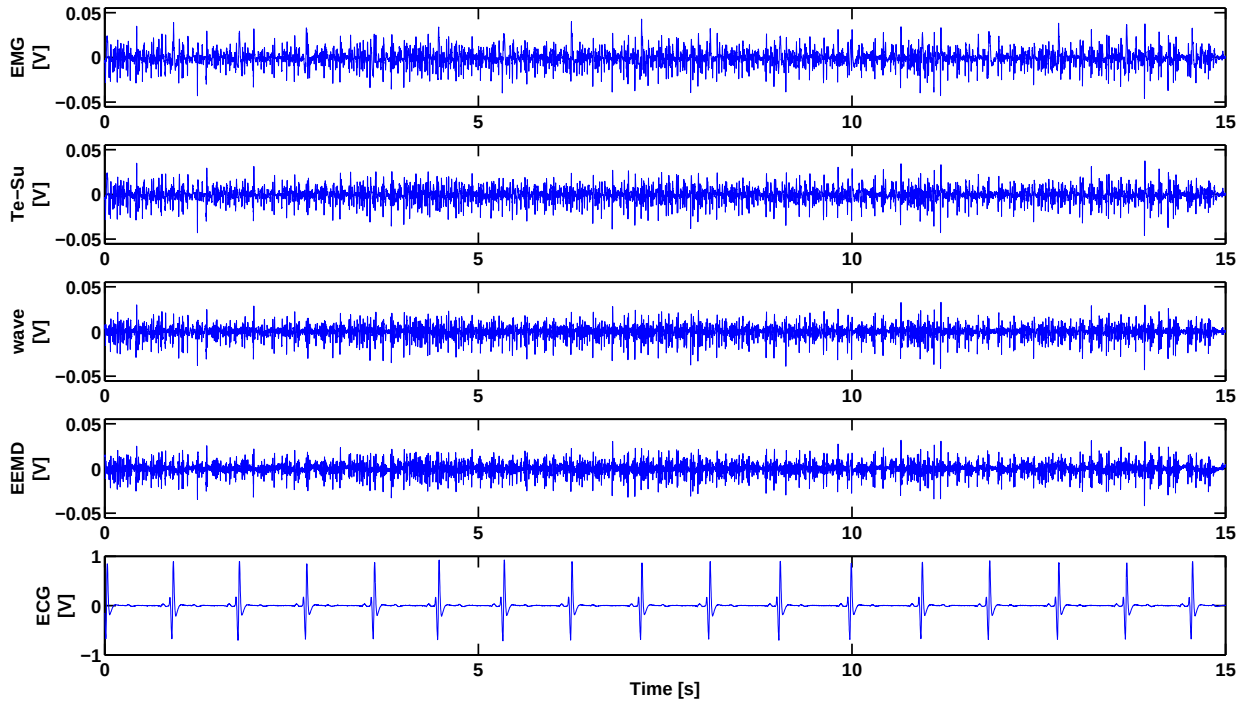


Figure 13: *ECG removal on real life signal 5 using the* ***two channel*** *(sEMG and corresponding ECG channel) approach. The top figure shows the contaminated sEMG signal. The middle three figures show the results after cleaning with the template subtraction (Te-Su) algorithm, after wavelet-ICA (wave) and Ensemble Empirical Mode Decomposition-ICA (EEMD). The lower trace show the corresponding ECG channel for validation.*

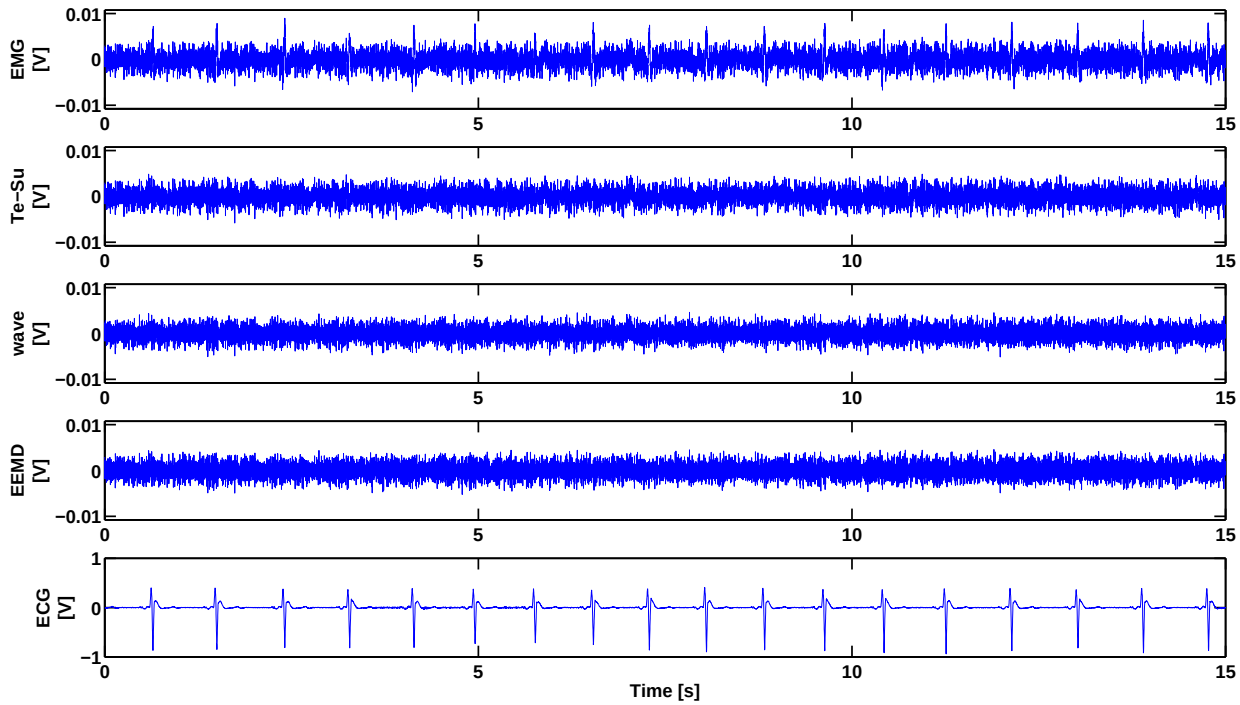


Figure 14: *ECG removal on real life signal 6 using the* ***two channel*** *(sEMG and corresponding ECG channel) approach. The top figure shows the contaminated sEMG signal. The middle three figures show the results after cleaning with the template subtraction (Te-Su) algorithm, after wavelet-ICA (wave) and Ensemble Empirical Mode Decomposition-ICA (EEMD). The lower trace show the corresponding ECG channel for validation.*

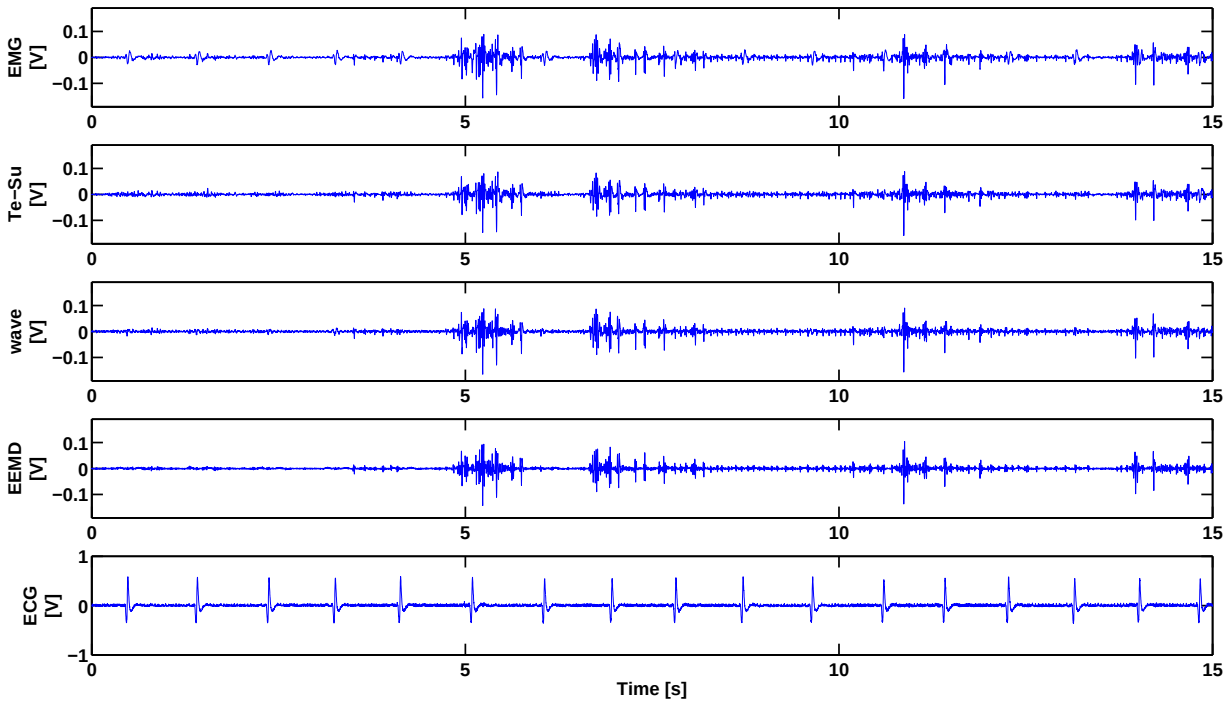


Figure 15: *ECG removal on real life signal 7 using the* ***two channel*** *(sEMG and corresponding ECG channel) approach. The top figure shows the contaminated sEMG signal. The middle three figures show the results after cleaning with the template subtraction (Te-Su) algorithm, after wavelet-ICA (wave) and Ensemble Empirical Mode Decomposition-ICA (EEMD). The lower trace show the corresponding ECG channel for validation.*

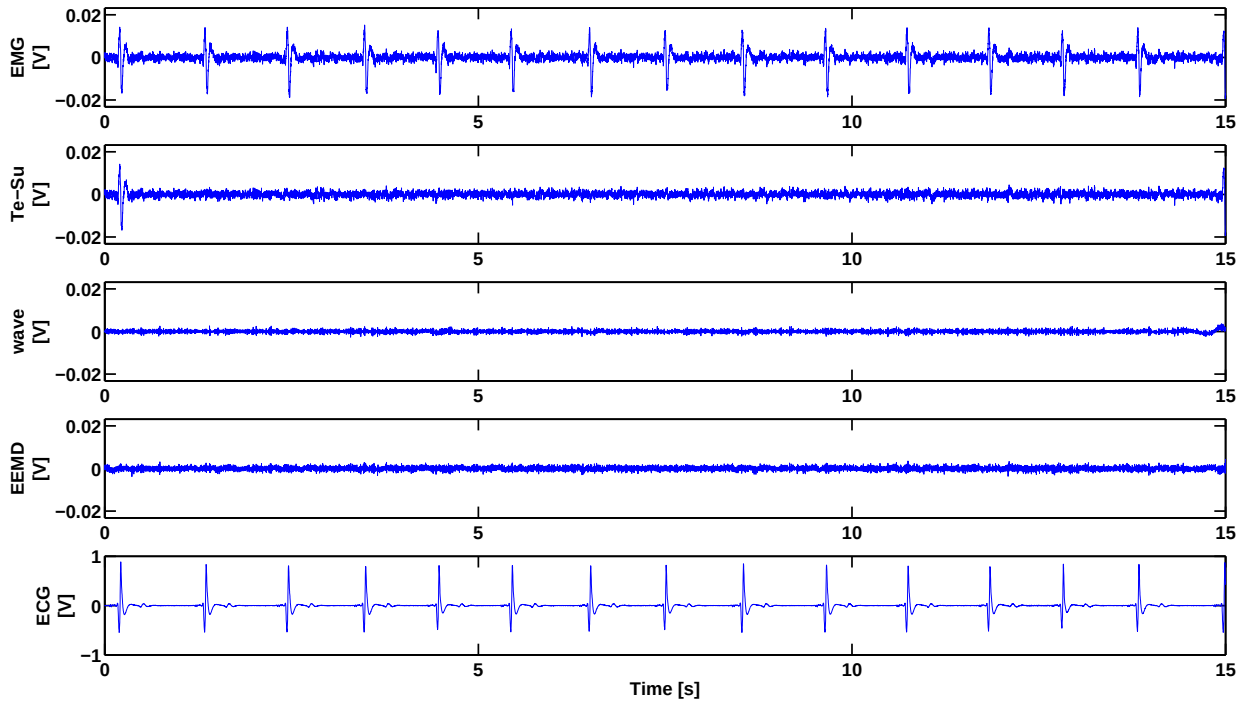


Figure 16: *ECG removal on real life signal 8 using the* ***two channel*** *(sEMG and corresponding ECG channel) approach. The top figure shows the contaminated sEMG signal. The middle three figures show the results after cleaning with the template subtraction (Te-Su) algorithm, after wavelet-ICA (wave) and Ensemble Empirical Mode Decomposition-ICA (EEMD). The lower trace show the corresponding ECG channel for validation.*

Bibliography

[1] S. Akselrod, D. Gordon, F.A. Ubel, D.C. Shannon, A.C. Berger, and C.J. Cohen. Power spectrum analysis of heart rate fluctuation: a quantitative probe of beat-to-beat cardiovascular control. *Science*, 213:220–222, 1981.

[2] J.A. Albright and R.A. Brand. *The scientific basis of orthopaedics. Occupational biomechanics*. John Wiley and sons, New york, 1984.

[3] M.U. Altaf, T. Gautama, T. Tanaka, and D.P. Madic. Rotation invariant compex empirical mode decomposition. In *Proceedings of the IEEE International Conference on Acoustics, Speech and Signal Processing (ICASSP)*, pages 1009–1012, Honolulu, April 2007.

[4] J.-P. Antoine. Wavelet analysis and some of its applications in physics. In *Contemporary problems in mathematical physics. Proceedings of the Third International Workshop*, pages 384–413, Cotonou, Republic of Benin, November 2003.

[5] E.A. Ashley and J. Niebauer. *Cardiology Explained*. Remedica, London, England, 2004.

[6] A.K. Au and P.J. Keir. Interfering effect of multitasking on muscle activity in the upper extremity. *Journal of Electromyography and Kinesiology*, 17:578–586, 2007.

[7] F. Auger, P. Flandrin, P. Gonçalvès, and O. Lemoine. Time-frequency toolbox. *CNRS France-Rice University*, 1996.

[8] B. Azzerboni, M. Carpentieri, F. La Foresta, and F.C. Morabito. Neural-ICA and Wavelet Transform for artifacts removal in EMG. In *Proceedings Of the IEEE International Joint Conference on Neural Networks*, volume 4, pages 3223–3228, Budapest, Hungary, 2004.

[9] R. Bailón, P. Laguna, L. Mainardi, and L. Sörnmo. Analysis of Heart Rate Variability Using Time-Varying Frequency Bands Based on Respiratory Frequency. In *Proceedings of the 29th Annual International Conference of the IEEE EMBS*, pages 6674–6677, Lyon, France, 2007.

[10] R. Bailón, L. Sörnmo, and P. Laguna. Ecg-derived respiratory frequency estimation. In G. D. Clifford, editor, *Advanced methods and tools for ECG data analysis*, pages 215–244. Artech House Inc, 2006.

[11] D. Bartlett. Origin and regulation of spontaneous deep breaths. *Respiration Physiology*, 12:230–238, 1971.

[12] A. Bartolo, C. Roberts, R. Dzwonczyk, and E. Goldman. Analysis of diaphragm EMG signals: comparison of gating vs. subtraction for removal of ECG contamination. *Journal of Applied Physiology*, 80:1898–1902, 1996.

[13] J.V. Basmajian and C.J. De Luca. *Muscles Alive. Their function revealed by electromyography.* Williams & Wilkens, 1985.

[14] E.A.C. Beenakker. *Duchenne muscular dystrophy quantification of muscular parameters and prednisone therapy.* PhD thesis, Rijksuniversiteit Groningen, 2005.

[15] L. Bernardi, A. Porta, L. Gabutti, L. Spicuzza, and P. Sleight. Modulatory effects of respiration. *Autonomic Neuroscience: Basic & Clinical*, 30:47–56, 2001.

[16] L. Bernardi, J. Wdowczyk-Szulc, C. Valenti, S. Castoldi, C. Passino, and G. Spadacini G. Effects of controlled breathing, mental activity and mental stress with or without verbalization on heart rate variability. *Journal of the American College of Cardiology*, 35:1462–1469, 2000.

[17] J.G. Bloemsaat, R.G.J. Meulenbroek, and G.P. Van Galen. Differential effects of mental load on proximal and distal arm muscle activity. *Experimental Brain Research*, 167:622–634, 2005.

[18] P. Bonato, T. DAlessio, and M. Knaflitz. A statistical method for the measurement of muscle activation intervals from surface myoelectric signal during gait. *IEEE Transactions on Biomedical Engineering*, 45:287–298, 1998.

[19] E. Bonilla, C.E. Samitt, A.F. Miranda, A.P. Hays, G. Salviati, S. DiMauro, L.M. Kunkel, E.P. Hoffman, and L.P. Rowland. Duchenne muscular dystrophy: deficiency of dystrophin at the muscle cell surface. *Cell*, 54:447–452, 1988.

[20] R.F. Bonner, R. Nossal, S. Havlin, and G.H.J. Weiss. Model for photon migration in turbid biological media. *Journal of the Optical Society of America*, 4:423432, 1987.

[21] N.A. Campbell and J.B. Reece. *Biology.* Pearson, 2004.

[22] C.G. Caro, J. Butler, and A.B. Dubois. Some effects of restriction of chest cage expansion on pulmonary function in man: an experimental study. *The Journal of clinical investigation*, 39:573–583, 1960.

[23] B. Chance, M. T. Dait, C. Zhang, T. Hamaoka, and F. Hagerman. Recovery from exercise-induced desaturation in the quadriceps muscles of elite competitive rowers. *American Journal of Physiology. Cell physiology*, 262(3):C766–775, 1992.

[24] E.A. Clancy, E.L. Morin, and R. Merletti. Sampling, noise-reduction and amplitude estimation issues in surface electromyography. *Journal of Electromyography and Kinesiology*, 12:1–16, 2002.

[25] F. Clariá, M. Vallverdu, R. Baranowski, L. Chojnowska, and P. Caminal. Heart rate variability analysis based on time-frequency representation and entropies in hypertrophic cardiomyopathy patients. *Physiological Measurements*, 29:401–416, 2008.

[26] L. Cohen. *Time-frequency analysis: theory and applications*. Prentice-Hall, Inc., Upper Saddle River, NJ, USA, 1995.

[27] S. Cohen, T. Kamarck, and R. Mermelstein. A global measure of perceived stress. *Journal of Health and Social Behavior*, 24:385–396, 1983.

[28] W.N. Colier, I.B. Meeuwsen, H. Degens, and B. Oeseburg. Determination of oxygen consumption in muscle during exercise using near infrared spectroscopy. *Acta anaesthesiologica Scandinavica. Supplementum*, 107:151–155, 1995.

[29] G.M. cooper and R.E. Hausman. *The Cell, A Molecular Approach*. Sinauer Associates Inc., 2009.

[30] M. Cope and D.T. Delpy. A system for long term measurementof cerebral blood and tissue oxygenation in newborn infants by near infrared transillumination. *Medical and Biological Engineering and Computing*, 26:289–294, 1988.

[31] J.L. Cox, J.M. Holden, and R. Sagovsky. Detection of postnatal depression. Development of the 10-item Edinburgh Postnatal Depression Scale. *The British journal of psychiatry : the journal of mental science*, 150(6):782, 1987.

[32] A.G. Crenshaw, M. Djupsjöbacka, and A. Svedmark. Oxygenation, emg and position sense during computer mouse work. impact of active versus passive pauses. *European Journal of Applied Physiology*, 97:59–67, 2006.

[33] D.A. Crist, C.H. Rickard, S. Prentice-Dunn, and H.R. Barker. The relaxation inventory: self-report scales of relaxation training effects. *Journal of Personality Assessment*, 53:716–726, 1989.

[34] I. Daubechies. *Ten lectures on wavelets*. Society for Industrial and Applied Mathematics, Philadelphia, PA, USA, 1992.

[35] I. Daubechies, J. Lu, and H.-T. Wu. Synchrosqueezed wavelet transforms: a tool for empirical mode decomposition. Arxiv preprint arXiv:0912.2437, 2010.

[36] M.E. Davies and C.J. James. Source separation using single channel ICA. *Signal Processing*, 87:1819 – 1832, 2007.

[37] W. Deburchgraeve. *Development of an automated neonatal EEG seizure monitor*. PhD thesis, Department of electrical engineering, Katholieke Universiteit Leuven, September 2010.

[38] W. Deburchgraeve, P.J. Cherian, M. De Vos, R.M. Swarte, J.H. Blok, G.H. Visser, P. Govaert, and S. Van Huffel. Automated neonatal seizure detection mimicking a human observer reading EEG. *Clinical Neurophyiology*, 119:2447–2454, 2008.

[39] P.B. Defares, H.M. van der Ploeg, and C.D. Spielberg. Een nederlandstalige bewerking van Spielberger State-Trait Anxiety Inventory: de Zelf-Beoordelingsvragenlijst. *De psycholoog*, 15:460–467, 1980.

[40] J.P.A. Delaney and D.A. Brodie. Effects of short-term psychological stress on the time and frequency domains of heart-rate variability. *Perceptual and Motor Skills*, 91:515–524, 2000.

[41] D.T. Delpy and M. Cope. Quantification in tissue near-infrared spectroscopy. *Philosophical Transactions of the Royal Society*, 352:649–659, 1997.

[42] J.W. Denver, S. Reed, and S. Porges. Methodological issues in the quantifcation of respiratory sinus arrhythmia. *Biological Psychology*, 74:286–294, 2007.

[43] S. Devuyst, T. Dutoit, P. Stenuit, M. Kerkhofs, and E. Stanus. Cancelling ECG artifacts in EEG using a modified independent component analysis approach. *EURASIP Journal on Advances in Signal Processing*, pages 1–13, 2008.

[44] A. Duncan, J.H. Meek, M. Clemence, C.E. Elwell, L. Tyszczuk, M. Cope, and D.T. Delpy. Optical pathlength measurements on adult head, calf and forearm and the head of the newborn-infant using phase-resolved optical spectroscopy. *Physics in Medicine and Biology*, 40:295–304, 1995.

[45] R.H.T. Edwards. Human muscle function and fatigue. *Ciba Foundation symposium*, 82:1–18, 1981.

[46] EuroSTRESS project. http://www.esf.org/activities/eurocores/running-programmes/eurostress.html.

[47] D. Farina, D. Zennaro, M. Pozzo, R. Merletti, and T. Läubli. Single motor unit and spectral surface emg analysis during low-force, sustained contractions of the upper trapezius muscle. *European Journal of Applied Physiology*, 96:157–164, 2006.

[48] F. Felici, V. Quaresima, L. Fattorini, P. Sbriccoli, G.C. Filligoi, and M. Ferrari. Biceps bracii myoelectric and oxygenation changes during static and sinusoidal isometric exercises. *European Journal of Applied Physiology*, 92:e1–e11, 2009.

[49] M. Ferrari, T. Binzoni, and V. Quaresima. Oxidative metabolism in muscle. *Philosophical Transactions of the Royal Society of London. Series B, Biological sciences*, 352:677–683, 1997.

[50] L. Finsen, K. Sogaard, C. Jensen, V. Borg, and H. Christensen. Muscle activity and cardiovascular response during computer-mouse work with and without memory demands. *Ergonomics*, 44:1312–1329, 2001.

[51] P. Flandrin, G. Rilling, and P. Goncalves. Empirical mode decomposition as a filter bank. *IEEE Signal Processing Letters*, 11:112–114, 2004.

[52] European Agency for Safety and Health at work. Repetitive strain injuries in the member states of the european union: the results of an information request. Technical report, European Commission, 2000.

[53] European Agency for Safety and Health at work. Research on work-related stress. Technical report, European Commission, 2000.

[54] European Agency for Safety and Health at work. Work-related musculoskeletal disorders: prevention report. Technical report, European Commission, 2000.

[55] European Agency for Safety and Health at work. Commission asks workers and employees what action should be taken to combat musculoskeletal disorders. Press Release IP/04/1358, European Commission, November 2004.

[56] P. Franco, D. Verheulpen, F. Valente, I. Kelmanson, A. de Broca, S. Scaillet, J. Groswasser J, and A. Kahn. Autonomic responses to sighs in healthy infants and in victims of sudden infant death. *Sleep mMedicine*, 4:569–577, 2003.

[57] B. Freriks and H.J. Hermens. *European Recommendations for Surface ElectroMyoGraphy, results of the SENIAM project.* Roessingh Research and Development, 1999.

[58] A.W.K. Gaillard and C.J.E. Wientjes. Mental load and work stress as two types of energy mobilization. *Work Stress*, 8:141–152, 1994.

[59] A. Galindo, J. Barthelemy, M. Ishikawa, P. Chavet, V. Martin, J. Avela, P. V. Komi, and C. Nicol. Neuromuscular control in landing from supra-maximal dropping height. *Journal of Applied Physiology*, 106:539547, 2009.

[60] A.H. Garde, B. Laursen, A.H. Jorgensen, and B.R. Jensen. Effects of mental and physical demands on heart rate variability during computer work. *European Journal of Applied Physiology*, 87:456 – 461, 2002.

[61] R. Gauthy. Musculoskeletal disorders: where we are, and where we could be. *HESA newsletter*, 27:22–27, 2005.

[62] G. Gerdle, S. Karlsson, S. Day, and M. Djupsjobacka. Acquisition, processing and analysis of the surface electromyogram. In H. Johansson U. Windhorst, editor, *Modern Techniques in neuroscience research*, chapter 26, pages 705–755. Springer Verlag, 1999.

[63] E.J. De Geus, L.J. van Doornen LJ, D.C. de Visser, and J.F. Orlebeke. Existing and training induced differences in aerobic fitness: the relationship to physiological response patterns during different types of stress. *Psychophysiology*, 27:457–478, 1990.

[64] K.A. Glass, G.A. Frishkoff, R.M. Frank, C. Davey, J. Dien, A.D. Malony, and D.M. Tucker. A framework for evaluating ica methods of artifact removal from multichannel eeg. In Carlos G. Puntonet and Alberto Prieto, editors, *Independent Component Analysis and Blind Signal Separation*, volume 3195 of *Lecture Notes in Computer Science*, pages 1033–1040. Springer Berlin / Heidelberg, 2004.

[65] R. González-Camarena, S. Carrasco-Sosa, R. Román-Ramos, M.J. Gaitán-González, V. Medina-Ba nuelos, and J. Azpiroz-Leehan. Effect of static and dynamic exercise on heart rate and blood pressure variabilities. *Medicine and Science in Sports and Exercise*, 32:1719–1728, 2000.

[66] J.P. Grossman and E. Taylor. Toward understanding respiratory sinus arrhythmia: Relations to cardiac vagal tone, evolution and biobehavioral functions. *Biological Psychology*, 74:263–285, 2007.

[67] G.M. Hägg and A. Aström. Load pattern and pressure pain treshold in the upper trapezius muscle and psychosocial factors in medical secretaries with and without shoulder/neck disorders. *International Archive of Occupational and Environmental Health*, 69:423–432, 1996.

[68] J.N. Han, R. Schepers, K. Stegen, O. Van den Bergh, and K.P. Van de Woestijne. Psychosomatic symptoms and breathing pattern. *Journal of Psychosomatic Research*, 49:319–333, 2008.

[69] J. Hartikainen, K. Tahvanainen, and T. Kuusela. Short-term measurement of heart rate variability. In M. Malik Jr., editor, *Clinical Guide to Cardiac Autonomic Tests*, pages 149–176. Kluwer Academic, 1998.

[70] V. Hermans, A.J. Spaepen, and M. Wouters. Relation between differences in electromyographic adaptations during static contractions and the muscle function. *Journal of Electromyography and Kinesiology*, 18:253–261, 1999.

[71] N. Hjortskov, D. Rissen, A.K.K. Blangsted, N. Fallentin, U. Lundberg, and K. Sogaard. The effect of mental stress on heart rate variability and blood pressure during computer work. *European Journal of Applied Physiology*, 92:84 – 89, 2004.

[72] A. Holobar and D. Zazula. Multichannel blind source separation using convolution kernel compensation. *IEEE Transactions on Biomedical Engineering*, 55:4487 – 4496, 2007.

[73] K.A. Holte and R.H. Westgaard. Daytime trapezius muscle activity and shoulder-neck pain of service workers with work stress and low biomechanical exposure. *American Journal of Industrial Medicine*, 41:393–405, 2002.

[74] B. Van Houdenhove. *In wankel evenwicht. Over stress, levensstijl en welvaartsziekten.* Lannoo, Tielt, Belgium, 2005.

[75] N.E. Huang, Z. Shen, S.R. Long abd M.C. Wu, H.H. Shih, Q. Zheng, N. Yen, C.C. Tung, and H.H. Liu. The empirical mode decomposition and the Hilbert spectrum for nonlinear and non-stationary time series analysis. *Proceedings of the Royal Society of London A*, 454:903995, 1998.

[76] A. Hyvarinen. Fast and robust fixed-point algorithms for independent component analysis. *IEEE Transactions on Neural Networks*, 10:625–634, 1999.

[77] A. Hyvärinen, J. Karhunen, and E. Oja. *Independent Component Analysis.* John Wiley & sons, 2001.

[78] A. Hyvärinen and E. Oja. Independent component analysis: algorithms and applications. *Neural Networks*, 13:411–433, 2000.

[79] A. Ishimaru. Diffusion of a pulse in densely distributed scatters. *Journal of the Optical Society of America*, 68:10451050, 1978.

[80] F.F. Jöbsis. Noninvasive, infrared monitoring of cerebral and myocardial oxygen sufficiency and circulatory parameters. *Science*, 198:1264–1267, 1977.

[81] J.F. Kaiser. On a simple algorithm to calculate the energy of a signal. *IEEE International Conference on Acoustics Speech Signal Processing (ICASSP)*, pages 381–384, 1990.

[82] L.A.C. Kallenberg, H.J. Hermens, and M.M.R. Vollenbroek-Hutten. Distinction between computer workers with and without work-related neck-shoulder complaints based on multiple surface emg parameters. *International Journal of Industrial Ergonomics*, 36:921–929, 2006.

[83] M.V. Kamath and E.L. Fallen. Correction of the heart rate variability signal for ectopic and missing beats. In M. Malik and A.J. Camn, editors, *Heart Rate Variability*, pages 75–85. Futura, 1995.

[84] M.J. Katz. Fractals and the analysis of waveforms. *Computers in biology and medicine*, 18:145–156, 88.

[85] R.M. Kelsey, J. Blascovich, C.L. Leitten, T.R. Schneider, J. Tomaka, and S. Wiens. Cardiovascular reactivity and adaptation to recurrent psychological stress: The moderating effects of evaluative observation. *Psychophysiology*, 37:748–756, 2000.

[86] R. Kleiger, J. Miller, J.T.Jr. Bigger, and A. Moss. Decreased heart rate variability and its association with increased mortality after acute myocardial infarction. *The American Journal of Cardiology*, 59:256–262, 1987.

[87] M. Klemm, J. Haueisen, and G. Ivanova. Independent component analysis: comparison of algorithms for the investigation of surface electrical brain activity. *Medical and Biological Engineering and Computing*, 47:413–423, 2009.

[88] M. Kobayashi and T. Musha. 1/f fluctuations of heart beat period. *IEEE Transactions on Biomedical Engineering*, 29:456–457, 1982.

[89] G. Krantz, M. Forsman, and U. Lundberg. Consistency in physiological stress responses and electromyographic activity during induced stress exposure in women and men. *Integrative Physiological and Behavioral Science*, 39:105–118, 2004.

[90] S.G. Kuklin, A.A. Dzizinskii, Y.M. Titov, and A.A. Temnikov. Continuous wavelet analysis: a new method for studying nonstationary oscillations in the cardiac rhythm. *Human Physiology*, 32:116–121, 2006.

[91] L. De Lathouwer, B. De Moor, and J. Vandewalle. An introduction to independent component analysis. *Journal of chemometrics*, 14:123–149, 2000.

[92] B. Laursen, B.R. Jensen, A.H. Garde, and A.H. Jorgensen. Effect of mental and physical demands on muscular activity during the use of a computer mouse and a keyboard. *Scandinavian Journal of Work Environmental Health*, 28:215–221, 2002.

[93] M. Lidierth. A computer based method for automated measurement of the periods of muscular activity from an emg and its application to locomotor emgs. *Electroencephalography and Clinical Neurophysiology*, 64:378380, 1986.

[94] C.J. De Luca. The use of surface electromyography in biomechanics. *Journal of Applied Niomechanics*, 13:135–163, 1997.

[95] U. Lundberg, I. Elfsberg Dohns, B. Melin, L. Sandsjo, G. Palmerud, R. Kadefors, M. Ekstrom, and D. Parr. Psychosocial stress responses, muscle tension and neck and shoulder pain among supermarket cashiers. *Journal of Occupational Health Psychology*, 4:245–255, 1999.

[96] U. Lundberg, R. Kadefors, B. Melin, G. Palmerud, P. Hassmen, M. Engström, and I. Elfsberg Dohns. Psychophysiological stress and emg activity of the trapezius muscle. *International Journal of Behavioral Medicine*, 4:354–370, 1994.

[97] D.M. Mancini, L. Bolinger, H. Li, K. Kendrick, B. Chance, and J.R. Wilson. Validation of near-infrared spectroscopy in humans. *Journal of Applied Physiology*, 77:2740–2747, 1994.

[98] S.E. Mathiassen and T. Aminoff. Motor control and cardiovascular responses during isoelectric contractions of the upper trapezius muscle: evidence for individual adaptation strategies. *European Journal of Applied Physiology*, 76:434–444, 1997.

[99] K.K. McCully and T. Hamaoka. Near-infrared spectroscopy: What can it tell us about oxygen saturation in skeletal muscle. *Exercise and Sport Sciences Reviews*, 28:123–127, 2000.

[100] B.S. McEwen. Protective and damaging effects of stress mediators. *New England Journal of Medicine*, 338:171–179, 1998.

[101] B.S. McEwen and E. Stellar. Stress and the individual: mechanisms leading to disease. *Archives of Internal Medicine*, 153:2093–2101, 1993.

[102] Home version of the MENSA IQ test, December 2007. http://www.mensa.be/.

[103] R. Merletti, A. Holobar, and D. Farina. Analysis of motor units with high-density surface electromyography. *Journal of Electromyography and Kinesiology*, 18:879–890, 2008.

[104] R. Merletti and P.A. Parker. *Electromyography. Physiology, Engineering and Noninvasive applications*. Wiley-Interscience, 2004.

[105] E.S. Mezzacappa, R.M. Kelsey, E.S. Katkin, and R. Sloan. Vagal rebound and recovery from psychological stress. *Psychosomatic Medicine*, 63:650–657, 2001.

[106] B. Mijovic, M. De Vos, I. Gligorijevic, J. Taelman, and S. Van Huffel. Source separation from single-channel recordings by combining empirical mode decomposition and independent component analysis. *IEEE Transactions on Biomedical Engineering*, 57:2188–2196, 2010.

[107] H. Miura, H. Araki, H. Matoba, and K. Kitagawa. Relationship among oxygenation, myoelectric activity, and lactic accumulation in vastus lateralis muscle during exercise with constant work rate. *International Journal of Sports Medicine*, 21:180–184, 2000.

[108] G. Morren. *Advanced signal processing applied to in-vivo spectroscopy and Heart Rate Variability*. PhD thesis, Department of electrical engineering, Katholieke Universiteit Leuven, May 2004.

[109] G.R. Morrow and A.H. Labrum. The relationship between psychological and physiological measures of anxiety. *Psychological Medicin*, 8(1):95–101, 1978.

[110] E.J.H. Mulder, P.G. Robles de Medina, A.C. Huizink, B.R.H. Van den Bergh, J.K. Buitelaar, and G.H.A. Visser. Prenatal maternal stress: effects on pregnancy and the (unborn) child. *Early human development*, 70(1-2):3–14, 2002.

[111] M. Myrtek, D. Weber, and G. Brügner W. Müller. Occupational stress and strain of female students: results of physiological, behavioural, and psychological monitoring. *Psychophysiology of Workload*, 42:379–391, 1996.

[112] G. Naulaers. *Non-invasive measurement of the neonatal cerebral and splanchnic circulation by near-infrared spectroscopy*. PhD thesis, Faculty of Medicine, Katholieke Universiteit Leuven, 2003.

[113] K.B. Nilsen, T. Sand, L.J. Stovner, R.B. Leistad, and R.H. Westgaard. Autonomic and muscular responses and recovery to one-hour laboratory mental stress in healthy subjects. *BMC Musculoskeletal Disorders*, 2007:8:81, 2007.

[114] R.P. Nolan, M.V. Kamath, J.S. Floras, J. Stanley, C. Pang, and P. Picton. Heart period variability biofeedback as a behavioral neurocardiac intervention to enhance vagal heart rate control. *American Heart Journal*, 149:1137, 2005.

[115] C. Nordander, G.A. Hansson, L. Rylander, P. Asterland, J.U. Bystrom, K. Ohlsson, I. Balogh, and S. Skerfving. Muscular rest and gap frequency as emg measures of physical exposure: the impact of work tasks and individual related factors. *Ergonomics*, 43:1904–1919, 2000.

[116] M. Orini, R. Bailon, R. Enk, S. Koelsch, L. Mainardi, and P. Laguna. A method for continuously assessing the autonomic response to music-induced emotions through HRV analysis. *Medical & Biological Engineering & Computing*, 48:423–433, 2010.

[117] H. Owen-Reece, M. Smith, C.E. Elwell, and J.C. Goldstone. Near infrared spectroscopy. *British Journal of Anaesthesia*, 82:418–426, 1999.

[118] M. Pagani, G. Mazzuero, A. Ferrari, D. Liberati, S. Cerutti, D. Vaitl, L. Tavazzi, and A. Malliani. Sympathovagal interaction during mental stress. A study using spectral analysis of heart rate variability in healthy control subjects and patients with prior myocardial infarction. *Circulation*, 83:43–51, 1991.

[119] M.D. Pagel, G. Smilkstein, H. Regen, and D. Montano. Psychosocial influences on new born outcomes: a controlled prospective study. *Social Science & Medicine*, 30(5):597–604, 1990.

[120] J. Pan and W.J. Tompkins. A real time qrs detection algorithm. *IEEE Transactions on Biomedical Engineering*, 32:230–236, 1985.

[121] M.S. Patterson, B. Chance, and B.C. Wilson. Time resolved reflectance and transmittance for the non-invasive measurement of tissue optical properties. *Applied optics*, 28:2331–2336, 1989.

[122] C.K. Peng, S. Havlin, J.M. Hausdorff, J.E. Mietus, H.E. Stanley, and A.L. Goldberger. Fractal mechanisms and heart rate dynamics. *Journal of electrocardiology*, 28:59–64, 1996.

[123] R. Perini, S. Milesi, N.M. Fisher, D.R. Pendergast, and A. Veicsteinas. Heart rate variability during dynamic exercise in elderly males and females. *European Journal of Applied Physiology*, 82:8–15, 2000.

[124] Y.B. Pesin. Characteristic lyapunov exponents and smooth ergodic theory. *Russian Mathematical Surveys*, 32:55114, 1977.

[125] E.I. Plotkin and M.N.S. Swamy. Nonlinear signal processing based on parameter invariant moving average modeling. *Proceedings of the 21st Annual Canadian Conference on Electrical and Computer Engineering (CCECE)*, 1, 1992.

[126] C.S. Poon and M. Barahoma. Titration of chaos with added noise. *PNAS*, 98:7107–7112, 2001.

[127] S.W. Porges and D.C. Raskin. Respiratory and heart rate components of attention. *Journal of Experimental Psychology*, 81:497–503, 1969.

[128] M. Poyhonen, S. Syvaoja, J. Hartikainen, E. Ruokonen, and J. Takala. The effect of carbon dioxide, respiratory rate and tidal volume on human heart variability. *Acta anaesthesiologica Scandinavia*, 48:93–101, 2001.

[129] H.M. Van Praag. Crossroads of corticopin releasing hormone, corticosteroids and monoamines. About the interface between stress and depression. *Neurotoxicity Research*, 4:531–555, 2002.

[130] M. Praagman, H. E. J. Veeger, E. K. J. Chadwick, W. N. J. M. Colier, and F. C. T. van der Helm. Muscle oxygen consumption, determined by nirs, in relation to external force and emg. *Journal of Biomechanics*, 36(7):905 – 912, 2003.

[131] C.U. Ranniger and D.L. Akin. EMG mean power frequency determination using wavelet analysis. In *Proceedings of the 19th Annual International Conference of the IEEE Engineering in Medicine and Biology Society*, volume 4, pages 1589 – 1592, Chicago, IL , USA, 1997.

[132] N. Rehman and D.P. Mandic. Multivariate Empirical Mode Decomposition. *Proceedings of the Royal Society A*, 466:1291–1302, 2010.

[133] J.C. Rekling, G.D. Funk, D.A. Bayliss, X.W. Dong, and J.L. Feldman. Synaptic Control of Motoneuronal Excitability. *physiological reviews*, 80:767,852, 2000.

[134] J.S. Richman and R.J. Moorman. Physiological time-series analysis using approximate entropy and sample entropy. *American journal of physiology. Heart and circulatory physiology*, 278:2039–2049, 2000.

[135] D. Rissen, B. Melin, L. Sandsjo, I. Dohns, and U. Lundberg. Surface emg and psychophysiological stress reactions in women during repetitive work. *European Journal of Applied Physiology*, 83:215–222, 2000.

[136] T. Ritz. Studying noninvasive indices of vagal control: The need for respiratorycontrol and the problem of target specificity. *Biological psychology*, 80:158–168, 2009.

[137] Z. Sahul, J. Black, B. Widrow, and C. Guilleminault. EKG artifact cancellation from sleep EEG using adaptive filtering. *Sleep Research*, 24:486, 1995.

[138] G. Sammer. Heart period variability and respiratory changes associated with physical and mental load: nonlinear analysis. *Ergonomics*, 41:746 – 755, 1998.

[139] L. Sandsjo, B. Melin, D. Rissen, I. Dohns, and U. Lundberg. Trapezius muscle activity, neck and shoulder pain and subjective experiences during monotonous work in women. *European Journal of Applied Physiology*, 83:235–238, 2000.

[140] M. Santello and M.J.N. McDonagh. The control of timing and amplitued of emg activity in landing movements in humans. *Experimental Physiology*, 83(06):857–874, 1998.

[141] A. Santos, M. Duret, J. Mancini, C. Gire, and C. Deruelle. Preterm birth affects dorsal-stream functioning even after age 6. *Brain & Cognition*, 69(3):490–494, 2009.

[142] J.P. Saul, P. Albrecht, R.D. Berger, and R.J. Cohen. Analysis of long term heart rate variability: methods, 1/f scaling and implications. In *Proceedings of the* 14^{th} *Annual International Conference of Computers in Cardiology (CinC)*, volume 14, pages 419–422, Washington, DC, USA, 1987.

[143] J. Seghers, A. Jochem, and A. Spaepen. Posture, muscle activity and muscle fatigue in prolonged VDT work at different screen height settings. *Ergonomics*, 46:714–730, 2003.

[144] H. Selye. *The stress of life*. McGraw-Hill, New York, USA, 1956.

[145] H. Selye. Confusion and controversy in the stress field. *Journal of Human Stress*, 1:37–44, 1975.

[146] G. Sjogaard, U. Lundberg, and R. Kadefors. The role of muscle activity and mental load in the development of pain and degenerative processes at the muscle cell level during computer work. *European Journal of Applied Physiology*, 83:99–105, 2000.

[147] R.P. Sloan, J.B. Korten, and M.M. Myers. Components of heart rate reactivity during mental arithmetic with and without speaking. *Psychophysiology*, 50:1039–1045, 1991.

[148] R.P. Sloan, J.B. Korten, and M.M. Myers. Cardiac vagal tone: a physiological index of stress. *Neuroscience and Biobehavioral Reviews*, 19:225–233, 1995.

[149] R.P Sloan, P.A. Shapiro, E. Bagiella, S.M. Boni, M. Paik, J.T. Bigger Jr, R.C. Steinman, and J.M. Gorman. Effect of mental stress throughout the day on cardiac autonomic control. *Biological Psychology*, 37:89–99, 1994.

[150] A.J. Spaepen, W. Baumann, and H. Maes. Relation between mechanical load and EMG-activity of selected muscles of the trunk under isometric conditions. In G. Bergmann, R. Klbel, and A. Rohlmann, editors, *Biomechanics: basic and applied research*, pages 595–600. Dordrecht: Martinus Nijhoff Publishers, 1985.

[151] G. Staude, C. Flachenecker, M. Daumer, and W. Wolf. Onset detection in surface electromyographic signals: a systematic comparison of methods. *EURASIP Journal of Applied Signal Processing*, 2001(1):67–81, 2001.

[152] J.L. Stephenson. Discharge behaviors of trapezius motor units during exposure to low and high levels of acute psychosocial stress. *Journal of Clinical Neurophysiology*, 27:52–61, 2010.

[153] P. Sterling and J. Eyer. Allostasis: A new paradigm to explain arousal pathology. In S. Fisher and J. Reason, editors, *Handbook of Life Stress, Cognition and Health*. John Wiley and Sons, New York, 1988.

[154] I. Stevenson and H.S. Ripley. Variations in respirations and respiratory symptoms during changes in emotion. *Psychosomatic Medicine*, 14:476–490, 1952.

[155] Subcommittee on Instrumentation Committee on Electrocardiography American Heart Association. Recommendation for instruments in electrocardiography and vectorcardiography. *IEEE Transactions on Biomedical Engineering*, 14:60–68, 1967.

[156] J. Taelman, W. Deburchgraeve, K. Van Damme, T. Adriaensen, A. Spaepen, and S. Van Huffel. Detection Algorithm for Single Motor Unit Firing in sEMG of the Trapezius Muscle. *Methods of information in Medicine*, 49:492–495, 2010.

[157] J. Taelman, B. Mijovic, S. Devuyst, T. Dutoit, A. Spaepen, and S. Van Huffel. ECG artifact removal from surface EMG signals by combining empirical mode decomposition and independent conponent analysis. In *Proceedings of the International Conference on Bio-inspired Systems and Signal Processing, subconference of the 4th International Joint Conference on Biomedical Engineering Systems and Technologies (BIOSTEC 2011)*, January 2011. to appear.

[158] J. Taelman, A. Spaepen, and S. Van Huffel. Estimation of the rest state of a muscle extracted form the frequency domain of the electromyography signals. In *Annual Symposium of the IEEE/EMBS Benelux Chapter*, page 62, Heeze, The Netherlands, December 2007.

[159] J. Taelman, A. Spaepen, and S. Van Huffel. Wavelet Independent Component Analysis to remove electrocardiography contamination in surface electromyography. *Proceedings of Engineering in Medicine and Biology Society*, 2007:682–685, 2007.

[160] J. Taelman, S. Vandeput, A. Spaepen, and S. Van Huffel. Influence of mental stress on heart rate and heart rate variability. In *Proceedings of 4th European Congress of the International Federation for Medical and Biomedical Engineering (ECIFMBE)*, pages 1366–1369, Antwerp, Belgium, November 2008.

[161] J. Taelman, S. Vandeput, E. Vlemincx, A. Spaepen, and S. Van Huffel. Instantaneous changes in heart rate regulation due to mental load in simulated office work. *European Journal of Applied Physiology*, 2010. Accepted for publication.

[162] J. Taelman, S. Vandeput, D. Widjaja, M. Braeken, R. Otte, B. Van den Bergh, and S. Van Huffel. Stress during pregnancy: Is the autonomic nervous system influenced by anxiety? In *Proceedings. of 37th Annual Computing in Cardiology (CinC)*, Belfast, Northern Ireland, September 2010. to appear.

[163] J. Taelman, J. Vanderhaegen, M. Robijns, G. Naulaers, A. Spaepen, and S. Van Huffel. Estimation of muscle fatigue using surface electromyography and near-infrared spectroscopy. *Advances in Experimental Medicine and Biology*, 701, 2010. to appear.

[164] T. Tanaka and D.P. Mandic. Complex empirical mode decomposition. *IEEE Signal Processing Letters*, 14:101–104, 2007.

[165] Task Force of the European Society of Cardiology and the North American Society of Pacing and Electrophysiology. Heart rate variability: standards of measurement, physiological interpretation and clinical use. *Circulation*, 93:1043–1065, 1996.

[166] S.E. Taylor. Biobehavioral responses to stress in females: tend-and-befriend, not fight-or-flight. *Annual Review of Psychology*, 107:411–429, 2000.

[167] S. Thorn, K. Sogaard, L.A.C. Kallenberg, L. Sandsjo, G. Sjogaard, H.J. Hermens, R. Kadefors, and M. Forsman. Trapezius muscle rest during standardised computer work - A comparison of female computer users with and without self-reported neck/shoulder complaints. *Journal of Electromyography and Kinesiology*, 17:420–427, 2007.

[168] L.C.K. Tripathi. Respiration and heart rate variability: a review with special reference to its application in aerospace medicine. *Indian Journal of Aerospace Medicine*, 48:64–75, 2004.

[169] B.R.H. Van den Bergh, E.J.H. Mulder, M. Mennes, and V. Glover. Antenatal maternal anxiety and stress and the neurobehavioural development of the fetus and child: links and possible mechanisms. A review. *Neuroscience and Biobehavioral Reviews*, 29(2):237–258, 2005.

[170] S. Vandeput. *Heart rate variability: linear and nonlinear analysis with applications in human physiology.* PhD thesis, Department of electrical engineering, Katholieke Universiteit Leuven, October 2010.

[171] S. Vandeput, J. Taelman, A. Spaepen, and S. Van Huffel. Heart rate variability as a tool to distinguish periods of physical and mental stress in a laboratory environment. In *Proceedings of the 6th International Workshop on Biosignal Interpretation (BSI)*, pages 187–190, New Haven, Connecticut, June 2009.

[172] S. Vandeput, J. Taelman, A. Spaepen, and S. Van Huffel. Distinction between physical and mental stress in a laboratory environment using heart rate variability characteristics. *Journal of NeuroEngineering and Rehabilitation*, 2010. Revised.

[173] O. Vasseljen and R.H. Westgaard. Can stress-related shoulder and neck pain develop independently of muscle activity? *Pain*, 64:221–230, 1995.

[174] A. Vincent, F.I.M. Craik, and J.J. Furedy. Cardiac vagal tone: a physiological index of stress. *International Journal of Psychophysiology : Official Journal of the International Organization of Psychophysiology*, 23:181–198, 1996.

[175] E. Vlemincx, I. Van Diest, P.M. Lehrer, A.E. Aubert, and O. Van den Bergh. Respiratory variability preceding and following sighs: A resetter hypothesis. *Biological Psychology*, 84:82–87, 2010.

[176] E. Vlemincx, J. Taelman, I. Van Diest, and O. Van den Bergh. Take a deep breath: The relief effect of spontaneous and instructed sighs. *Physiology & Behavior*, 101:67–73, 2010.

[177] E. Vlemincx, J. Taelman, S. De Peuter, I. Van Diest, and O. Van den Bergh. Sigh rate and respiratory variability during mental load and sustained attention. *Psychophysiology*, 47:1–4, 2010.

[178] A. Voss, S. Schulz, R. Schroeder, M. Baumert, and P. Caminal. Methods derived from nonlinear dynamics for analysing heart rate variability. *Philosophical Transactions of thr Royal society A: Mathematical, physical and engineering sciences*, 367:277–296, 2009.

[179] T. Vrijkotte, L. van Doornen, and E. de Geus. Effects of work stress on ambulatory blood pressure, heart rate, and heart rate variability. *Hypertension*, 35:880, 2000.

[180] J. Wahlstrom, M. Hagberg, P.W. Johnson, J. Svensson, and D. Rempel. Influence of time pressure and verbal provocation on phsyiological and psychological reactions during work with a computer mouse. *European Journal of Applied Physiology*, 87:257–263, 2002.

[181] J. Wahlstrom, A. Lindegard, G. Ahlborg, A. Ekman, and M. Hagberg. Perceived muscular tension, emotional stress, pshychological demands and physical load during vdu work. *International Archive of Occupational and Environmental Health*, 76:584–590, 2003.

[182] D. Watson, L.A. Clark, and A. Tellegen. A development and validation of brief measures of positive and negative affect: the PANAS scales. *Journal of Personal and Social Psychology*, 54:1063–1070, 1988.

[183] N. Wessel, M. Riedl, and J. Kurths. Is the normal heart rate chaotic due to respiration? *Chaos*, 19:028508, 2009.

[184] C. Westad, R.H. Westgaard, and C.J. De Luca. Motor unit recruitment and derecruitment induced by brief increase in contraction amplitude of the human trapezius muscle. *Journal of Physiology*, 552:645–656, 2003.

[185] R. Westgaard, P. Bonato, and C. Westad. Respiratory and stress-induced activation of low-threshold motor units in the human trapezius muscle. *Experimental Brain Research*, 175:689–701, 2006.

[186] R.H. Westgaard, O. Vasseljen, and K.A. Holte. Trapezius muscle activity as a risk indicator for shoulder and neck pain in female service workers with low biomechanical exposure. *Ergonomics*, 44:339–353, 2001.

[187] D. Widjaja, S. vandeput, J. Taelman, M. Braeken, R. Otte, B. Van den Bergh, and S. Van Huffel. Accurate R Peak Detection and Advanced Preprocessing of Normal ECG for Heart Rate Variability Analysis. In *Proceedings of 37th Annual Computing in Cardiology (CinC)*, Belfast, Northern Ireland, September 2010. to appear.

[188] D. Widjaja, S. Vandeput, J. Taelman, M.A.K.A. Braeken, R.H. Otte, B.R.H. Van den Bergh, and S. Van Huffel. Accurate R Peak Detection and Advanced Preprocessing of Normal ECG for Heart Rate Variability Analysis. In *Proc of Computing in Cardiology 2010*, Belfast, Northern Ireland, September 2010.

[189] C.J. Wientjes and P. Grossman. Overreactivity of the psyche or the soma? Inter-individual associations between psychosomatic symptoms, anxiety, heart rate, and end-tidal partial carbon dioxide pressure. *Psychosomatic Medicine*, 53:533–540, 1994.

[190] Z. Yang and L. Yang. A new definition of the intrinsic mode function. *World Academy of Science, Engineering and Technology*, 60:822–825, 2009.

[191] Y. Yoshitake, H. Ue, M. Miyazaki, and T. Moritani. Assessment of lower-back muscle fatigue using EMG, MMG and NIRS. *European Journal of Applied Physiology*, 84:174–179, 2001.

[192] V. Zarzoso and P. Common. Comparative speed analysis of fastica. In *Proceedings of the 7th international conference on Independent component analysis and signal separation*, volume 7, pages 293–300, London, UK, 2007.

[193] X. Zhong, H.J. Hilton, G.J. Gates, S. Jelic, Y. Stern, M.N. Bartels, R.E. DeMeersman, and R.C. Basner. Increased sympathetic and decreased parasympathetic cardiovascular modulation in normal humans with acute sleep deprivation. *Journal of Applied Physiology*, 98:2024–2032, 2005.

Publication List

Papers in international journals

1. E. Vlemincx, **J. Taelman**, S. De Peuter, I. Van Diest and O. Van den Bergh. Sigh rate and respiratory variability during mental load and sustained attention. Psychophysiology, vol. 47, 2010, pp. 1-4.

2. E. Vlemincx, **J. Taelman**, I. Van Diest and O. Van den Bergh. Take a deep breath: The relief effect of spontaneous and instructed sighs. Physiology and Behavior, vol. 101, 2010, pp. 67-73.

3. B. Mijovic, M. De Vos, I. Gligorijevic, **J. Taelman** and S. Van Huffel. Source separation from single-channel recordings by combining empirical mode decomposition and independent component analysis. IEEE Transactions on Biomedical Engineering, vol. 57 (9), 2010, pp. 2188-2196.

4. **J. Taelman**, W. Deburchgraeve, K. Van Damme, T. Adriaensen, A. Spaepen and S. Van Huffel. Detection Algorithm for Single Motor Unit Firing in sEMG of the Trapezius Muscle. Methods of information in Medicine, vol. 49, Nov. 2010, pp. 492-495.

5. **J. Taelman**, J. Vanderhaegen, M. Robijns, G. Naulaers, A. Spaepen and S. Van Huffel. Estimation of muscle fatigue using surface electromyography and near-infrared spectroscopy. Advances in Experimental Medicine and Biology, to be published in vol. 701, 2010.

6. **J. Taelman**, S. Vandeput, E. Vlemincx, A. Spaepen and S. Van Huffel. Instantaneous changes in heart rate regulation due to mental load in simulated office work. Accepted for publication in European Journal of Applied Physiology, December 2010.

Papers submitted to international journals

7. S. Vandeput, **J. Taelman**, A. Spaepen and S. Van Huffel. Distinction between physical and mental stress in a laboratory environment using heart rate variability characteristics. Journal of NeuroEngineering and Rehabilitation, resubmitted July 2010.

Abstracts in international journals

8. E. Vlemincx, K. Van Damme, T. Adriaensen, **J. Taelman**, A. Wittebrood, A. Peeters, S. De Peuter, I. Van Diest, A. Spaepen and O. Van den Bergh. The effect of mental stress on sigh rate and respiratory variability. Biological Psychology: vol. 83 (1).

9. M.A.K.A Breaken, R.A. Otte, D. Widjaja, S. Vandeput, **J. Taelman**, S. Van Huffel and B. Van den Bergh. Mental stress and heart rate variability during the first pregancy trimester. Developmental Psychobiology, in Press.

Papers in proceedings of international conferences

10. **J. Taelman**, T. Adriaensen , A. Spaepen, G.R. Langereis, L. gourmelon and S. Van Huffel. Contactless emg sensors for continuous monitoring of muscle activity to prevent musculoskeletal disorders. Proceedings of 1^{st} symposium of the IEEE/EMBS Benelux Chapter. (IEEE EMBS), Brussel, Belgium, Dec. 2006, pp. 223-226.

11. **J. Taelman**, S. Van Huffel and A. Spaepen. Wavelet-Independent Component Analysis to remove Electrocardiography Contamination in surface Electromyography. Proceedings of 29^{th} Annual International Conference of the IEEE, Engineering in Medicine and Biology Society (IEEE/EMBC), Lyon, France, Aug. 2007, pp. 682-685

12. **J. Taelman**, T. Adriaensen , C. van der Horst, T. Linz and A. Spaepen. Textile Integrated Contactless EMG Sensing for Stress Analysis. Proceedings of 29^{th} Annual International Conference of the IEEE, Engineering in Medicine and Biology Society (IEEE/EMBC), Lyon, France, Aug. 2007, pp. 3966-3969.

13. A. Sipilä, P. Tolvanen and **J. Taelman**. sEMG measuring by garments. Proceedings of 39^{th} Nordic Ergonomics Society Conference (NES), Göteborg, Sweden, Oct. 2007.

14. **J. Taelman**, S. Vandeput, A. Spaepen and S. Van Huffel. Influence of mental stress on heart rate and heart rate variability. Proceedings of 4^{th} European Congress of the International Federation for Medical and Biomedical Engineering (ECIFMBE), Antwerp, Belgium, Nov. 2008, pp. 1366-1369.

15. **J. Taelman**, W. Deburchgraeve, K. Van Damme, T. Adriaensen, A. Spaepen and S. Van Huffel. Detection of the firing of a single motor unit in surface electromyography from the trapezius muscle during a mental task. Proceedings of the 6^{th} International Workshop on Biosignal Interpretation (BSI), New Haven, Connecticut, USA, June 2009, pp. 116-119.

16. S. Vandeput, **J. Taelman**, A. Spaepen and S. Van Huffel. Heart rate variability as a tool to distinguish periods of physical and mental stress in a laboratory environment. Proceedings of the 6^{th} International Workshop on Biosignal Interpretation (BSI), New Haven, Connecticut, USA, June 2009, pp. 187-190.

17. M.A.K.A. Braeken, R.A. Otte, D. Widjaja, S. Vandeput, **J. Taelman**, S. Van Huffel and B.R.H. Van den Bergh. Mental stress and cardiovascular reactivity in pregnant women. Proceedings of the 7^{th} World Congress on Stress, Leiden, the Netherlands, Aug. 2010.

18. D. Widjaja, S. Vandeput, **J. Taelman**, M.A.K.A. Braeken, R.A. Otte, B.R.H. Van den Bergh and S. Van Huffel. Accurate R peak detection and advanced preprocessing of normal ECG for heart rate variability analysis. Proceedings of the 37^{th} Annual Computing in Cardiology (CinC), Belfast, Northern Ireland, Sep. 2010, accepted.

19. D. Widjaja, **J. Taelman**, S. Vandeput, M.A.K.A. Braeken, R.A. Otte, B.R.H. Van den Bergh and S. Van Huffel. ECG derived respiration: comparison and new measures for respiratory variability. Proceedings of the 37^{th} Annual Computing in Cardiology (CinC), Belfast, Northern Ireland, Sep. 2010, accepted.

20. **J. Taelman**, D. Widjaja, S. Vandeput, M.A.K.A. Braeken, R.A. Otte, B.R.H. Van den Bergh and S. Van Huffel. Stress during pregnancy: Is the autonomic nervous system influenced by anxiety? Proceedings of the 37^{th} Annual Computing in Cardiology (CinC), Belfast, Northern Ireland, Sep. 2010, accepted.

21. **J. Taelman**, B. Mijovic, S. Devuyst, T. Dutoit and S. Van Huffel. ECG artifact removal from surface EMG signals by combining empirical mode decomposition and independent component analysis Proceedings of the International Conference on Bio-inspired Systems and Signal Processing, subconference of the 4^{th} International Joint Conference on Biomedical

Engineering Systems and Technologies (BIOSTEC 2011), Rome, Italy, Jan. 2011, accepted.

Abstracts in proceedings of (inter)national conferences

22. **J. Taelman**, A. Spaepen and S. Van Huffel. Estimation of the rest state of a muscle extracted form the frequency domain of the electromyography signals Annual Symposium of the IEEE/EMBS Benelux Chapter, Heeze, The Netherlands, Dec. 2007, pp 62.

23. E. Vlemincx, K. Van Damme, T. Adriaensen, **J. Taelman**, A. Wittebrood, A. Peeters, S. De Peuter, I. Van Diest, A. Spaepen and O. Van den Bergh. The effect of mental stress on sigh rate and respiratory variability Proceedings of the International Society of the Advancement of Respiratory Psychophysiology (ISARP), Ann Arbor, Michigan, Oct. 2008.

24. E. Vlemincx, K. Van Damme, T. Adriaensen, **J. Taelman**, A. Wittebrood, A. Peeters, S. De Peuter, I. Van Diest, A. Spaepen and O. Van den Bergh. Sigh rate during mental stress Annual meeting society for psychophysiological research, Austin, Oct. 2008.

25. E. Vlemincx, **J. Taelman**, S. De Peuter, I. Van Diest and O. Van den Bergh. The Effect of an Imposed Sigh Following Mental Stress Annual meeting society for psychophysiological research, Berlin, Oct. 2009.

26. E. Vlemincx, **J. Taelman**, S. De Peuter, I. Van Diest and O. Van den Bergh. The relief effect of spontaneous sighs as opposed to imposed sighs AAnnual Meeting & Symposium on Respiratory Psychophysiology, Berlin, Oct. 2009.

27. M.A.K.A Breaken, R.A. Otte, D. Widjaja, S. Vandeput, **J. Taelman**, S. Van Huffel and B. Van den Bergh. Mental stress and cardiovascular reactivity in pregnant women. Proceedings of the 7^{th} World Congress on Stress, Leiden, the Netherlands, Aug. 2010.

28. D. Widjaja, **J. Taelman**, S. Vandeput, M.A.K.A. Braeken, R.A. Otte, B.R.H. Van den Bergh and S. Van Huffel. Influence of stress and anxiety on the autonomic nervous system during pregnancy. The Belgian Day on Biomedical Engineering, Brussels, Belgium, Nov. 2010.

Curriculum vitae

Joachim Taelman was born in Roeselare, Belgium on April 10, 1982. He received the degree of engineer cum laude in electronics at the Katholieke Hogeschool Brugge-Oostende, Belgium in 2004. He also received the degree of electrotechnical-mechanical engineer with specialization in biomedical techniques, cum laude from the Katholieke Universiteit Leuven, Belgium in July 2006.

Since July 2006, he worked as scientific researcher in the laboratory of ergonomics in the department of biomedical kinesiology, Katholieke Universiteit Leuven under the supervision of Prof. Dr. Ir. Arthur Spaepen and Prof. Dr. Ir. Sabine Van Huffel. He was involved in the European project ConText (Contactless sensors incorporated in Textiles; IST-027291). The project ended in December 2008. Since January 2009, he has been working as researcher at the Electrical Engineering Department ESAT of the Katholieke Universiteit Leuven under the supervision of Prof. Dr. Ir. Sabine Van Huffel on a K.U. Leuven PhD grant.

Arenberg Doctoral School of Science, Engineering & Technology
Faculty of Engineering
Department of Electrical Engineering
Research group SISTA-BIOMED
Kasteelpark Arenberg 10, B - 3001 Leuven

KATHOLIEKE UNIVERSITEIT LEUVEN

ASSOCIATIE K.U.LEUVEN